The role of *TBK1* mutations in amyotrophic lateral sclerosis and frontotemporal dementia

Alaa Osama Doubi

Department of Neuroscience Faculty of Medicine, Dentistry and Health

University of Sheffield

A thesis submitted to the University of Sheffield in partial fulfilment of the requirements for the degree of Doctor of Philosophy

Submission Date: September 2021

Declaration

I, Alaa Doubi, confirm that the work presented in this confirmation review is my own. I also would like to acknowledge that the *tbk1*^{SH570} Zebrafish model have been previously generated in University of Sheffield and *optn*^{SA0143} obtained from Sanger Institute.

Acknowledgements

I would like to sincerely express my deep gratitude to my supervisor Dr Andrew Grierson. He was most helpful, offered invaluable assistance, and always been there for me as an excellent academic supervisor. Furthermore, I would like to thank my second supervisor Dr Kurt De Vos, who gave me valuable advice and helpful suggestions. I would also like to thank my colleague Mirinda Tattan and Kathryn Adamson for their help and support.

I owe thanks to the Sheffield Institute for Translational Neuroscience (SITraN) group and the Bateson Centre for offering advice and support. Additionally, I am thankful to Richard Shepherd and Michael Thomson at the Bateson Centre for assistance with zebrafish husbandry and Sarah Baxendale from Bioscience for helping with the viewpoint.

I want to acknowledge the support of King Faisal specialist hospital and research centre for sponsoring me, and I also would like to thank my boss, Dr Brian Meyer, for his support.

I am also deeply grateful to my friends Hayfa, Hatoon, Amani and my cousin Mawadah for their support during the lockdown period. Finally, I would like to thank my family, and I could not have gotten to this point without my parents, brothers, and sister's encouragement.

Abstract

Dominantly inherited loss of function mutations in human TANK binding kinase (*TBK1*) predispose to neurodegenerative diseases of the central nervous system including amyotrophic lateral sclerosis (ALS) and frontotemporal dementia (FTD). TBK1 regulates several pathways, including autophagy, nuclear factor κb (NFκB) and interferon regulatory factor 3 (IRF3) signaling. Zebrafish have been used effectively as an *in vivo* model to analyse the molecular and functional aspects of many neuroinflammatory and neurodegenerative diseases. In order to investigate the role of TBK1 in ALS/FTD we have generated zebrafish *tbk1* models carrying loss of function mutations. The aims of this study are to characterise the ALS/FTD phenotype of the *tbk1* zebrafish models by utilising swimming and shoaling behaviour studies, and to establish assays for analysing NFκB, IRF3 and autophagy in control and *tbk1* mutant siblings. In order to determine disease mechanisms, we will then attempt to restore activity of specific pathways and determine whether or not this rescues the ALS/FTD phenotype of the zebrafish.

We successfully generated zebrafish models carrying a frameshift mutation in the *tbk1* gene that are similar to those reported in ALS and FTD patients. Our *tbk1* homozygous mutant zebrafish models show some promising evidence of phenotypic effects that are similar to those reported in other ALS models. Our *tbk1*$^{SH570/SH570}$ mutant zebrafish survive to adulthood and show reduced swimming behaviour similar to ALS patients. Also, they show a loss of thigmotaxis and a defect in shoaling, which may represent altered social behaviour observed in FTD patients. The *tbk1*$^{SH570/SH570}$ show increased NFκB signaling and increased expression of genes that are known to be downstream targets of NFκB (*il1β, il6, il8* and *tnfα*). Since we observe increased NFκB signaling we used a crispant approach to target *map3k14a* in the *tbk1*^{SH570} zebrafish to attempt to reduce NFκB signaling and investigate the effect on swimming behaviour. This approach was unsuccessful, and in future studies we suggest that this result should be investigated again using a stable *map3k14a* mutant.

Table of Contents

List of figures

List of tables

Abbreviations

ANOVA: analysis of variance
ALS: amyotrophic lateral sclerosis
ALS2: alsin Rho Guanine Nucleotide exchange Factor
ANG: angiogenin
cAMP: cyclic adenosine monophosphate
CEP170: centrosomal Protein 170
C9ORF72: chromosome 9 open reading frame 72
CHMP2B: chromatin- modifying protein 2B
COX: cyclooxygenase
Cas9: CRISPR-associated protein 9
cDNA: complementary DNA
CREB: (cAMP) response element binding protein
DCTN1: dynactin
DNA: deoxyribonucleic acid
Dpf: days post-fertilisation
dsRNA: double-stranded RNA dsRNA
EDTA: ethylenediaminetetraacetic acid
EBP: enhancer-binding protein beta
eef1a1b: eukaryotic translation elongation factor 1 alpha 1b
ExoSAP: Exonuclease I and shrimp alkaline phosphatase
FTD: frontotemporal dementia
FUS: fused in sarcoma
gRNA: guide RNA
GRN: granulin
Kif2b: Kinesin Family Member 2B
HRM: high-resolution melt
HRMA: high-resolution melt analysis
IKK: inhibitor of nuclear factor kappa kinase
IKKα: inhibitor of nuclear factor kappa-B kinase subunit alpha
IKKβ: inhibitor of nuclear factor kappa-B kinase subunit beta
IKKε: inhibitor of nuclear factor kappa-B kinase subunit epsilon
IFN: interferon
IL: interleukin
IL1β: interleukin β
IL6: interleukin 6
IL8: interleukin 8
IRF3: interferon regulatory factor 3
IRF7: interferon regulatory factor 7
LC3: microtubule associated 1 light chain 3
LRRK2: leucine rich repeat kinase 2
LPS: lipopolysaccharide

LRR: leucine-rich repeat (segment of extracellular part of TLR)
MAPT: microtubule- associated protein tau
MAP3K14a: Mitogen-activated protein kinase kinase kinase 14a
mRNA: messenger RNA
MND: motor neuron disease
NAK: NFκB activating kinase
NAP1: NAK-associated protein 1
NEMO: NF-kappa-B essential modulator
NIK: NFκB inducing kinase
NDP52: nuclear dot 52kDa
NF: nuclear transcription factor
NFκB: nuclear transcription factor kappa-light chain enhancer of activated B cells
NIK: nuclear factor κB-inducing Kinase
OPTN: optineurin
PGE_2 : prostaglandin E_2
TRAF: TNF receptor associated factor
TNF: tumor necrosis factor
TLR:toll-like receptor
P62: SQSTM1 p62
P65: transcription factor p65
PNFA: progressive nonfluent aphasia
PPA: primary progressive aphasia
Poly(I : C): Polyinosinic : polycytidylic acid
qPCR: quantitative real-time PCR
RNA: ribonucleic acid
SIGMAR1: sigma non-opioid intracellular receptor
SINTBAD: similar to NAP1 TBK1 adaptor
SOD1: superoxide dismutase 1
SQSTM1: Sequestosome 1
STAT6: Signal Transducer and Activator Of Transcription 6
STING: Stimulator of interferon genes
TANK: TRAF (TNF (tumour necrosis factor) receptor-associated factor)
TBK1: TANK binding kinase 1
TIR domain: Toll- Interleukin -1 receptor domain
TLR: Toll-like receptor
TNF: tumour necrosis factor alpha
TARDBP: TAR DNA binding protein
UBQLN2: Ubiquilin 2
ULD: Ubiquitin-like domain
VAPB: vesicle-associated membrane protein B
VCP: valosin containing protein

Chapter 1

1. Introduction

1.1 Amyotrophic lateral sclerosis (ALS)

Amyotrophic lateral sclerosis (ALS) also known as Lou Gehrig's disease is a progressive motor neuron disease, which is characterised by the premature degeneration and loss of structure and function of both upper and lower neurons leading to the death of the neurons (Hardiman et al., 2017).

Annually around 1.5-2.5 per 100,000 people among Caucasian populations are diagnosed with ALS, which makes it a relatively rare disease (Logroscino et al., 2008). Twin study implies that environmental factors contribute to 40% risk of developing ALS (Al-Chalabi et al., 2010) while 60% are heritability; however, genome-wide association indicates that heritability accounts for only 21% (Keller et al., 2014). The only confirmed risk factors for ALS are family history of the disease, age, and male gender. Approximately 10% of ALS cases are familial and 90% are sporadic with no clear genetic linkage (Ahmeti et al., 2013). However, several environmental factors have been proposed to play a role in ALS, including head injury, toxins such as insecticides and pesticides, infections, autoimmune reactions (Beard and Kamel, 2015) and strenuous exercise(Julian et al., 2021). Other possible risk factors remain unconfirmed, including electromagnetic field exposure, electric shock, profession, and physical trauma (Pasinelli and Brown, 2006, Gardner and Yaffe, 2015).

ALS symptoms vary between patients depending on the disease presentation and progression but, usually, disability starts to present in one part of the body, followed by progression that leads to involvement of other parts (Hobson and McDermott, 2016). Some ALS patients have spinal-onset disease symptoms are characterised by muscle weakness of the limbs, such as cramps and spasticity. Other patients can present with bulbar-dysfunction, which causes dysarthria (speech problems) and dysphagia (difficulty swallowing) (Hardiman et al., 2017).

Other common symptoms includes pain, fatigue, emotional lability, depression, anxiety, dry mouth, excessive respiratory secretions, excessive oral secretions and respiratory failure (Hobson and McDermott, 2016).

The rate of progression of symptoms determines the average survival duration in ALS patients. Typically survival is in the range of 2–5 years, but for some patients the disease progression is much slower and the survival time could last longer (Beghi et al., 2006).

Diagnosis of ALS is challenging and usually based on a physical examination for upper and lower motor neurons. Electromyographic used to diagnose lower motor neuron MRI of the brain and the spinal cord used to diagnose upper motor neuron (Menke et al., 2014, Sekiguchi et al., 2014).

The neuropathological hallmark of ALS includes motor neuron degeneration in the motor cortex and spinal cord also the presence of inclusion bodies (TDP-43, FUS, SOD1) in the cytoplasm of the motor neuron. Other pathological features of ALS include vacuolization, spongiosis, loss and atrophy of nerve fibers, loss of myelinated axons in the spinal cord, decreases in size of anterior horn of the spinal cord, and a reduction of neurons in the anterior horn, lower cranial motor nuclei of the brainstem, and Betz cells in the motor cortex(Saberi et al., 2015, Hardiman et al., 2017).

TDP-43 is a heterogeneous nuclear ribonucleoprotein that is normally expressed in the nucleus of the neuron and glial cells. It has many functions, including mRNA stability, processing, transport, and translocation. TDP-43 has been observed in both sporadic and familial ALS. It is the main component of ubiquitinated inclusions in ALS, and it manifests by a loss of nuclear TDP-43 and the formation of pathological aggregates in the cytoplasm(Saberi et al., 2015).(Buratti, 2001)

1.1.1 Lessons from ALS genetics

The causes of ALS are still not fully known, however the continuing discovery of genetic mutations in familial ALS patients is providing strong support for a number of shared molecular pathogenic mechanisms (S.H. Appel, 2011). ALS is a genetically heterogeneous disease with causal mutations identified in more than 40 genes (Hardiman et al., 2017, Renton et al., 2014) (See Figure (1.1). The pathogenesis of ALS disease is caused by several genetic defects that interplay in various molecular mechanisms and pathways (see Figure (1.1) (Sheng Chen1, 2013). A list of confirmed ALS genes are given in table (1.1).

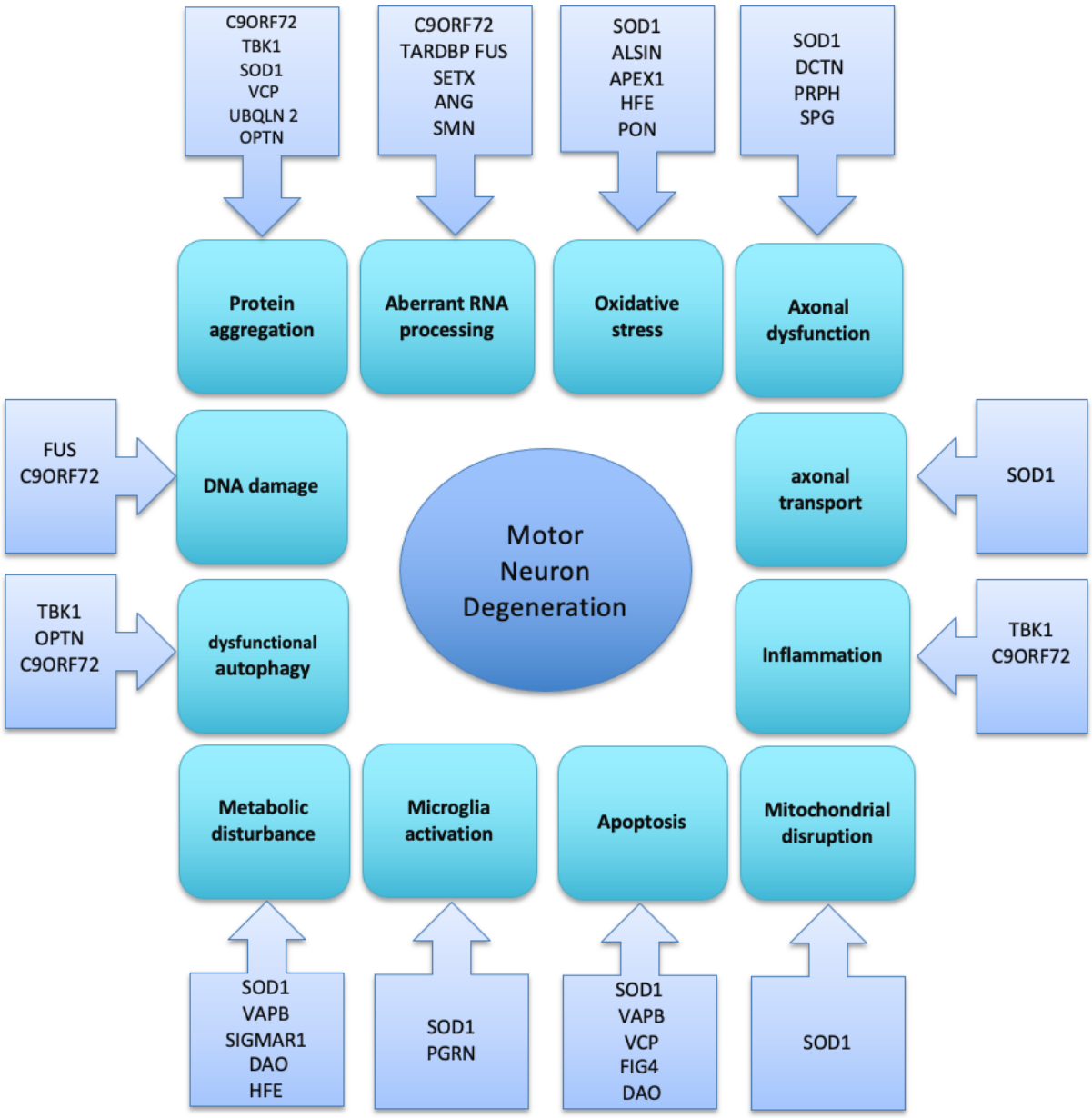

Figure 1.1 ALS/MND is likely to be caused by the interaction of several molecular pathways. Figure shows the genes (blue boxes) and pathways involved in motor neuron degeneration (violet boxes).

Table 1. 1 Genes that have been associated with ALS

Gene Symbol	Gene Name	Reference
ALS2	alsin Rho guanine nucleotide exchange factor	(Shinji Hadano1 et al., 2001)
ALS3	Amyotrophic Lateral Sclerosis 3	(Collette K. Hand et al., 2002)
ANG	Angiogenin	(Greenway et al., 2006)
ANXA11	annexin A11	(Smith et al., 2017)
ARPP21	CAMP Regulated Phosphoprotein 21	(Chun Hao Wong, 2018)
ATXN2	ATXN2	(Elden et al., 2010)
C9ORF72	chromosome 9 open reading frame 72	(DeJesus-Hernandez et al., 2011)
C19ORF12	Chromosome 19 Open Reading Frame 12	(Deschauer et al., 2012)
CHCHD10	Coiled-Coil-Helix-Coiled-Coil-Helix Domain	(Bannwarth et al., 2014)
CHMP2B	Charged Multivesicular Body Protein 2B	(N. Parkinson et al., 2006)
CHRNA4	Cholinergic Receptor Nicotinic Alpha 4	(Sabatelli et al., 2009)
CHRNB4	Cholinergic Receptor Nicotinic Beta 4 Subunit	(Sabatelli et al., 2009)
DCTN1	Dynactin Subunit 1	(C. Münch and J. Prudlo, 2004)
DAO	D-Amino Acid Oxidase	(Mitchell et al., 2010)
ELP3	Elongator Acetyltransferase Complex Subunit	(Simpson et al., 2009)
ERBB4	Erb-B2 Receptor Tyrosine Kinase 4	(Takahashi et al., 2013)
EWSR1	EWS RNA Binding Protein 1	(Couthouis et al., 2012)
FUS	FUS RNA Binding Protein	(T. J. Kwiatkowski Jr. et al., 2009)
FIG4	FIG4 Phosphoinositide 5-Phosphatase	(Chow et al., 2009)
GLE1	GLE1 RNA Export Mediator	(Aditi et al., 2016)
GLT8D1	Glycosyltransferase 8 Domain Containing 1	(Cooper-Knock et al., 2019)
HNRNPA2B1	Heterogeneous Nuclear Ribonucleoprotein	(Kim et al., 2013a)
HNRNPa1	Heterogeneous Nuclear Ribonucleoprotein A1	Kim et al., 2013)
KIF5A	Kinesin Family Member 5A	(Nicolas et al., 2018)
MATR3	Matrin 3	(Johnson et al., 2014)
NEFH	Neurofilament, Heavy Polypeptide	(A Al-Chalabi 1, 1999)
NEK1	NIMA (Never In Mitosis Gene A)-Related	(Kenna et al., 2016)
OPTN	optineurin	(Maruyama et al., 2010b)
PFN1	Profilin 1	(Wu et al., 2012)
PNPLA6	Patatin Like Phospholipase Domain	(Rainier et al., 2008)
PRPH	Peripherin	(C. Münch and J. Prudlo, 2004, Gros-Louis et
SETX	Senataxin	(Butterfield et al., 2009)
SIGMAR1	Sigma Non-Opioid Intracellular Receptor 1	(Luty et al., 2010)
SOD1	Superoxide Dismutase 1	(Daniel R. Rosen* et al., 1993)
SPAST	Spastin	(T. Meyer and A. Hopt, 2005)
SPG11	SPG11 Vesicle Trafficking Associated,	(Orlacchio et al., 2010)
SQSTM1	Sequestosome 1	(Faisal Fecto et al., 2011)
SS18L1	Subunit Of BAF Chromatin Remodeling	(Teyssou et al., 2014)
TAF15	TATA-Box Binding Protein Associated Factor	(Ticozzi et al., 2011)
TARDBP	TAR DNA Binding Protein	(Rutherford et al., 2008)
TBK1	TANK Binding Kinase 1	(Cirulli et al., 2015a)

TUBA4A	Tubulin Alpha 4a	(Smith et al., 2014)
UBQLN2	Ubiquilin 2	(Deng et al., 2011)
VAPB	VAMP Associated Protein B And C	(Nishimura et al., 2004)
VCP	Valosin Containing Protein	(Johnson et al., 2010)

1.1.2 Evolving themes in ALS genetics

Numerous genome-wide association studies (GWAS) published in both familial and sporadic ALS have made significant contributions to our understanding of ALS, these studies indicate that unlike schizophrenia and other diseases that are associated with common variants the genetic architecture of ALS is based mainly on rare variants with large effects (Hardiman et al., 2017). The rare genetic variants that present risk in ALS could be specific to individuals, families and ancestral populations, which makes GWAS in ALS more complicated. For example in Finland GWAS of ALS identified association signals on chromosome 9 (analogous to *C9ORF72*) and on chromosome 21 (analogous *SOD1*) these two loci account for almost all familial ALS cases in Finland (Laaksovirta et al., 2010). While in a Sardinian GWAS study they identified association signals at the *TARDBP* gene locus, which accounts for approximately 28% of both sporadic and familial ALS cases (Chio et al., 2011).

In 2015 a whole exome sequencing (WES) study of 2,874 ALS cases and 6,405 controls identified genetic variants associated with ALS (Cirulli et al., 2015a). Based on WES analysis of the presence or absence of variants predicted to be deleterious in each gene, 51 genes were predicted to be associated with ALS (Renton et al., 2014). TANK-Binding Kinase 1 (*TBK1*) mutations were found to be associated with ALS ($p = 1.13x10^{-5}$, a replication $p = 5.78x10^{-7}$, and a combined $p = 3.63x10^{-11}$) with loss-of-function variants occurring in 0.382% of cases and 0.034% of controls (Cirulli et al., 2015a). In addition, rare damaging loss-of-function variants in 0.620% of ALS cases and 0.228% of controls were observed in Optineurin (*OPTN*), a known substrate of *TBK1* (Cirulli et al., 2015a, Richter et al., 2016b). TBK1 and Optn proteins are both important regulators of inflammation and autophagy, which suggests that these important processes may be damaged in ALS and FTD patients with *TBK1* or *OPTN* mutations (Cirulli et al., 2015a). Furthermore, another WES study identified a frontotemporal lobar degeneration (FTLD) case that carried both a loss of function (LOF) p.Arg117x mutation in the *TBK1* gene and a deletion p.Gly538Glux27 in the *OPTN* gene (Pottier et al., 2015a). This indicates that these LOF mutations may act synergistically in FTLD.

1.2 Frontotemporal dementia

Frontotemporal dementia (FTD), also referred to as FTLD or Pick's Disease, is a neurodegenerative disease characterised by progressive neuronal atrophy of the frontal and temporal lobes of the brain (Hodges and Miller, 2001). Most cases of FTD are diagnosed in people aged 45-65, but it has also been diagnosed in people younger than 45 or older than 65. The prevalence of FTD in adults aged <65 years varies between 3 to 15 per 100,000 (Bang et al., 2015, Rabinovici and Miller, 2010). FTD is a complex heterogeneous disorder where the disease mechanisms are embroiled in significant genetic variability, a wide range of clinical symptoms and differential pathological indications (Ferrari et al., 2014). Common signs and symptoms of FTD are personality changes, with socially inappropriate behaviour, language defects, executive dysfunction, and problems with mental abilities, but with a relative preservation of memory and cognitive functions (Rabinovici and Miller, 2010).

The main clinical syndromes of FTD can be classified into three clinical subtypes, namely behavioural variant FTD (bvFTD), semantic dementia (SD), and progressive nonfluent aphasia (PNA) (Miller1, 2001). bvFTD is the most common form of FTD, the main signs are personality changes where patients have an inappropriate social behaviour, lack of empathy, defects in executive function and lack of good judgment (Pressman and Miller, 2014). SD symptoms include difficulty of reading, spelling, or finding the right word or understanding the meaning of a word (Diehl et al., 2005). Patients with PNA have problems with grammar, sentence comprehension and motor speech agrammatism (M.L. Gorno-Tempini et al., 2011). In addition, FTD also overlaps clinically with motor neurone disease /amyotrophic lateral sclerosis (FTD-MND/ALS) and also with the atypical Parkinsonian disorders and progressive supranuclear palsy (Rohrer and Warren, 2011). However motor neuron disease arises frequently in patients with bvFTD dementia and less often in patients with semantic-variant primary progressive aphasia (PPA) or non- fluent variant PPA (Bang et al., 2015). This clinical overlap is reflected in a shared genetic basis for the disorders (see Section 2.1).

Treatments for FTD are limited, although AD and FTD share certain symptoms, the pharmacological agents designed for AD are unlikely to benefit patients with FTD, because the cholinergic systems are not affected in FTD (Snowden et al. 2002).

1.2.1 Molecular Genetics of FTD

FTD is a genetically and pathologically heterogeneous disorder. The majority of cases are familial with autosomal dominant inheritance but heritability varies between the different syndromes such as behavioural variant FTD and PPA (J.D. Rohrer et al., 2009). Genetic linkage and sequencing studies have provided efficient approaches for detecting common and rare genetic variations associated with FTD (Rainero, 2017). Mutations in the microtubule-associated protein tau (*MAPT)*, granulin *(GRN)* and *C9orf72* genes are most commonly associated with FTD. Additional rare mutations have been identified in the following genes: valosin-containing protein (*VCP*), *TARDBP,* chromatin- modifying protein 2B *(CHMP2B*), ubiquilin 2 (*UBQLN2*), fused-in-sarcoma (*FUS*), Triggering receptor expressed on myeloid cells 2 *(TREM2),* coiled-coil-helix-coiled-coil-helix domain containing 10 (*CHCHD10), OPTN, TBK1* and sequestosome 1 (*SQSTM1*) (Rademakers et al., 2004, Finch et al., 2009, Sharon J. Sha et al., 2012, Watts et al., 2007, Borroni et al., 2009, Borroni et al., 2014, A.M. Isaacs1, 2011, Synofzik et al., 2012, Vance et al., 2009, Woo et al., 2017, Le Ber et al., 2013).
Interestingly mutations in *C9orf72, VCP, TARCBP, UBQLN2, FUS, OPTN* and *TBK1* been reported previously in ALS cases (Ilse Gijselinck et al., 2015, Manuela Neumann et al., 2006, Renton et al., 2011, Johnson et al., 2010, Maruyama et al., 2010b, Vance et al., 2009, Deng et al., 2011). These data support the evidence that ALS and FTD are part of a disease spectrum and re-emphasises an important role for the overlapping genetic basis of the OPTN/TBK1 pathway in ALS and FTD (Pottier et al., 2015a, Freischmidt et al., 2015b). A number of studies have reported the identification of several different mutations in ALS and FTD genes in individual patients. It is not clear yet whether all these mutations are pathogenic, however it seems to indicate that there may be an oligogenic basis for ALS and FTD (Keogh et al., 2018). Specifically relevant to this project, there are reports of *TBK1* and *OPTN* mutations in individual patients (Pottier et al., 2015a).

1.3 TANK binding kinase 1

The TANK binding kinase 1 (*TBK1*) gene also known as NFκB -activating kinase (*NAK*) encodes an 84 kDa serine/threonine kinase. The TBK1 protein is a member of the Inhibitor of nuclear factor kappa kinase (IKK) family. *TBK1* is located on chromosome 12q14.2, comprises 21 exons encoding a 729 amino acid protein (NM_013254) (NP_037386). Human *TBK1* is highly conserved evolutionarily and does not tolerate polymorphisms. According to the Exome Aggregation Consortium (ExAC) out of 66,706 WES samples only one common missense variant has been reported in *TBK1*.

1.3.1 Functional domains of TBK1

The TBK1 protein has 4 characterised functional domains, including a serine/ threonine kinase domain (KD) (amino acids 1-308), ubiquitin-like domain (amino acids 309-383), a helical scaffold dimerization domain at the N-terminus and two putative coiled-coil domains (CCDs); CCD1 (amino acids 407-658), and CCD2 (amino acids 659-729) at the C-terminus (see Figure (1.2) (Larabi et al., 2013, Ahmad et al., 2016).

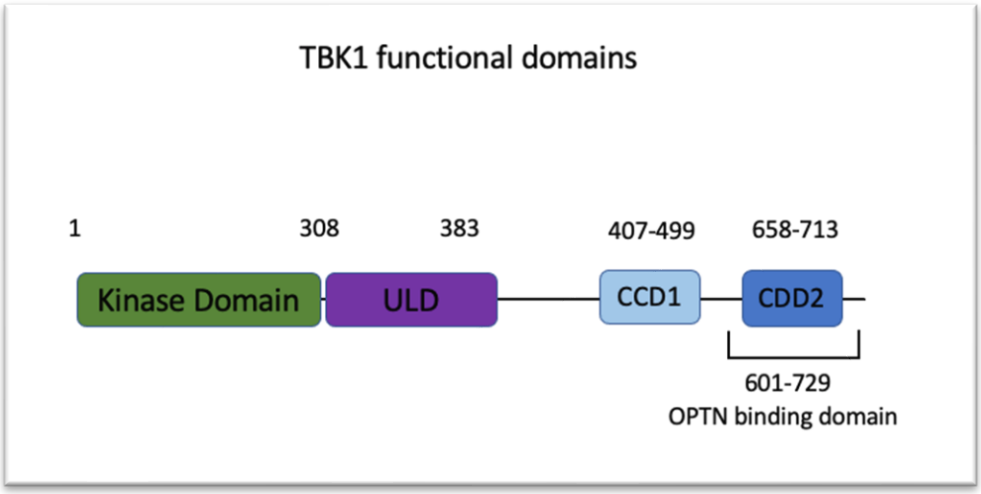

Figure 1.2 Structure of TBK1. Figure shows the locations of the kinase domain, ubiquitin like domain (ULD) and the two coiled coil domains (CCDs) 1 & 2. The OPTN binding domain in the C-terminal region of TBK1 is indicated.

TBK1 functions as a dimer, but within the configuration of the dimer the TBK1 kinase active sites are in opposite orientations. This obstructs the dynamic kinase-kinase interaction within the dimer, thus in the absence of upstream signaling, TBK1 activation and auto-phosphorylation will be restricted (Helgason et al., 2013). Auto-phosphorylation of the TBK1 KD is controlled by several mechanisms to ensure that TBK1 is inactive in the absence of pathway stimulation (Helgason et al., 2013). Localisation plays a key role in the activation of TBK1 protein, where adaptor proteins are recruited to signaling complexes that auto-phosphorylate ether by high local concentrations or by other kinases that are localised to the same molecular platform (Hou et al., 2011, Clark et al., 2011). It was shown in one study that the subcellular localisation of TBK1 has different functions in several pathways as different adaptors such as TRAF family member associated NF-kappa-B activator (TANK), similar to NAP1 TBK1 adaptor (SINTBAD) and nuclease assembly protein (NAP1) compete to interact with TBK1 (Goncalves et al., 2011). Activation of TBK1 involves an adaptor binding motif and upstream signaling. However, localisation-based regulation of TBK1 can be activated in the lack of an adaptor binding motif or pathway catalyst when it is overexpressed (Hou et al., 2011, Clark et al., 2011).
Mutations in *TBK1* and *OPTN* are associated with ALS and FTD, and TBK1 also regulates OPTN by phosphorylating it to trigger autophagy, as OPTN is an autophagy receptor (Li et al., 2016). TBK1 has the ability to interact with full length OPTN where the N-terminal region of OPTN binds to the C-terminal region of TBK1. However, mutation in either the C-terminal (amino acids 601-729) of TBK1 or the N-terminus of OPTN (amino acids 1-119) could prevent formation of this complex (Li et al., 2016, Morton et al., 2008).

1.3.2 *TBK1* mutations in human disease

Mutations in human *TBK1* predispose to neuroinflammatory/neurodegenerative diseases of the central nervous system including ALS, FTD, normal tension glaucoma (NTG) and childhood herpes simplex encephalitis (HSE) (see Table 1.1). These diseases suggest genetic heterogeneity of *TBK1* where mutations in a single gene can cause various phenotypes (Ahmad et al., 2016). *TBK1* mutations play a part in defining the disease phenotype and can vary from loss of function, gain of function, haploinsufficiency and dominant negative mutants. In NTG gain of function results from *TBK1* duplication, while ALS and FTD are associated with heterozygous loss of function mutations that result in haploinsufficiency (Ahmad et al., 2016). To date none of the mutations characteristic of NTG and HSE have been discovered in ALS or FTD patients. HSE mutations arise singularly in the KD causing a loss of interferon-beta (IFNb) induction, whereas in ALS and FTD nonsense, missense, deletion, splice site and frameshift mutations have been found in all *TBK1* domains and have been proposed to result in impaired optineurin binding (Freischmidt et al., 2015b) and loss of kinase activity(De Majo et al., 2018). Proteomic studies have demonstrated that TBK1 has different subcellular localisations and through interactions with adaptor protein such as TANK, SINTBAD and NAP1, TBK1 forms independent complexes (Li et al., 2011, Goncalves et al., 2011). It remains to be established if all missense mutations found in *TBK1* alter specific interactions and/or alter subcellular localisation of the protein, but both truncating (S357X) and missense (pG217R) mutations have been shown to prevent TBK1 from binding to OPTN (De Majo et al., 2018). Consequently, the different diseases that are associated with mutations in *TBK1* may be characterised by a combination of domain specific mutations, alterations in protein-protein interactions, subcellular localisation and tissue specificity (Freischmidt et al., 2015b).

Table 1. 2 *TBK1* mutations reported in human diseases

Mutation type	Nucleotide Variation	Residue change	Phenotype	References	Domains
Missense	c.10A>G	p.T4A	ALS -FTD	(Le Ber et al., 2015)	
Missense	c.77G>A	p.G26E	ALS -FTD	(Le Ber et al., 2015)	
Deletion	c.86delA	p.K29Rfsx15	FTD	(van der Zee et al., 2017)	
Missense	c.92A>G	p.T31A	ALS	(De Majo et al., 2018)	
Missense	c.140G>A	p.R47H	ALS	(Freischmidt et al., 2015b)	
Missense	c.149A>C	p.D50A	HSE	(Herman et al., 2012)	
Duplication	c.176dupT	p.C58fs	ALS	(Pozzi et al., 2017)	
Deletion	c.236_238delCAA	p.T79del	FTD-ALS	(van der Zee et al., 2017)	
Missense	c.281T>C	p.L94S	ALS	(van der Zee et al., 2017)	
Deletion	c.288delT	p.V97Ffsx2	ALS	(van der Zee et al., 2017)	
Nonsense	c.349C>T	p.R117X	ALS	(Cirulli et al., 2015a)	
Missense	c.352G>A	p.D118N	ALS	(Pozzi et al., 2017)	
Splicing	c.358+2T>C	_	ALS	(Freischmidt et al., 2015b)	
Splicing	c.358+5G>A	_	ALS	(Pozzi et al., 2017)	
Missense	c.362G>A	p.G121D	ALS	(van der Zee et al., 2017)	KD
Nonsense	c.379C>T	p.R127X	ALS	(van der Zee et al., 2017)	
Missense	c.427C>T	p.R143C	ALS -FTD	(Le Ber et al., 2015)	
Deletion	c.467_468delCA	p.T156RfsX6	FTD-ALS	(Le Ber et al., 2015)	
Missense	c.476G>C	p.G159A	HSE	(Herman et al., 2012)	
Deletion	c.501_503delTGA	p.D167del	ALS	(Verheijen et al., 2018)	
Nonsense	c.555T>A	p.Y185X	ALS	(Freischmidt et al., 2015b)	
Missense	c.619A>G	p.I207V	HSE	(Itan et al., 2015)	
Missense	c.687G>T	p.R229S	ALS	(van der Zee et al., 2017)	
Missense	c.731G>T	p.G244V	ALS -FTD	(van der Zee et al., 2017)	
Missense	c.737T>C	p.I246T	ALS	(van der Zee et al., 2017)	
Missense	c.916C>A	p.L306I	ALS -FTD	(Pottier et al., 2015a)	
Missense	c.923G>A	p.R308Q	ALS	(Freischmidt et al., 2015b)	
Missense	c.959C>T	p.T320I	ALS -FTD	(Le Ber et al., 2015)	
Splicing	c.991+1G>T	-	FTD	(Verheijen et al., 2018)	ULD
Missense	c.1073G>A	p.R358H	ALS	(De Majo et al., 2018)	
Missense	c.1150C>T	p.R384W	ALS	(Borghero et al., 2016)	
Missense	c.1190T>C	p.I397T	ALS	(Pozzi et al., 2017)	
Deletion	c.1192delT	p.S398PfsX11	ALS	(Verheijen et al., 2018)	
Missense	c.1252A>G	p.I418V	FTD	(van der Zee et al., 2017)	
Missense	c.1270T>G	p.Y424D	ALS	(Pottier et al., 2015a)	
Missense	c.1331G>A	p.R444Q	ALS	(Borghero et al., 2016)	
Nonsense	c.1335G>A	p.W445X	ALS	(van der Zee et al., 2017)	CCD1
Deletion	c.1349_1352delTTAA	p.I450KfsX15	ALS-FTD	(Freischmidt et al., 2015b)	
Deletion	c.1358_1388delCAGA	p.T462Kfs∗ 3	FTD-ALS	(van der Zee et al., 2017)	
Deletion	c.1414delA	p.I472Sfs*8	ALS	(Kim et al., 2017)	

Deletion	c.1432delA	p.Q475fs	MND	(Black et al., 2017)	CCD1
Deletion	c.1436_1437delTG	p.V479EfsX4	ALS-FTD	(Freischmidt et al., 2015b)	
Deletion	c.1436_1437delTG	p.V479EfsX4	ALS-FTD	(Freischmidt et al., 2015b)	
Nonsense	c.1446T>G	p.Y482X	ALS -FTD	(Le Ber et al., 2015)	
Deletion	c.1470delG	p.D490fs	ALS	(Borghero et al., 2016)	
Insertion	c.1551_1552insTT	p.E517fs	ALS	(Verheijen et al., 2018)	
Deletion	c.1644-5_1644-	_	ALS	(Pozzi et al., 2017)	
Duplication	c.1653dupA	p.E551fs	ALS	Cirulli et al., 2015)	
Missense	c.1676T>G	p.M559R	ALS	(Freischmidt et al., 2015b)	
Missense	c.1717C>G	p.R573G	PLS	(Gomez-Tortosa et al.,	
Missense	c.1792A>G	p.M598V	ALS	(Freischmidt et al., 2015b)	
Deletion	c.1869_1875del	p.M623fs	ALS	(De Majo et al., 2018)	
Deletion	c.1887_1890del	p.Q629fs	ALS	(De Majo et al., 2018)	
Deletion	c.1928_1930delAAG	p.E643del	ALS-FTD	(Freischmidt et al., 2015b)	
Splicing	c.1960-2A>G	_	FTD	(Le Ber et al., 2015)	
Nonsense	c.1963C>T	p.Q655X	ALS -FTD	(Le Ber et al., 2015)	
Missense	c.1985T>C	p.M662T	ALS -FTD	(Le Ber et al., 2015)	CCD2
Nonsense	c.2107G>T	p.E703X	ALS -FTD	(Lamb et al., 2019)	
Deletion	c.2115_2127del13	p.E704	MND	Black et al., 2017)	

KD: Kinase Domain, ULD: Ubiquitin like domain, CCD1: Coiled coil domain 1 and CCD2: Coiled coil domain 2

1.3.3 TBK1 Function

TBK1 is a kinase with a large number of characterised substrates, and regulates many signaling pathways including I-kappaB Kinase/ NF-kappaB signaling, immune response, Interferon Regulatory Factor, autophagy, inflammation, insulin signaling and cell proliferation and growth (Helgason et al., 2013). TBK1 is a non-canonical IkB kinase that participates in a variety of inflammation signaling pathways such as those regulating the Interferon Regulatory Factor 3 (*IRF3*), Interferon Regulatory Factor 7 (*IRF7*), Signal Transducer and Activator of Transcription 6 (*STAT6*) and transcription factor p65 (*P65*). TBK1 colocalises with kinase substrates such as leucine rich repeat kinase 2 (LRRK2), Inhibitor Of Nuclear Factor Kappa B Kinase Subunit Beta (IKKβ), Inhibitor Of Nuclear Factor Kappa-B Kinase Subunit Alpha (IKKα), Inhibitor Of Nuclear Factor Kappa B Kinase Subunit Epsilon (IKKε) and Nuclear Factor κB-inducing Kinase (NIK) which may be critical for driving kinase specificity (Helgason et al., 2013).

TBK1 recruits the adaptor proteins TANK, stimulator of interferon genes (STING), NF-kappa-B essential modulator (NEMO), OPTN and SQSTM1 (p62) to form mutually exclusive complexes that directly modify the functions of several downstream substrates (Helgason et al., 2013, Goncalves et al., 2011). In mitophagy TBK1 phosphorylates the autophagy receptors optineurin and p62 leading to the formation of autophagosome (Zhang et al., 2014) (see Figure(1.3).

TBK1 is an IκB kinase (IKK)-related kinase that can directly phosphorylate and activate IKK (Yuichiro Tojima et al., 2000b, Yuichiro Tojima et al., 2000a) . The kinase domain of TBK1 has high similarity with IKKα/β, but it functions as an IKK kinase rather than an IkB kinase (Karin, 1999).

As a response to growth factors that trigger protein kinase C-ε (PKCε) activity, according to (Clement et al., 2008) TBK1 mediates IKK and nuclear factor kappa-light-chain-enhancer of activated B cells (NFκB) activation as TBK1 phosphorylates the inhibitor of NFκB (IκB) leading to its ubiquitination, and releases P50/P65 which translocate to the nucleus (Yuichiro Tojima et al., 2000b) The translocation of P50/P65 triggers the transcription of NFκB target genes leading to the production of proinflammatory cytokines(Ben-Neriah, 2000).

However recent data suggest that TBK1 and IKKε work together in a complex to inhibit NFκB signal transduction (Moser et al., 2015). NFκB inducing kinase (NIK) activates non-canonical NFκB signaling by phosphorylating IKKα which is then ubiquitinated. This releases P100 and RelB which translocate to the nucleus. TBK1 negatively regulates non-canonical NFκB signaling via phosphorylation of NIK leading to its ubiquitination and degradation into the proteasome (Jin et al., 2012) (see Figure (1.3).

Tumour necrosis factor Receptor Associated Factor 3 (TRAF3) activates the TBK1-interacting proteins SINTBAD, TANK and NAP1 which subsequently activate the TBK1/IKKε complex that directly phosphorylates IRF3 and translocates it to the nucleus. Within the nucleus IRF3 initiates the transcription of IFN and interferon stimulated genes (ISGs) (Unterholzner et al., 2011) (see Figure (1.3).

Studies show that TBK1 also acts as a mitotic kinase and has functions in microtubule dynamics and mitosis (Pillai et al., 2015). TBK1 regulates mitosis by regulating microtubule motion and mitotic progress via phosphorylating the Forkhead, centrosome- and spindle microtubule -associated domain protein centrosomal protein 170 (CEP170) and the nuclear mitotic apparatus *protein* (NuMA) (Radulescu and Cleveland, 2010, Giulia Guarguaglini, 2004). During mitosis active phospho-TBK1 is confined to centrosomes, mitotic spindles and the midbody (Pillai et al., 2015). TBK1 phosphorylates the microtubule-binding protein CEP170 that is required for interaction with the kinesin 13 family member Kif2b and with centrosomes (Pillai et al., 2015). Disabling the TBK1–CEP170 complex or reducing the interaction of CEP170 with centrosomes inhibits mitosis and increases microtubule stability (Giulia Guarguaglini, 2005).

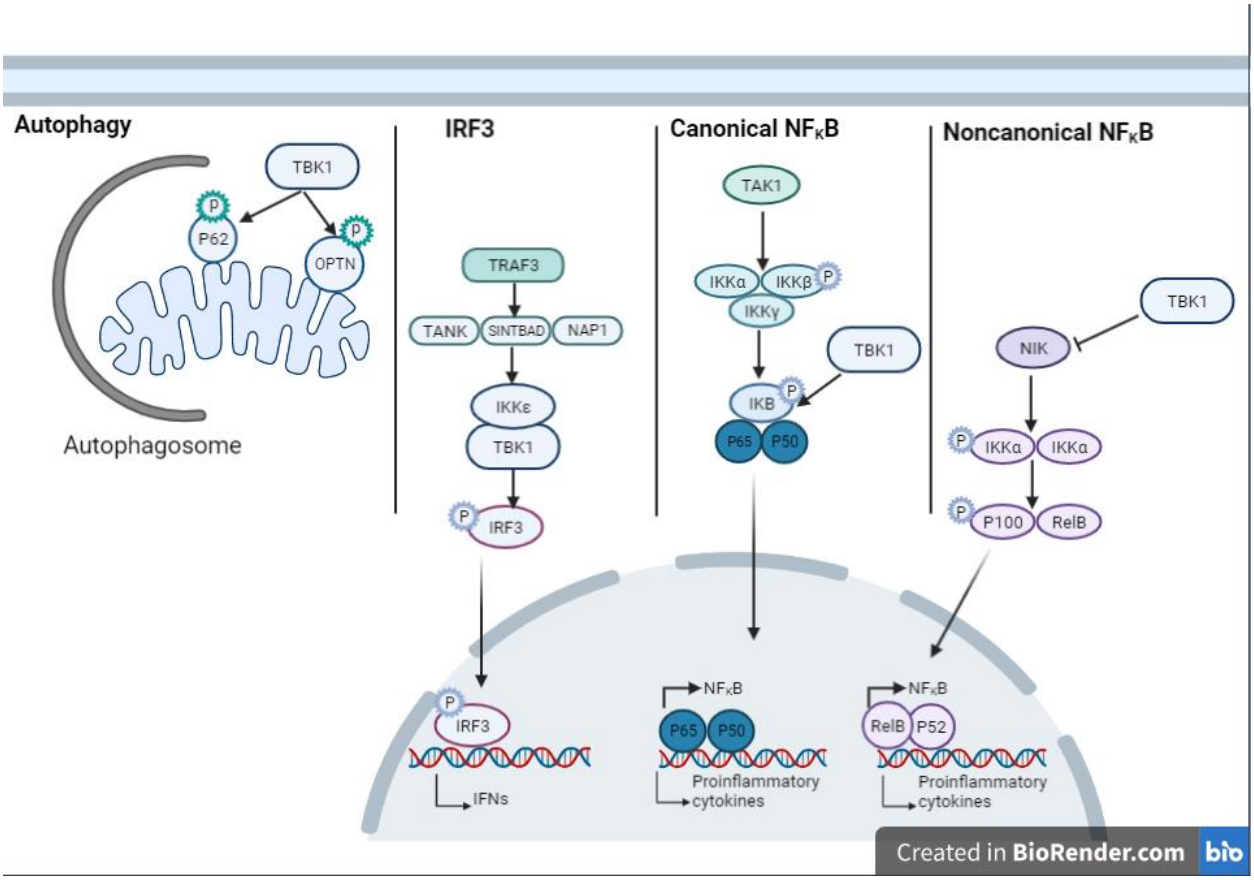

Figure 1.3 TBK1 functional pathways. In Autophagy, TBK1 phosphorylates the autophagy receptors OPTN and p62 which triggers mitophagy. In IRF3, TBK1 directly phosphorylates IRF3 that translocates to the nucleus and produces IFNs.In Canonical NFκB, TBK1 phosphorylates IKB leading to the translocation of P65 and P50 to the nucleus and initiates the transcription of canonical NFκB signaling and the production of proinflammatory cytokines. In Noncanonical NFκB, TBK1 phosphorylates NIK leading to its proteasomal degradation. NIK is needed to activate noncanonical NFκB signaling as NIK phosphorylates IKKα that phosphorylate p100 and RelB. This leads to their translocation to the nucleus where they initiate the transcription of non-canonical NFκB target genes and the production proinflammatory cytokines.

1.3.3.1 Role of TBK1 in innate immune Responses

One of the major causes of chronic disease is inflammation, and there are more than 100 types of inflammatory disease (Yu et al., 2012). It is recognised that inflammation is an essential mechanism of the innate immune response triggered when immune cells detect infection or tissue injury. Pattern recognition receptors (PRRs) are host sensors that recognise cell damage or pathogen invasion with intracellular or surface-expressed pathogens in the innate immune system (Kumar et al., 2011). PRRs are expressed in macrophages, fibroblasts, dendritic cells, mast cells, neutrophils and monocytes (Newton and Dixit, 2012). PRRs identify, both directly and indirectly, pathogen-associated molecular patterns such as damage-associated molecules released from injured cells, microbial nucleic acids, carbohydrates, and lipoproteins (Newton and Dixit, 2012). PRRs promote activation of transcription factors Activator Protein 1 (AP1), NFκB, enhancer-binding protein beta (c/EBP), cyclic adenosine monophosphate (cAMP) response element binding protein (CREB), and IRFs that generate signaling cascades that trigger the release of factors that stimulate enrolment of leukocytes (Xiao, 2017). In response to ligand- specific recognition of double-stranded RNA (dsRNA) of viruses, or bacterial lipopolysaccharide, TBK1 contributes to the regulation of the IRF-3 and IRF-7 activation pathways via the Toll like receptors (TLRs), TLR3 and TLR4. TLR activation and internalisation induces TIR-domain-containing adapter-inducing interferon-β (*TRIF*), which in turn induces activation of the transcriptional regulator type I interferon 3 (IFN 3), and the expression of IFN-β and of interferon (IFN) inducible genes through the activation of TBK1 and inhibition of kappaB kinase ε (IKKε) (Fitzgerald et al., 2003b, Toshchakov et al., 2002).

Several studies suggest that TBK1 regulates inflammatory mediators like IL6, TNFα, or IFN-β, and indicate that TBK1-deficient cells express strong defects in IFN induction (Xie et al., 2012, Hemmi et al., 2004). TLRs also have a role in NFκB and IRF-3 activation however TBK1 is an important regulator in the interferon response to viral infection and is involved in both NFκB and IRF-3 pathways (Sharma et al., 2003, Shen and Hahn, 2011, Fitzgerald et al., 2003b, Mikko Hallman, 2001).

Subsequent to the activation of TLRs, TBK1 connects with TRAF3 and TANK at multiple serine and threonine residues to phosphorylate IRF-3, IRF-5, and IRF-7 (Cheng et al., 2006, Lin, 1998). These outcomes show that TBK1 and IKKε are necessary for interferon signaling (Shen and Hahn, 2011). IRFs heterodimerise and translocate to the nucleus which induces expression of antiviral and proinflammatory genes such as IFN-α/β and ISGs (Mitsuharu Sato et al., 2000).

1.3.3.2 Regulation of signaling by TBK1 kinase activity

Phosphorylation of IkB is a critical regulatory step in the activation of NFκB signaling (Gilmore, 2006). Phosphorylation of the IKK complex by TBK1 induces IkB degradation and activates the transcription factor NFκB. This occurs through TBK1 phosphorylating one of the two regulatory serines that are needed for induction of IkB degradation. The activation of NFκB occurs through IKKb, when TBK1 phosphorylates the subunit adjacent to IKK through intramolecular trans-autophosphorylation (Karin, 1999).

NFκB is regulated by cytoplasmic proteins such as IkB that prevent nuclear translocation of P65 (Christian et al., 2016, Oeckinghaus and Ghosh, 2009, Liu et al., 2017). Nuclease assembly protein (NAP1) interacts with TBK1 and stimulates its kinase activity, facilitates its oligomerisation, and promotes TBK1-induced activation of canonical NFκB (Fujita et al., 2003)

In basal conditions, the TRAF2-TRAF3-cIAP complex continually mediates the proteasomal degradation of NIK to regulate the activity of noncanonical NFκB signaling. However, upon stimulation the TRAF2-TRAF3-cIAP complex is recruited to activate lymphotoxin-β receptor (LTβR) which enables NIK to interact with IKKα and release NFκB2/RelB to activate transcription (Thu and Richmond, 2010). This pathway, termed noncanonical NFκB signaling, is negatively regulated by TBK1, as TBK1 induces the destruction of NIK. During cell stimulation TBK1 is activated downstream of TACI and triggers the proteasome-dependent destruction of NIK by phosphorylating it at Ser862 (Bram, 2012).

NFκB induces expression of target genes proinflammatory cytokines such as tumour necrosis factor alpha (*TNFα*), interleukin 1 beta (IL*1β*), interleukin 6 (*IL6*), interleukin 8 (*IL8*) and cyclooxygenase-2, in response to stress and inflammation (Liu et al., 2017, Oeckinghaus and Ghosh, 2009). TNFα stimulates the TBK1-NAP1 complex to phosphorylate serine 536 of the p65/RelA subunit of NFκB to enhance NFκB transcriptional activity (Fujita et al., 2003). Overexpression of NAP1 enhanced cytokine induction of an NFκB -dependent reporter whereas reduction of NAP1 reduced NFκB dependent reporter gene expression and sensitised cells to *TNFα*-induced apoptosis (Fujita et al., 2003).

1.3.3.3 Role of TBK1 in Autophagy Regulation

Autophagy is an important evolutionarily conserved homeostatic mechanism responsible for protein degradation by the lysosome. Autophagy is necessary for cells to tolerate environmental, developmental and disease-associated changes (Klionsky, 2007). Cellular stress, infections, metabolic and inflammatory disease trigger autophagy. Recent research has identified cross talk between autophagy and inflammation, as autophagy contributes to, controls and balances inflammation (Yuk and Jo, 2013).

Several studies have highlighted the important role of TBK1 in autophagy (Stolz et al., 2014). In particular TBK1 directly phosphorylates several proteins involved in autophagy to regulate their activity (Ahmad et al., 2016). For example, TBK1 phosphorylates the autophagy receptor optineurin to promote autophagy of mitochondria, a process termed mitophagy (Richter et al., 2016b). TBK1 is involved in pathogen clearance and contributes to cell-autonomous immunity through autophagic destruction of intracellular invading pathogens. Autophagic killing of mycobacteria in macrophages is mediated by TBK1-dependent production of a key proinflammatory cytokine, IL-1b (Pilli et al., 2012). Furthermore, the maturation of the autophagosome into the hydrolytic autophagolysosome involves TBK1.

TBK1 phosphorylates the autophagic adaptor p62/SQSTM1 and coordinates the autophagic machinery leading to its degradation and its associated cargo (Pilli et al., 2012). Damaged mitochondria undergo a form of autophagy referred to as mitophagy (Lockshin, 1977). The key role of mitophagy is keeping the cell healthy, promoting turnover of mitochondria and preventing accumulation of dysfunctional mitochondria which may lead to cell death (Pickrell and Youle, 2015). Assembly of ubiquitin chains on damaged mitochondria activates the autophagy adaptor kinase TBK1, which phosphorylates autophagy adaptors optineurin, nuclear dot 52kDa protein (NDP52), and SQSTM1 to facilitate efficient mitophagy (Heo et al., 2015). Mitochondria recruit mitophagy receptors via ubiquitin binding and mediate autophagic engulfment by their involvement with microtubule-associated protein light chain 3 (LC3) (Moore and Holzbaur, 2016a). Effective autophagosome formation can be obstructed by inhibition or reduction of TBK1 or OPTN, which indicates that TBK1 and OPTN are required in mitochondrial response to stress as they have a role in functional redundancy among mitophagy receptors and efficient sequestration of damaged mitochondria. Therefore ALS/FTD-linked mutations in *TBK1* and *OPTN* could delineate a major pathophysiological mechanism leading to neurodegenerative disease via dysfunctional autophagy (Moore and Holzbaur, 2016a).

1.4 Optineurin

The *OPTN* gene is located on chromosome 10p13 and contains 3 noncoding exons and 13 coding exons. It encodes a 577 amino acid coiled coil adaptor protein optineurin, which interacts with many other proteins. The protein has 2 coiled coil domains in the N-terminal region, and a third coiled coil domain, ubiquitin binding domain (UbBD) and zinc finger domain in the C-terminal region (Figure(1.2). These functional domains interact with many partner proteins such as TBK1 (through amino acids 1-127), RAB8 (58-209), LC3 (through amino acids 150-168) and MYO6 (through amino acids 412-520) (Weil et al., 2018, Wild et al., 2011, Shen et al., 2015) (see Figure(1.4).

OPTN also interact with itself forming a homo-hexamer (Ying et al., 2010). The stable autophagy OPTN-TBK1 hetero-tetramer complex forms by the interaction of OPTN N-terminal domain with TBK1 C-terminal domain (Li et al., 2018). Both UbBD and CCD3 in OPTN are essential for binding to polyubiquitinated inclusion bodies (Shen et al., 2015).

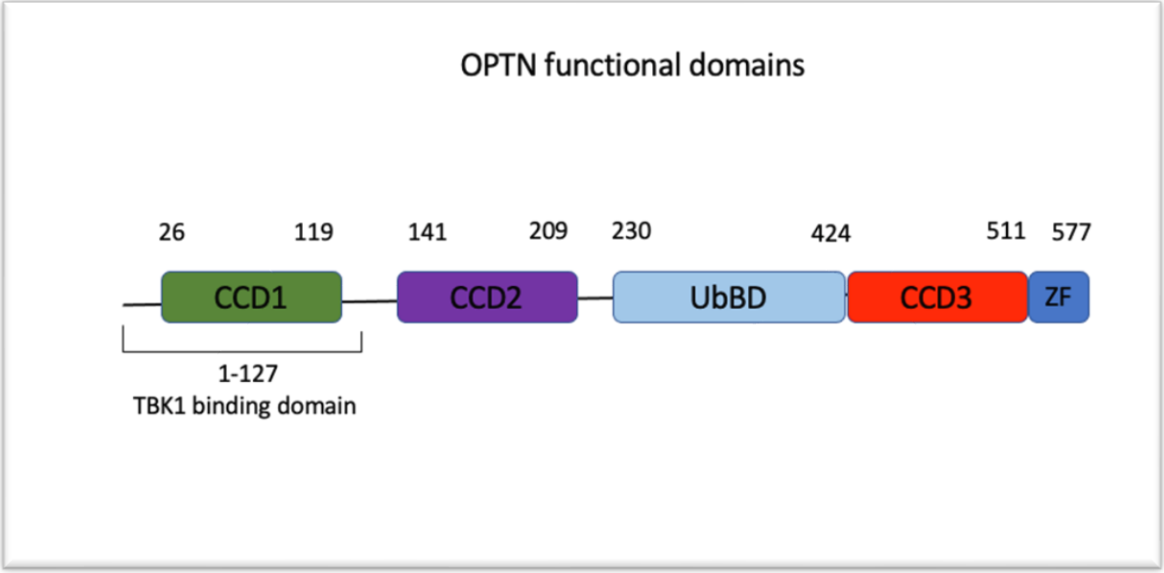

Figure 1.4 Structure of OPTN. Figure shows the locations of coiled coil domain1 (CCD1), coiled coil domain 2 (CCD2), ubiquitin binding domain (UbBD), coiled coil domain 3 (CCD3) and zinc finger domain (ZF). The TBK1-binding domain in the N-terminal region of OPTN is indicated.

1.4.1 *OPTN* mutations in disease

Mutations in the *OPTN* gene cause many clinical phenotypes including Adult-Onset Primary Open-Angle Glaucoma (POAG) (Rezaie, 2002), normal tension glaucoma (NTG) (Toda et al., 2003), ALS (Maruyama et al., 2010a) and ALS with FTD (Feng et al., 2019, Deng, 2011). Also, as mentioned earlier *OPTN* been associated with *TBK1* to cause ALS with or without FTD (Pottier et al., 2015b). Additionally, a GWAS study identified some *OPTN* variants that were associated with Paget's disease of bone (Omar M E Albagha1, 2011). Although mutations in *OPTN* are associated with degenerative disease, the mechanism of pathogeneses is not fully understood. Mutations in *OPTN* include missense, nonsense and deletions in its functional domains. NTG can also be caused by duplication of *TBK1* (Kawase et al., 2012). Mutations associated with ALS/FTD can be dominantly or recessively inherited (Ying and Yue, 2012, Gotkine et al., 2021). Even though the majority of ALS mutations are located in C-terminal region of *OPTN* which is not responsible for TBK1 binding, they still may impair autophagy (Zhu et al., 2007, Maruyama et al., 2010a, Li et al., 2016).

1.4.2 OPTN function

OPTN has many binding partners that are involved in a range of cellular processes and pathways including autophagy, inflammation, antiviral signaling, and protein aggregation. OPTN plays role in selective autophagy (mitophagy and xenophagy) as a ubiquitin-binding autophagy receptor due to its polyubiquitin binding ability (Weil et al., 2018). The process of mitophagy involves the activation of PINK1-parkin that mediates the phosphorylation of OPTN via TBK1 on the damaged mitochondria leading to autophagosome formation (He et al., 2017). Additionally upon infection TBK1 phosphorylates OPTN and enhances an interaction with microtubule-associated proteins 1A/1B light chain 3B (LC3) that stimulates autophagic clearance of the pathogens (Wild et al., 2011). It was suggested that non-phosphorylated OPTN binds protein aggregates via its ubiquitin binding domain before being phosphorylated by TBK1 leading to the recruitment of LC3 and activation of autophagy.

Depletion of OPTN in an *in vitro* study results in an increase of SOD1 aggregation suggesting the role of OPTN in autophagic degradation of protein aggregates(Korac et al., 2013).
OPTN is also involved in inflammatory signaling by NFκB and IRF3. During bacterial infection xenophagy triggers the recruitment of both OPTN and NEMO that induce IKK activation and NFκB signaling (Noad et al., 2017). OPTN and NEMO share sequence homology in their UbBDs, however OPTN is not sufficient to fulfil the role of NEMO in activating NFκB signaling (Zhu et al., 2007). OPTN competes with NEMO to bind polyubiquitinated receptor-interacting protein (RIP), a process which is thought to dampen NFKB activation in response to TNFα. Bone-marrow-derived macrophages from *optn*$^{-/-}$ mice showed a decrease in neutrophil recruitment and reduced TNFα and IL6 expression level when infected with Citrobacter colitis and E. coli peritonitis. Similar findings were also observed in *optn* knockdown zebrafish infected with pathogens (Chew et al., 2015). The tumour suppressor deubiquitinase CYLD (CYLD Lysine 63 Deubiquitinase) is an optineurin-interacting protein that regulates TNFα induced NFκB activation (Nagabhushana et al., 2011). OPTN mediates the interaction of CYLD with ubiquitinated receptor interacting protein (RIP) leading to the deubiquitination of RIP and inhibits TNFα induced NFκB activation. Interestingly a mutation in CYLD (M719V) that increased deubiquitinase activity caused a rare inherited form of ALS/FTD and was associated with inhibition of NFkB signalling and impairment of autophagy when overexpressed in cell culture(Dobson-Stone et al., 2020). OPTN is also essential for IRF3 activation in the immune response. An *OPTN* knock-in mouse model that carries a C-terminal deletion shows a reduction in toll like receptor 4 (TLR4)-induced IFN-β (Munitic et al., 2013). Another study of bone marrow derived macrophages from the *OPTN* mouse model suggest that in response to lipopolysaccharide and poly(I:C) stimulation OPTN binds to polyubiquitylated species which activate TBK1 leading to the phosphorylation of IRF3 and IFNβ production (Gleason et al., 2011). However, contrary to what has been suggested *in vivo* studies, *in vitro* studies suggest that OPTN negatively regulates IFNβ production in response to viral infection (Mankouri et al., 2010). Additionally, an *in vitro* study suggested upregulation of TBK1 activation of NFkB signaling during mitosis, when CYLD and OPTN, both negative regulators of TBK1, translocate to the nucleus (Génin et al., 2015).

Clearly these regulatory pathways are complex and interconnected, and there are discrepancies found between *in vivo* and *in vitro* studies. However, the involvement of at least three genes that cause ALS/FTD in this pathway make it an important, but somewhat understudied area in ALS/FTD research.

1.5 MAP3K14/NIK

Mitogen-activated protein kinase kinase kinase 14 is also known as NFκB-inducing kinase NIK. MAP3K14 is a serine/threonine protein-kinase that is located on chromosome 17q21 in man and encodes a protein that shares sequence similarity with other MAPKK kinases. It has four major domains- a TRAF3 binding domain (amino acids 30-120) and a negative regulatory domain NRD (amino acids 121–318) in the N-terminal region, and a serine/threonine kinase domain (amino acids 390–660) and a non-catalytic region (NCR, amino acids 661-947) in the C-terminal region (Xiao and Sun, 2000) and (see Figure(1.5).

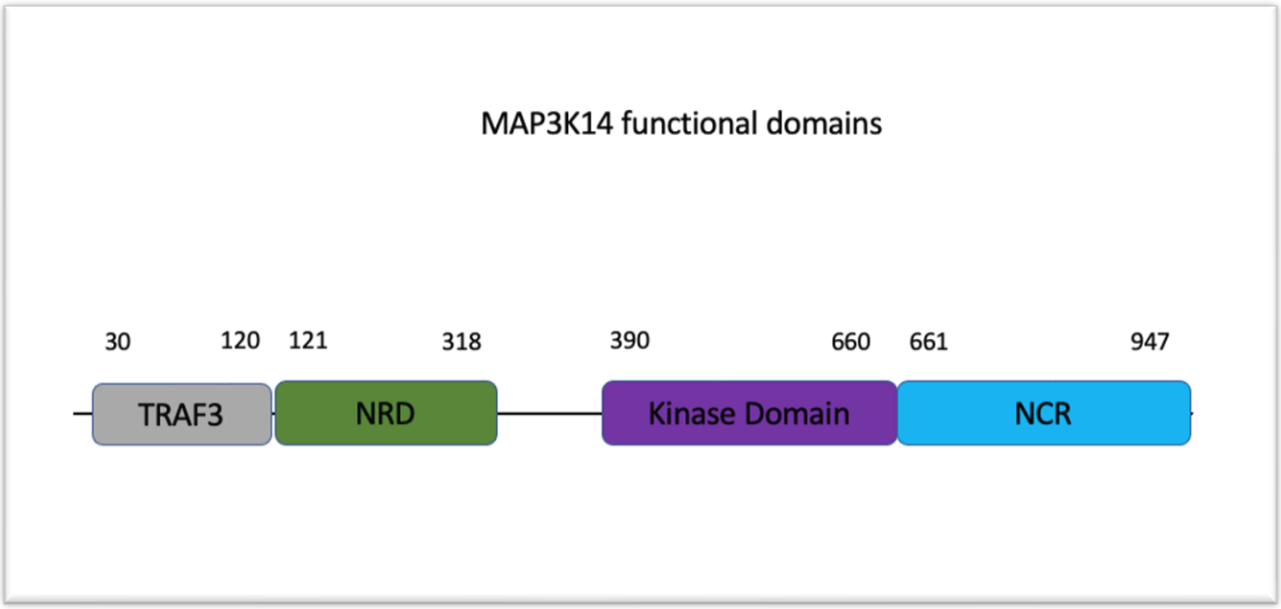

Figure 1.5 Structure of MAP3K14. Figure shows the locations of the TRAF3 binding domain, negative regulatory domain NRD, kinase domain and non-catalytic region NCR.

1.5.1 *MAP3K14/NIK* mutations in human disease

Biallelic loss of function mutations (Pro565Arg and Val345Met) in *MAP3K14* causes patients to present with recurrent infections that progress to the development of various malignancies. (Willmann et al., 2014) (Schlechter et al., 2017). These mutations reduce the kinase function of *MAP3K14* causing a significant reduction in phosphorylation of IkappaB kinase-alpha (IKKα).

1.5.2 *MAP3K14* function

Initial studies indicated the role of *MAP3K14* in activating NFκB however disruption of *MAP3K14* had no effect on the activation of the IKK complex p65 and p50, thus it did not impair canonical NFκB signaling (Yin, 2001). It was later demonstrated that *MAP3K14* has an essential role in upstream regulation of the noncanonical NFκB pathway (Pflug and Sitcheran, 2020). Stimulation of the noncanonical NFκB pathway activates MAP3K14 leading to phosphorylation of IKKα, which subsequently phosphorylated p100 to stimulate p52/RelB nuclear signaling (Sun, 2012). In resting cells MAP3K14a levels are tightly regulated to limit noncanonical signaling. One mechanism involves TBK1 phosphorylation of MAP3K14 leading to its proteasomal degradation (Jin et al., 2012). In addition, canonical NFκB signaling plays a role in suppressing non-canonical NFκB signaling as NEMO deficient cells show an accumulation of MAP3K14 (Gray et al., 2014).

MAP3K14 is a key player of the immune system as it has a crucial role in immune cell development and function. Alymphoplasia (aly) is a spontaneous autosomal recessive mutant mouse, which carries a point mutation in the C-terminal region of *Map3k14* (Shinkura et al., 1999). These mice show a reduction in viral control, adaptive immunity and antiviral CD8+T cells immunity when infected with virus suggesting a crucial role for *Map3k14* in regulating the adaptive immune response to viral Infection, although failure of lymphoid organogenesis contributes to this phenotype (Hamdan et al., 2020).

1.6 Zebrafish disease models

The zebrafish (Danio rerio) is a small teleost fish that was initially used for developmental biology, but has become increasing popular in all fields of biological science (Fishman, 2001). Zebrafish is the first vertebrate that can be used for *in vivo* genome-wide screening which was previously only possible in invertebrates such as fruit flies and nematodes. Due to the similarities between zebrafish and mammalian biology it has been described as 'the canonical vertebrate' (Fishman, 2001, Rubinstein, 2003).

While the zebrafish genome size is almost half that of human genome most gene families present in mammals are represented by one or more orthologues in the zebrafish (J. Wittbrodt, 1998, Rubinstein, 2003). Due to ancient genome duplication events multiple copies of mammalian genes exist in zebrafish (J. Wittbrodt, 1998, Allan Force, 1998). The zebrafish provides multiple significant advantages over mammalian models, as it is less expensive, small, and contains organs and cell types similar to that of mammals with some notable exception. Furthermore, zebrafish produce hundreds of offspring which develop externally, and these embryos are transparent allowing easy visualisation of tissues and organs. These advantages have together endorsed phenotype-based genetic screening using zebrafish (Ahmed et al., 2016, Rubinstein, 2003).

On the other hand, using zebrafish to model human disease has some limitations; as mentioned earlier, some zebrafish genes have two copies of human disease genes instead of one(Kalueff et al., 2014). Unlike mammals, gender in zebrafish is not genetically determined, and zebrafish embryos lack the placenta(Lardelli, 2017). Some zebrafish skeletal and brain structures are not similar to the human, such as the head skeleton and the cortex, making it challenging to map their counterparts (Kalueff et al., 2014, Bruneel and Witten, 2015). As zebrafish used to study many neurodevelopmental diseases it is challenging to validate complex behaviours such as social behaviour since some of the symptoms cannot be fully recapitulated in zebrafish (Sakai et al., 2018). Additionally, when it comes to drug delivery, administrating water-insoluble drugs to zebrafish is an obstacle; also, the blood-brain barrier is similar to humans yet there are some differences in permeability of certain drugs (Kalueff et al., 2014).

Different methods are available to disrupt zebrafish genes such as chemicals, irradiation or viral insertion and genome editing tools (Bandmann and Burton, 2010). Genome editing, or genome engineering, has contributed to creating animal models that resemble human diseases. Genome editing tools include clustered regularly interspaced short palindromic repeats (CRISPR), zinc finger nucleases (ZFNs) and transcription activator like effector-based nucleases (TALENs) (Richard, 2015).

Numerous knock-out zebrafish models of neurodegenerative disease genes have shown phenotypes that resemble the severity and progression of the human disease (Bandmann and Burton, 2010).

Although human behaviours are different from those of zebrafish, the evolutionarily conserved nature of the central nervous system implies that human and zebrafish may share many phenotypes arising from conserved genetic and physiological factors (Kalueff et al., 2014).

Several zebrafish models have been generated to study motor neuron disease genes such as *sod1, tardbp* and *ccnf.* Although most autosomal dominant forms of neurodegenerative diseases can arise via gain of function mutations, such as *SOD1* and *CCNF* some dominant forms are thought to cause loss of function, such as mutations in *TARDBP*(Ramesh et al., 2010, Hogan et al., 2017, Hewamadduma et al., 2013).

These zebrafish models have motor neuron phenotypes that mimic those observed in human ALS patients. A zebrafish transgenic model overexpressing mutant *sod1* shows several motor neuron phenotypes which includes a defect at the neuromuscular junction, loss of spinal cord motor neurons, muscle atrophy, reduced swimming endurance, incomplete paralysis and eventually premature death (Ramesh et al., 2010). Knockdown of *tardpb1* in zebrafish causes a motor phenotype, which includes shortening of the motor axons, a movement defect and premature death (Hewamadduma et al., 2013). Axonopathy is a common phenotype in ALS zebrafish models and has been recently characterised in a mutant *ccnf* overexpression model. The gain of function mutation in *ccnf* zebrafish disturbed the cell death pathway and damaged axonal outgrowth, resulting in reduced motor function in zebrafish (Hogan et al., 2017).

1.6.1 *TBK1* Disease Models

TBK1 is highly conserved across species. The human TBK1 protein shares 94.10% homology with the mouse (Mus musculus) orthologue and 71.39% with the zebrafish (Danio rerio) orthologue (NM_001044748.2_ NP_001038213.2) (see Figure (1.6). Understanding TBK1 function in pathways such as autophagy, NFκB and inflammation has come from *in vitro* manipulation of TBK1 in cell culture. However *in vivo* phenotypes associated with human *TBK1* mutations have not been forthcoming (Ahmad et al., 2016) although *Tbk1* deficient mouse models have contributed greatly to our understanding of TBK1 function, the characterisation of TBK1 function *in vivo* remains a major task, as homozygous *Tbk1* knockout mice are embryonic lethal due to severe hepatic tissue apoptosis at embryonic day 14.5 (Hemmi et al., 2004).
Finding an alternative animal model that could survive homozygous *TBK1* deficiency is beneficial, and although mammalian models share more similarity with humans and have many advantages, they are costly, more difficult to manipulate embryonically, and cost-limiting for large-scale genetic studies (Chau et al., 2008). Therefore, alternative vertebrate studies should be prioritised in a different model organism.

1.6.1.1 *tbk1* in zebrafish

Zebrafish *tbk1* has a single orthologue located on chromosome 4, and contains a 3025 base pair transcript encoding a 727 amino acid protein (NM_001044748; NP_001038213). According to a Clustal Omega alignment, zebrafish tbk1 protein has a high degree of identity with human and mouse proteins (71.39% with human and 71.11% with mouse), (see Figure (1.6). tbk1 in zebrafish has a conserved kinase domain, and a conserved ubiquitin like domain (Chi et al., 2011). High sequence identity and conserved domains suggest a conserved or similar function despite a large evolutionary distance (Pearson, 2013). There is some evidence to support a conserved role for zebrafish tbk1 in regulating IFN signaling (Li 2017), but to date a zebrafish *tbk1* knockout has not been reported.

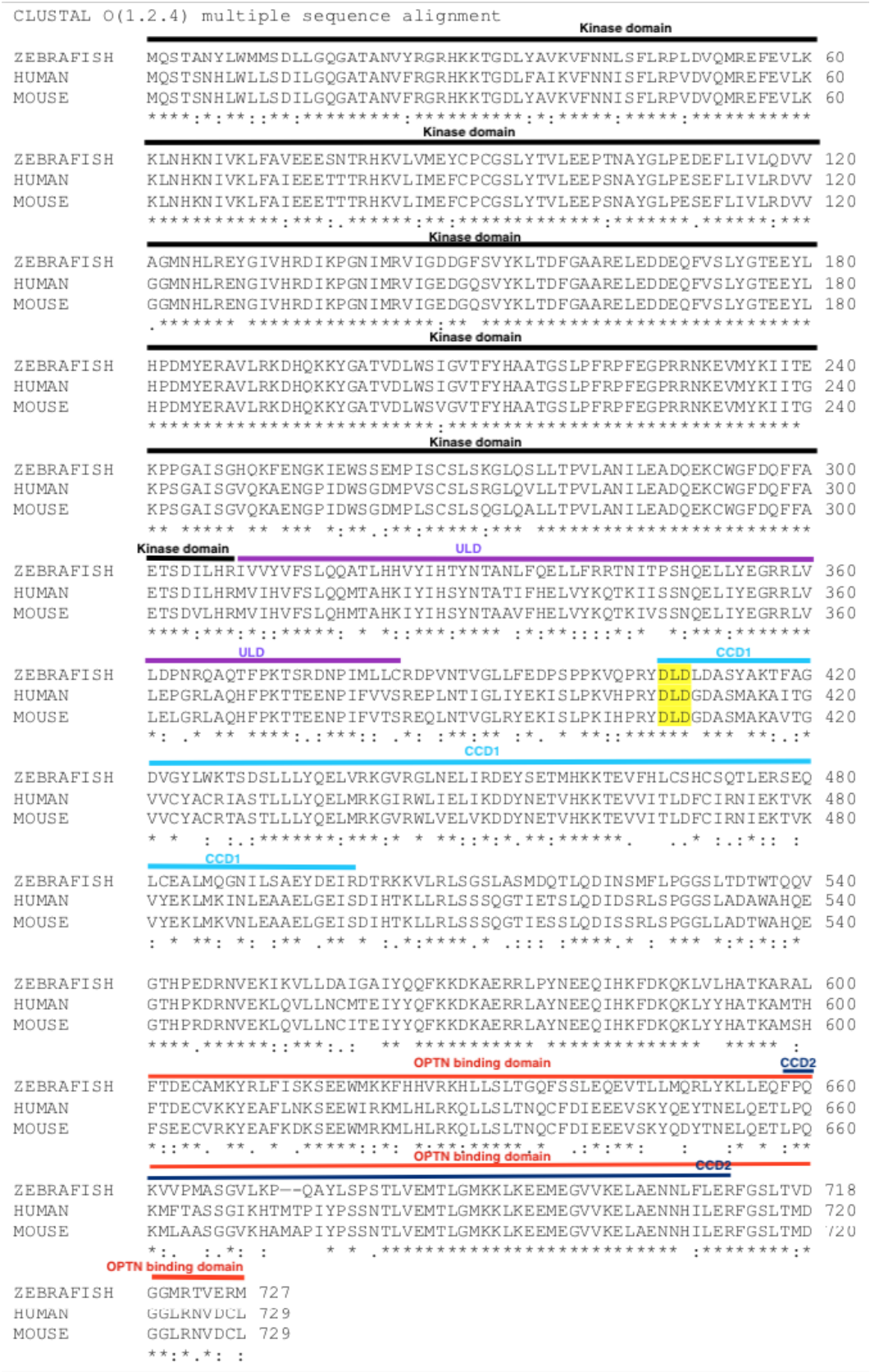
CLUSTAL O(1.2.4) multiple sequence alignment
Kinase domain
ZEBRAFISH MQSTANYLWMMSDLLGQGATANVYRGRHKKTGDLYAVKVFNNLSFLRPLDVQMREFEVLK 60
HUMAN MQSTSNHLWLLSDILGQGATANVFRGRHKKTGDLFAIKVFNNISFLRPVDVQMREFEVLK 60
MOUSE MQSTSNHLWLLSDILGQGATANVFRGRHKKTGDLYAVKVFNNISFLRPVDVQMREFEVLK 60
Kinase domain
ZEBRAFISH KLNHKNIVKLFAVEEESNTRHKVLVMEYCPCGSLYTVLEEPTNAYGLPEDEFLIVLQDVV 120
HUMAN KLNHKNIVKLFAIEEETTTRHKVLIMEFCPCGSLYTVLEEPSNAYGLPESEFLIVLRDVV 120
MOUSE KLNHKNIVKLFAIEEETTTRHKVLIMEFCPCGSLYTVLEEPSNAYGLPESEFLIVLRDVV 120
Kinase domain
ZEBRAFISH AGMNHLREYGIVHRDIKPGNIMRVIGDDGFSVYKLTDFGAARELEDDEQFVSLYGTEEYL 180
HUMAN GGMNHLRENGIVHRDIKPGNIMRVIGEDGQSVYKLTDFGAARELEDDEQFVSLYGTEEYL 180
MOUSE GGMNHLRENGIVHRDIKPGNIMRVIGEDGQSVYKLTDFGAARELEDDEQFVSLYGTEEYL 180
Kinase domain
ZEBRAFISH HPDMYERAVLRKDHQKKYGATVDLWSIGVTFYHAATGSLPFRPFEGPRRNKEVMYKIITE 240
HUMAN HPDMYERAVLRKDHQKKYGATVDLWSIGVTFYHAATGSLPFRPFEGPRRNKEVMYKIITG 240
MOUSE HPDMYERAVLRKDHQKKYGATVDLWSVGVTFYHAATGSLPFRPFEGPRRNKEVMYKIITG 240
Kinase domain
ZEBRAFISH KPPGAISGHQKFENGKIEWSSEMPISCSLSKGLQSLLTPVLANILEADQEKCWGFDQFFA 300
HUMAN KPSGAISGVQKAENGPIDWSGDMPVSCSLSRGLQVLLTPVLANILEADQEKCWGFDQFFA 300
MOUSE KPSGAISGVQKAENGPIDWSGDMPLSCSLSQGLQALLTPVLANILEADQEKCWGFDQFFA 300
Kinase domain
ULD
ZEBRAFISH ETSDILHRIVVYVFSLQQATLHHVYIHTYNTANLFQELLFRRTNITPSHQELLYEGRRLV 360
HUMAN ETSDILHRMVIHVFSLQQMTAHKIYIHSYNTATIFHELVYKQTKIISSNQELIYEGRRLV 360
MOUSE ETSDVLHRMVIHVFSLQHMTAHKIYIHSYNTAAVFHELVYKQTKIVSSNQELIYEGRRLV 360
ULD
CCD1
ZEBRAFISH LDPNRQAQTFPKTSRDNPIMLLCRDPVNTVGLLFEDPSPPKVQPRYDLDLDASYAKTFAG 420
HUMAN LEPGRLAQHFPKTTEENPIFVVSREPLNTIGLIYEKISLPKVHPRYDLDGDASMAKAITG 420
MOUSE LELGRLAQHFPKTTEENPIFVTSREQLNTVGLRYEKISLPKIHPRYDLDGDASMAKAVTG 420
CCD1
ZEBRAFISH DVGYLWKTSDSLLLYQELVRKGVRGLNELIRDEYSETMHKKTEVFHLCSHCSQTLERSEQ 480
HUMAN VVCYACRIASTLLLYQELMRKGIRWLIELIKDDYNETVHKKTEVVITLDFCIRNIEKTVK 480
MOUSE VVCYACRTASTLLLYQELMRKGVRWLVELVKDDYNETVHKKTEVVITLDFCIRNIEKTVK 480
CCD1
ZEBRAFISH LCEALMQGNILSAEYDEIRDTRKKVLRLSGSLASMDQTLQDINSMFLPGGSLTDTWTQQV 540
HUMAN VYEKLMKINLEAAELGEISDIHTKLLRLSSSQGTIETSLQDIDSRLSPGGSLADAWAHQE 540
MOUSE VYEKLMKVNLEAAELGEISDIHTKLLRLSSSQGTIESSLQDISSRLSPGGLLADTWAHQE 540
ZEBRAFISH GTHPEDRNVEKIKVLLDAIGAIYQQFKKDKAERRLPYNEEQIHKFDKQKLVLHATKARAL 600
HUMAN GTHPKDRNVEKLQVLLNCMTEIYYQFKKDKAERRLAYNEEQIHKFDKQKLYYHATKAMTH 600
MOUSE GTHPRDRNVEKLQVLLNCITEIYYQFKKDKAERRLAYNEEQIHKFDKQKLYYHATKAMSH 600
OPTN binding domain
CCD2
ZEBRAFISH FTDECAMKYRLFISKSEEWMKKFHHVRKHLLSLTGQFSSLEQEVTLLMQRLYKLLEQFPQ 660
HUMAN FTDECVKKYEAFLNKSEEWIRKMLHLRKQLLSLTNQCFDIEEEVSKYQEYTNELQETLPQ 660
MOUSE FSEECVRKYEAFKDKSEEWMRKMLHLRKQLLSLTNQCFDIEEEVSKYQDYTNELQETLPQ 660
OPTN binding domain
CCD2
ZEBRAFISH KVVPMASGVLKP--QAYLSPSTLVEMTLGMKKLKEEMEGVVKELAENNLFLERFGSLTVD 718
HUMAN KMFTASSGIKHTMTPIYPSSNTLVEMTLGMKKLKEEMEGVVKELAENNHILERFGSLTMD 720
MOUSE KMLAASGGVKHAMAPIYPSSNTLVEMTLGMKKLKEEMEGVVKELAENNHILERFGSLTMD 720
OPTN binding domain
ZEBRAFISH GGMRTVERM 727
HUMAN GGLRNVDCL 729
MOUSE GGLRNVDCL 729

Figure 1.6 Protein sequence alignment of zebrafish, human and mouse TBK1. Alignment of zebrafish (top sequence) human (middle sequence) and mouse (bottom sequence) TBK1 proteins using ClustalW2 software showed 71% homology between the two orthologues. Conserved regions are shown as follows: The black line is the kinase domain, the purple line is the ubiquitin like domain, the blue line is the coiled coil domain 1, the navy line is coiled coil domain 2 and the red line is OPTN binding domain. The position of the CRISPR induced mutation is highlighted in yellow.

1.6.1.2 Generating a loss of function *tbk1* zebrafish

CRISPR-Cas9 is a natural immune mechanism found in bacteria as a response to viral infection where Cas9 cleaves the viral DNA at specific sites (Ran et al., 2013). The repair of the double strand breaks that are generated is error prone, which leads to introduction of an insertion/deletion (Ran et al., 2013). In the CRISPR-Cas9 genome editing method a short guide RNA (gRNA) directs Cas9 endonuclease to cut the genome at a specific location in the presence of a protospacer adjacent motif (PAM) that mediates the cleavage of double stranded DNA (Riordan et al., 2015). A custom gRNA is needed to target each genomic region in CRISPR-Cas9 genome editing. In the lead up to this project, work in our laboratory used a gRNA targeting exon 10 of zebrafish *tbk1* to introduce a loss of function mutation as a frameshift mutation (for example c.1349_1352delTTAA p.Ile450LysfsX15 (Freischmidt et al., 2015), present in the CCD1 of an ALS patient. A 5 bp deletion (c.1227_1231delCCTGG, p.D409Efsx10)was introduced in exon 10 of the *tbk1* gene that causes a frameshift mutation resulting in a premature stop codon (see Figure (1.7). A stable line (*tbk1*^{SH570}) of zebrafish carrying this loss of function mutation has been raised in our aquarium.

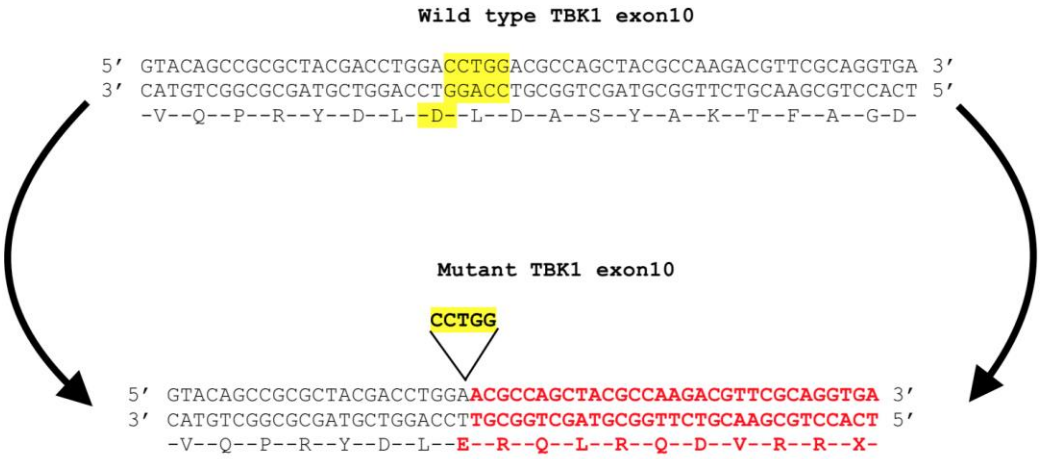

Figure 1.7 Introduced mutation in zebrafish *tbk1* gene. Top line represents the *tbk1* wild type cDNA and amino acid sequence the yellow highlighted sequence is the 5 bp deletion. Bottom line represents mutant *tbk1* cDNA and amino acid sequence that leads to the premature stop codon c.1227_1231delCCTGG, p.D409Efsx10.

1.6.2 *OPTN* disease models

The human *OPTN* gene shares 78.63% similarity with the mouse OPTN and 41.19% with zebrafish see (Figure(1.8). Current understanding of OPTN function comes from in vivo and *in vitro* studies. *OPTN in vivo* disease models have been used to study many diseases such Parkinson's disease, normal tension glaucoma, ALS and FTD. An *Optn* knockout mouse model was significantly more prone to pathogen infection which was attributed to a reduction in proinflammatory cytokine expression (Chew et al., 2015). Overexpression of the OPTN E50K mutation that is found in patients with NTG in a mouse model led to retinal degeneration similar to the glaucoma phenotype (Chi et al., 2010). A homozygous *Optn* deficient mouse model showed loss of hypoglossal motor neurons that led to degeneration of the respiratory motor unit and demonstrated respiratory deficiency under hypercapnic and hypoxic stress (McCall et al., 2020).

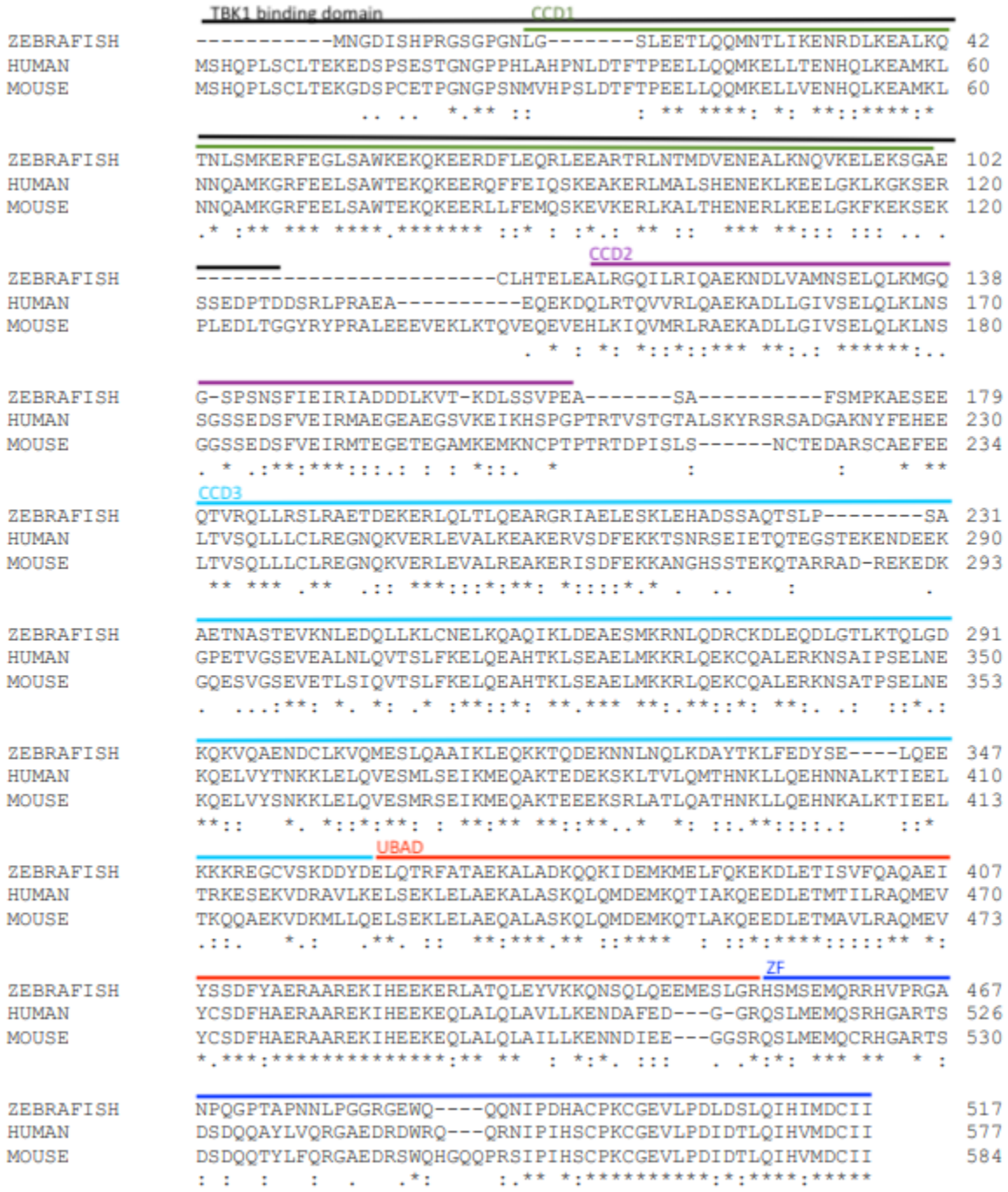

Figure 1.8 Protein sequence alignment of zebrafish, human and mouse OPTN. Alignment of zebrafish (top sequence) human (middle sequence) and mouse (bottom sequence) OPTN proteins using Clustal software showed 78.63% identity between human and mouse and 41.19% identity between human and zebrafish. The green line is coiled coil domain 1, the black line is the TBK1 binding domain, the purple line is coiled coil domain 2, the light blue line is coiled coil domain 3, the red line is ubiquitin binding domain, and the blue line is zinc finger domain.

1.6.2.1 *optn* in zebrafish

In zebrafish *optn* has singel orthologue located on chromosome 4 with one non-coding and 13 coding exons that encode a 517 amino acid peptide ENSDART00000014036.11. A zebrafish *optn* morpholino model shows motor axonopathy similar to what has been observed in other ALS zebrafish models. Furthermore, *optn* reduction in a *sod1* G93A zebrafish model specifically enhances the axonopathy phenotype (Korac et al., 2013). A loss of function *optn* zebrafish model $optn^{SA0143}$ that carries a null mutation (p.L278X) has been generated as part of the Zebrafish Mutation Project at the Sanger Institute (Paulus and Link, 2014). This model didn't demonstrate a strong ALS-like phenotype but altered axonal trafficking and an increase in cell death were reported. Interestingly the authors say they were unable to demonstrate upregulation of NFκ
B target genes (*casp8*, *tp53*, *rela*, *tnfα* and *ikbaa*) using qRT-PCR, however this data was not shown in the published paper.

1.6.3 *MAP3K14* disease models

The human MAP3k14 protein shares 84% similarity with mouse *map3k14* and 37% with zebrafish *map3k14a* see (Figure (1.9). As mentioned previously, loss of MAP3K14 function in humans leads to immunodeficiency that presents with repeated infections, and patients develop tumours. There are mouse models that mimic this effect, such as the spontaneous mutant carrying a p.G855R mutation (Shinkura et al., 1999, Reiko Shinkura1* and Katsumi Kogishi2, 1999)

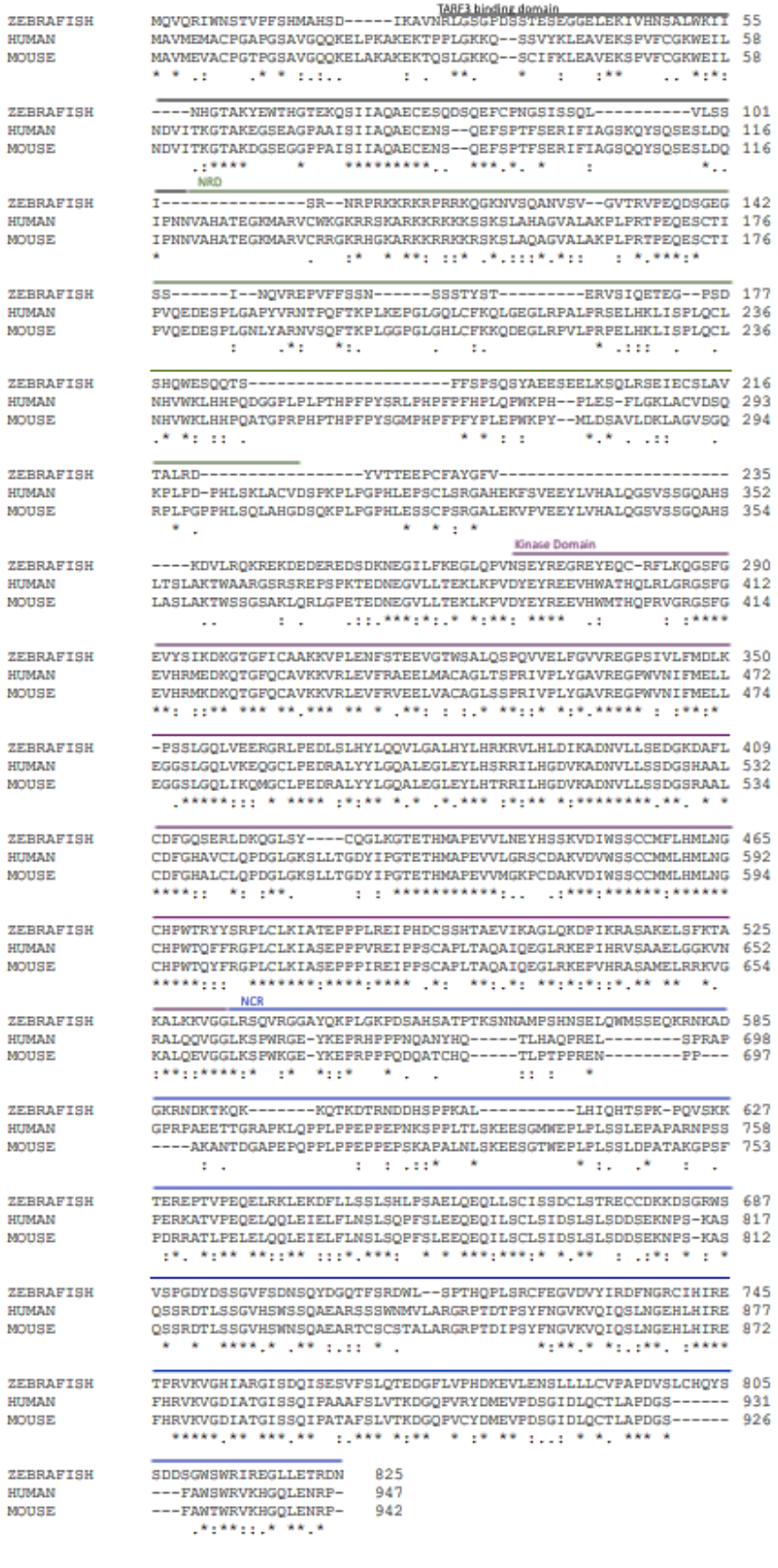
TARF3 binding domain
NRD
Kinase Domain
NCR

Figure 1.9 Protein sequence alignment of zebrafish, human and mouse *map3k14.* Alignment of zebrafish (top sequence) human (middle sequence) and mouse (bottom sequence) *map3k14* proteins using Clustal software showed 84% between human and mouse and 37% similarity between human and zebrafish. black line is the TARF3 binding domain, green line is negative regulatory domain, purple line is kinase domain, and light blue line is non catalytic domain

1.6.3.1 *MAP3K14a* in zebrafish

The zebrafish information network (ZFIN) has two protein-coding genes MAP3K14A and MAP3K14b. However, MAP3K14b poorly characterised, so we focused on map3k14a. Zebrafish *map3k14a* is located on chromosome 3 with one non-coding and 15 coding exons that encode an 825 amino acid peptide ENSDART00000151236.3. A recent study on *map3k14a* in zebrafish (Chen et al., 2020) demonstrates, using the zebrafish ZF4 cell line, that map3k14a mediates IRF3 and NFκB activation in response to viral infection. They show by immunoblot analysis that transfected map3k14a phosphorylates IRF3 but not IRF7, and then used qRT-PCR to demonstrate significantly increased of *ifnφ1* and *isg15* mRNA expression level after transfection. On the other hand, when *map3k14a* was silenced, it led to decreased *ifnφ1* and *isg15* mRNA expression levels. Additionally, using a luciferase reporter assay they demonstrated that transfected map3k14a activates a NFκB reporter gene. Furthermore, knocking down *map3k14a* using morpholinos inhibited the antiviral response in zebrafish embryos when infected with spring viremia of carp virus, and was associated reduced mRNA levels of *ifnφ1* and *isg15*. As the authors point out zebrafish map3k14a has poor conservation with at the amino acid level, however the kinase domain seems well conserved, which is consistent with the effect on phosphorylation and gene expression. The N-terminus is particularly poorly conserved, but importantly the critical TRAF3-binding motif ISIIAQA is well conserved in zebrafish, suggesting the orthologue may fully recapitulate the functions of the mammalian protein.

1.7 Research questions

1) Does *tbk1* mutation cause an ALS/FTD like phenotype in zebrafish?

If the *tbk1* frameshift mutant zebrafish is a model of ALS/FTD we predict to see symptoms in both *tbk1* heterozygous and homozygous mutants, reminiscent of the human disease. For example, defects in motor neuron function causing altered swimming behaviour are common in ALS zebrafish models and altered social and swimming behaviour may indicate changes reminiscent of FTD.

2) Which mechanisms are associated with the phenotype?

Loss of function mutations in the *tbk1* gene lead to neuroinflammatory/neurodegenerative disorders of the central nervous system such as ALS and FTD. As described previously the disease phenotypes arising from mutations in *tbk1* might be mediated through several different mechanisms, namely dysfunctional autophagy, NFκB or IRF-3 signaling. To investigate these mechanisms, we aim to characterise autophagy, NFκB and IRF-3 pathways in the *tbk1* zebrafish model and determine their involvement in driving the phenotypes observed in the model. This will provide crucial information about which pathway(s) should be targeted for effective therapeutic intervention in ALS/FTD patients with *tbk1* mutations.

1.8 Aims and hypothesis

We hypothesise that loss of function of *tbk1* leads to ALS/FTD through defects in autophagy, NFκB or IRF-3 pathways.

To test this hypothesis, we will:

1) Characterise the ALS/FTD phenotype of the *tbk1* zebrafish model
2) Establish assays to quantify autophagy, NFκB and IRF-3 function and quantify these in control and *tbk1* mutant siblings
3) For any pathways where we find a defect, we will attempt a rescue experiment of the pathway and determine whether this rescues the ALS/FTD phenotype.

In this way we hope to identify the critical pathways that are related to *tbk1* mutation *in vivo* and lay the foundation for developing therapies for *tbk1* mutation carriers in the clinic.

Chapter 2

2. Materials and Methods

2.1 Materials

The following materials have been used during the study.

2.1.1 Behavioural Analysis

12 well cell culture plates (Greiner Ltd, UK) Catalogue number #665180

24 well cell culture plates (Greiner Ltd, UK) Catalogue number #662160

96 well cell culture plates (Bio-One Ltd, UK) Catalogue number #655180

2.1.2 Molecular Biology

TAE buffer: (40 mM Tris-acetate, 1 mM EDTA)

96 well PCR plate: (4titude, UK) Catalogue number #4ti-0741

Agarose, Molecular Grade 500g (BIOLINE) Catalogue number #BIO-41025

Chloroform: (Sigma 650498-1L, UK)

DNA Markers: Hyper Ladder V (25bp), Hyper Ladder IV (100bp) (Bioline Ltd, UK).

Ethidium Bromide: (10mg/ml) from Sigma

Exonuclease I: (New England Biolabs, UK)

PCR plate seal: eXTReme Seal from EXCEL Scientific, Catalogue number #XTR100

PCR plate caps: 4titude Strips of 8 flat optical clear caps Catalogue number #4ti-0751

PCR Reaction Mix: 5x FIREPol Master mix ready to load (Solis BioDyne, Estonia) Catalogue number #04-12-00s15

Primers: From IDT

Guide RNA: Sigma

Cas9 enzyme: New England Biolabs, UK

Quick Extract: (Lucigen, UK) Catalogue number # QE09050

Restriction enzymes: New England Biolabs, UK

Reverse transcriptase reaction Mix: 5x qScript mix (Quanta-bio) Catalogue number #95048-100

q-RT PCR mix: 5x FIREPol EvaGreen qPCR supermix (Solis BioDyne, Estonia) Catalogue number #08-36-00008

HRM mix: 5x Hot FIREPol EvaGreen HRM mix (No ROX) (Solis BioDyne, Estonia) Catalogue number #08-31-00001

Shrimp Alkaline Phosphatase: (New England Biolabs, UK)

Trizol: ambion by life technologies Catalogue number #15596026

2.1.3 Primer oligonucleotides

IDT is the supplier for all the primers, we used primer3 https://primer3.ut.ee/ to design all the primers except for *optn* (Paulus and Link, 2014), *il-6 and il-8 (*Kasica-Jarosz et al., 2018)*, ifnφ1, isg15* and *mxa* (Hamilton et al., 2020*), β acti n*(Podlasz et al., 2012) and *eef1a1b* (Bai et al., 2016). The specificity of primers was confirmed using UCSC in silico PCR tools https://genome.ucsc.edu.

Table 2. 1 of zebrafish Genomic DNA primer sequences

Primer name	Direction	Sequence 5' →3'	product length (bp)
tbk1-Exon10-*1*	Forward	TGTAAAACGACGGCCAGT CGCCGCTACTGTTGAAGAGA	256
	Reverse	TTGATTCAGTTTGATTCAGTGTTGA	
tbk1-Exon10-2	Forward	TGTAAAACGACGGCCAGT TCATGCTCCTGTGCAGAGAC	358
	Reverse	TTCAATTCAGCTCATAAGAGAATCA	
tbk1 Exon 4-1	Forward	TGTAAAACGACGGCCAGT AGTGGACGTCAAGCAGAACT	233
	Reverse	TGAACTTGTATTAATCCTGTGTTATTAC	
tbk1 Exon 4-2	Forward	TGTAAAACGACGGCCAGT GCTAATGATGCGGTGTTGTG	214
	Reverse	TGTGTGTGTGGTGAACTTG	
optn Exon9	Forward	CCCATCTCCTGCTTTGTCTTCAGATCCAAAGATT	140
	Reverse	ATCGCCGCTTGGAGGCTTTCC	
map3k14a-Exon4	Forward	TGTAAAACGACGGCCAGT TGCGGTTTACATGTTTTGTGA	256
	Reverse	TGTTTTTACAATTTTCATCAGTTGTT	
map3k14a-Exon5	Forward	TGTAAAACGACGGCCAGT CCAGTGTTCTTCAGCAGCAA	158
	Reverse	TTCAGCTCCTCGCTCTCTTC	
map3k14a-Exon11	Forward	TGTAAAACGACGGCCAGT CATCTCTGCGTAGGCGTAAA	174
	Reverse	AAGGAGAGCTCTTTGGCAGA	
map3k14a-Exon12	Forward	TGTAAAACGACGGCCAGT AAAACCATACATGTACAAATTACTGC	233
	Reverse	CGTCAGCCTTGTTCCTCTTC	

Table 2. 2 of zebrafish c.DNA primer sequences

Primer name	Direction	Sequence 5' →3'	product length (bp)	Primer concentration
tbk1	Forward	ACATCACTCCGTCCCATCAG	94	5 nm
	Reverse	CTGGAGGTCTTGGGAAAGGT		
map3k14a	Forward	AGCATCAAAGACAAAGGCACA	199	5 nm
	Reverse	AAGAGTTCCACCACCTGAGG		
tnfα	Forward	TGAGAGATCGCATTTCACAAGG	277	10 nm
	Reverse	CTGAAGAAAAGGCCTGGTCC		
il1β	Forward	GCTGGAGATCCAAACGGATA	114	10 nm
	Reverse	ATACGCGGTGCTGATAAACC		
il6	Forward	TCAACTTCTCCAGCGTGATG	73	2.5 nm
	Reverse	TCTTTCCCTCTTTTCCTCCTG		
il8	Forward	GTCGCTGCATTGAAACAGAA	253	1.25 nm
	Reverse	AGGGGTCCAGACAGATCTCC		
ifnφ1	Forward	ACGGCAGCCTGAAATACGTT	241	10 nm
	Reverse	GTCCTCCACCTTTGACTTGT		
isg15	Forward	AACTCGGTGACGATGCAGC	124	10 nm
	Reverse	TGGGCACGTTGAAGTACTGA		
mxa	Forward	GACCGTCTCTGATGTGGTTA	207	10 nm
	Reverse	GCATGCTTTAGACTCTGGCT		
eef1a1b	Forward	GGATTGCCACACGGCTCACATT	177	5 nm
	Reverse	GGTGGATAGTCTGAGAAGCTCTC		
β actin	Forward	CTCTTCCAGCCTTCCTTCCT	247	10 nm
	Reverse	CACCGATCCAGACGGAGTAT		

2.1.4 Zebrafish

Zebrafish strains are listed in Table2.3.

E3 medium: 5mM NaCl; 0.17mM KCl; 0.33mM CaCl2; 0.33mM Mg2SO4; 0.1mg/l Methylene Blue in dH2O

Tricaine methane sulfonate (MS222) (Sigma, UK):100-200mg/l

L-Rotifers (Brachionus plicatilis) cultured in salt water and fed an algal mix consisting of Nannochloropsis which contains nutrients perfect for fry growth / health.

Table 2. 3 Zebrafish strains

Strain	Reference
Wild type AB	Zebrafish International Resource Center (ZIRC)
Wild type Nacre	(Lister et al., 1999)
NFKB; GFP	(Kanther et al., 2011b)
MXA;Mcherry	(Levraud et al., 2007)
***optn*^{SA0143}**	(Paulus and Link, 2014)

2.1.5 Equipment

Cold microcentrifuge: SciQuip 1-15PK from Sigma

Centrifuge: ALC PK 120CWS from ANNITA

Cordless handheld homogeniser Kimble 749540

Data Viewer Zebrabox Viewpoint behaviour technology ZEBRALAB Digital tracking-1 Zebrabox-HIBW-newWizard

Microscope: S6 E from Leica

Scales: AND HM-120 Digital Analytical Balance

Sigma Nano drop Spectrophotometer: ND-1000 & NanoDrop 1000

Thermo-cycler: From G-STORM

The Apex Minigrab microscopes camera

UV illumination on a Syngene G: box

2.2 Methods

2.2.1 Zebrafish Husbandry

The University of Sheffield aquarium has a semi-closed system to maintain optimum conditions for zebrafish. Several filtration devices are utilised to obtain water quality for zebrafish, including a carbon filter, an ultraviolet steriliser, a pressurised sand filter, a fluidised sand filter and a biological filter. In addition, zebrafish are maintained in water with parameters similar to what is found in the wild i.e. 28°C temperature, pH 7.5, and a 14 hour light/10 hour dark cycle. Zebrafish are fed twice daily with live artemia, and zebrafeed 400-600 by sparos.
Zebrafish fry between (5-10 dpf) are fed L-Rotifers if the fry has a particular phenotype and/or poor swim ability it would be fed longer. The rotifers themselves offer little nourishment but once enriched with the algal formula provide an excellent early life cycle diet for fry.

2.2.2 Zebrafish breeding

For both in crosses and out-crosses, a pair of zebrafish (male and female) were removed from holding tanks and placed in a breeding tank that contained a divider to separate them. The divider was removed the following morning to allow breeding. Several hours later zebrafish embryos were collected using a small strainer, rinsed in aquarium water, and then transferred to petri dishes containing E3. Any dead or unfertilised embryos were removed then embryos were sorted into batches of 60 per Petri dish containing approximately 50ml of E3. Zebrafish embryos were kept in a 28°C incubator up to 5.2 days post fertilisation (dpf).
The *tbk1* lines were crossed with the NFκB reporter line to facilitate identification of homozygous mutants on the basis of increased fluorescence (see chapter 3). Generated *tbk1* zebrafish lines are listed in table 2.4.

Table 2. 4 Generated *tbk1* zebrafish lines

ZEBRAFISH LINE	MUTATION
***TBK1*^{SH570}**	D409Efsx10
***TBK1*^{SH643}**	Glu109fsX20
***TBK1*^{SH570} *OPTN*^{SA0143}**	D409Efsx10; L278X
***TBK1*^{SH570} NFκB;GFP$^{+/-}$**	D409Efsx10; NFκB;GFP$^{+/-}$
***TBK1*^{SH570} MXA;MCHERRY$^{+/-}$**	D409Efsx10; MXA;Mcherry$^{+/-}$
***TBK1*^{SH643} NFκB;GFP$^{+/-}$**	Glu109fsX20; NFκB;GFP$^{+/-}$
***TBK1*^{SH570} *TBK1*^{SH643}**	D409Efsx10; Glu109fsX20
***TBK1*^{SH570} MAP3K14A**	D409Efsx10;NA

2.2.3 Zebrafish Euthanasia

Zebrafish larvae older than 5.2 dpf were euthanised in 20µl of ice cold Tricaine and then frozen. Adult zebrafish were culled using Tricaine (4.2ml/100ml system water) for 20 min followed by a schedule 1 method (decapitation or freezing).

2.2.4 Fin clipping

Zebrafish were transferred into a tank containing Tricaine (4.2ml/100ml system water) and left for 1 minute until anaesthetised. Using a small spoon, a zebrafish was removed, and a small amount of tail fin tissue was obtained using a scalpel. Clipped tissue was placed in a 96 well plate-containing 20µl of QuickExtract per well. After clipping zebrafish were transferred to individual tanks labelled with the corresponding plate location.

2.2.5 CRISPR/Cas9 injection in Zebrafish embryos

CRISPR Cas9 mix for scrambled and TBK1-Exon4 gRNA were prepared by adding:

H_2O	1µl
Phenol red	1µl
RNA tracer	1µl of 100µM
gRNA	1µl of 100µM
Cas9	1µl of 20µM

TBK1-EX4 gRNA were designed using online resources from the Zhang Laboratory https://zlab.bio/guide-design-resources.

Scrambled gRNA and MAP3K14a gRNA sequences were obtained from (Wu et al., 2018).

tbk1-EX4 gRNA: TGAGGAACTCGTCCTCCGGC

Scrambled gRNA: GCAGGCAAAGAATCCCTGCCG

map3k14 gRNA Target_1: GCTGTCCTGTTCTGGCACTC

map3k14 gRNA Target_2: AGTATCCATCCAGGAAACCG

map3k14 gRNA Target_3: GGGATTTCTCTCAGTGGCGG

map3k14 gRNA Target_4: GGACTACGCAGCCAAGTGAG

CRISPR Cas9 mix for MAP3k14a were prepared by adding:

H_2O	1µl
Phenol red	1µl
RNA tracer	1µl of 100µM
gRNA target_1	0.25µl of 100µM
gRNA target_2	0.25µl of 100µM
gRNA target_3	0.25µl of 100µM
gRNA target_4	0.25µl of 100µM
Cas9	1µl of 20µM

2.2.5.1 Generating frameshift mutations in zebrafish

After confirming the efficiency of the CRISPR Cas9 mutagenesis (see below), F0 zebrafish were raised to adulthood. F0 zebrafish were outcrossed with AB zebrafish then their progeny were screened for founders that transmit a frameshift mutation, then F1 offspring were raised to adulthood. Adult F1 were fin clipped to identify confirmed founders that carry a frameshift mutation. F1 founders were outcrossed with AB to generate F2 *tbk1* heterozygous zebrafish. F2 *tbk1* heterozygous zebrafish were in-crossed to produce F3 (wild type, heterozygous and homozygous) zebrafish.

2.2.6 Zebrafish DNA Extraction

Zebrafish samples, either fin clips or individual embryos <5.2dpf, were arrayed in 96 well-PCR plates. All E3 or system water was carefully removed with a pipette and discarded. 20µl of QuickExtract was added to each well and the plate was sealed with a film lid or caps. After a brief spin to bring the contents to the bottom of the wells, the plate was transferred to a thermo-cycler (G-Storm) and incubated at 65°C for 2 hours followed by 99°C for 2 minutes. DNA extracts were then diluted 1: 6 by adding 100ul deionised H_2O (dH_2O) to each well. For older larvae 30µl of QuickExtract was used and the DNA was diluted 1:400 in dH_2O.

2.2.7 Zebrafish genotyping PCR

A standard 10µl PCR reaction mix contains:

dH_2O	6.8µl
5x FIREPol	2µl
Forward primer (100µM)	0.1µl
Reverse Primer (100µM)	0.1µl
DNA Template	1µl

An appropriate amount of master mix was made up on ice in a designated pre-PCR area and pipetted into a 96 well plate. Diluted template DNAs were added using a multichannel pipette and the plate sealed.

Samples were amplified using a standard touchdown PCR programme:

Denaturation	94°C for 3 minutes
Touchdown (15 cycles)	94°C for 30 seconds
	65°C - 50°C for 45 seconds*****
	72°C for 1 minute 30 seconds
	***decrease temperature by 1°C per cycle**
Conventional Cycles (30 cycles)	94°C for 30 seconds
	58°C for 45 seconds
	72°C for 1 minute 30 seconds
Elongation	72°C for 10 minutes
Store	10°C

2.2.7.1 Restriction digests of PCR products

Genotyping of *tbk1* and *optn* DNA samples takes advantage of restriction enzyme sites that are disrupted by the mutations. A standard digest mix is as follows:

H_2O	7.6µl
10x appropriate buffer	2µl
Enzyme (10 units/µ l)	0.4µl
PCR product	10µl

Digests were incubated for 12 hours at the recommended temperature.
BslI restriction enzyme was used for *tbk1* genotyping.
tbk1 Exon 10-1 the expected digested product sizes for wild type are 157 and 117 bp, heterozygous 274, 157 and 117 bp, and homozygous 274 bp. For *tbk1* Exon 10-2 expected digested product sizes for wild type are 203 and 155 bp, heterozygous 358, 203 and 155 bp, and homozygous 358 bp.
tbk1 Exon 4-1 the expected digested product sizes for wild type are 160 and 73 bp, heterozygous 233, 160 and 73 bp, and homozygous 233 bp. For *tbk1* Exon 4-2 expected digested product sizes for wild type are 128 and 86 bp, heterozygous 214, 128 and 86 bp, and homozygous 214 bp.

For *optn* genotyping a BstXI restriction enzyme digest was used. Expected digested product sizes for wild type are 110 and 30bp, heterozygous 140, 110 and 30bp, and homozygous 140bp.

2.2.8 Agarose gel electrophoresis

PCR products and restriction digests were evaluated on 2-3% agarose gels as appropriate for the expected fragment sizes. A 2% gel was prepared by adding 3g of agarose to 150ml 1x Tris-Acetate EDTA (TAE) buffer then the solution was heated in a microwave for 3 minutes. The agarose was cooled down to approximately 50°C then 1.5µl of Ethidium bromide (0.2-0.5 µg/ml) was added and mixed well. The agarose was poured into a 15cm electrophoresis tray, and 17 well combs were inserted before leaving the gel to solidify for 30 minutes.
The gel was positioned into an electrophoresis tank containing 1x TAE buffer. 1.5µl of 100bp ladder (Hyperladder IV, Bioline) was loaded in each row next to the samples. The gel was run until DNA fragments were resolved, then images were captured under UV illumination on a Syngene G:box.

2.2.9 Sequencing PCR products

The forward PCR primers contain M13F extensions to facilitate sequencing using the University of Sheffield Core Genomics Service. Prior to sequencing the PCR is checked on an agarose gel, then 5µl of PCR product is prepared using exonuclease I and shrimp alkaline phosphatase treatment:

PCR product	5µl
H_2O	3.95µl
Exonuclease I (New England Biolabs, UK)	1µl
Shrimp Alkaline Phosphatase (New England Biolabs, UK)	0.05 µl

Samples are incubated at 65°C for 45 minutes then 80°C for 15 minutes. At this point samples were handed to the Core Genomics Facility, who returned the data as ab1 files. Raw sequence data was analysed using the https://benchling.com website, and sequences were aligned against Ensembl reference sequences *tbk1:* ENSDART00000163280.2 and *map3k14a:* ENSDART00000151236

2.2.10 High resolution melt (HRM) analysis

HRMA was used to test CRISPR Cas9 efficiency to introduce mutations in exon 4 of *tbk1*, and exons 4, 5, 11 and 12 of *map3k14a*.

HRM 10µl PCR reaction mix contains:

H_2O	6µl
5x Hot FIREPol HRM Mix	2µl
Forward primer	0.5µl
Reverse primer	0.5µl
DNA template	1µl

HRM cycling parameters as following:

Initial denaturation	95°C for 15 minutes
Conventional Cycle (40 cycles)	95°C for 15 seconds
	60°C for 30 seconds
	72°C for 30 seconds
	PCR plate read
Denaturation	95°C for 30 seconds
Heteroduplex formation	60°C for 1 minute Ramp 0.1°C/cycle
Duplex Melting (150 cycles)	65°C to 95°C for 10 seconds*
	*Increase temperature by 0.2°C/minute
	PCR Plate read
Hold	10°C

2.2.11 Assessment of larval swimming behaviour

Swimming behaviour of zebrafish larvae at different ages was conducting using a Zebrabox system (Viewpoint, France). For 5 day old zebrafish 96 well plates (Bio-One Ltd, UK, Catalogue number #655180) were used. For 8, 14 and 19 day old larvae 24 well plates (Greiner Ltd, UK, Catalogue number #662160) were used. For 12 day old zebrafish 12 well plates (Greiner Ltd, UK, Catalogue number #662160) were used. Zebrafish were arrayed into plates in the period immediately prior to experiments. A repeat of three independent experiments were conducted for each time point and zebrafish line expect for *tbk1*^{SH640} for which only one experiment was conducted.

2.2.11.1 Zebrafish viewpoint protocol for swimming behaviour

All behavioural tests were conducted between 9.00AM and 6.00PM.
After initiation the Zebrabox was allowed to equilibrate for 30 minutes before commencing experiments. Zebrafish arrayed in plates were individually acclimatised to the Zebrabox for 30 minutes in light (10% intensity). The detection threshold was set according to the age of zebrafish in order to eliminate a reflection of the fish on the side of the wells. A threshold for fast movement was set at 6.4 mm/second and slow movement at 3 mm/second. To induce swimming and analyse behaviour we used the photomotor response method based on the Burton group protocol (Zhou et al., 2014) whereby zebrafish are induced to swim by switching from light to darkness. Our standard protocol consisted of:
Acclimatisation: 30 minutes light
5 minutes dark
5 minutes light
5 minutes dark
5 minutes light
5 minutes dark
5 minutes light
End

Throughout this period an infrared camera captured images at video frame rate (25Hz). Viewpoint software then integrated various movement parameters for each 5-minute period such as (distance, slow movement, fast movement and active duration).

2.2.11.2 Statistical analysis of swimming behavior

The following parameters were analysed:
Active duration - the total time spent moving during a 5 minute period
Slow movement - distance moved at a speed between 3 and 6.4 mm/second during a 5 minute period
Fast movement - distance moved at a speed >6.4 mm/second during a 5 minute period
Total distance- total distance moved in a 5-minute period
For each embryo we calculated the average of each parameter across the 3 dark periods and the 3 light periods.
After genotyping the embryos, we calculated the mean light and dark swimming parameters for each genotype. Experiments were repeated on several days to ensure reproducibility.
One-way ANOVA was performed to determine significant differences at a 95% confidence interval, and Tukey's multiple comparisons test was performed to determine significant differences between each genotype. All values in the graphs are shown as means +/- standard deviation.

2.2.12 Viewpoint protocol for thigmotactic behaviour

A repeat of three independent experiments were conducted for thigmotactic behaviour. 12 day old zebrafish were arrayed in a 12 well plate and acclimatised to the Zebrabox for 30 minutes in light (10% intensity) prior to the experiment. Detection threshold background was set to 36, in order to eliminate a reflection of the fish movement on the wells, while the threshold for fast movement was set at 6.4mm/sec and the slow movement at 3mm/sec.

Two areas were created to calculate swimming parameters, one covers the whole well (25mm) and the second covers just the centre of the well(1.5mm)
To induce swimming and analyse behaviour we used the photomotor response method as described above.

2.2.12.1 Statistical analysis of thigmotactic behavior

For each embryo we calculated the proportion of total time they spend swimming in the centre across the 3 dark periods and the 3 light periods. After genotyping the embryos, we calculated the mean light and dark swimming parameters for each genotype. Experiments were repeated on several days to ensure reproducibility.

2.2.13 RNA extraction

RNA was extracted from 5 and 12 day old zebrafish embryos after genotyping. We performed tail biopsies on anaesthetised embryos under a dissecting microscope. Tails were arrayed in a 96 well plate and processed for DNA extraction, PCR and restriction digest as described in sections 2.2.2-2.2.4. The rest of the larvae were placed in individual tubes containing 20µl of TRIZOL and stored at -80°C until needed. When the genotyping was complete a sample of 10 zebrafish in Trizol were pooled in tubes according to the genotype. The samples were homogenised using a handheld homogeniser. RNA was extracted using phenol-chloroform (0.2x of Trizol volume) and centrifugation at 4°C for 15 minutes at 12000g to separate RNA into the aqueous phase, which was transferred into RNAse free tubes. 100% isopropanol (0.2x of Trizol volume) was added to precipitate RNA under centrifugation at 4°C for 15 minutes at 12,000g. The supernatant was removed, and the pellet was washed with 75% ethanol then centrifuged at 4°C for 5 minutes at 7,500g. After removing the supernatant, the pellet was dried at room temperature for 10 min. RNA was resuspended in 10µl RNAse free water, and the concentration and purity (OD260/280) was determined using a Sigma Nanodrop Spectrophotometer ND-1000.

2.2.14 cDNA synthesis

Reverse Transcriptase was used to synthesise cDNA from RNA as follows:

8µl of RNA (1µg)

1µl of 10x buffer (NEB)

1µl of Dnase1(NEB)

Incubate at 37°C for 10 minutes

Add 1µl of EDTA (2.5mM) and heat inactivate at 75°C for 10 minutes.

Add the following to each sample:

5µl of RNase free dH_2O

4µl of 5x qScript mix (Quanta-bio) (containing oligo dT and random hexamers)

Vortex and spin-down

Incubate at:

22°C for 5 minutes

42°C for 30 minutes

85°C for 5 minutes

Store at 4°C

2.2.15 Quantitative Real time PCR (qRT-PCR)

All primers were optimized for qPCR to establish optimal concentrations without primer-dimers or non-specific amplification products. Primers were initially diluted to a 100µM concentration were subsequently tested at the following dilutions: 10µM, 5µM, 2.5µM and 1.25µM. cDNA was subsequently diluted to between 1/5 to 1/78125 to optimise and determine the optimum template input, by analysing the standard curve that has a CT value lower than 35, an efficiency close to the range of 90-110% and a ratio of sample to dye around 0.95 or more.

Three groups of independently collected samples and a reference gene were included in each experiment to calculate the relative mRNA level. *eef1α1b* was used as a reference gene for *tbk1* and *map3k14a* while *β actin* used as a reference for *tnfα, il1β, il6, il8, ifnφ1, isg15* and *mxa.*

A standard 10µl qPCR reaction mix contains:

H_2O	6µl
EVA green	2µl
Forward primer (varying concentrations)	0.5µl
Reverse Primer (varying concentrations)	0.5µl
cDNA Template	1µl

An appropriate amount of master mix was made up on ice in a designated pre-PCR area and pipetted into a 96 well plate. Diluted template c.DNAs were added using a multichannel pipette and the plate sealed.

Samples were amplified using a standard RT-qPCR programme:

Denaturation	95°C for 10 minutes
Conventional Cycles (39 cycles)	94°C for 30 seconds
	60°C for 1 minute
	72°C for 1 minute
Plate read (60 cycles)	
Denaturation	95°C for 1 minute
Annealing	65°C for 30 seconds
Melt curve	65°C for 5 seconds (+0.5°C/cycle)
Store	10°C

Bio-Rad CFX Manager software produced (Ct) values for each reaction and relative mRNA expression was calculated using this (Schmittgen and Livak, 2008) formula:

Fold change = $2^{-(\Delta Ctsample - \Delta Ctcontrol)}$

2.2.16 Whole body weight and length of zebrafish

Length was obtained from several age groups 14 dpf, 21 dpf, 6 months and 1 year old zebrafish using a millimetre scale ruler and weight was obtained using an analytical scale.

2.2.17 Assessment of adult swimming behaviour

Adult zebrafish were sorted in separate tanks according to their genotype, in each group we obtained the same number of males and females. It is very important not to feed the fish on the day of the experiment but feed them at the end of it. A swim tunnel that has a flow meter has been used to assess zebrafish swimming endurance and calculate critical swimming speed (Ramesh et al., 2010, Chapman et al., 2013). Zebrafish were transferred to the swim tunnel and started to swim against water flow with initial speed of 6.57cm/s, water flow was increased by 6.57cm/s every 5 minutes until the fish got exhausted and couldn't swim anymore. At this point the swimming time was recorded. At the end of the experiment, zebrafish were anesthetized, and body length and weight were obtained. The critical swimming speed calculated by using the following formula:

Ucrit/body length = $(U_i + (U_{ii}(T_i))/T_{ii})/B$

Ui = the highest velocity maintained for a full 5 min period (cm/s) Uii = the velocity increment (6.57 cm/s)

Ti = the time to exhaustion (s)

Tii = the time interval (5 min)

B = body length (cm)

A repeat of three independent experiments were conducted for the six month old *tbk1*^{SH570} zebrafish but only two independent experiments were conducted for the one year old *tbk1*^{SH570} zebrafish.

2.2.18 Shoaling swimming behaviour

Three independent experiments were conducted for shoaling behaviour, and each time two groups were used. 21dpf zebrafish had been raised in separate tanks according to their genotype (*tbk1*$^{+/+\&+/SH5770}$ in one tank and *tbk1*$^{SH570/SH570}$ in another) and shoaling behaviour was conducted using a Viewpoint Zebrabox system. A group of six zebrafish from the same genotype were placed in a concave watch glass plate (46mm diameter) with 3ml E3 water and acclimatised for 30 min before starting the shoaling analysis.

Viewpoint Zebrabox Shoaling software was used to quantify 4 shoaling parameters (speed, polarisation, inter individual distance and nearest neighbour distance) every minute (Miller and Gerlai, 2007) through an infrared camera at video frame rate (25Hz). The mean and a standard deviation were calculated for the total of 10 minutes.

Chapter 3

3. Characterisation of *tbk1* zebrafish

3.1 Introduction

Haploinsufficiency loss of function mutations in the human *TBK1* gene cause ALS/FTD. We predict that point mutation or a frameshift mutation would resemble haploinsufficiency in the heterozygous model and a gene knockout in the homozygous one (De Majo et al., 2018). The *TBK1* knockout mouse is embryonic lethal (Bonnard, 2000) which makes the development of alternative animal models an important area for research. We chose to investigate effects of *tbk1* LOF mutations in a zebrafish model. Our first aim was to characterise a newly generated zebrafish *tbk1* mutant and investigate if it causes loss of function. Furthermore, we wished to see if mutant zebrafish show symptoms and phenotypes observed in ALS/FTD patients. In order to assess loss of function we looked at mRNA levels using quantitative PCR, as cells usually degrade mRNA that contain a premature stop codon by a mechanism called nonsense-mediated mRNA degradation. Another major question was about the viability of the model and whether it would reach adulthood. In order to confirm our findings, we also generated a new *tbk1* model targeting the kinase domain.

Our second aim was to address whether *tbk1* mutant zebrafish model showed a motor phenotype like ALS, or a behavioural phenotype like FTD. To address this, we performed a series of swimming studies to characterise motor function.

Evaluating an FTD-like phenotype in zebrafish is challenging as there are no published FTD zebrafish models, and the structure of the human cortex is not particularly comparable with the zebrafish forebrain. However, we chose to look for abnormal behaviour which is a feature of some forms of human FTD. In particular we measured the effects of mutant *tbk1* on larval zebrafish shoaling behaviour and thigmotaxis, which may mimic the behavioural FTD phenotypes seen in patients.

3.2 Genetic characterisation of *tbk1*$^{SH570/SH570}$ zebrafish

In order to investigate the effect of the *tbk1* mutation in zebrafish we first sequenced *tbk1*$^{SH570/+}$ in cross progeny to make sure they carried the expected mutation.

3.2.1 Sequencing of *tbk1*$^{SH570/+}$ in cross progeny

Sequence analysis of *tbk1* heterozygous in cross zebrafish progeny confirmed a 5bp frameshift deletion in exon10, c.1227_1231delCCTGG, resulting in a premature stop codon p.D409Efsx10 (Figure (3.1). This was confirmed by restriction enzyme digestion with BslI. The mutation abolishes the BslI restriction site (see Figure (3.2). The frameshift introduces 10 novel amino acids and a stop codon downstream of amino acid 409. This is expected to cause either a loss of function mutation through nonsense-mediated degradation of the mutant transcript, or the generation of a truncated protein.

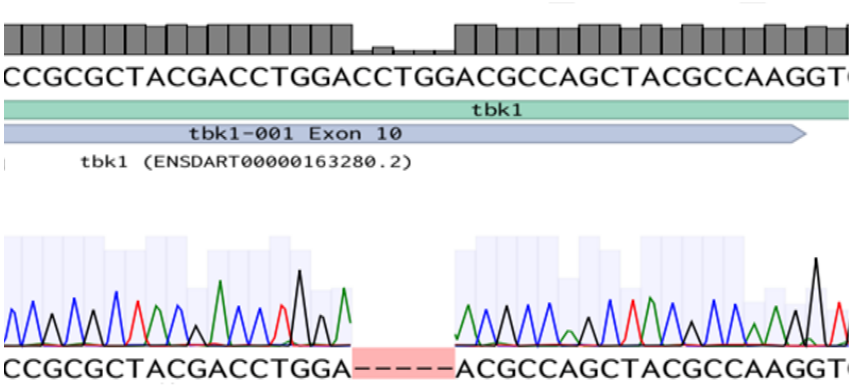

Figure 3. 1 Sequence analysis of *TBK1* mutant zebrafish. The top sequence is the ensembl reference sequence (ENSDART00000163280.2), the bottom sequence shows a homozygous deletion of CCTGG at position 1227 of the mRNA.

3.2.2 Genotyping *tbk1*$^{SH570/+}$ in-cross progeny

Genotyping analysis of *tbk1* heterozygous in cross zebrafish progeny was performed to distinguish the wild type, heterozygous and homozygous offspring. The expected size of the PCR product using exon 10 primers Fw1 and Rv1 is 274 bp. BslI will digest the wild type allele at position 157 bp, giving rise to products of 157 & 117 bp. In mutants the BslI site is lost, so the PCR product will remain 274 bp. Therefore, BslI digest of heterozygotes will yield 3 bands of 274, 157 and 117 bp (see Figure(3.2).

In the course of these experiments, we observed a problem with PCR contamination, leading to amplification in the no template control. To overcome this issue new primers were designed that generate a 358 bp PCR product, which is digested to give bands of 155 & 203bp in wild type, but not digested in homozygotes. Heterozygotes give bands of 155, 203 and 358 bp (see Figure(3.3).

a)

CAAGACCTCCAGAGACAATCCCATCATGCTCCTGTGCAGAGACCCCGTCAACACCGTCGG

CCTGCTGTTTGAGGACCgtgagtctggcgccgctactgttgaagagatgatgcagttatt

Fw1

attgtagatcagctcaacagttatcatgtgttaatagctgatcataaccctgccctgtgt

gtctgcagCCAGCCCACCCAAAGTACAGCCGCGCTACGACCTGGACCTGGACGCCAGCTA

Exon10

CGCCAAGgtgacaaacactgaactccactccaccaatcaaccacgaaccaaacttaaata

ctattgaactgaactgaatcaacactgaatcaaactgaatcaaaaaggaaactaactgat

Rv1

tctcttatgagctgaattgaatcaacactgaactgaagtgaatcaatatttaactgaacc

PCR product size: 274bp
Wild type: 157 & 117bp
Heterozygous: 274, 157 &117bp
Homozygous:274bp

b)

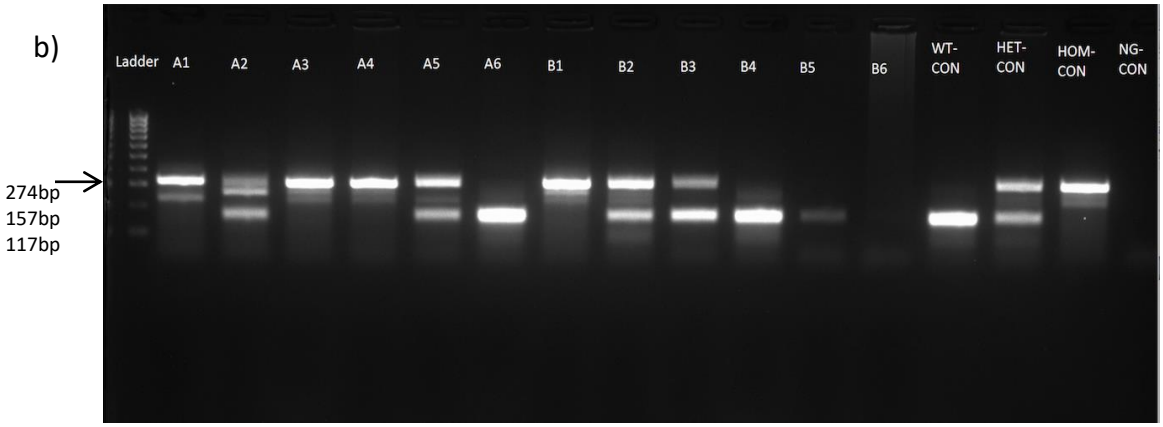

Figure 3. 2 Genotyping of *tbk1* exon 10. a) Diagram depicting location of forward (FW1) and reverse (RV1) primer binding sites within the *tbk1* gene, 5bp deletion (red letters) and BslI restriction site (highlighted in yellow, underlined A where the enzyme cuts). b) Gel image of *tbk1* exon 10 genotyping, wild type gives bands of 157 & 117 bp, heterozygous gives bands of 274, 157 & 117bp and homozygous gives a band at 274 bp. Positive controls (wild type, heterozygous, homozygous) and negative controls (no DNA template) were included.

a)

CAAGACCTCCAGAGACAATCCCATCATGCTCCTGTGCAGAGACCCCGTCAACACCGTCGG

Fw2 →

CCTGCTGTTTGAGGACCgtgagtctggcgccgctactgttgaagagatgatgcagttatt

attgtagatcagctcaacagttatcatgtgttaatagctgatcataaccctgccctgtgt

gtctgcagCCAGCCCACCCAAAGTACAGCCGCGCTACGACCTGGACCTGGACGCCAGCTA

Exon10

CGCCAAGgtgacaaacactgaactccactccaccaatcaaccacgaaccaaacttaaata

ctattgaactgaactgaatcaacactgaatcaaactgaatcaaaaaggaaactaactgat

tctcttatgagctgaattgaatcaacactgaactgaagtgaatcaatatttaactgaacc

← Rv2

PCR product size:358bp
Wild type:203 & 155bp
Heterozygous:358, 203 &155bp
Homozygous:358bp

b)

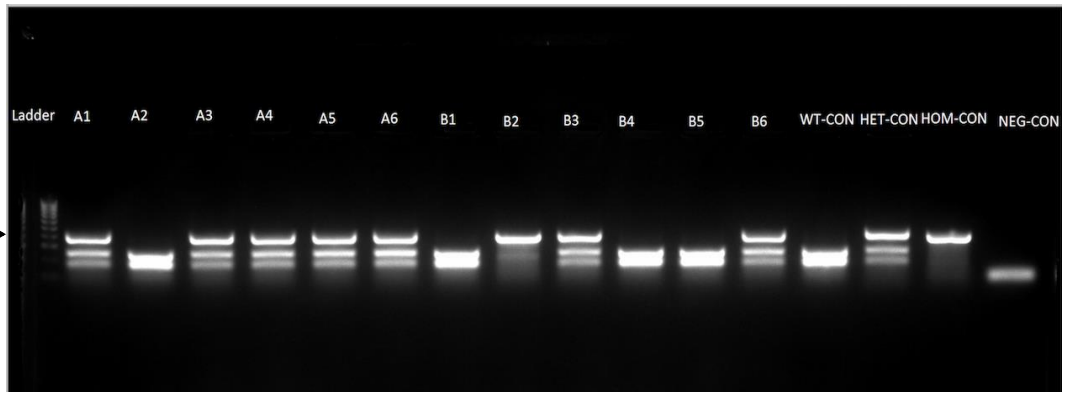

Figure 3. 3 Genotyping of *tbk1* exon 10. a) Diagram depicting location of forward (FW2) and reverse (RV2) primers binding sites within *TBK1* gene, 5bp deletions (red letters) and BslI restriction site (highlighted in yellow, underline A is where the enzyme cut). b) Gel image of *TBK1* exon 10 genotyping, wild type genotyping show one band at size 203 & 155 bp, heterozygous bands 358, 203 & 155 bp and homozygous band at 358 bp. Positive controls (wild type, heterozygous, homozygous) and negative controls (no DNA template) were included.

3.2.3 Survival rate of *tbk1*$^{SH570/SH570}$ zebrafish

tbk1 homozygous knockout mice (see section 1.4) are embryonic lethal due to liver apoptosis (Marchlik et al., 2010). In order to determine whether the zebrafish *tbk1* mutation is also embryonic lethal we determined viability of offspring obtained from a series of experimental *tbk1*$^{SH570/+}$ in crosses obtained by marbling the same tank of *tbk1*$^{SH570/+}$ fish over a number of weeks. Embryos were collected and randomly assigned to groups in batches of 60. These groups were then maintained for 7-35 days using standard husbandry, before being killed using tricaine, and genotyped.

Table 3. 1 Frequencies of each genotype obtained from *tbk1*$^{SH570/+}$ in crosses

Age (days)	n	*tbk1* $^{+/+}$	*tbk1*$^{SH570/+}$	*tbk1*$^{SH570/SH570}$
7	49	24.5%	51%	24.5%
14	47	23%	45%	32%
21	42	26.2%	57.1%	16.7%
28	57	33%	51%	16%
35	51	31%	55%	14%

This experiment showed that 24.5% of progeny were homozygotes at 7 days, which is almost exactly the expected Mendelian frequency (25%). At 14 days homozygotes accounted for 32% of the fish, which is slightly higher than the Mendelian ratio, but not indicative of decreased survival. However, fish collected at 21, 28 and 35 days old all had less than 17% homozygotes. Therefore, we find evidence that during these experiments a proportion of the homozygous mutants are dying after 14 days of age.

3.2.4 tbk1 mutant zebrafish are smaller

The mean weight and length of 14 day old *tbk1* zebrafish was calculated for 5 wild types, 9 heterozygotes and 9 homozygotes. One-way ANOVA for the weight shows a significant difference between groups ($p<0.0001$) and Tukey's multiple comparisons test shows significant difference between wild type and homozygous mutants ($p=0.0120$). Likewise One-way ANOVA for the length showed a significant difference between groups ($p=0.0001$) and Tukey's multiple comparisons test shows a significant difference between wild type and homozygous mutants ($p<0.0001$) (see Figure (3.4). In addition to the small size of 14 day old *tbk1* homozygous zebrafish the 12 and 14 day old *tbk1* homozygous lack the anterior swim bladder and they shows an empty gut compared to wild type and heterozygous siblings (see Figure (3.5). This suggests that *tbk1* deficiency may cause broad developmental defects.

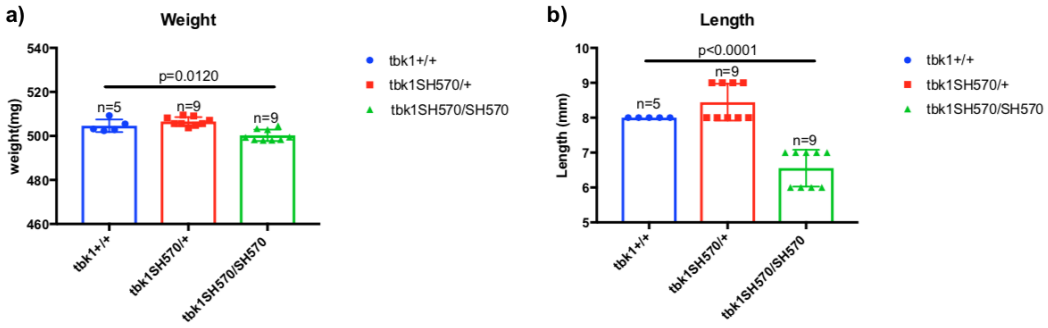

Figure 3. 4 Weight and length of *tbk1* zebrafish larvae. a) Weight was significantly different between wild type and homozygous larvae (p=0.012) b) Length was significantly different between wild type and homozygous larvae (p<0.0001).

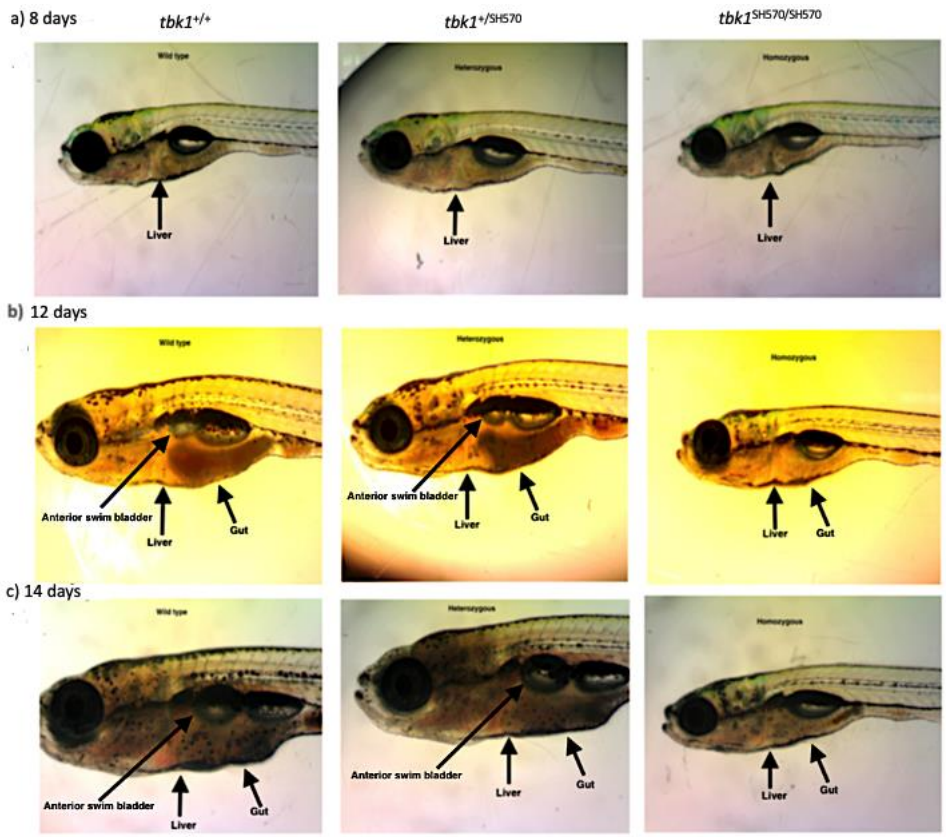

Figure 3. 5 Morphology of *tbk1* larvae at different ages. Morphology of *tbk1* larvae at different ages. a) 8 days old. b) 12 days old, homozygous lack anterior swim bladder and the gut is empty. c) 14 days old, homozygous are smaller in size, lack anterior swim bladder and the gut is empty. At all ages arrows are used to indicate the structures mentioned in the text.

3.2.5 Expression level of *tbk1* mRNA during development

We wished to establish the expression level of tbk1 during larval development, in order to understand more about the potential effect of loss of tbk1. Gene expression is often quantified at the mRNA level, particularly when there is no antibody available to measure protein levels. In order to evaluate *tbk1* expression we collected embryos at the following developmental stages: 16 cells, 50% epiboly, gastrulation, 1 dpf, 2 dpf, 3 dpf, 4 dpf, 5 dpf, 6 dpf, 7 dpf and 12 dpf. Total RNA was extracted from a pool of 10 whole body embryos per stage. cDNA was synthesised using a kit containing a mixture of oligo dT and random hexamers and we performed quantitative RT-PCR (qRT-PCR). A housekeeping gene, eukaryotic elongation factor 1 alpha 1b (eef1a1b) was used as a reference. qPCR of the target transcript *tbk1* and the reference *eef1a1b* was carried out and relative mRNA levels were calculated using delta-delta Ct method. The data was then normalised with the level at 5 dpf being set to 1. (Figure (3.6) shows that *tbk1* mRNA levels are high at the 16 cell stage, and then drop rapidly. This suggests maternal inheritance of *tbk1* mRNA that is present in the oocyte. At 2 dpf there is an increase in expression, which seems to peak at 3 dpf, then reaches a steady state at 5-6dpf.

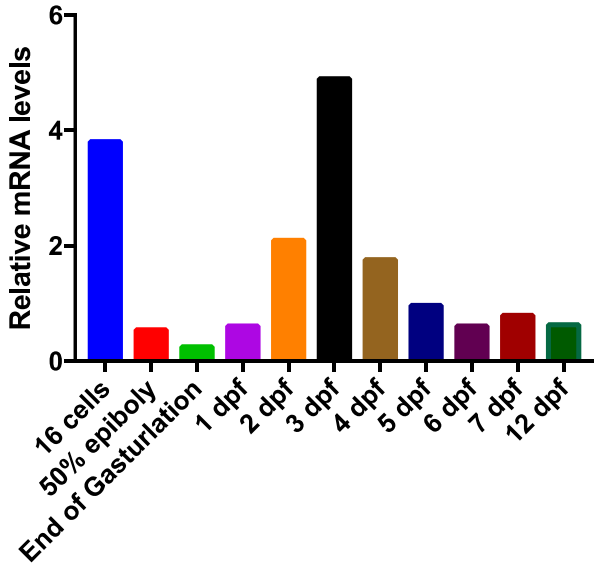

Figure 3. 6 Expression level of *TBK1* mRNA in wild type Zebrafish through development. Figure shows the relative mRNA level of *TBK1* at different stages: 16 cell, 50% epiboly, end of gastrulation, 1dpf, 2dpf, 3dpf, 4dpf, 5dpf, 6dpf, 7dpf and 12dpf in wild type zebrafish.

3.2.6 The *tbk1*^{SH570} allele leads to nonsense mediated degradation

The purpose of this project is to study loss of *tbk1* function. Therefore, we wish to study *tbk1* alleles that lead to reduced/loss of tbk1 protein. Frameshift mutations that do not occur in the final coding exon of a gene are very likely to induce nonsense mediated degradation, resulting in loss of tbk1 protein rather than expression of a truncated protein. To look for evidence of nonsense mediated degradation we used qRT-PCR to quantify *tbk1* mRNA levels in embryos derived from a *tbk1*$^{SH570/+}$ in-cross (3.7).

We measured relative *tbk1* mRNA levels in 5 dpf *tbk1*$^{+/+}$, *tbk1*$^{SH570/+}$ and *tbk1*$^{SH570/SH570}$ zebrafish. From each genotype we collected a pool of 10 embryos, then we extracted the total RNA and performed qRT-PCR using the approach described above. One way ANOVA did not reveal a significant difference between the 3 groups (p=0.6252) (see Figure (3.7).

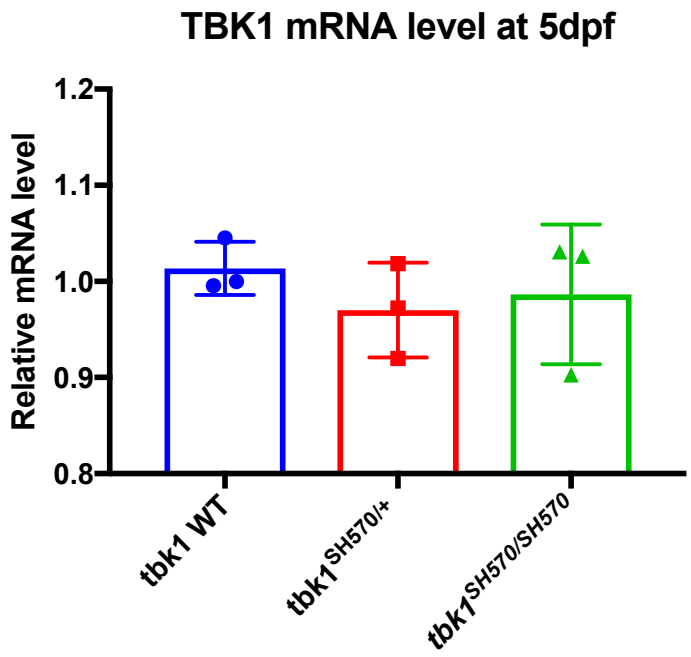

Figure 3. 7 Expression level of *tbk1* mRNA at 5 dpf in *tbk*$^{+/+}$, *tbk1*$^{SH570/+}$ and *tbk1*$^{SH570/SH570}$ zebrafish. Relative *tbk1* mRNA level in 5 dpf *tbk1*$^{+/+}$, *tbk1*$^{SH570/+}$ and *tbk1*$^{SH570/SH570}$ zebrafish shows no significant difference between the groups (p=0.6252). Each point represents a pool of 10 larvae from 3 independent group.

Because we did not see evidence of nonsense mediated degradation at 5 dpf (Figure (3.7), and since we suspected strong maternal contribution of *tbk1* mRNA from the oocyte (Figure (3.6) we decided to investigate *tbk1* levels at 12dpf, when we assumed that the maternal mRNA contribution would be diminished.

We then measured *TBK1* relative mRNA level in 12d pf *tbk1*$^{+/+}$, *tbk1*$^{SH570/+}$ and *tbk1*$^{SH570/SH570}$ zebrafish. From each genotype we collected a pool of 10 embryos, then we extracted the total RNA and performed qRT-PCR. We observed a slight reduction in the expression of *tbk1*$^{SH570/SH570}$ at 12dpf, however one-way ANOVA did not show a significant difference between the 3 groups (p=0.1540) (see Figure (3.8).

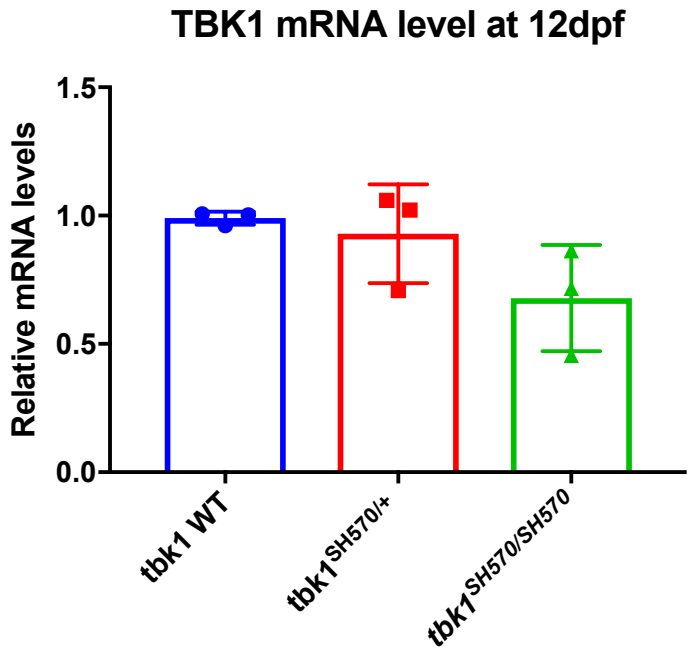

Figure 3. 8 Expression level of *tbk1* mRNA at 5 dpf in *tbk*$^{+/+}$, *tbk1*$^{SH570/+}$ and *tbk1*$^{SH570/SH570}$ zebrafish. Relative *tbk1* mRNA level in 12 dpf *tbk1*$^{+/+}$, *tbk1*$^{SH570/+}$ and *tbk1*$^{SH570/SH570}$ zebrafish shows no significant difference between the groups (p=0.1540). Each point represents a pool of 10 larvae from 3 independent group.

3.2.6.1 Expression level of *tbk1*^{SH570} mRNA in mutants without maternal contribution of wild type *tbk1* mRNA

To assess if maternally inherited wild type *tbk1* mRNA is what we detected in homozygous progeny of in crosses been heterozygous parents we set up in crosses of *tbk1*$^{+/+}$ siblings alongside in crosses of *tbk1*$^{SH570/SH570}$ siblings. A pool of 10 embryos from each cross was collected at 5 dpf, RNA was extracted, and a qRT-PCR was performed. An unpaired t test with Welch's correction shows a significant reduction in *tbk1*^{SH570} mRNA compared to wild type mRNA ($p=0.0233$) (see Figure (3.9a). We also extracted RNA from 12 dpf *tbk1*$^{SH570/SH570}$ and wild type larvae without maternal contribution and demonstrated a significant reduction in the mutant mRNA (Welch's t test $p<0.0001$), (see Figure (3.9b). Therefore, we conclude that wild type mRNA from the oocyte was the signal we detected at 5 and 12 dpf in the homozygous progeny of heterozygous in crosses.

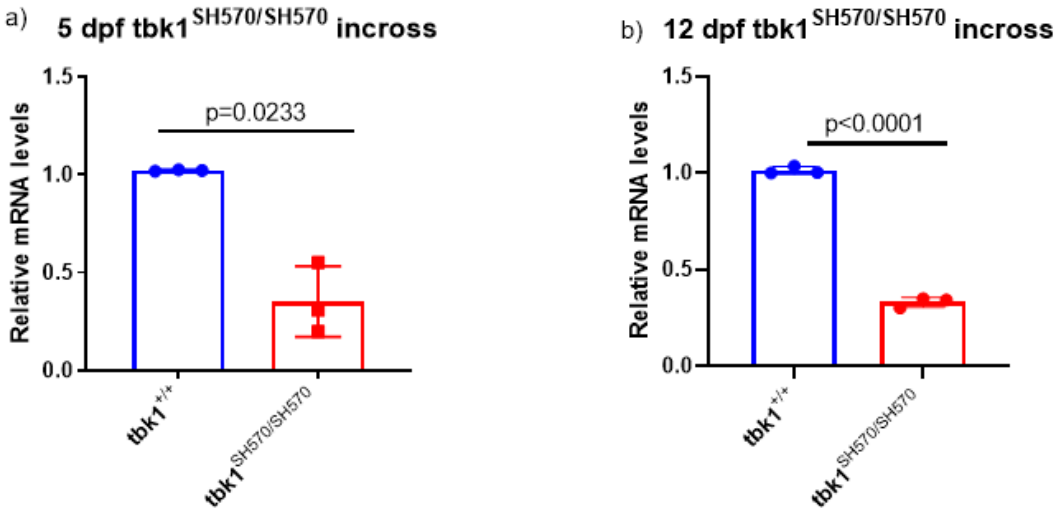

Figure 3. 9 Expression level of *TBK1* mRNA without maternal contribution at 5dpf and 12dpf *TBK1* Zebrafish. A)*TBK1* relative mRNA level in 5dpf *tbk1*$^{SH570/SH570}$ incross Zebrafish shows a significant reduction compared to the *tbk1*$^{+/+}$ incross with p=0.0233.b)*TBK1* relative mRNA level in 12dpf *tbk1*$^{SH570/SH570}$ incross Zebrafish shows a significant reduction compared to the *tbk1*$^{+/+}$ incross with p<0.0001. Each point represents a pool of 10 larvae from 3 independent group.

To verify these finding and to confirm the effect of the frameshift mutation that predicted to produce a premature stop codon that leads to a loss of function in *TBK1* gene, and since we still observe a relative *TBK1* mRNA level in the *tbk1*$^{SH570/SH570}$ Zebrafish at 12dpf, western blot should be performed to look at tbk1 protein level.

3.3 Generating a new loss of function model

3.3.1 Sequence verification of the CRISPR target region of zebrafish *tbk1* exon 4

To confirm the finding in the *tbk1*$^{SH570/SH570}$ zebrafish model that carries a mutation in exon 10 which encodes CCD1, we wished to generate a second mutant allele that would eliminate tbk1 kinase activity.

A guide RNA was designed (see section 2.2.5) to target a conserved region in exon 4 located in the kinase domain of zebrafish *tbk1* which overlaps a BslI site. We used PCR to amplify and sequence the target region in zebrafish from the University of Sheffield aquarium and demonstrated that the sequence of the target region is the same as that in the ensemble database. The expected size for PCR product of *TBK1* exon 4 is 233bp (see Figure (3.10).

a)

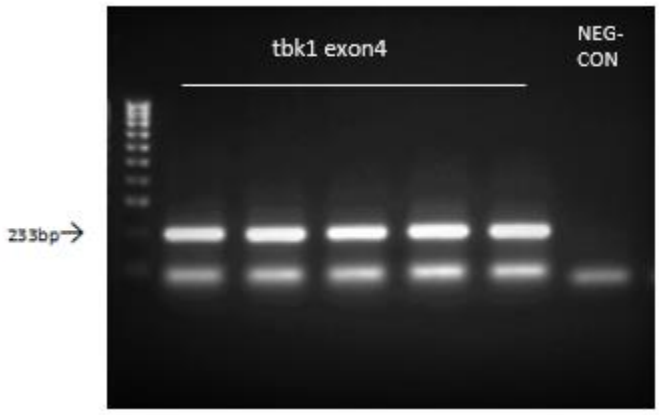

b)

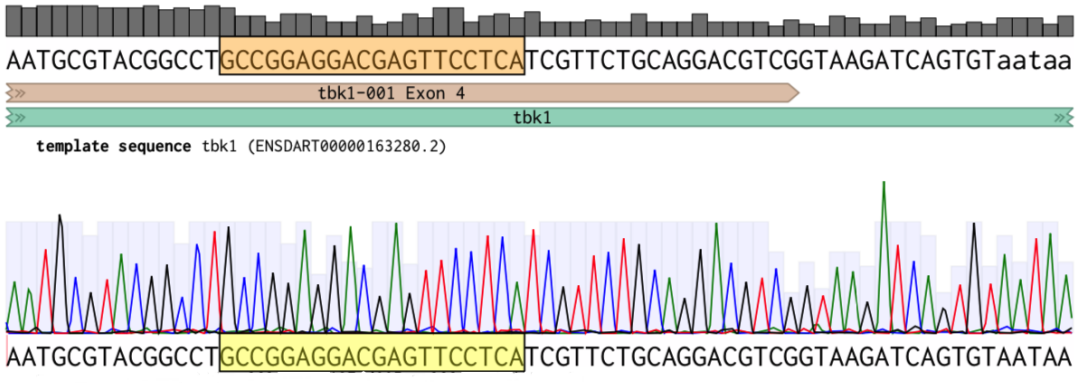

Figure 3. 10 Target region for mutagenesis of *tbk1* exon 4. The BslI site is underlined. A) Gel image of *tbk1* exon 4 showing a single product at 233bp the 2nd lower band are primer dimers also present in negative control (NEG-CON). B) Sequence analysis of *tbk1* exon 4. The top sequence is the nsemble reference sequence (ENSDART00000163280.2) and the bottom sequence shows a wild type sequence of exon 4 with the gRNA region highlighted in yellow.

3.3.2 Mutagenesis of *tbk1* exon 4

To induce indel mutations 2nl and 4nl of mixes containing gRNA and recombinant Cas9 were injected into one-cell stage zebrafish embryos. At 2 dpf, injected embryos were collected, and DNA was extracted. A BslI digest was performed to determine whether mutations have been introduced. BslI will digest the wild type PCR product after 160 bp, giving rise to products of 160 & 73 bp. In mutants the BslI site is lost, so the PCR product will remain 233bp after restriction enzyme digestion. Therefore, a BslI digest of embryos where one copy of *tbk1* has been mutated will yield 3 bands of 233, 160 and 73 bp.

HMRA detects changes in the melting temperature of DNA duplexes. Heteroduplexes melt differently to homoduplexes, and this can be seen as a shift in the melt curve. If mutagenesis is working efficiently, we would expect to see shifts caused by the presence of mutant and wild type DNA templates. The melt curve was shifted in some of the *TBK1* exon 4 CRISPR injected embryos compared to scrambled injected controls, indicating that a mutation has been introduced in the targeted *tbk1* region (see Figure (3.11).

a)

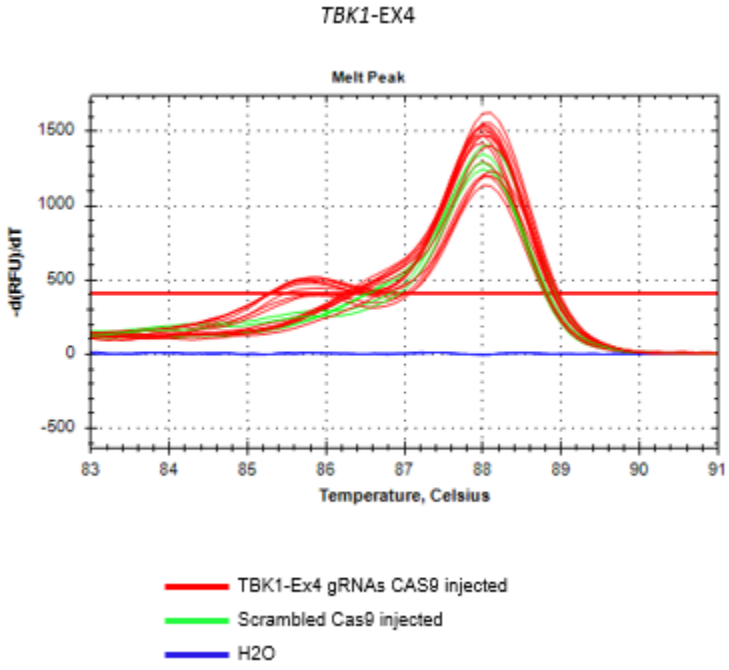

b)

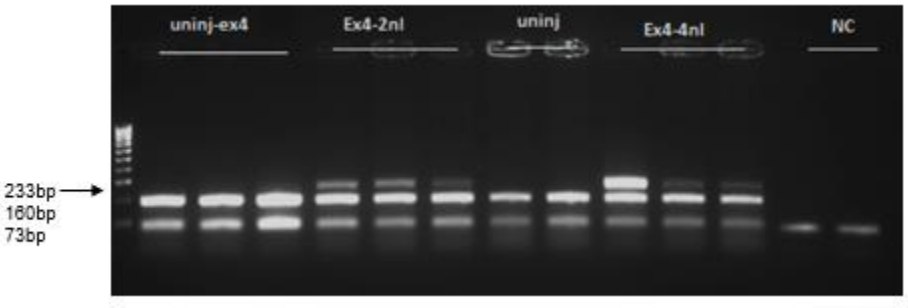

Figure 3. 11 PCR and BslI restriction digest of CRISPR/Cas9 *tbk1* exon4 gRNA-injected embryos and High-resolution melt analysis (HRMA) indicates that mutations have been introduced in CRISPR embryos. a) The first 3 lanes are uninjected embryos with the expected band sizes of 160 and 73bp the next 3 lanes are embryos from the same parents injected with 2nl CRISPR/Cas9 *tbk1* exon 4 gRNA that in addition shows a band of 233 bp. Lanes 7 and 8 are un-injected embryos, while lanes 9-11 are the fourth 3 wells 3 wells are embryos from the same parents that were injected with 4nl CRISPR/Cas9 t*bk1* exon 4 gRNA, that show the 233 bp undigested band. The last 2 lanes are no template controls. B) Melt curves are shown for WT scrambled gRNA CRISPR (green lines), *tbk1* exon4 gRNA CRISPR (red lines) and negative control is (blue lines)

3.3.2.1 Characterising mutations in exon 4

F0 zebrafish embryos that have been injected with CRISPR/Cas9 and gRNA will become genetic mosaics. We wished to identify F0 fish with germline mutations of tbk1, therefore we outcrossed 13 randomly selected adult F0 with wild type zebrafish. From each cross we collected 2 dpf F1 embryos and performed PCR and BslI restriction digests. Out of 200 genotyped embryos 19 embryos carried a mutation, (see Figure (3.12) for example.
Next, we sequenced the exon 4 PCR product for all F1 embryos with a 233 bp undigested band following BslI digest. We detected various heterozygous insertion or deletion mutations (see Figure (3.13) and Table (3.2). Novel frameshift mutations introduced by CRISPR/Cas9 are expected to be deleterious for protein function (see Figure (3.14). Therefore, we selected the F0 zebrafish that transmitted frameshift mutations and performed outcrosses with wild type (AB strain).

gacgtcaagcagaactagtaacactaacgctaatgatgcggtgttgtgttgttctgtcag

FW1 →

TCGAACACACGTCATAAGGTGCTGGTGATGGAGTACTGCCCCTGCGGGAGTCTCTACACC

Exon4

GTCCTGGAGGAGCCCACCAATGCGTACGGCCTGCCGGAGGACGAGTTCCTCATCGTTCTG

CAGGACGTCGgtaagatcagtgtaataacacaggattaatacaagttcaccacacacaca

← RV1

cacacacacacacacacacacacacacacacacacacacacacacacacactaata

PCR product size: 233bp
Wild type: 160 and 73bp
Heterozygous: 233, 160 and 73bp
Homozygous: 233bp

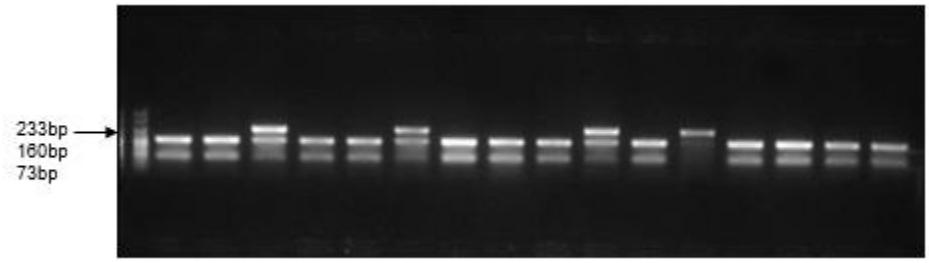

Figure 3. 12 Genotyping of F1 *TBK1* exon 4 embryos. Gel image of *TBK1* exon 4 genotyping, wild type embryos show bands at 160 and 73 bp, and F1 carrying mutations show bands of 233, 160 and 73bp.

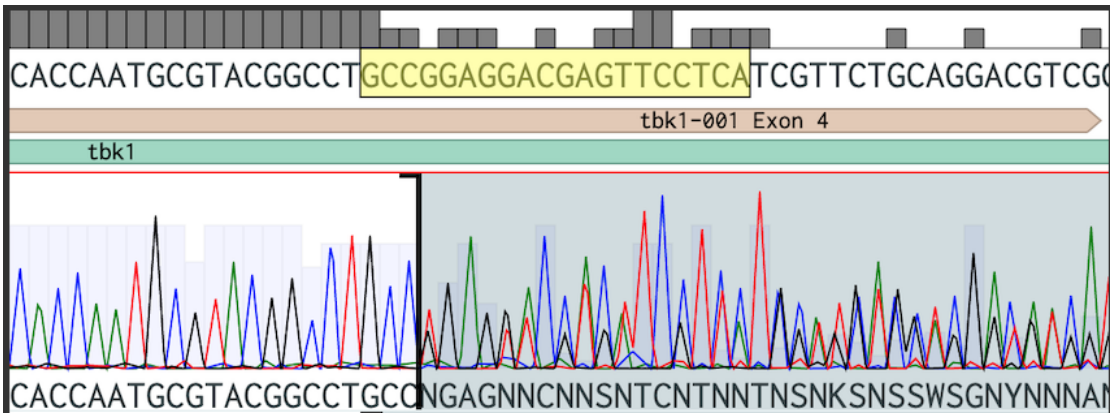

Figure 3. 13 Example of Sequence chromatogram of *TBK1* exon 4 F1 mutant zebrafish. Sequence analysis of an F1 fish carrying a 7 bp deletion.

Figure 3. 14 Characterisation of frameshift mutations in exon 4 F1 embryos. DNA and protein translation sequences of F1 mutant alleles. The wild type reference sequence is labelled 1. Samples 2-9 represent independent F1 fish. Deleted and inserted nucleotides, as well as novel stop codons, are highlighted in red.

Table 3. 2 Novel mutations identified in F1 zebrafish embryos:

F0	#0f embryos	Type of mutation	Mutation
1	0	NA	NA
2	1	5bp deletion(GGAGG)	c.323_327del5;p.Glu109_Asp110del
3	1	9bp deletion(CCGGAGGAC)	c.321_329del9;p.Pro107_Asp110del
4	5	7bp deletion(GGAGGAC)insertion(T)	c.323_329del7GGAGGACinsT;p.Glu109fs
		7bp deletion(GGAGGAC)insertion(T)	c.323_329del7GGAGGACinsT;p.Glu109fs
		7bp deletion(GGAGGAC)insertion(T)	c.323_329del7GGAGGACinsT;p.Glu109fs
		7bp deletion(GGAGGAC)	c.323_329del7;p.Glu109fsX13
		7bp deletion(GGAGGAC)	c.323_329del7;p.Glu109fsX13
5	0	NA	NA
6	2	6bp deletion(GGAGGA)	c.323_328del6;p.Glu109_Asp110del
		6bp deletion(GGAGGA)	c.323_328del6;p.Glu109_Asp110del
7	2	10bp deletion(GCCGGAGGAC)	c.323_328del6;p.Glu109_Asp1109del
		17bp deletion(GCCTGCCGGAGGACGAG)	c.316_332del17;p.Gly105del
8	2	7bp deletion(GGAGGAC)insertion(T)	c.323_329del7GGAGGACinsT;p.Glu109fs
		7bp deletion(GGAGGAC)insertion(T)	c.323_329del7GGAGGACinsT;p.Glu109fs
9	0	NA	NA
10	0	NA	NA
11	4	7bp deletion(GGAGGAC)	c.323_328del6;p.Glu109_Asp110del
		14bp insertion(TTCAGGCACCTTCA)	c.323_329del7;p.Glu109fsX13
		14bp insertion(TTCAGGCACCTTCA)	c.323_324ins14;p.Glu109fsX20
		14bp insertion(TTCAGGCACCTTCA)	c.323_324ins14;p.Glu109fsX20
12	2	7bp deletion(GGAGGAC)insertion(T)	c.323_329del7GGAGGACinsT;p.Glu109fs
		7bp deletion(GGAGGAC)insertion(T)	c.323_329del7GGAGGACinsT;p.Glu109fs
13	0	NA	NA

3.3.2.1.1 Characterisation of novel mutations in tbk1 exon 4

3.3.2.1.1.1 Sequence analysis of F1 fish to be taken forward for further investigation

F1 adult fish were fin clipped and genotyped by BslI digest (see Figure (3.15). 29 of F1 showed undigested products and 61 out of 90 progeny showed digested products. These were sequenced for exon 4 to identify frameshift mutations, (see Figure (3.16). Sequence analysis showed that 13 of the 29 carried frameshift mutations, see tables (3.3 &3.4).

In the course of these experiments, we observed a problem with PCR amplification, possibly due to a polymorphism. To overcome this issue new primers were designed that generate a 214 bp PCR product, which is digested to give bands of 128 & 86 bp in wild type, but not digested in homozygotes. Heterozygotes give bands of 214, 128 and 86 bp (see Figure (3.15).

Figure 3. 15 Genotyping of adult F1 *TBK1* exon 4 using to sets of primers. Gel image of new exon 4 *tbk1* genotyping, wild type genotyping show two bands of size 128 & 86 bp, and fish carrying a mutation showing bands 214,128 and 86 bp. Negative controls (no DNA template) were included.

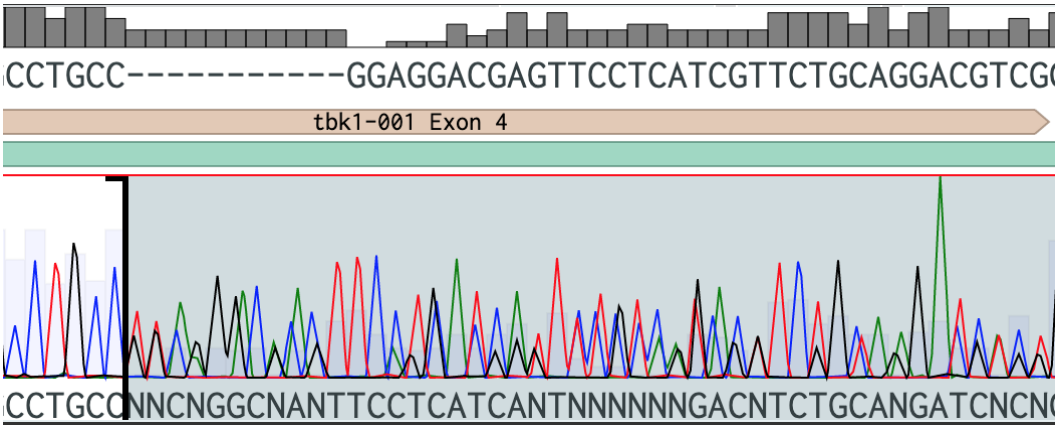

Figure 3. 16 Sequence chromatogram of adult *tbk1* exon4 F1 mutant zebrafish. The double read shows the location of the mutant allele. Deconvolution of these 2 sequences demonstrated that this mutation was a 14 bp insertion

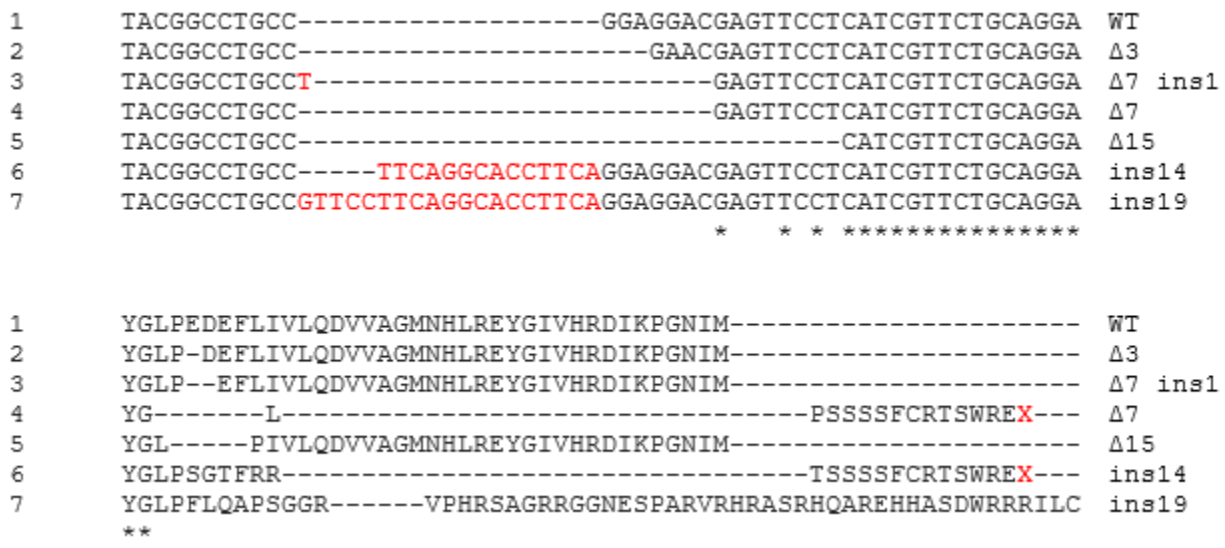

Figure 3. 17 Mutations in targeted *tbk1* exon4 F1 zebrafish adults. DNA and protein translation sequences of F1 mutant alleles. The wild type reference sequence is labelled 1. Samples 2-7 represent independent F1 fish. Deleted and inserted nucleotides, as well as novel stop codons, are highlighted in red.

Table 3. 3 Summary of mutations found in F1 zebrafish.

# of TBK1-Ex4	Result	Mutation
3	15bp deletion(GGAGGACGAGTTCCT)	c.317_332del15; p.Leu106_Asp110del
5	7 bp deletion(GGAGGAC) insertion (T)	c.323_329del7GGAGGAC insT; p.Glu109fs
11	14 bp insertion(TTCAGGCACCTTCA)	c.323_324ins14; p.Glu109fsX20
2	7 bp deletion(GGAGGAC)	c.323_329del7; p.Glu109fsX13
1	3bp deletion (GTT)	c.336_339delGTT; p.Glu112del

Table 3. 4 Percentage of F1 zebrafish carrying frameshift mutations

	TBK1-Ex4
#of Zebrafish	90
#of mutated	29
#of Negative	61
Percentage	32.22%
#of Frameshift mutation	13
Percentage	45%

Zebrafish carrying the c.323_324ins14 p;Glu109fsX20 frameshift mutation were out crossed with wild type to generate the F2 generation. This allele was given the name *tbk1*^{SH643}. To generate F3 animals, F2 fish were crossed to either NFkB:GFP or wild type (AB).

3.3.2.2 *tbk1* mRNA expression level in *tbk1*^{SH643} zebrafish

The first step to evaluate the new mutation (c.323_324ins14; p.Glu109fsX20) is to measure the *tbk1* mRNA levels in homozygous mutants. F3 fish were in crossed, and RNA was extracted from 10 individual offspring of each genotype from three independent parents at two time points- day 5 and day 12. At day 5, qRT-PCR was performed to measure relative *tbk1* mRNA levels in *tbk1*$^{+/+}$, *tbk1*$^{+/SH643}$ and *tbk1*$^{SH643/SH643}$ offspring.

One-way ANOVA reveal a significant difference between the 3 groups (p=0.0026) and Tukey's multiple comparisons test show a significant difference between wild type and homozygous (p=0.0252). At 12 dpf one-way ANOVA also shows a significant difference between the 3 groups (p=0.0007) and Tukey's multiple comparisons test showed a significant difference between wild type and heterozygous (p=0.0088) as well as wild type and homozygous progeny (p=0.0006), (see Figure (3.18).

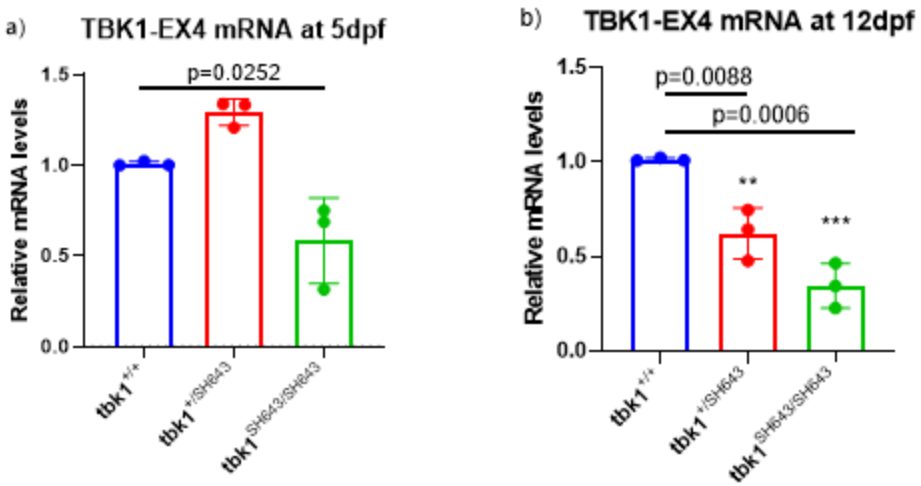

Figure 3. 18 *tbk1* mRNA expression level in *tbk1*^{SH643} zebrafish. *tbk1* expression levels were determined relative to *eef1α1*b and normalised to the level in wild type which was set to 1. a) Relative *tbk1* mRNA level in 5 dpf *tbk1*$^{SH643/SH643}$ shows a significant reduction compared to *tbk1*$^{+/+}$ siblings p=0.0252. b) Significant differences in the relative *tbk1* mRNA level in 12 dpf *tbk1*$^{SH643/SH643}$ (p=0.0088), and *tbk1*$^{+/SH643}$ (p=0.0006 compared *tbk1*$^{`+/+}$ siblings (One-way ANOVA with Tukey's multiple comparisons test). Each point represents a pool of 10 larvae from 3 independent group.

3.4 Investigating whether *tbk1* mutants have an ALS-like motor dysfunction phenotype

Due to anatomical and functional similarities zebrafish have been shown to provide excellent vertebrate models of ALS. In particular due to their small size and rapid development it is possible to investigate effects of gene mutations on motor function (swimming) in microtiter plate assays.

3.4.1 Characterisation of swimming behaviour in *tbk1*^{SH570} larvae

Mutation of the zebrafish *tbk1* gene is expected to be deleterious to motor neurons, but it is not clear whether this effect will be detectable in early life stages. Swimming behaviour of the *tbk1* zebrafish progeny was assessed at different ages using Viewpoint video tracking to study locomotor behaviour. Their swimming and their response to light/dark stimulation was assessed and analysed (section 2.2.11.2). It is known that 5 day old zebrafish embryos respond to light/dark switching by increased swimming in the dark (Zhou et al., 2014). We used this property to investigate darkness-provoked swimming in *tbk1* mutants. Using the Viewpoint analysis system, we quantified the following swimming parameters:

Active duration - the total time spent moving during a 5 minute period.

Slow movement - distance moved at a speed between 3 - 6.4 mm/second.

Fast movement - distance moved at a speed >6.4 mm/second.

Total distance- total distance moved in a 5-minute period.

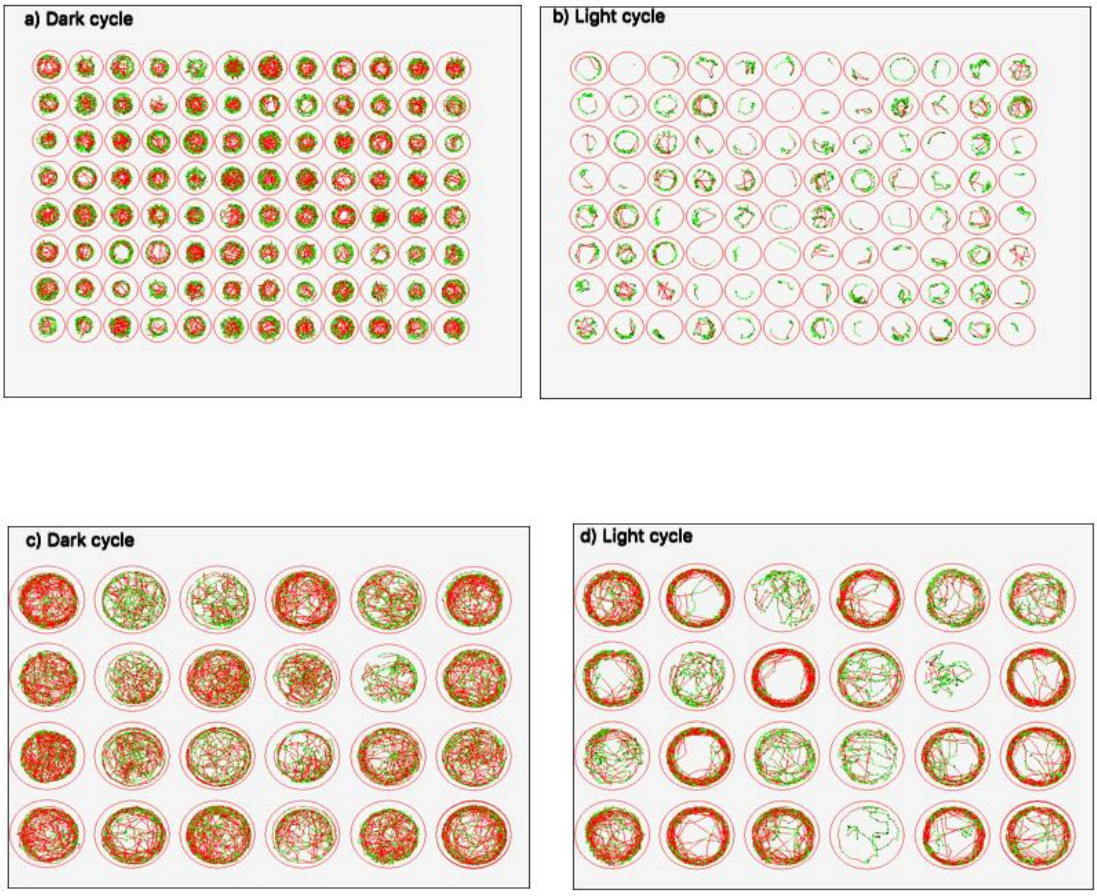

Figure 3. 19 Examples of swimming behaviour in *tbk1* zebrafish. a) 5 day old larvae in a 96 well plate (single larva in each well) showing the swimming of zebrafish in the dark cycle (0-300 seconds) b) the same plate showing swimming of zebrafish in the light cycle (300-600 seconds) c) 8 day old larvae in a 24 well plate showing the swimming of zebrafish in the dark cycle (0-300 seconds) d) is the same plate showing swimming of zebrafish in the light cycle (300-600 seconds). In all cases a red line represents fast movement, and a green line represents slow movement.

3.4.1.1 Swimming Analysis

Analysis was performed on different batches of larvae used at 5, 8, 12, 14 and 19 days of age. For 5 days we used 96 well plates and for 8, 12, 14 and 19 days we used 24 well plates. A summary of the numbers and genotypes is given in Table 3.5.

Table 3. 5 Summary of zebrafish used for swimming analysis

Age	Number of independent experiments	Wild type	Heterozygous	Homozygous
5 Days	3	54	120	83
8 Days	2	24	48	25
12 Days	2	28	48	20
14 Days	1	11	21	15
19 Days	1	9	27	5

3.4.1.1.1 Active duration

Figure (3.20) shows the active duration data. In all cases individual data points were obtained for each embryo to generate the first graph in each panel (i.e. a, d, g, j, m). This allows us to observe the overall response of the different genotype groups to light/dark switching (see Table 3.5). Active duration in the light and dark is shown in the remaining two panels for each age. Wild type siblings show increased swimming in darkness at 5 and 8 days old, but this response is lost from 12 days onwards. In *tbk1*$^{SH570/SH570}$ the response to light>dark switching continues until day 12. At 8 and 12 days old one-way ANOVA shows significant changes in swimming in the light and in the dark, and Tukey's multiple comparison test is also significant when comparing *tbk1*$^{+/+}$ and *tbk1*$^{SH570/SH570}$ siblings under these conditions (3.6). The largest difference in active duration is a 30% reduction observed in *tbk1*$^{SH570/SH570}$ in the light on day 12. At 14 and 19 days old one-way ANOVA shows no significant changes between wild type and homozygous in the active duration light and dark cycles since it was underpowered.

Table 3. 6 One-Way ANOVA and Tukey's multiple comparisons test p-value of active duration

Age	One way ANOVA between group (p-value)		Tukey's multiple comparisons test between Wild type & Homozygous (p-value)	
	Dark	Light	Dark	Light
5 days	0.2965	0.0119	0.5878	0.1930
8 days	0.0081	0.0001	0.0270	0.0004
12 days	0.0133	0.0002	0.0095	0.0016
14 days	0.4786	0.0014	0.9969	0.0779
19 days	0.2871	0.1534	0.8150	0.2392

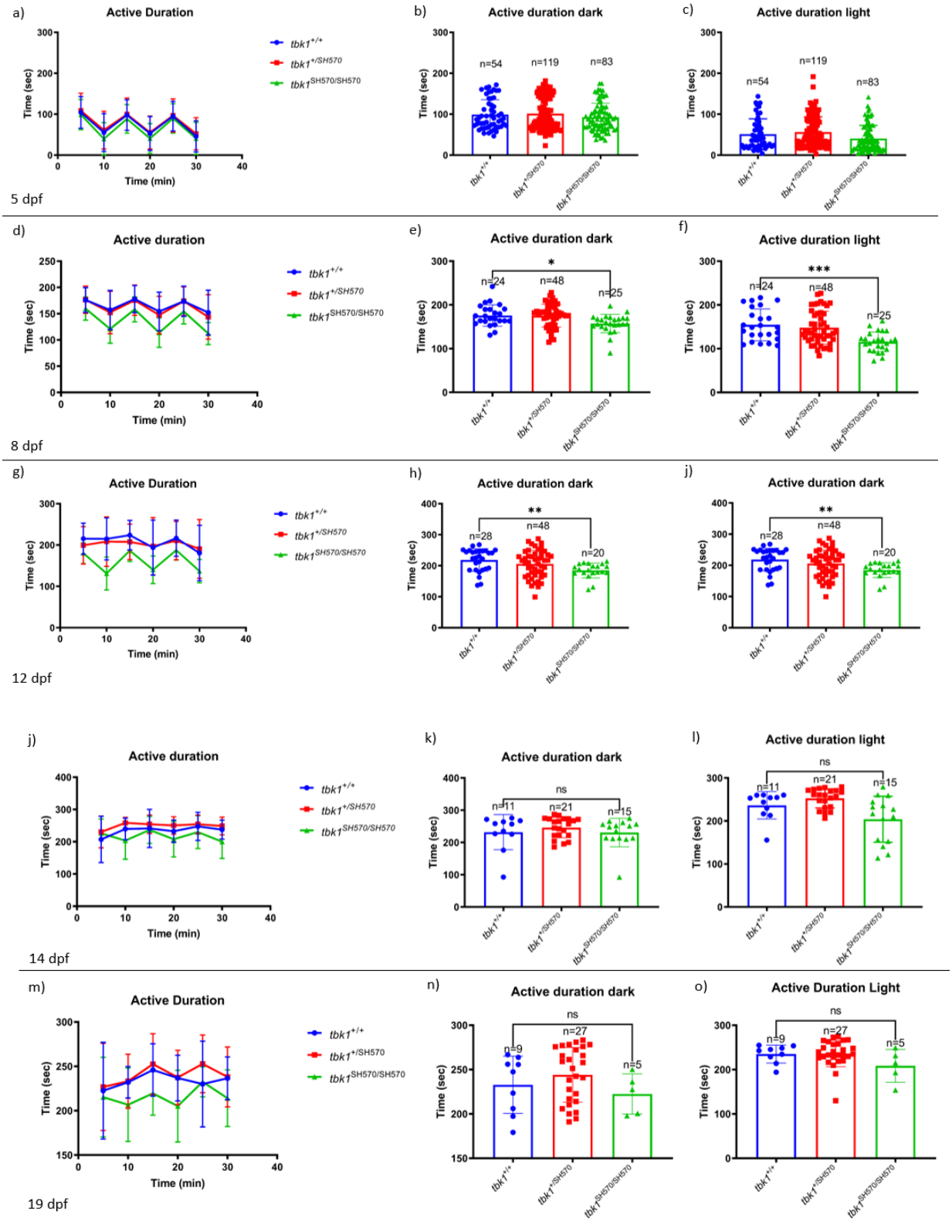
a)
Active Duration
Time (sec)
Time (min)
tbk1+/+
tbk1+/SH570
tbk1SH570/SH570
5 dpf
b)
Active duration dark
n=54
n=119
n=83
c)
Active duration light
n=54
n=119
n=83
d)
Active duration
8 dpf
e)
Active duration dark
*
n=24
n=48
n=25
f)
Active duration light
***
n=24
n=48
n=25
g)
Active Duration
12 dpf
h)
Active duration dark
**
n=28
n=48
n=20
j)
Active duration dark
**
n=28
n=48
n=20
j)
Active duration
14 dpf
k)
Active duration dark
ns
n=11
n=21
n=15
l)
Active duration light
ns
n=11
n=21
n=15
m)
Active Duration
19 dpf
n)
Active duration dark
ns
n=9
n=27
n=5
o)
Active Duration Light
ns
n=9
n=27
n=5

Figure 3. 20 Active duration data for 5, 8, 12, 14 and 19 day old *tbk1* zebrafish. a) Cumulative plots of 5 day old zebrafish progeny for active duration during dark light switching. b) Histogram of 5 day old zebrafish for active duration in dark cycles. c) Histogram of 5 day old zebrafish for active duration in light cycles. d) Cumulative plots of 8 day old zebrafish progeny for active duration for dark light switching. e) Histogram of 8 day old zebrafish for active duration in dark cycles shows significant difference between wild type and homozygous (p=0.027). f) Histogram of 8 day old zebrafish for active duration in light cycles shows significant difference between wild type and homozygous (p=0.0004). g) Cumulative plots of 12 day old zebrafish progeny for active duration for dark light switching. h) Histogram of 12 day old zebrafish for active duration in dark cycles shows significant difference between wild type and homozygous (p=0.0095). i) Histogram of 12day old zebrafish for active duration in light cycles shows significant difference between wild type and homozygous (p=0.0016). j) Cumulative plots of 14 day old zebrafish progeny for active duration for dark light switching. k) Histogram of 14 day old zebrafish for active duration in dark cycles. l) Histogram of 14 day old zebrafish for active duration in light cycles. m) Cumulative plots of 19 day old zebrafish progeny for active duration for dark light switching. n) Histogram of 19 day old zebrafish for active duration in dark cycles. o) Histogram of 19 day old zebrafish for active duration in light cycles.

3.4.1.1.2 Slow movement

Figure (3.21) shows the distance travelled using slow speed swimming (3 – 6.4 mm/second). In all cases individual data points were obtained for each embryo to generate the first graph in each panel (i.e. a, d, g, j, m). This allows us to observe the overall response of the different genotype groups to light/dark switching (see Table 3.7). The total distance travelled at a slow speed in the light and dark is shown in the remaining two panels for each age. *Tbk1*$^{SH570/SH570}$ larvae show significant reductions in slow swimming in light and dark at 8 days of age. One-way ANOVA for dark cycles shows a significant difference (p=0.0016) between groups for the total distance travelled at a slow speed and Tukey's multiple comparisons test shows a significant difference between wild type and homozygous (p=0.0265). Similarly, one-way ANOVA for light cycles showed a significant difference (p<0.0001) between groups, and Tukey's multiple comparisons test showed a significant difference between wild type and homozygous larvae (p=0.0005). At 12 days *tbk1*$^{SH570/SH570}$ larvae show significant reductions in slow speed swimming in the light. One-way ANOVA for the mean of each larva from three light cycles show a significant difference (p=0.0034) between groups and Tukey's multiple comparisons test show a significant difference between wild type and homozygous (p=0.0174). At 14 and 19 days old one-way ANOVA shows no significant changes between wild type and homozygous in the slow movement light and dark cycles since it was underpowered.

The magnitude of the effect appears larger for swimming in the light. The largest difference in slow swimming is a 23% reduction observed in *tbk1*$^{SH570/SH570}$ in the light on day 12.

Table 3. 7 One-Way ANOVA and Tukey's multiple comparisons test p-value of slow movement.

	One way ANOVA between group (p-value)		Tukey's multiple comparisons test between Wild type & Homozygous (p-value)	
Age	Dark	Light	Dark	Light
5 days	0.1489	0.0114	0.5394	0.1430
8 days	0.0016	0.0001	0.0265	0.0005
12 days	0.6209	0.0034	0.6662	0.0174
14 days	0.3226	0.8859	0.3028	0.9712
19 days	0.8027	0.6794	0.9982	0.9410

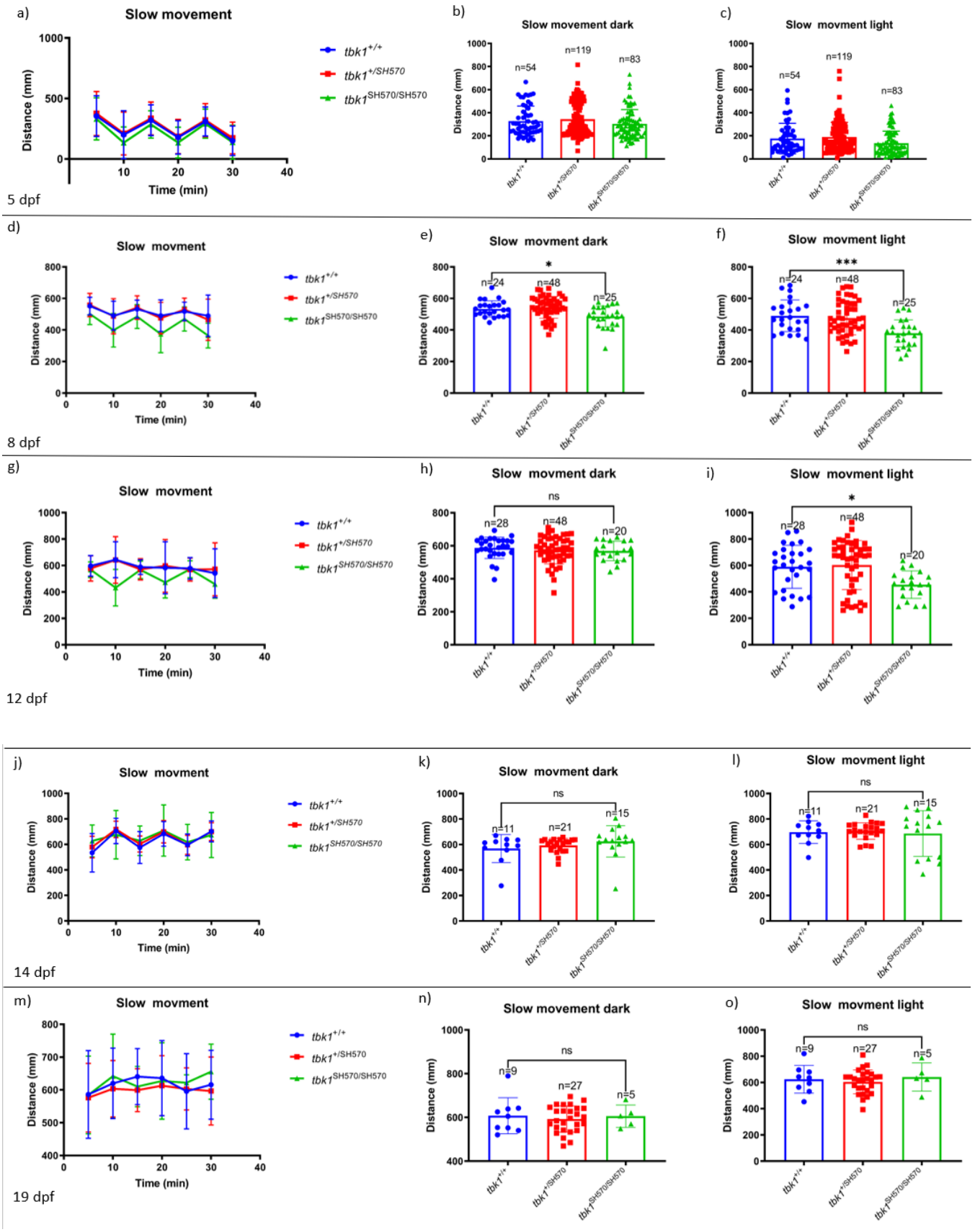
a)
Slow movement
Distance (mm)
Time (min)
tbk1+/+
tbk1+/SH570
tbk1SH570/SH570
b)
Slow movement dark
n=54
n=119
n=83
c)
Slow movment light
n=54
n=119
n=83
5 dpf
d)
Slow movment
e)
Slow movment dark
*
n=24
n=48
n=25
f)
Slow movment light
***
n=24
n=48
n=25
8 dpf
g)
Slow movment
h)
Slow movment dark
ns
n=28
n=48
n=20
i)
Slow movment light
*
n=28
n=48
n=20
12 dpf
j)
Slow movment
k)
Slow movment dark
ns
n=11
n=21
n=15
l)
Slow movment light
ns
n=11
n=21
n=15
14 dpf
m)
Slow movment
n)
Slow movement dark
ns
n=9
n=27
n=5
o)
Slow movment light
ns
n=9
n=27
n=5
19 dpf

Figure 3. 21 Slow movement data for 5, 8, 12, 14 and 19 day old *TBK1* zebrafish. A) Cumulative plots of 5 day old zebrafish progeny for slow movement for dark/light switching. B) Histogram of 5 day old zebrafish for slow movement in dark cycles. C) Histogram of 5 day old zebrafish for slow movement in light cycles. D) Cumulative plots of 8 day old zebrafish progeny for slow movement for dark/light switching.
e) Histogram of 8 day old zebrafish for slow movement in dark cycles shows significant difference between wild type and homozygous (p=0.0265). f) Histogram of 8 day old zebrafish for slow movement in light cycles shows significant difference between wild type and homozygous (p=0.0005). g) Cumulative plots of 12 day old zebrafish progeny for slow movement for dark light switching. H) Histogram of 12 day old zebrafish for slow movement in dark. I) Histogram of 12 day old zebrafish for slow movement in light cycles shows significant difference between wild type and homozygous (p=0.0174). j) Cumulative plots of 14 day old zebrafish progeny for slow movement for dark/light switching. K) Histogram of 14 day old zebrafish for slow movement in dark cycles. L) Histogram of 14 day old zebrafish for slow movement in light cycles. M) Cumulative plots of 19 day old zebrafish progeny for slow movement or dark light switching. N) Histogram of 19 day old zebrafish for slow movement in dark cycles. O) Histogram of 19 day old zebrafish for slow movement in light cycles.

3.4.1.1.3 Fast movement

According to published literature (Zhou et al., 2014) light>dark switching increases fast movement of zebrafish larvae. Figure (3.22) shows the distance travelled by fast swimming (>6.4 mm/second). In all cases individual data points were obtained for each embryo to generate the first graph in each panel (i.e. a, d, g, j, m). This allows us to observe the overall response of the different genotype groups to light/dark switching (see Table 3.7). At 8 days *tbk1*$^{SH570/SH570}$ larvae show significant reductions in fast speed swimming in the light. One-way ANOVA shows a significant difference (p=0.0011) between groups, and Tukey's multiple comparisons test shows a significant difference between wild type and homozygous larvae (p=0.0013). The total distance travelled at a fast speed in the light and dark is shown in the remaining two panels for each age. *Tbk1*$^{SH570/SH570}$ larvae show significant reductions in fast swimming in light and dark at 12 days of age. One-way ANOVA shows a significant difference (p=0.0273) between groups for the total distance at dark cycles, and Tukey's multiple comparisons test shows a significant difference between wild type and homozygous larvae (p=0.0201). Similarly, one-way ANOVA shows a significant difference (p<0.0001) in total distance during light cycles, and Tukey's multiple comparisons test shows a significant difference between wild type and homozygous larvae (p=0.0003). At 14 and 19 days *tbk1*$^{SH570/SH570}$ larvae show significant reductions in fast speed swimming in the light. One-way ANOVA shows significant difference (p=0.0002) between groups and Tukey's multiple comparisons test shows significant difference between wild type and homozygous (p=0.0473) at 14 days old. Likewise, at 19 days old one-way ANOVA shows a significant difference (p<0.0001) between groups and Tukey's multiple comparisons test shows significant difference between wild type and homozygous (p<0.0001).

The magnitude of the effect is larger for swimming in the light. The largest difference in fast swimming is an impressive 82% reduction observed in *tbk1*$^{SH570/SH570}$ in the light on day 12.

Table 3. 8 One-Way ANOVA and Tukey's multiple comparisons test p-value of fast movement.

Age	One way ANOVA between group (p-value)		Tukey's multiple comparisons test between Wild type & Homozygous (p-value)	
	Dark	Light	Dark	Light
5 days	0.7149	0.7338	0.0003	0.3952
8 days	0.3040	0.0011	0.3572	0.0013
12 days	0.0273	<0.0001	0.0201	0.0003
14 days	0.4277	0.0002	0.8313	0.0473
19 days	0.3999	<0.0001	0.9745	<0.0001

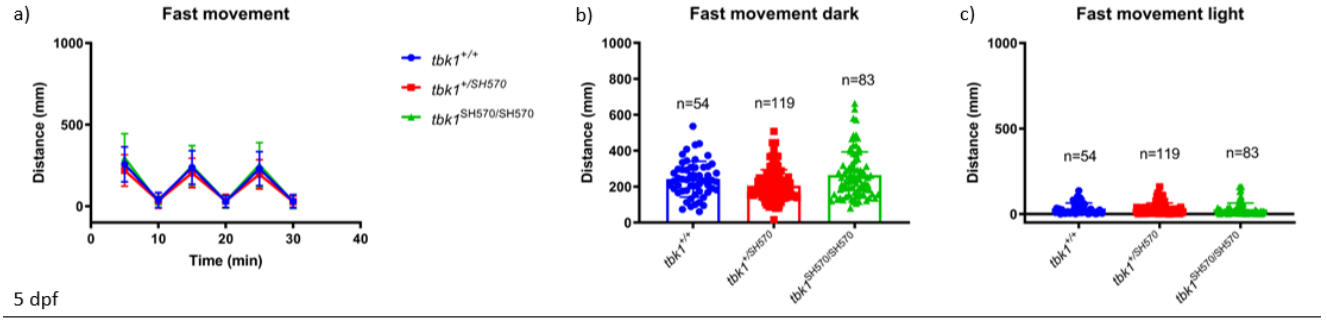
a)
Fast movement
Distance (mm)
Time (min)
tbk1+/+
tbk1+/SH570
tbk1SH570/SH570
b)
Fast movement dark
n=54
n=119
n=83
c)
Fast movement light
5 dpf

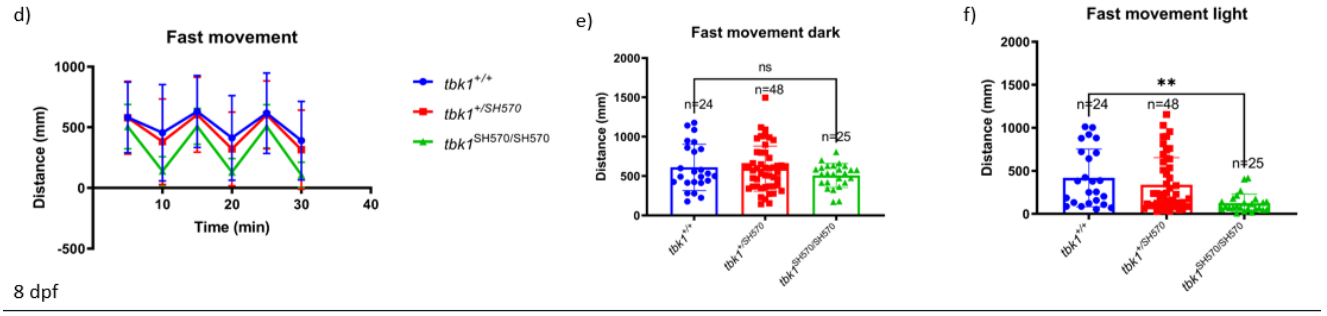
d)
Fast movement
e)
Fast movement dark
ns
n=24
n=48
n=25
f)
Fast movement light
**
8 dpf

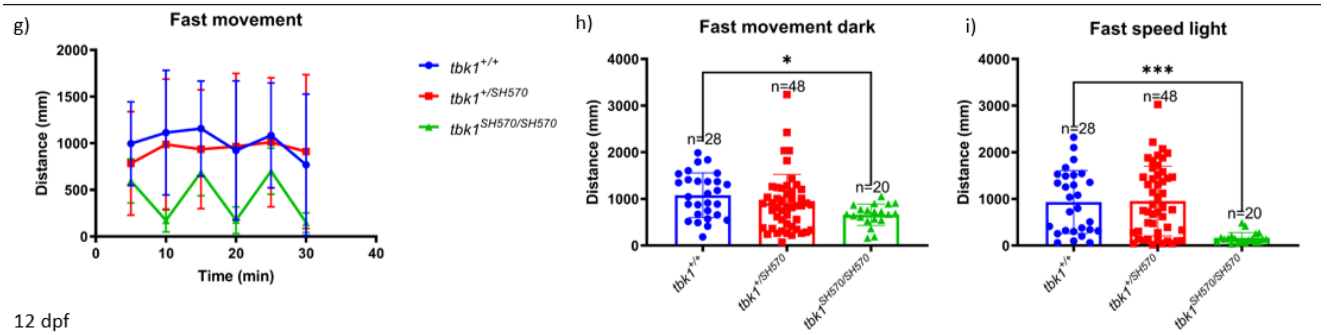
g)
Fast movement
h)
Fast movement dark
*
n=28
n=48
n=20
i)
Fast speed light
***
12 dpf

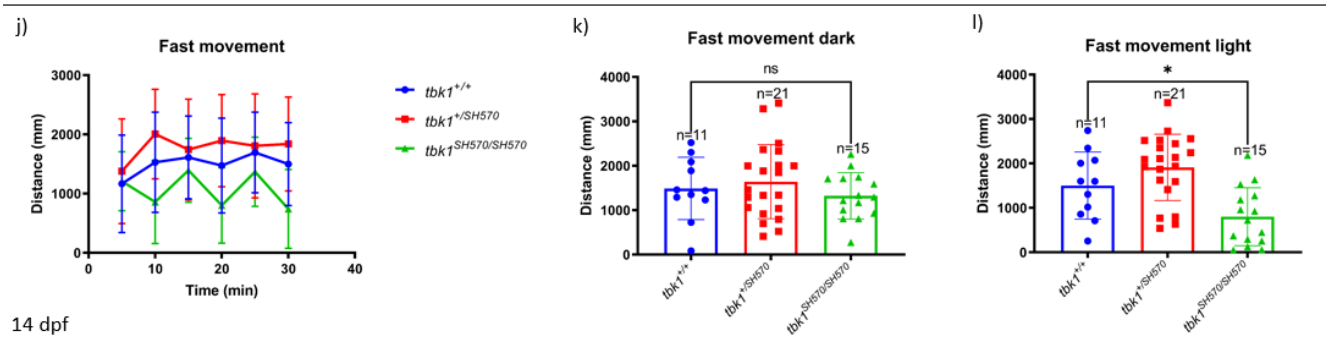
j)
Fast movement
k)
Fast movement dark
ns
n=11
n=21
n=15
l)
Fast movement light
*
14 dpf

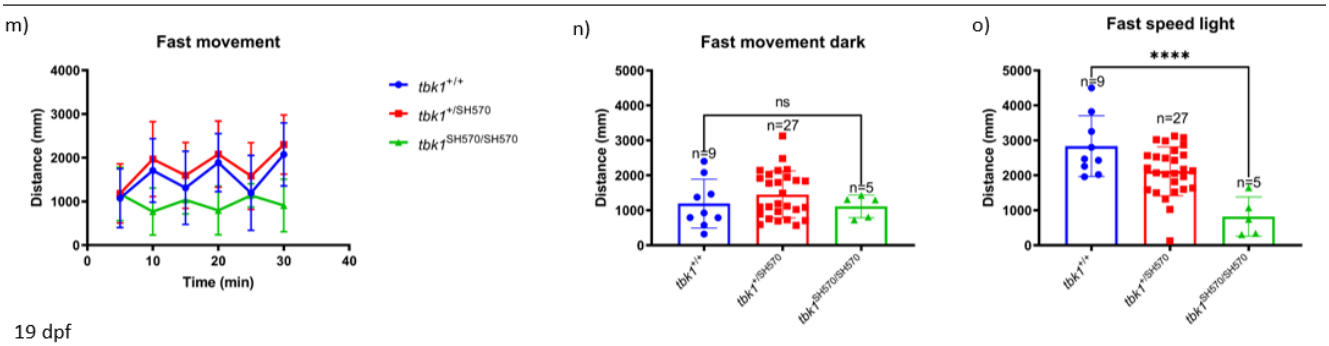
m)
Fast movement
n)
Fast movement dark
ns
n=9
n=27
n=5
o)
Fast speed light
****
19 dpf

Figure 3. 22 Fast movement data for 5, 8, 12, 14 and 19 day old *TBK1* zebrafish. A) Cumulative plots of 5 day old zebrafish progeny for fast movement for dark light switching. B) Histogram of 5 day old zebrafish for fast movement in dark cycles. C) Histogram of 5day old zebrafish for fast movement in light cycles.
d) Cumulative plots of 8 day old zebrafish progeny for fast movement for dark light switching. E) Histogram of 8 day old zebrafish for fast movement in dark cycles. F) Histogram of 8 day old zebrafish for fast movement in light cycles shows significant difference between wild type and homozygous ($p=0.0013$). g) Cumulative plots of 12 day old zebrafish progeny for fast movement for dark light switching. H) Histogram of 12 day old zebrafish for fast movement in dark shows significant difference between wild type and homozygous ($p=0.0201$). i) Histogram of 12 day old zebrafish for fast movement in light cycles shows significant difference between wild type and homozygous ($p=0.0003$). j) Cumulative plots of 14 day old zebrafish progeny for fast movement for dark light switching. K) Histogram of 14 day old zebrafish for fast movement in dark cycles. L) Histogram of 14 day old zebrafish for fast movement in light cycles shows significant difference between wild type and homozygous ($p=0.0473$). m) Cumulative plots of 19 day old zebrafish progeny for fast movement or dark light switching. N) Histogram of 19 day old zebrafish for fast movement in dark cycles. O) Histogram of 19 day old zebrafish for fast movement in light cycles shows significant difference between wild type and homozygous ($p<0.0001$).

3.4.1.1.4 Total distance

Figure (3.23) shows the total distance travelled by in light and dark periods. In all cases individual data points were obtained for each embryo to generate the first graph in each panel (i.e. a, d, g, j, m). This allows us to observe the overall response of the different genotype groups to light/dark switching (see Table 3.9). The total distance travelled is shown in the remaining two panels for each age. *Tbk1*$^{SH570/SH570}$ larvae show significant reductions in total swimming distance in light at all ages, though 14 and 19 days old was underpowered. This reaches significance at 8, 12 and 19 days old. At 8 days old, one-way ANOVA show a significant difference (p=0.0003) between groups and Tukey's multiple comparisons test show a significant difference between wild type and homozygous larvae (p=0.0005). One-way ANOVA shows a significant difference (p<0.0001) between groups and Tukey's multiple comparisons test show a significant difference between wild type and homozygous (p=0.0004) at 12 days old. Similarly, at 19 days old one-way ANOVA shows a significant difference (p=0.0019) between groups and Tukey's multiple comparisons test shows significant difference between wild type and homozygous larvae (p=0.0209). At 12 days old the total distance travelled in the dark was also significantly reduced, one-way ANOVA shows significant difference (p=0.0329) between groups and Tukey's multiple comparisons test show a significant difference between wild type and homozygous (p=0.0245). The magnitude of the effect is larger for swimming in the light. The largest difference in total distance travelled is a 60% reduction observed in *tbk1*$^{SH570/SH570}$ in the light on day 12.

Table 3. 9 One-Way ANOVA and Tukey's multiple comparisons test p-value of total distance

	One way ANOVA between group (p-value)		Tukey's multiple comparisons test between Wild type & Homozygous (p-value)	
Age	Dark	Light	Dark	Light
5 days	0.5432	0.0146	0.9992	0.1379
8 days	0.0973	0.0003	0.1705	0.0005
12 days	0.0329	<0.0001	0.0246	0.0004
14 days	0.5075	0.0003	0.9261	0.0577
19 days	0.4200	0.0019	0.9721	0.0209

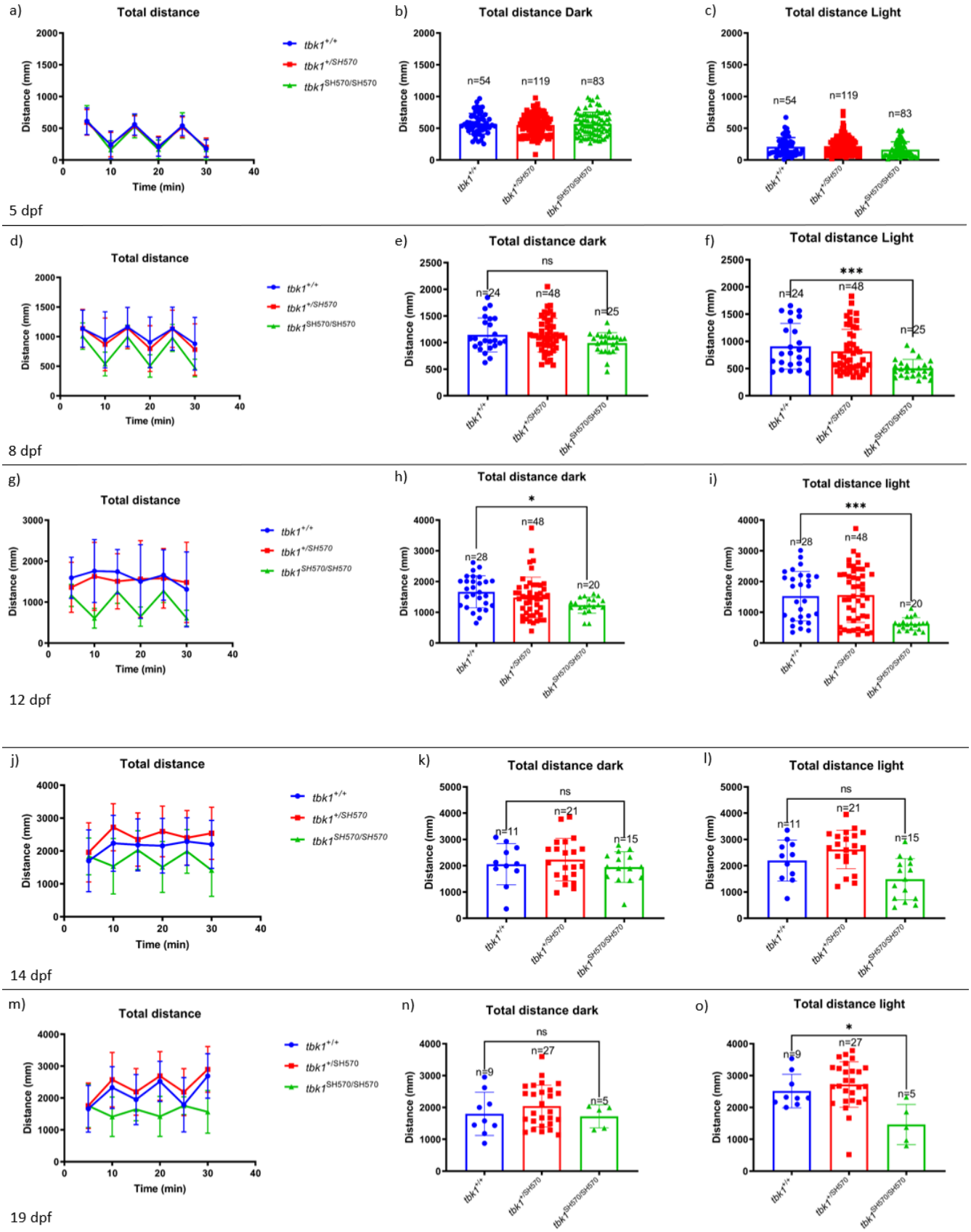
a)
Total distance
Distance (mm)
Time (min)
tbk1+/+
tbk1+/SH570
tbk1SH570/SH570
b)
Total distance Dark
n=54
n=119
n=83
c)
Total distance Light
n=54
n=119
n=83
5 dpf
d)
Total distance
e)
Total distance dark
ns
n=24
n=48
n=25
f)
Total distance Light
***
n=24
n=48
n=25
8 dpf
g)
Total distance
h)
Total distance dark
*
n=28
n=48
n=20
i)
Total distance light
***
n=28
n=48
n=20
12 dpf
j)
Total distance
k)
Total distance dark
ns
n=11
n=21
n=15
l)
Total distance light
ns
n=11
n=21
n=15
14 dpf
m)
Total distance
n)
Total distance dark
ns
n=9
n=27
n=5
o)
Total distance light
*
n=9
n=27
n=5
19 dpf

Figure 3. 23 Total distance data for 5, 8, 12, 14 and 19 day old *TBK1* zebrafish. a) Cumulative plots of 5 day old zebrafish progeny for total distance for dark light switching. b) Histogram of 5 day old zebrafish for total distance in dark cycles. c) Histogram of 5 day old zebrafish for total distance in light cycles. d) Cumulative plots of 8 day old zebrafish progeny for total distance for dark light switching.
e) Histogram of 8 day old zebrafish for total distance in dark cycles. f) Histogram of 8 day old zebrafish for total distance in light cycles shows significant difference between wild type and homozygous ($p=0.0005$). g) Cumulative plots of 12 day old zebrafish progeny for total distance for dark light switching. h) Histogram of 12 day old zebrafish for total distance in dark shows significant difference between wild type and homozygous ($p=0.0246$). i) Histogram of 12 day old zebrafish for total distance in light cycles shows significant difference between wild type and homozygous ($p=0.0004$). j) Cumulative plots of 14 day old zebrafish progeny for total distance for dark light switching. k) Histogram of 14 day old zebrafish for total distance in dark cycles. l) Histogram of 14 day old zebrafish for total distance in light cycles. m) Cumulative plots of 19 day old zebrafish progeny for total distance or dark light switching. n) Histogram of 19 day old zebrafish for total distance in dark cycles. o) Histogram of 19 day old zebrafish for total distance in light cycles shows significant difference between wild type and homozygous ($p<0.0209$).

3.4.1.2 Reduced swimming in 12dpf *tbk1*$^{SH570/SH570}$ larvae

Although swimming studies of *tbk1*$^{SH570/SH570}$ larvae of different ages (5, 8, 12, 14 and 19 dpf) showed significant reductions in swimming at 12 days, we were concerned that the magnitude of the effect may be limited by the total swimming area available as the larvae grow. Therefore, we performed three independents experiments at 12 dpf using 12 well plates, which have double the surface area compared to 24 well plates.
Figure (3.24) shows the four parameters of the swimming study (active duration, slow movement, fast movement and total distance). In all cases individual data points were obtained for each embryo to generate the first graph in each panel (i.e. a, d, g, j). This allows us to observe the overall response of the different genotype groups to light/dark switching. Active duration in the light and dark cycles shows a significant reduction in total swimming duration as One-way ANOVA (p value <0.0001) and Tukey's multiple comparisons test show a significant difference between wild type and homozygous larvae ($p<0.0001$). A significant reduction was observed in the dark light cycles of all the four parameters with One-way ANOVA (p values <0.001) and Tukey's multiple comparisons tests between wild type and homozygous larvae (all $p<0.0001$). The magnitude of the effect is larger for swimming in the light in the fast movement and total distance.

Looking at Figure (3.24 a, d, g and h) it is possible to see that 12 day old wild type and heterozygous zebrafish have lost the response to light/dark switching seen but in the homozygous mutants an increase in swimming in the dark is still observed. The largest difference in fast movement is a 67% reduction observed in *tbk1*$^{SH570/SH570}$ in the light cycles.

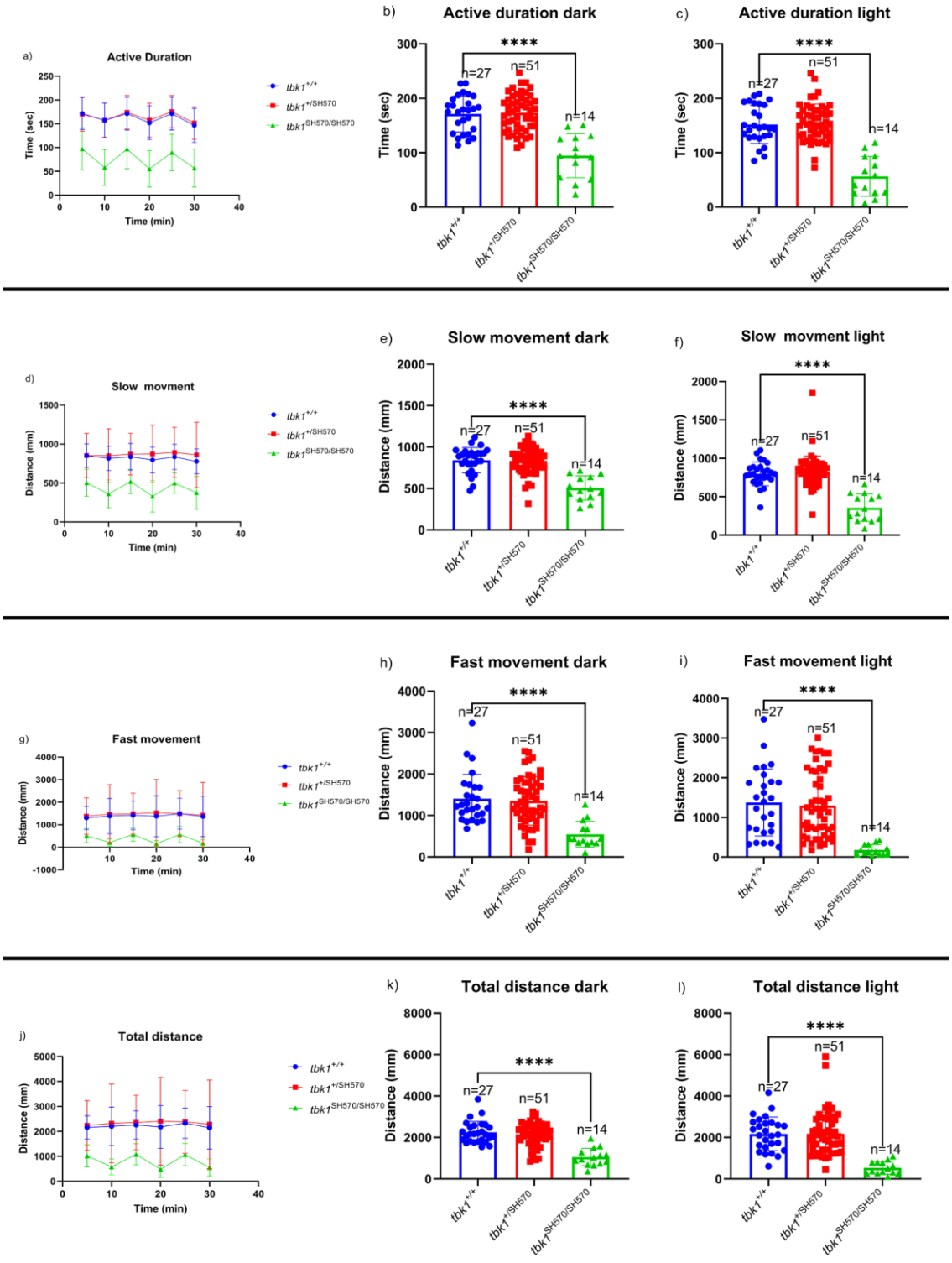
a)
Active Duration
Time (sec)
Time (min)
tbk1+/+
tbk1+/SH570
tbk1SH570/SH570
b)
Active duration dark
c)
Active duration light
d)
Slow movment
Distance (mm)
e)
Slow movement dark
f)
Slow movment light
g)
Fast movement
h)
Fast movement dark
i)
Fast movement light
j)
Total distance
k)
Total distance dark
l)
Total distance light
****
n=27
n=51
n=14

Figure 3. 24 **swimming study data for a 12 day old *tbk1*$^{SH570/SH570}$ zebrafish.** a) Cumulative plots of 12 day old zebrafish progeny for active duration during dark light switching. b) Histogram of 12 day old zebrafish for active duration in dark cycles shows significant difference between wild type and homozygous ($p<0.0001$). c) Histogram of 12day old zebrafish for active duration in light cycles shows significant difference between wild type and homozygous ($p<0.0001$). d) Cumulative plots of 12 day old zebrafish progeny for slow movement during dark light switching. e) Histogram of 12 day old zebrafish for slow movement in dark cycles shows significant difference between wild type and homozygous ($p<0.0001$). f) Histogram of 12day old zebrafish for slow movement in light cycles shows significant difference between wild type and homozygous ($p<0.0001$). Cumulative plots of 12 day old zebrafish progeny for fast movement during dark light switching. h) Histogram of 12 day old zebrafish for fast movement in dark cycles shows significant difference between wild type and homozygous ($p<0.0001$). i) Histogram of 12day old zebrafish for fast movement in light cycles shows significant difference between wild type and homozygous ($p<0.0001$). j) Cumulative plots of 12 day old zebrafish progeny for total distance during dark light switching. k) Histogram of 12 day old zebrafish for total distance in dark cycles shows significant difference between wild type and homozygous ($p<0.0001$). l) Histogram of 12day old zebrafish for total distance in light cycles shows significant difference between wild type and homozygous ($p<0.0001$).

3.4.1.3 Reduced swimming in 5dpf *tbk1*$^{SH570/SH570}$ in-cross larvae

At 5 dpf the *tbk1* mRNA level was significantly reduced in *tbk1*$^{SH570/SH570}$ in cross progeny whereas in *tbk1*$^{+/SH570}$ in cross homozygous progeny it was not. We believe this may be due to a maternal contribution of wild type *tbk1* mRNA from the oocyte in the *tbk1*$^{+/SH570}$ in cross progeny. To confirm the functional effect of wild type *tbk1* on zebrafish motor function we performed a swim study on 5 dpf *tbk1*$^{SH570/SH570}$ in cross progeny and *tbk1*$^{+/+}$ in cross progeny.

Figure (3.25) shows four parameters of the swimming study (active duration, slow movement, fast movement and total distance). In all cases individual data points were obtained for each embryo to generate the first graph in each panel (i.e. a, d, g, j). This allows us to observe the overall response of the wild type and homozygous larvae to light/dark switching. A significant reduction was observed in the dark and light cycles for all four parameters see table (3.10).

These findings support the idea that loss of wild type maternal *tbk1* mRNA contributes to the phenotype of *tbk1*$^{SH570/SH570}$ in cross progeny at 5 dpf.

Table 3. 10 t test and Welch's correction p-value of 5dpf *tbk1*$^{SH570/SH570}$ in-cross larvae

5days	Unpaired t test with Welch's correction (p-value)	
	Dark	Light
Active duration	<0.0001	<0.0001
Slow movement	0.0005	<0.0001
Fast movement	<0.0001	0.0001
Total distance	<0.0001	<0.0001

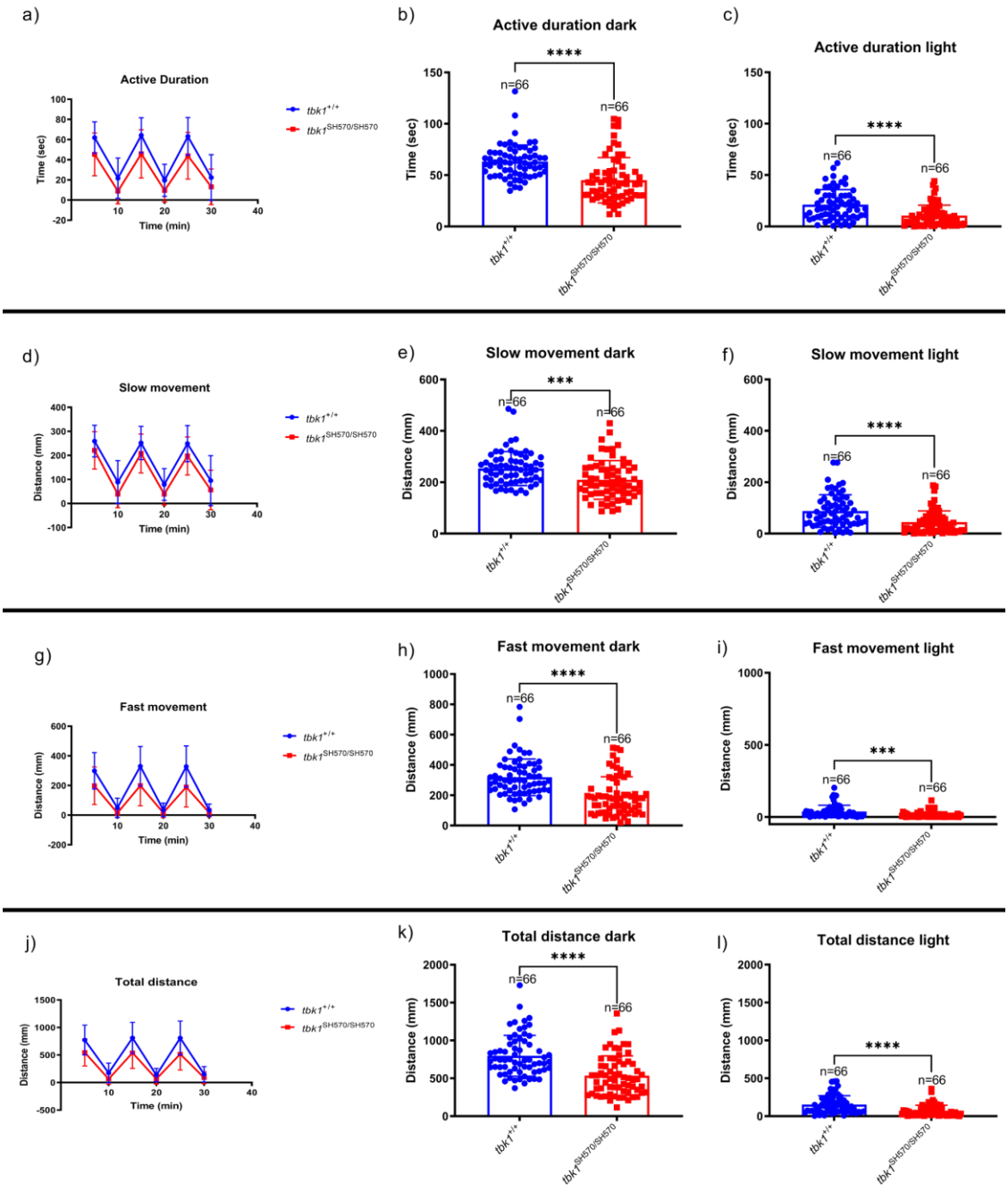

Figure 3. 25 Swimming data for 5 day old *tbk1*$^{SH570/SH570}$ zebrafish derived from homozygous mutant parents. a) Cumulative plots of 5 day old zebrafish in cross progeny for active duration during dark light switching. b) Histogram of 5 day old zebrafish for active duration in dark cycles shows a significant difference between wild type and homozygous (p=0.0001). c) Histogram of 5day old zebrafish for active duration in light cycles shows a significant difference between wild type and homozygous (p<0.0001). d) Cumulative plots of 5 day old zebrafish in cross progeny for slow movement during dark light switching. e) Histogram of 5 day old zebrafish for slow movement in dark cycles shows a significant difference between wild type and homozygous (p=0.0005). f) Histogram of 5 day old zebrafish for slow movement in light cycles shows a significant difference between wild type and homozygous (p<0.0001). g) Cumulative plots of 5 day old zebrafish in cross progeny for fast movement during dark light switching.

h) Histogram of 5 day old zebrafish for fast movement in dark cycles shows a significant difference between wild type and homozygous larvae ($p<0.0001$). i) Histogram of 5 day old zebrafish for fast movement in light cycles shows a significant difference between wild type and homozygous larvae ($p<0.0001$). j) Cumulative plots of 5 day old zebrafish in cross progeny for total distance during dark light switching. k) Histogram of 5 day old zebrafish for total distance in dark cycles shows a significant difference between wild type and homozygous larvae ($p=0.0001$). l) Histogram of 5 day old zebrafish for total distance in light cycles shows a significant difference between wild type and homozygous larvae ($p<0.0001$).

3.4.2 Reduced swimming in 12dpf *tbk1*$^{SH643/SH643}$ larvae

To confirm that the *tbk1*^{SH643} mutant allele causes a similar swimming phenotype to *tbk1*^{SH570} we investigated the response of *tbk1*$^{+/SH643}$ in cross progeny to light/dark switching in a 12 well plate. Due to time limitations, we were only able to perform one repeat of this experiment. The Viewpoint apparatus was used to study the same four swimming parameters (active duration, slow movement, fast movement and total distance).

Figure (3.26) shows that in all cases individual data points were obtained for each embryo to generate the first graph in each panel (i.e. a, d, g, j). This allows us to observe the overall response of the different genotype groups to light/dark switching. All parameters were statistically significant when tested using one-way ANOVA (Table 3.11). Tukey's multiple comparison tests showed that *tbk1*$^{SH643/SH643}$ showed significantly reduced swimming duration and movement for all parameters when compared to *tbk1*$^{+/+}$ siblings. Interestingly, fast movement in the light showed the most dramatic reduction of all parameters in *tbk1*$^{SH643/SH643}$ larvae. This precisely phenocopies the effect of the *tbk1*^{SH570} allele.

Table 3. 11 One-Way ANOVA and Tukey's multiple comparisons test p-value of 12dpf *tbk1*$^{SH643/SH643}$ larvae

12days	One way ANOVA between groups (p-value)		Tukey's multiple comparisons test between wild type and homozygous (p-value)	
	Dark	Light	Dark	Light
Active duration	0.0001	<0.0001	0.0029	0.0014
Total distance	0.0396	0.0035	0.0378	0.0230
Slow movement	0.0118	<0.0001	0.0167	0.0008
Fast movement	0.0077	<0.0001	0.0100	0.0016

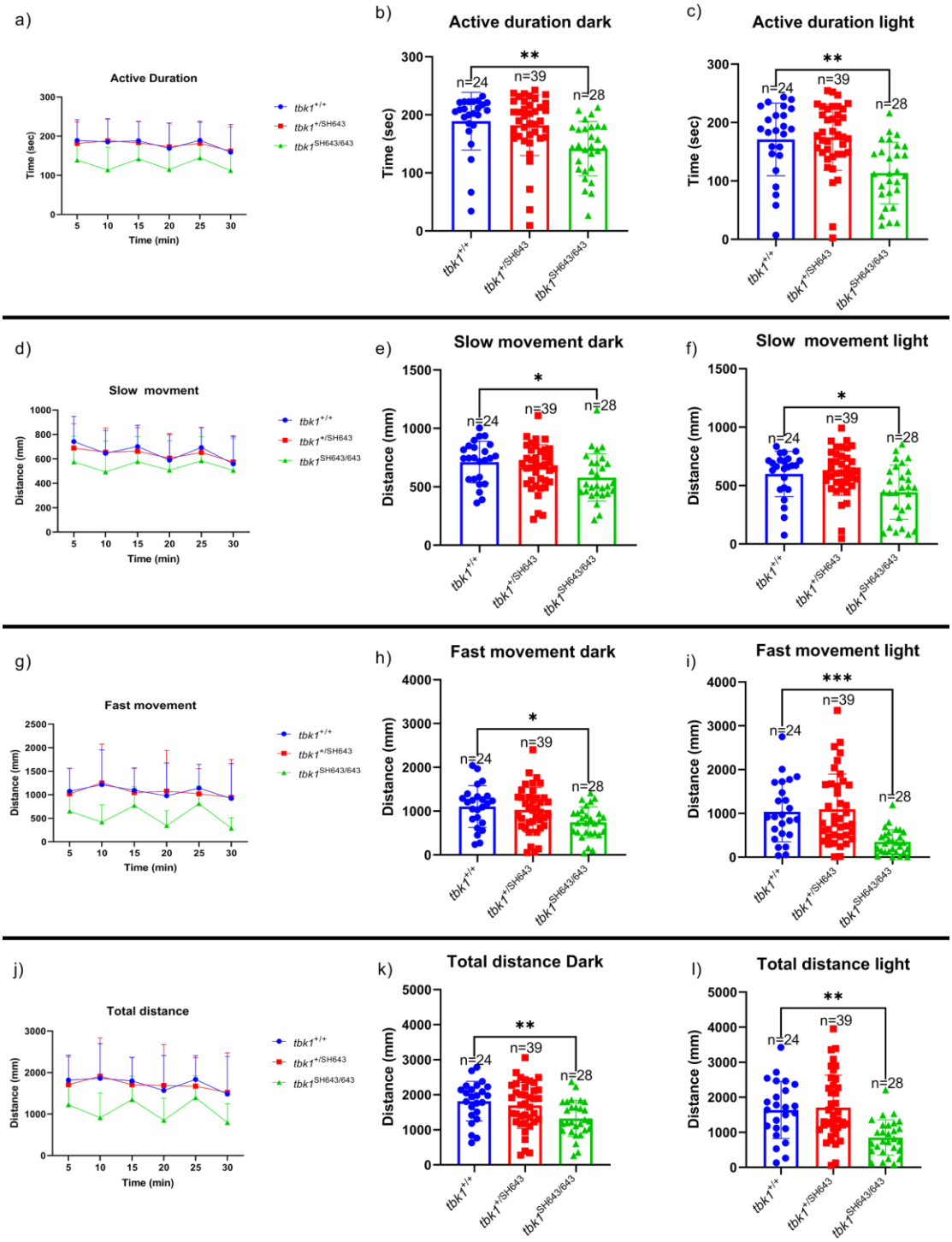

Figure 3. 26 Swimming data for 12 day old *tbk1*$^{SH643/SH643}$ zebrafish. a) Cumulative plots of 12 day old zebrafish progeny for active duration during dark light switching. b) Histogram of 12 day old zebrafish for active duration in dark cycles shows a significant difference between wild type and homozygous larvae (p=0.0029).

c) Histogram of 12 day old zebrafish for active duration in light cycles shows a significant difference between wild type and homozygous larvae ($p=0.0014$). d) Cumulative plots of 12 day old zebrafish progeny for slow movement during dark light switching. e) Histogram of 12 day old zebrafish for slow movement in dark cycles shows a significant difference between wild type and homozygous larvae ($p=0.0378$). f) Histogram of 12 day old zebrafish for slow movement in light cycles shows a significant difference between wild type and homozygous larvae ($p=0.0230$). Cumulative plots of 12 day old zebrafish progeny for fast movement during dark light switching. h) Histogram of 12 day old zebrafish for fast movement in dark cycles shows a significant difference between wild type and homozygous larvae ($p=0.0167$). i) Histogram of 12 day old zebrafish for fast movement in light cycles shows a significant difference between wild type and homozygous larvae ($p=0.0008$). j) Cumulative plots of 12 day old zebrafish progeny for total distance during dark light switching. k) Histogram of 12 day old zebrafish for total distance in light cycles shows a significant difference between wild type and homozygous larvae ($p<0.0100$). l) Histogram of 12 day old zebrafish for total distance in light cycles shows a significant difference between wild type and homozygous larvae ($p<0.0016$).

3.4.3 Reduced swimming endurance in adult *tbk1*$^{SH570/SH570}$ zebrafish

We observed a swimming defect in 12 day old *tbk1*$^{SH570/SH570}$ larvae, but we did not observe any swimming defect in the 12 day old *tbk1*$^{+/SH570}$ larvae. *TBK1* mutations cause autosomal dominant ALS/FTD that manifests in adulthood. Thus, we reasoned that hemizygous mutation of *tbk1* may cause an adult onset swimming phenotype in zebrafish.

In order to investigate this, we used a swim tunnel apparatus (Ramesh et al., 2010) to measure the swimming endurance of adult *tbk1*^{SH570} fish. Critical swimming speed (Ucrit) was determined in sex-matched groups of *tbk1* zebrafish. To account for the known effect of body length on Ucrit (PLAUT, 2000, Chapman et al., 2013) we normalised data to body length (Figure 3.27). A significant reduction in the critical swimming speed of *tbk1* homozygous mutants compared to wild type zebrafish was observed at 6 (One-way ANOVA p=0.0001) and 12 (p=0.0044) months. Tukey's multiple comparison test showed significant differences between wild type and *tbk1*$^{SH570/SH570}$ homozygous siblings at 6 (p=0.0002) and at 12 (p=0.0034) months. Hemizygous mutants did not show a significant difference at either age. To confirm effects on Ucrit were not due to differences in body length we compared length data for all genotype at each age (Figure 3.27). Group sizes at the 12 month time point were smaller as one cohort of fish reached the 12 month timepoint during lockdown when the laboratory was closed.

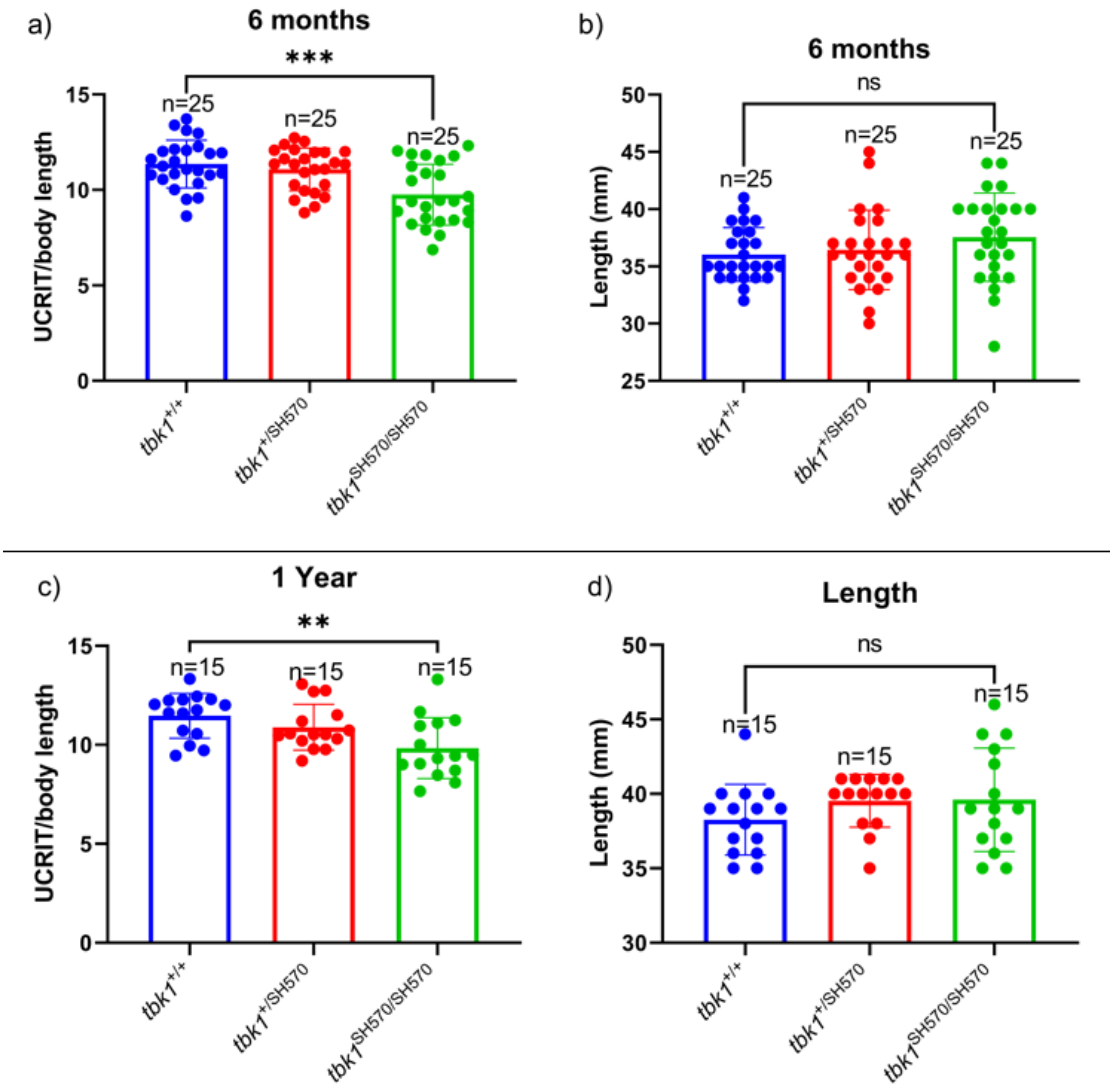

Figure 3. 27 Reduced swimming endurance in adult *tbk1*$^{SH570/SH570}$ zebrafish. a) Histogram of critical swimming speed in 6 month old zebrafish shows a significant difference between wild type and homozygous fish (p=0.0002). b) Histogram of body length in 6 month old zebrafish shows no difference between wild type and homozygous fish. c) Histogram of critical swimming speed in 12 month old zebrafish shows a significant difference between wild type and homozygous fish (p=0.0034). d) Histogram of body length in 12 month old zebrafish shows no difference between wild type and homozygous fish

3.5 Investigating whether *tbk1* mutants have an FTD like phenotype (abnormal social behaviour)

Although precise modelling of FTD in zebrafish is likely to be challenging, zebrafish have been used to model many neurodegenerative disorders including Parkinson's, Huntington's, and Alzheimer's disease as well as behavioural disorders including autism, schizophrenia, anxiety, addiction, psychoses and depression(Cheran et al., 2018, Kalueff et al., 2014, Stewart et al., 2014, Eachus et al., 2017, Chapman et al., 2013). Functional conservation between human disease genes and their zebrafish orthologues can impact the manifestation of pathological, morphological and behavioural phenotypes and the underlying biochemical abnormalities (Xi et al., 2011, Ziv et al., 2013). Thus, we need to assume that *tbk1* functions in conserved biochemical pathways, and equivalent cell types, in the human and zebrafish CNS, in order to affect behaviour. Numerous behavioural studies have been conducted to study zebrafish behaviour such as tests of anxiety, shoaling, social preferences, predator avoidance and many others(Gerlai, 2010, Miller and Gerlai, 2012). To model behavioural aspects of FTD we chose to study abnormal behaviour in zebrafish (Kalueff et al., 2014, Stewart et al., 2014, Miller and Gerlai, 2007, Wright and Krause, 2006). Anxiety can be studied by quantifying thigmotaxis (Schnörr et al., 2012a, Schnörr et al., 2012b), and shoaling behaviour can be used to evaluate abnormal social behaviour in our zebrafish model.

3.5.1 Characterising of thigmotaxis in *tbk1*$^{SH570/SH570}$ larvae

We predicted that mutation of the zebrafish *tbk1* gene may increase anxiety in the zebrafish model. Thigmotactic behaviour was assessed at 8 and 12 days of age. Their swimming and their response to swimming in the centre of the well during light/dark cycles was assessed and analysed (see section 2.2.12.1). It is known that zebrafish tend to swim around the edge of the wells and avoid swimming in the centre of the well in a well illuminated environment (Norton, 2012, Schnörr et al., 2012a, Schnörr et al., 2012b) . We used this property to investigate thigmotaxis in *tbk1* mutants. Using the Viewpoint analysis system, we quantified the proportion of the total time larvae spent swimming in the centre compared to whole well. (See Figure (3.28)

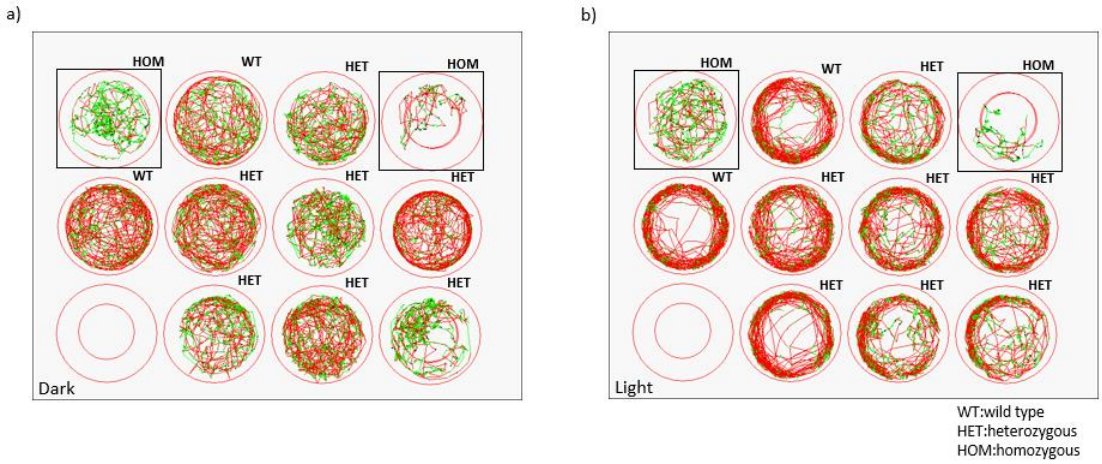

Figure 3. 28 Examples of thagmotaxis in *tbk1* zebrafish. 12 day old larvae in a 12 well plate (single larva in each well) showing the swimming of zebrafish in the center compared to the edge in light cycle. Black squares indicate *tbk1*$^{SH570/SH570}$ larvae. a) Swimming in dark cycles. b) Swimming in light cycles.

3.5.1.1 Thigmotaxis in 8 day old *tbk1*$^{SH570/SH570}$ mutant zebrafish

We first tested thigmotaxis at 8 days of age. Progeny of a *tbk1*$^{+/SH570}$ in cross were placed in a 12 well plate and imaged as described in section 2.2.12.1. We calculated the proportion of time each larva spent swimming in the centre of the well and then genotyped the larvae. Figure (3.29) shows the proportions of time spent swimming in the centre during dark and light cycles. Dark cycles act as a negative control, because the fish are not aware of their location relative to the centre of the well. In darkness there was no significant difference in the time spent swimming in the centre between wild type and homozygous larvae (one-way ANOVA p=0.1353). Interestingly we also saw no significant difference in the time spent in the centre of the well during light cycles (one-way ANOVA p=0.4192), suggesting that at this age zebrafish larvae do not show thigmotaxis under these experimental conditions. Therefore, we decided to look in 12 dpf larvae, an age at which we have already seen a significant effect on motor function.

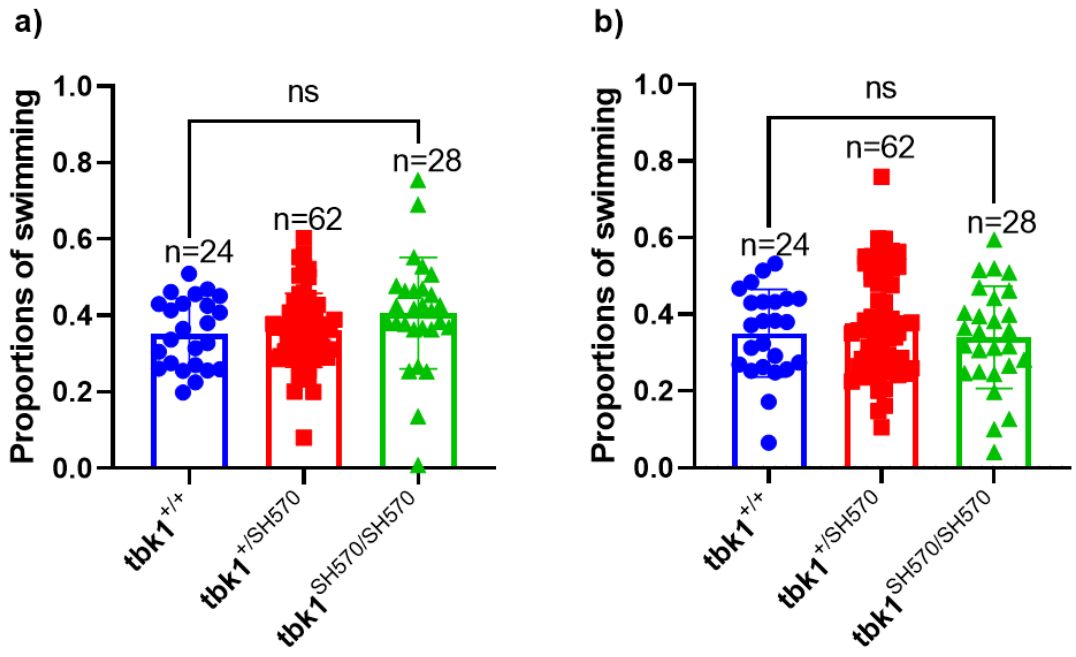

Figure 3. 29 8 day old zebrafish do not show thigmotaxis. No significant difference was seen in thigmotactic behaviour between genotypes in (a) dark cycles (b) light cycles.

3.5.1.2 Reduced thigmotaxis in 12 day old *tbk1*$^{SH570/SH570}$ mutants Zebrafish

Progeny of a *tbk1*$^{+/SH570}$ in cross were placed in a 12 well plate and imaged as described in section 2.2.12.1. We calculated the proportion of time each larva spent swimming in the centre of the well and then genotyped the larvae. Figure (3.30) shows the proportions of time spent swimming in the centre during dark and light cycles. In darkness there was no significant difference in the time spent swimming in the centre between wild type and homozygous larvae (one-way ANOVA p=0.0767). In the light cycles the average proportion of time spent in the centre of the well was significantly different between wild type and homozygous larvae (one-way ANOVA p=0.0073). Tukey's multiple comparisons test showed a significant difference between wild type and homozygous larvae, with *tbk1*$^{SH570/SH570}$ homozygotes showing reduced thigmotaxis (p=0.0052).

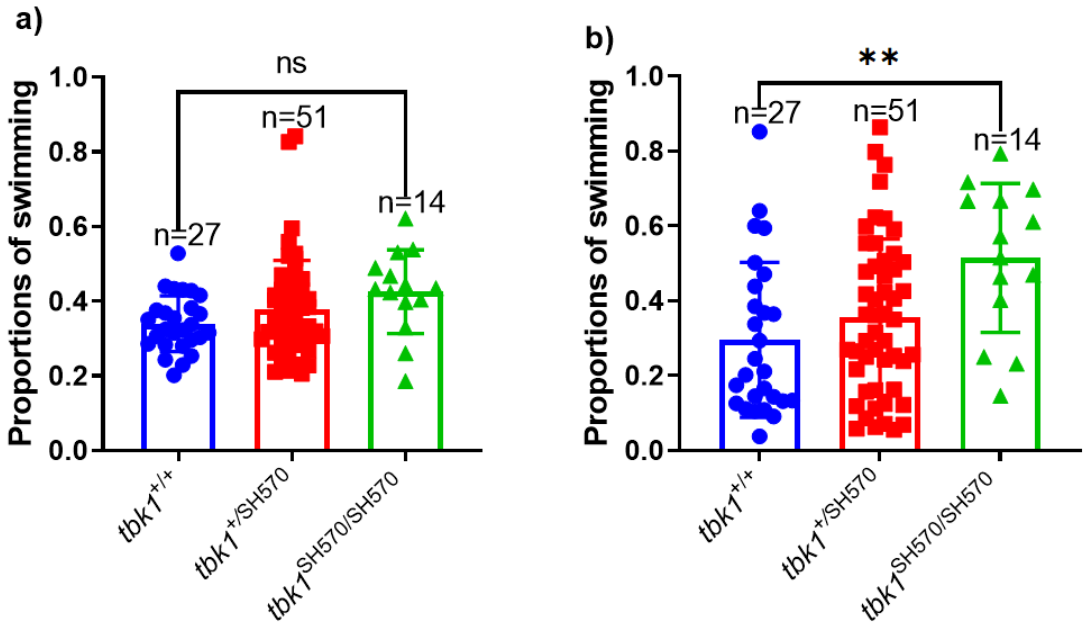

Figure 3. 30 12 day old *tbk1*$^{SH570/SH570}$ zebrafish show reduced thigmotaxis. a) During dark cycles there was no difference between genotypes (p=0.0650). b) During light cycles there was a significant difference in the proportion of time spent swimming in the centre of the field between wild type and homozygous siblings (p=0.0052).

3.5.2 Characterisation of shoaling behaviour in 21 day old *tbk1*^{SH570} zebrafish

Shoaling behaviour of *tbk1*^{SH570} progeny was assessed at 21 days old. It is known that at 21 days old zebrafish tend to shoal and swim in a group (Buske and Gerlai, 2011). Using the Viewpoint analysis system, we quantified the following shoaling parameters during a 10 minute period: Nearest neighbour distance, Inter individual distance, Polarization and Speed. *tbk1*$^{SH570/SH570}$ larvae were selected using NFkB:GFP fluorescence (Table 2.4) and raised to 21 days in a separate tank. A mixture of wild type and heterozygous siblings (weaker GFP fluorescence) were raised in a different tank. As we showed previously (section 2.2.18), *tbk1*$^{SH570/SH570}$ homozygous mutants are smaller, and at 21 days we also observed this phenotype (p=0.0002, (Figure (3.31a). We were concerned that the size of the zebrafish may directly or indirectly affect their shoaling behaviour, therefore from each clutch of larvae we selected the 12 largest homozygotes (Figure (3.31b) for the shoaling study. In this way we did not have a significant difference in size of the groups analysed for shoaling.

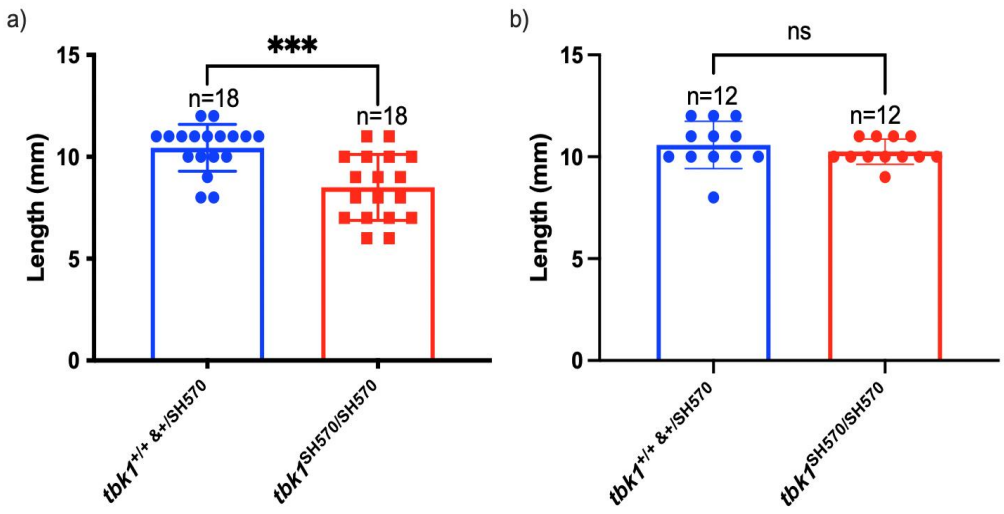

Figure 3. 31 Length of 21 day old *tbk1* zebrafish. a) Length was significantly different between the pooled *tbk1*$^{+/+}$ and *tbk1*$^{+/SH570}$ larvae and the *tbk1*$^{SH570/SH570}$ larvae (p=0.0002) . b) After size selection of the homozygous mutants, the length was no longer significantly different between the two groups.

3.5.2.1 Abnormal shoaling behaviour in 21 day old *tbk1*$^{SH570/SH570}$ Zebrafish

Using Viewpoint software, we analysed shoaling behaviour in groups of 6 *tbk1*$^{SH570/SH570}$ larvae and compared it with groups of 6 pooled *tbk1*$^{+/+}$ and *tbk1*$^{+/SH570}$ siblings. We looked at four shoaling parameters: Nearest neighbor distance, inter individual distance, speed, and polarisation. Nearest neighbor distance is the distance between a specified zebrafish and its nearest neighbor, Inter individual distance is the mean distance from a specified zebrafish to all the others, speed is the momentary speed of the fish and polarisation is the magnitude of the mean vector for all the zebrafish, in other words do they swim in the same direction or in opposite directions (Miller and Gerlai, 2007).

Figure (3.32) shows the shoaling data from six independent experiments of 21 day old *tbk1*^{SH570} zebrafish. The nearest neighbour distance shows a significant increase in the *tbk1*$^{SH570/SH570}$ group compared to the pooled *tbk1*$^{+/+}$ and *tbk1*$^{+/SH570}$ siblings (Figure (3.32a), Welch's t test p=0.0051). Inter individual distance also shows a significant increase in the *tbk1*$^{SH570/SH570}$ group (Figure (3.32b), Welch's t test p=0.0227). *tbk1*$^{SH570/SH570}$ larvae show a decrease in polarisation compared to the pooled *tbk1*$^{+/+}$ and *tbk1*$^{+/SH570}$ siblings (Figure (3.32c), Welch's t test p=0.0208). Lastly, and in keeping with the previous swimming analysis, there was a significant decrease in the speed of the *tbk1*$^{SH570/SH570}$ group compared to the pooled *tbk1*$^{+/+}$ and *tbk1*$^{+/SH570}$ siblings (Figure (3.32d), Welch's t test p=0.0166). Thus, *tbk1*^{SH570} homozygous mutants appear to show altered shoaling behaviour, which indicates aberrant social behaviour. Because we pooled wild type and heterozygous mutants, we are unable to determine if the heterozygotes show any difference in shoaling.

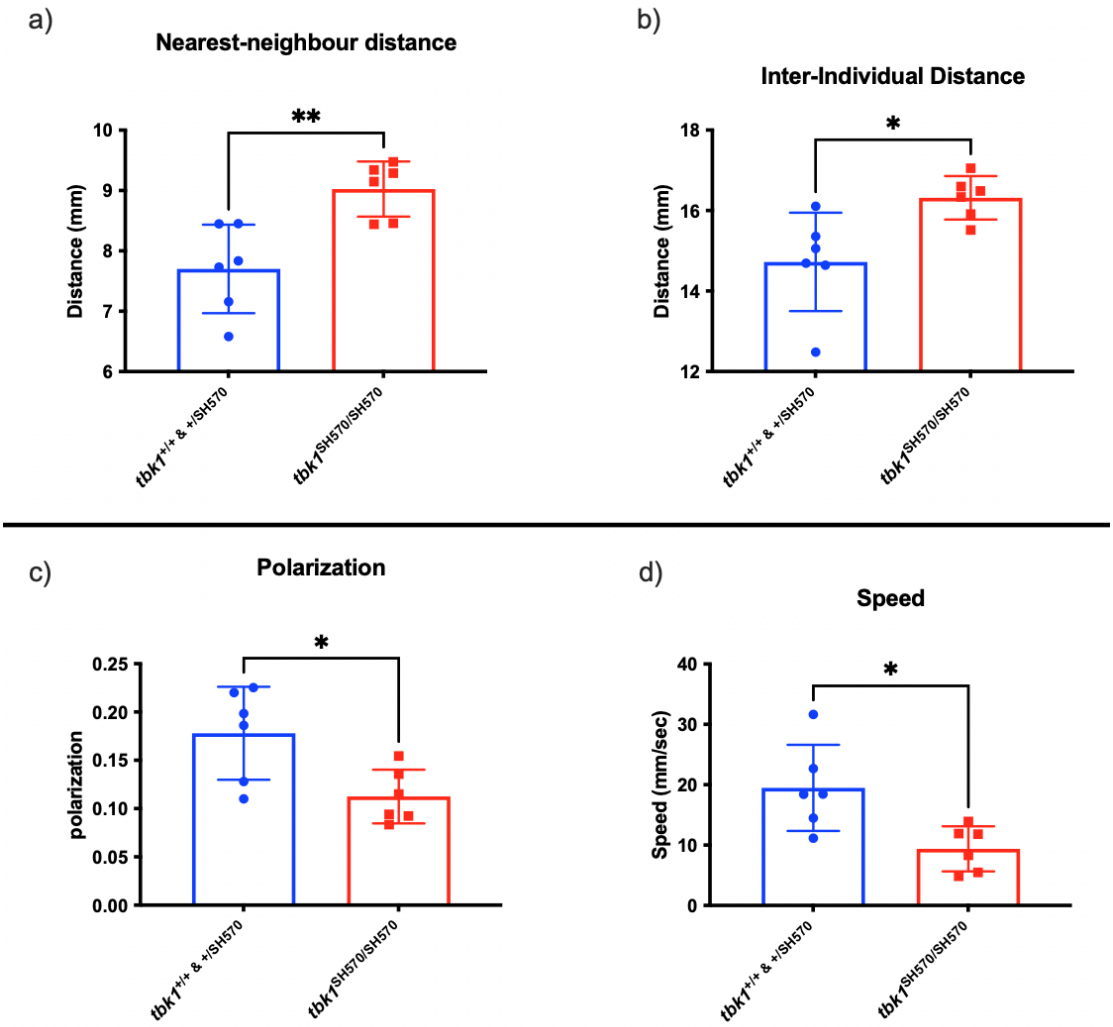

Figure 3. 32 *tbk1*$^{SH570/SH570}$ homozygotes show abnormal shoaling behaviour at 21 days old. a) Histogram of nearest neighbour distance shows a significant difference between *tbk1*$^{+/+}$/*tbk1*$^{SH570/+}$ and *tbk1*$^{SH570/SH570}$ (p=0.0051). b) Histogram of inter individual distance shows a significant difference between *tbk1*$^{+/+}$/ *tbk1*$^{SH570/+}$ and *tbk1*$^{SH570/SH570}$ (p=0.0270). c) Histogram of polarisation shows a significant difference between tbk1$^{+/+}$/*tbk1*$^{SH570/+}$ and *tbk1*$^{SH570/SH570}$ (p=0.0208). d) Histogram of speed shows a significant difference between *tbk1*$^{+/+}$/*tbk1*$^{SH570/+}$ and *tbk1*$^{SH570/SH570}$ (p=0.0166). each point represents an independent experiments.

3.6 Discussion

Our hypothesis is that *TBK1* mutations cause ALS/FTD by disrupting signaling pathways regulated by *TBK1*. To address that we first aimed to determine whether *tbk1* loss of function in zebrafish leads to the development of ALS/FTD related phenotypes. Using CRISPR/Cas9 genome editing we were able to introduce a frameshift mutation in coiled coil domain (*tbk1*^{SH570}) and the kinase domain (*tbk1*^{SH643}) of the *tbk1* gene.

3.6.1 Generation of the models used in this investigation

At the start of the project, we had available an uncharacterised *tbk1* mutant line that had been previously generated in the laboratory using CRISPR/Cas9 with a gRNA targeting exon 10 (*tbk1*^{SH570}). This region had been chosen on the basis that it had been shown to harbour pathogenic mutations in human ALS/FTD patients (for example c.1349_1352delTTAA p.Ile450LysfsX15 (Freischmidt et al., 2015), and because it contained an appropriate gRNA and PAM site that overlapped a BslI site. The restriction enzyme site is very useful to allow rapid screening during the identification of founder fish, and for genotyping experimental cohorts. Other high throughput methods such as Taqman and KASP genotyping are not optimal for CRISPR/Cas9 induced indel alleles, so the BslI allows us to avoid more expensive or time-consuming protocols such as sequencing or denaturing polyacrylamide gels. Another important feature of exon 10 was the ability to design PCR primers in the flanking intron sequence. Unusually, the zebrafish *tbk1* locus contains considerable amounts of microsatellite sequences and other repeats in the introns, which are very difficult to work around, and have caused considerable problems in the past in our laboratory.

The *tbk1*^{SH570} allele is a 5 bp deletion which leads to a premature stop codon in exon 10. Although this should give rise to either a non-functional tbk1 protein, or no protein at all, via nonsense mediated degradation, it was important during the course of this project to establish a new mutant line to validate our findings. In order to ensure that a new allele could not have any residual kinase activity we designed a new gRNA that targeted exon 4, in the middle of the kinase domain.

In addition, even though mutations found in patients are distributed across all Tbk1 domains it seems that the majority are located in the kinase or coiled coil domain, which are the two domains we have targeted in this project (Oakes et al., 2017). We identified a number of different *tbk1* mutations in the progeny of F0 fish and went on to raise F1 fish carrying a 14 bp insertion in exon 4 that leads to a premature termination codon (c.323_324ins14; p.Glu109fsX20). These fish were further outcrossed to generate a stable mutant line which transmitted the exon 4 mutation at a Mendelian frequency. This allele was named *tbk1*^{SH643}.

3.6.2 Determining whether *tbk1*^{SH570} and *tbk1*^{SH643} are loss of function mutations

For the purpose of this project, we require a *tbk1* mutation with no function. Because knockout technology does not exist in zebrafish in the same way as it does in mice, the most common approach is to study mutants containing upstream nonsense mutations that are predicted to lead to prematurely truncated transcripts. These mutations can either be generated by random mutagenesis (Kettleborough et al., 2013) or more commonly by using CRISPR/Cas9 mutagenesis. However, it can be challenging to determine whether a nonsense mutation actually causes the desired loss of function. The best approach would be to use an antibody to demonstrate that there is no protein present in homozygous mutant zebrafish, however zebrafish are severely limited in this respect, as very few specific primary antibodies are available, and the evolutionary divergence between humans and fish means that antibodies against the human protein do not recognise the zebrafish protein.

In the course of this project, we commissioned production of commercial antibodies recognising the N-terminus of the zebrafish protein. These would be useful as they would allow us to look for loss of protein expression, and to detect any truncated protein that might be produced. However, there was a delay in making the antibodies, and shortly after they were available for use, we went into lockdown. Thus, these reagents were not characterised as part of the project.

Another way to look for loss of function is to study mRNA levels. In cells, when an error occurs during transcription and translation that leads to incomplete polypeptides, a mechanism called nonsense mediated mRNA degradation destroys the aberrant mRNA. Thus, we expect that mRNAs containing *tbk1*^{SH570} or *tbk1*^{SH643} mutations will be subject to this degradation. We can therefore look at mRNA levels using a quantitative method such as qRT-PCR to determine whether the mutant transcripts are expressed.

Initially we checked the expression of *tbk1* mRNA at various embryonic stages starting from the 16 cell stage. The *tbk1* mRNA level was high at the 16 cell stage, then dropped to its lowest level by the end of gastrulation. After a peak on day 3, the mRNA level (measured at the level of the whole larvae) reaches steady state. After fertilisation, the earliest cell divisions in a zebrafish embryo are not accompanied by new transcription, so critical transcripts must be inherited from the oocyte. Because *tbk1* mRNA levels were so high in the 16 cell stage embryos we predicted that they are required early during development, and thus inherited from the mother. When we investigated *tbk1* mRNA expression in the mutant lines we were not able to demonstrate a significant reduction in *tbk1* in 5 day old *tbk1*^{SH570} homozygous mutants that were derived from in crosses of *tbk1*$^{+/SH570}$ parents (Figure (3.23).

However, we did see significant reduction, but not complete loss, of *tbk1* mRNA when we investigated *tbk1*^{SH570} homozygous mutants that were derived from in crosses of *tbk1*$^{SH570/SH570}$ parents (Figure (3.25). Together these results suggest that the *tbk1*^{SH570} allele does not cause efficient nonsense mediated degradation of the transcript, and thus it is possible that this mutant line will express some truncated protein.

To investigate this possibility and to formally demonstrate loss of tbk1 protein in the *tbk1*^{SH570} homozygous mutant, we would need to use an antibody recognising an N-terminal domain.

Turning to the exon 4 mutation, when we performed qRT-PCR on the progeny of *tbk1*$^{+/SH643}$ in crosses, at 5 dpf we were able to observe a significant reduction in the *tbk1* mRNA level between *tbk1*$^{+/+}$ and *tbk1*$^{SH643/SH643}$ groups, but there was no significant difference observed between *tbk1*$^{+/+}$ and *tbk1*$^{+/SH643}$.

However, by 12 dpf we observed a significant reduction in *tbk1* mRNA levels between both *tbk1*$^{+/+}$ and *tbk1*$^{SH643/SH643}$, and *tbk1*$^{+/+}$ and *tbk1*$^{+/SH643}$. Thus, it appears that unlike the SH570 allele, the SH673 allele is efficiently degraded by nonsense mediated degradation and will be useful to confirm that phenotypic effects observed in *tbk1*$^{SH643/SH643}$ mutants are true loss of function effects.

This difference in degradation between the two alleles could be related to the location of each mutation in the *tbk1* transcript, since secondary structure of the RNA is likely to influence its efficient recognition and degradation by the nonsense mediated degradation machinery (He and Jacobson, 2015).

3.6.3 Viability of the *tbk1* zebrafish model

One of the major concerns was the viability of this model, as a *TBK1* knockout mouse dies at an embryonic stage (Bonnard, 2000). However, we reasoned that even if this happened in zebrafish, since the embryos develop externally, we would still be able to gain valuable information, and potentially establish a rapid disease-relevant model.

Viability was reduced in *tbk1*$^{SH570/SH570}$ larvae compared to controls. The loss of viability seemed to occur at around 13-14 days which seems to be typical of a fish that fails to thrive. We were not permitted to conduct formal survival studies, so the data presented here comes from experiments to collect embryos for other analyses.

Once we understood the problem with raising *tbk1*$^{SH570/SH570}$ larvae we took two approaches. Firstly, we ensured that these larvae were raised on a diet that included rotifers. Observational studies in the Sheffield aquarium have suggested better overall survival of larvae when fed this particular diet. Secondly, once we became aware of the elevated NFkB:GFP expression in *tbk1*$^{SH570/SH570}$ larvae (see following chapter) we were able to select the homozygous mutants and house them separately. We know from previous experience that homozygous mutants with a swimming phenotype often fail to thrive when housed with their wild type or hemizygous siblings (Chapman et al., 2013).

We suspect this is because they are unable to compete for food in a mixed tank of 40-60 larvae. With these two improvements in husbandry, we were able to successfully breed *tbk1*$^{SH570/SH570}$ fish without loss of viability.

3.6.4 Phenotype of the *tbk1* zebrafish model

3.6.4.1 Size and possible developmental delay

When analysing a novel mutant phenotype, it is difficult to establish primary and secondary phenotypes. For example, in the section above we discussed the possibility that a swimming defect leads to reduced survival. We started to observe a possible delay in development at 12 days old as the *tbk1*$^{SH570/SH570}$ larvae lacked the anterior swimming bladder that was present in the 12 day old wild type larvae at this age. Using the microscope, we also noticed that the gut of the homozygous fish of this age appeared empty compared to their siblings, which could be due to them eating less.

By 21 days old, we demonstrated that *tbk1*$^{SH570/SH570}$ larvae are significantly smaller. This occurs despite improvements in husbandry, suggesting that it may be a mutation specific effect.

However, we know that by 6 months of age *tbk1*$^{SH570/SH570}$ raised separately in a tank containing up to 25 homozygous mutants will eventually reach the same length as their siblings.

Thus, there are some important effects of the tbk1 mutation on early development of the zebrafish, some of which may contribute to other phenotypes. This will be discussed below.

3.6.4.2 Impaired motor function in *TBK1* zebrafish model

As in other ALS zebrafish models motor function is one major feature to examine, and in common with other researchers we chose a microtitre plate imaging system (specifically a Zebrabox system from Viewpoint) to study swimming behaviour in *tbk1* larvae. Viewpoint systems evaluate the larvae swimming by quantifying 4 main parameters: Active duration, slow movement, fast movement and total swimming distance. We studied these parameters at several stages of larval development from 5 – 19 dpf.

Overall, we saw that the severity of the swimming phenotype in homozygous mutants was inversely correlated with the expression level of *tbk1* detected by qRT-PCR. As described earlier we think that *tbk1* mRNA detected in larvae could be wild type mRNA inherited from the mother via the oocyte, or alternatively it could be mutant mRNA that is not efficiently degraded by nonsense mediated degradation. At 5 dpf there is no reduction in the *tbk1* mRNA level in *tbk1*$^{SH570/SH570}$ progeny of a *tbk1*$^{+/SH570}$ in cross. Interestingly fish of this age and genotype did not show any significant defects in swimming. By 8 dpf we start to observe a significant reduction in all four swimming parameters during light cycles but not in the dark cycles. By 12 dpf we observed a significant reduction in all four parameters during both dark and light cycles. 14 and 19 dpf *tbk1*$^{SH570/SH570}$ did not reach significance because it was underpowered and also were influenced by the small arena size of the 24 well plate.

We selected the 12 dpf timepoint and replicated the swimming analysis using a 12 well plate instead of a 24 well plate. We were concerned that the 12 well plate might be too small to accurately measure swimming properties. Interestingly using the 12 well plate which is double the surface area allowed the fish to swim 30% further, and there was an increase in fast swimming compared to slow swimming, suggesting that the larvae were constrained in the smaller arena. Using the 12 well plate we observed the same effect on swimming, with significant reductions in the homozygotes in both light and dark cycles. Finally, we confirmed that this phenotype is consistent by investigating swimming at 12 dpf in *tbk1*$^{SH643/SH643}$ homozygotes derived from a heterozygote in cross. Due to time limitations this was only conducted once, but the results looked very similar to those obtained with *tbk1*$^{SH570/SH570}$.

As mentioned earlier, at 5 dpf the *tbk1* mRNA level in *tbk1*$^{SH570/SH570}$ progeny of a *tbk1*$^{SH570/}$^{SH570} in cross was significantly reduced. In order to confirm the impact of the reduced mRNA level on swimming behaviour we used viewpoint to examine their swimming. All four swimming parameters were significantly reduced in these homozygous mutants at 5 dpf. Since these larvae cannot possibly have wild type maternal mRNA, we can conclude that the inheritance of wild type mRNA (or perhaps protein) is likely to delay the onset of the swimming phenotype in the homozygous offspring of heterozygous *tbk1*^{SH573} parents. This seems a remarkably long-lasting effect, given the number of cell divisions that have occurred by 5 dpf.

At 12 days old *tbk1*$^{SH570/SH570}$ lack the anterior swimming bladder and older *tbk1*$^{SH570/SH570}$ larvae are much smaller in size compared to wild type thus the defects we observed in their swimming could be due wholly or in part to these factors. In addition, ALS is an autosomal dominant disease that appears at late adult hood, however *tbk1*$^{+/SH570}$ did not appear to show any symptoms or phenotype during larvae stages. Although the swimming data are consistent with a motor phenotype at the present time, we have no supporting pathology data. It is important to analyse the neuromuscular junction in affected larvae, to investigate the structure of post- and pre- synaptic markers. We should also quantify the number of motor neurons in the spinal cord at 12 dpf.

However, we did find that adult *tbk1*$^{SH570/SH570}$ zebrafish showed significant reduction in critical swimming speed (Ucrit) at 6 months and 1 year old. But 6 months and 1 year old *tbk1*$^{+/SH570}$ did not appear to show any swimming defects suggesting that it might lack the phenotype, to address that properly we need to examine swimming endurance at later age 18 months and 2 years. These experiments were hampered by lockdown, which reduced the group size at 12 months. Again, we need to conduct a detailed neuropathology to study the neuromuscular junction and spinal cord of these fish, which would support the finding that this is principally a neurological phenotype.

3.6.4.3 Abnormal social behaviour in the *tbk1* zebrafish model

Unlike ALS, modelling FTD in zebrafish is more challenging and there are no published FTD models. However, social behaviour has been investigated in many zebrafish models been and here we wished to determine if there were any behavioural changes in the *tbk1* model consistent with FTD phenotypes seen in patients. Thigmotactic or wall hugging behaviour is an indicator of anxiety that is evolutionary conserved in many species including fish and humans (Schnörr et al., 2012b). Using the viewpoint apparatus, *tbk1*^{SH570} larvae were subjected to 6 dark/light cycles in 12 well plates, then swimming data were collected from two areas; the centre of the well, and the whole well. To quantify thigmotaxis we measured the proportion of time spent in the centre of the field. An increase in this proportion would be a loss of thigmotaxis, which is a highly abnormal behaviour for a zebrafish, consistent with neurological dysfunction. At 8 days we found no overt thigmotaxis behaviour in larvae of any genotype.

However, at 12 dpf *tbk1*$^{SH570/SH570}$ larvae showed significantly reduced thigmotaxis in the light cycles but did not show any difference during the dark cycles. This suggests that when *tbk1*$^{SH570/SH570}$ larvae are aware of their surrounds (i.e. in the light) they do not avoid swimming in the centre of the field like their siblings do.

However, when the lights are switched of fish off all genotypes swim randomly in the whole field, demonstrating that there is no inherent preference from the edge of the well unless it is light. These findings suggest that 12 dpf *tbk1*$^{SH570/SH570}$ larvae lack thigmotactic behaviours. Although there is no evidence that bvFTD patients show increased anxiety, they can often have trouble controlling their behaviour, which could be a feature of the phenotype we observed in this assay.

The other social behaviour that we examined in zebrafish was shoaling. Shoaling in zebrafish develops with age and in zebrafish it is well developed at 3 weeks of age (Buske and Gerlai, 2012). *tbk1*$^{SH570/SH570}$ zebrafish were raised in a separate tank to maintain viability and normal body size. *tbk1*$^{+/+}$ and *tbk1*$^{+/SH570}$ were raised in another tank. The Viewpoint apparatus was used to examine shoaling in a watch glass. A group of six normally sized 21 day old *tbk1*$^{SH570/SH570}$ zebrafish were selected, acclimatized in Viewpoint apparatus for 30 minutes and allowed to swim for 10 minutes in light. A similar study was conducted for a mixed group of six *tbk1*$^{+/+}$ and *tbk1*$^{+/SH570}$ larvae. Four shoaling parameters (nearest neighbor distance, inter individual distance, polarisation and speed) were measured. A significant difference between *tbk1*$^{SH570/SH570}$ and the mixed group of tbk*1*$^{+/+}$ and *tbk1*$^{+/SH570}$ was observed for all shoaling parameters. Although we tried to control for larval size by selecting only the largest homozygous mutants for shoaling analysis, size could be a factor that could influences measurements based on distance (speed, neighbor distance, inter individual distance) as bigger fish swim faster and the space between the group of fish could be reduced. However, polarisation, which measures fish that swim 'together' i.e. in the same direction at the same time, appears to be independent of size, and therefore would not be affected by the size of the larvae. bvFTD patients show apathy, and perhaps this is related to the altered shoaling phenotype we observe

3.7 Conclusion

In conclusion, both *tbk1*$^{SH570/SH570}$ and *tbk1*$^{SH643/SH643}$ are viable when raised separately and provided with an optimal diet. Maternal wild type *tbk1* mRNA seems to reduce the phenotype of larvae obtained from heterozygous in crosses, and remarkably this effect is still observed at 3, 5 and 8 dpf. Both mutant lines show reduced swimming consistent with motor dysfunction, and in the *tbk1*^{SH570} line we know this also manifests in adults and is associated with abnormal social behaviour in larvae. More work is needed to support these observations, in particular neuropathology would allow us to draw a firm conclusion about the basis for these phenotypes.

Chapter 4

4. Investigating the role of signaling pathways in *tbk1* mutant zebrafish

4.1 Introduction

We hypothesise that TBK1 mutations cause ALS/FTD by disrupting TBK1 regulated signaling pathways. Thus, we aim to investigate which pathways downstream of TBK1 are involved in ALS/FTD pathogenesis in zebrafish. TBK1 is involved in many pathways but we have focused on pathways that we believe could be involved in ALS/FTD pathogenesis. Since many studies suggest a role for *TBK1* in mediating cross talk between the innate immune response, NF*κ*B and IRF3 signaling, and autophagy (Weidberg and Elazar, 2011) we are focusing on these three pathways.

There are many *in vitro* studies of the role of TBK1 in activating the canonical NF*κ*B pathway, and on the other hand there are other studies suggesting that TBK1 negatively regulates the non-canonical pathway. In order to investigate the effect of *in vivo* loss of TBK1 function on the NF*κ*B pathway we outcrossed our models with an NF*κ*B:GFP zebrafish reporter line (Kanther et al., 2011b). Furthermore, we looked at NFκB proinflammatory marker genes (*il1β*, *tnfα*, *il6* and *il8*). Finally, we generated and used a second zebrafish TBK1 model that carries a nonsense mutation in the kinase domain to investigate the role TBK1 in NF*κ*B signaling.

In vitro IRF3 could be directly phosphorylated and activated by TBK1 (Panne et al., 2007). To study the impact of TBK1 mutation on IRF3 signaling we studied expression of genes that respond to IRF3. This included crosses with transgenic mxa:mCherry zebrafish (Levraud et al., 2007) as well as investigation of mRNA levels of type1 IFN genes (*ifnφ1, isg15* and *mxa*).

TBK1 signaling is also involved in autophagy, since TBK1 phosphorylates autophagy receptors, particularly those on mitochondria that regulate mitophagy. Specifically, TBK1 phosphorylates OPTN to mediate formation of a complex that is essential for the depolarization of the damaged mitochondria (He et al., 2017).

Considering the potentially oligogenic basis of ALS and FTD (Van Blitterswijk et al., 2012b) and the presence of patients carrying hemizygous mutations in both TBK1 and OPTN (Pottier et al., 2015b) we also investigated epistasis between TBK1 and OPTN mutations in zebrafish. To this end, we generated zebrafish carrying loss of function mutations in both *TBK1* and *OPTN* and compared swimming behaviour between these fish with wild type and single mutants.

4.2 Increased NF*κ*B:GFP reporter gene levels in *tbk1*$^{SH570/SH570}$ mutants

To determine wither TBK1 regulates canonical NFκB signaling *in vivo* as some studies suggest (Abe and Barber, 2014, Jin et al., 2012) we outcrossed hemizygous transgenic NFκB:GFP zebrafish with in *tbk1*$^{+/SH570}$ zebrafish to generate a *tbk1*$^{+/SH570}$ NFκB:GFP reporter line. Then we outcrossed these fish with *tbk1*$^{+/SH570}$ zebrafish to produce *tbk1*$^{+/+}$, *tbk1*$^{+/SH570}$ and *tbk1*$^{SH570/SH570}$ progeny. Half of these offspring would be expected to carry the NFκB:GFP reporter gene. Under a binocular fluorescent microscope, at 3dpf, we sorted the progeny according to presence/absence of an GFP signal. Interestingly we observed two groups of GFP expressing zebrafish, one with a bright GFP signal and the other with a weaker GFP signal (Figure (4.1a and 4.1b). We collected both groups according to GFP intensity and extracted DNA for genotyping. remarkably this showed that all the bright GFP larvae were homozygous for the *tbk1* mutation while the weaker ones were a mix of *tbk1* wild type and heterozygous larvae (Figure (4.1c&d).

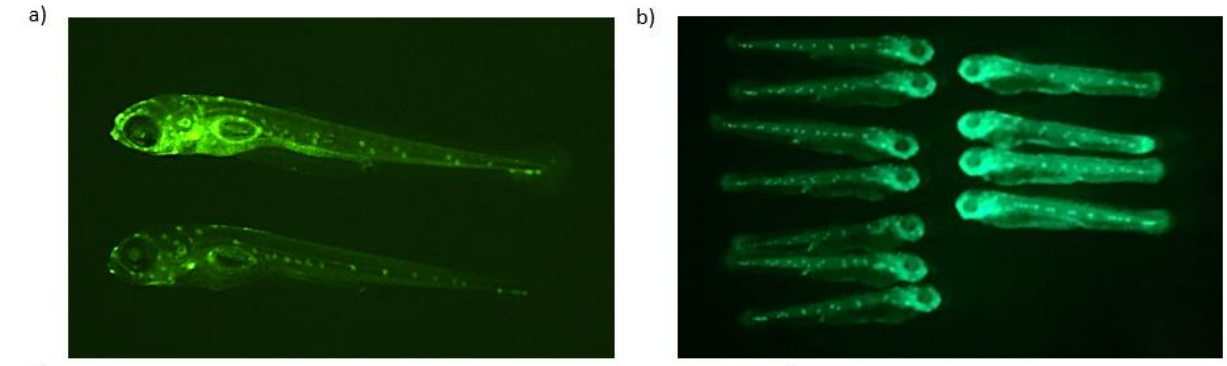

d)

Well #	genotype	Well #	genotype
1	*tbk1*$^{SH570/SH570}$	9	*tbk1*$^{+/+}$
2	*tbk1*$^{SH570/SH570}$	10	*tbk1*$^{+/SH570}$
3	*tbk1*$^{SH570/SH570}$	11	*tbk1*$^{+/SH570}$
4	*tbk1*$^{SH570/SH570}$	12	*tbk1*$^{+/SH570}$
5	*tbk1*$^{SH570/SH570}$	13	*tbk1*$^{+/+}$
6	*tbk1*$^{SH570/SH570}$	14	*tbk1*$^{+/+}$
7	*tbk1*$^{SH570/SH570}$	15	*tbk1*$^{+/SH570}$
8	blank control	16	*tbk1*$^{+/SH570}$

Figure 4. 1 NFκB:GFP reporter levels observed in progeny of a *tbk1*$^{+/SH570}$ incross. a) One bright NFκB:GFP zebrafish and one weaker NFκB:GFP zebrafish. b) A group of bright GFP zebrafish *are tbk1* $^{SH570/SH570}$ and a group of less bright EGFP zebrafish are a mixture of *tbk1*$^{+/+}$ and *tbk1*$^{+/SH570}$. c) Gel image of *tbk1* exon10 genotyping *tbk1*^{SH570} incross progeny that been selected according to the GFP signals, wild type genotyping show one band at size 203 & 155 bp, heterozygous bands 358, 203 & 155 bp and homozygous band at 358 bp, the 1st 7wells are *tbk1*$^{SH570/SH570}$. d) is a *tbk1* exon10 table of genotyping.

Furthermore, we used confocal microscopy to examine which cells and organs express NFκB:GFP and whether there is any difference between wild type and homozygous mutant larvae. NFκB:GFP was expressed in many epithelial cells and in neuromasts and the intensity of NFκB:GFP signal was higher in *tbk1*$^{SH570/SH570}$ compared to *tbk1*$^{+/+}$. Measuring the NFκB:GFP fluorescence intensity we observed a significant difference between the *tbk1* wild type and the homozygous, Welch's t-test p value is 0.0014 (see Figure(4.2e).

In conclusion there appears to be an increase in NFκB signalling in *tbk1*$^{SH570/SH570}$ zebrafish which is detectable using the reporter line from 3dpf.

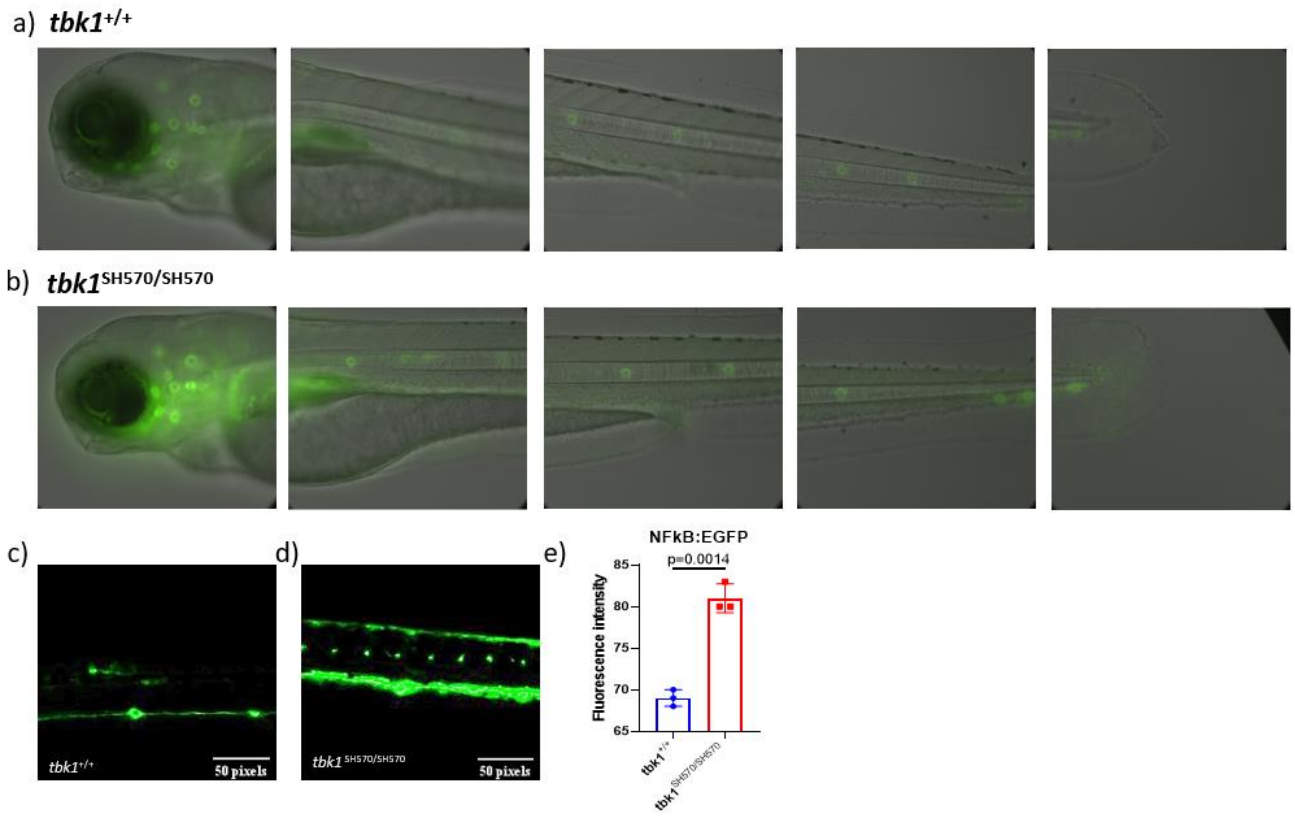

Figure 4. 2 Confocal imaging of *tbk1*$^{SH570/SH570}$ shows increased expression of NF*κ*B:GFP. a) *tbk1*$^{+/+}$ zebrafish expressing NF*κ*B:GFP in many cells b) *tbk1*$^{SH570/SH570}$ zebrafish have increased levels of NF*κ*B:GFP in many cells. c) section of *tbk1*$^{+/+}$ shows that NF*κ*B:GFP are expressed in neuromasts. d) section of *tbk1*$^{SH570/SH570}$ shows that NF*κ*B:GFP has increased expressed in neuromasts. e) NFκB:GFP florescence intensity is significantly different between *tbk1*$^{+/+}$ and *tbk1*$^{SH570/SH570}$ (p =) 0.0014.

4.2.1 Viral infection does not appear to contribute to NFκB signaling in *tbk1*$^{SH570/SH570}$

Since tbk1 regulation of canonical NFκB is involved in the inflammatory response to infection (Shih et al., 2011), we wanted to investigate whether increased NFκB:GFP expression could be due to viral infection.

Although the aquarium is a closed recirculating system, it is not a sterile environment, thus some pathogens will be present (Balla et al., 2020). Tbk1 is a crucial adaptor protein in the innate immune response to viruses, including picornavirus infection in human cells (Li et al., 2019). The only known zebrafish virus present in research aquaria is a picornavirus (Altan et al., 2019, Balla et al., 2020). Pathogen testing has demonstrated that this virus is carried by around 20% of the fish in the Sheffield aquarium where the *tbk1*^{SH570} line are housed. Picornavirus can be efficiently removed from embryos by standard bleaching protocols (Balla et al., 2020). Therefore, to reduce picornavirus infection we bleached embryos obtained from *tbk1*$^{+/SH570}$ x *tbk1*$^{+/SH570}$ NFκB:GFP crosses and maintained them in sterile autoclaved E3, and compared NF*κ*B:GFP in these embryos with siblings bleached and then maintained in autoclaved E3 supplemented with unfiltered water from the aquarium system, as well as a group that were left unbleached and raised according to our standard husbandry in non-sterile E3. The bleached embryos often remained in the chorions, which is expected. Examining the three groups under the microscope we observed the existence of bright and less bright zebrafish in all three groups. Genotyping revealed that all bright fish were *tbk1* homozygotes while the less bright ones were a mixture of wild type and *tbk1* heterozygous (see Figure (4.3).

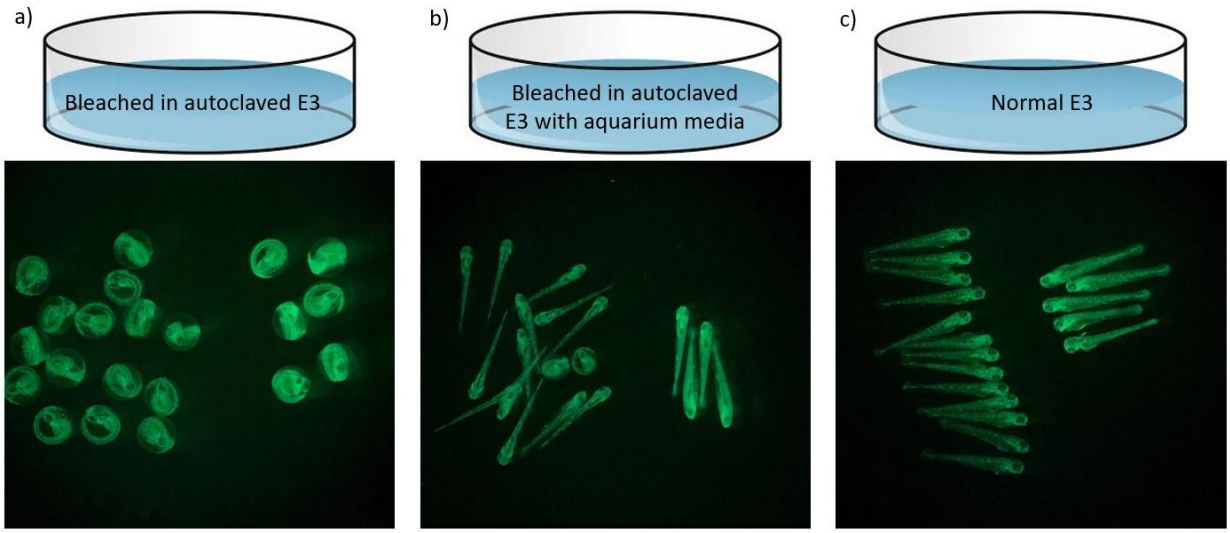

Figure 4. 3 Bleaching embryos to remove picornavirus does not alter the NFκB:GFP signal in *tbk1*$^{SH570/SH570}$. a) a group of 5 dpf tbk1^{SH570} siblings treated with bleach and raised in autoclaved E3.b) a group of 5 dpf tbk1^{SH570} siblings treated with bleach and raised in autoclaved E3 with aquarium media. c) a group of 5 dpf tbk1^{SH570} siblings raised in normal E3.

4.2.1.1 Over expression of proinflammatory cytokine genes in *tbk1*$^{SH570/SH570}$

Activating NFκB triggers a response involving upregulation of proinflammatory genes including *TNFα*, *IL1β, IL6* and *IL8* (Lawrence, 2009a). Therefore, we investigated whether increased NFκB signaling indicated by increased GFP was associated with changes in expression of the proinflammatory genes. We conducted three independent in crosses as above and sorted *tbk1*^{SH570} sibling embryos into two groups- those with bright NFκB:GFP and those with less bright NFκB:GFP, we pooled 10 larvae from each genotype on different days and extracted RNA at 5 and 12 dpf. By measuring the mRNA level of *tnfα*, *il1β*, *il6* and *il8* in 5 dpf tbk1^{SH570} zebrafish siblings we did not observe any significant difference in expression of *il1β*, *il6* and *il8* between groups. However, in 5 dpf *tbk1*$^{SH570/SH570}$ embryos we observed a significant increase in *tnfα* levels compared to the mixed wild type and heterozygous siblings (Welch's t-test p-value 0.0002) (see Figure (4.4).

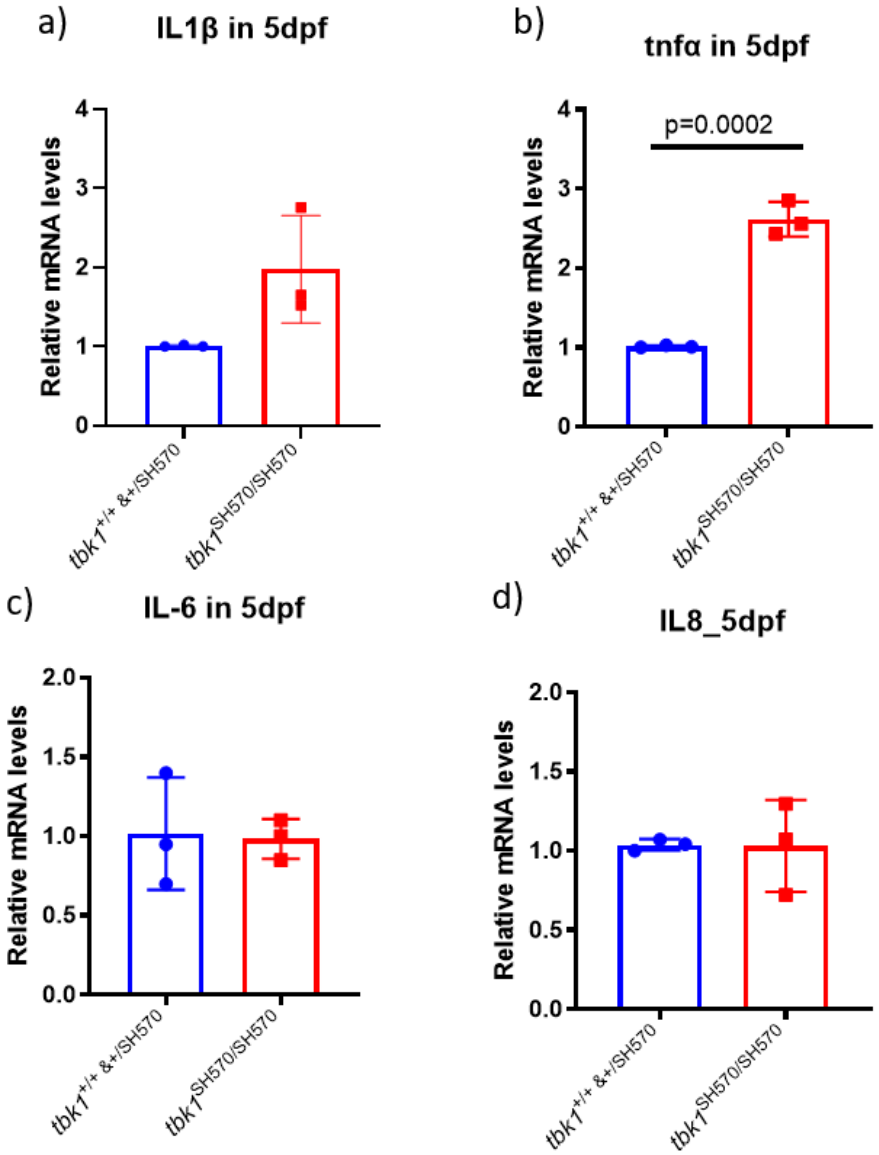

Figure 4. 4 Investigation of proinflammatory cytokine gene expression in 5 dpf *tbk1*$^{SH570/SH570}$. a) *il1β* mRNA level does not show any significant difference between *tbk1*$^{+/+}$& *tbk1*$^{+/SH570}$ sibling and *tbk1*$^{SH570/SH570}$ zebrafish. b) *tnfα* mRNA level shows significant difference between *tbk1*$^{+/+}$& *tbk1*$^{+/SH570}$ sibling and *tbk1*$^{SH570/SH570}$ zebrafish (p=0.0002). c) *il6* mRNA level does not show any significant difference between *tbk1*$^{+/+}$& *tbk1*$^{+/SH570}$ sibling and *tbk1*$^{SH570/SH570}$ zebrafish. d) *il*8 mRNA level does not show any significant difference between *tbk1*$^{+/+}$& *tbk1*$^{+/SH570}$ sibling and *tbk1*$^{SH570/SH570}$ zebrafish**.** Each point represents a pool of 10 larvae from 3 independent group.

Since the swimming defect in *tbk1*$^{SH570/SH570}$ zebrafish was detected at 12 dpf (Figure (3.24), we also measured levels of the proinflammatory genes at 12 dpf tbk1^{SH570}. We observed a significant increase of *tnfα*, *il1β*, *il6* and *il8* mRNA levels in the 12 dpf *tbk1*$^{SH570/SH570}$ compared the *tbk1*$^{+/+}$ and *tbk1*$^{+/SH570}$ siblings, (see Figure (4.5). Thus, we have demonstrated that proinflammatory genes are upregulated in *tbk1* mutants that have increased NFκB signalling, at a time when these fish manifest swimming and behavioural defects.

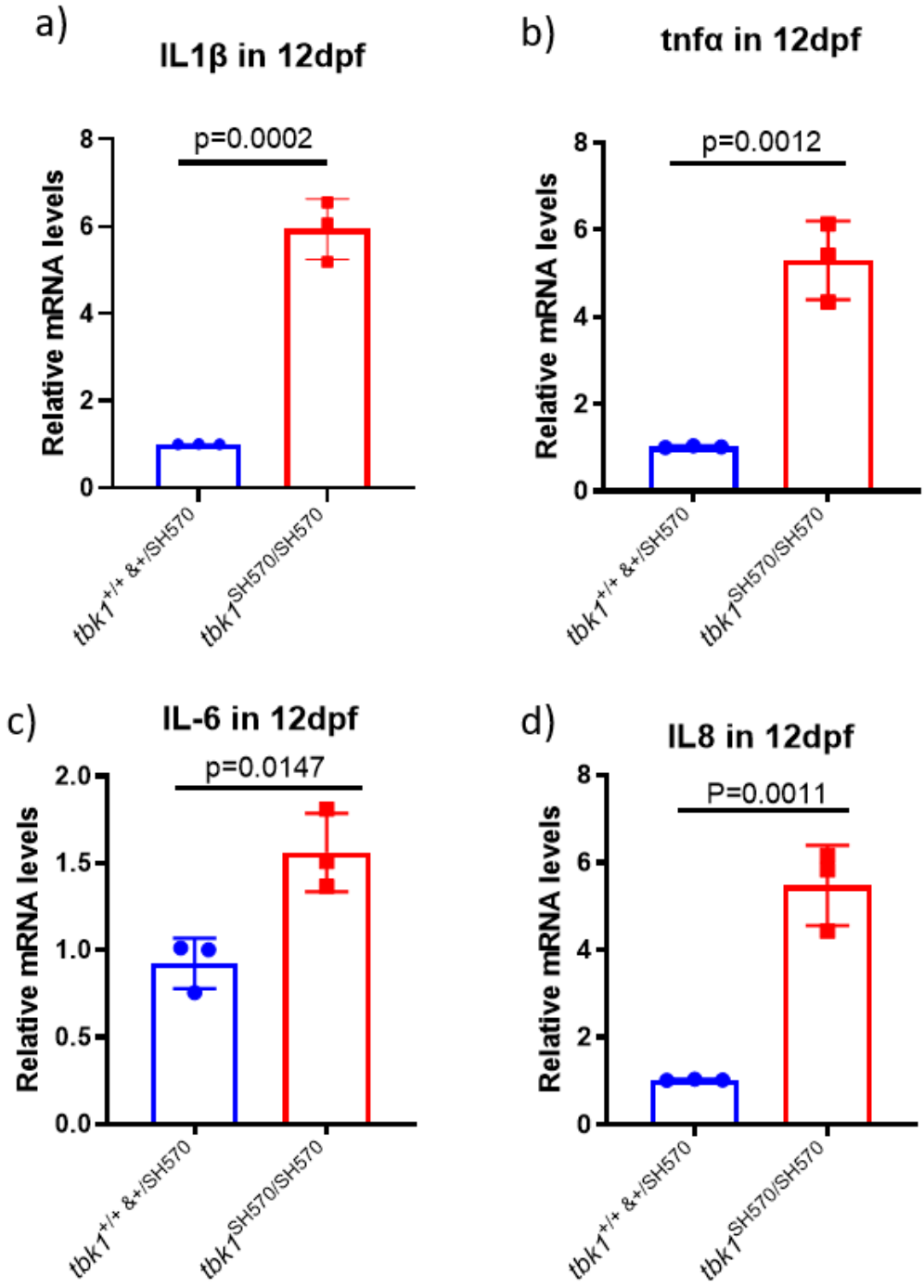

Figure 4. 5 Investigation of proinflammatory cytokine genes expression in 12 dpf *tbk1*$^{SH570/SH570}$. a) 12 dpf *tbk1*$^{SH570/SH570}$ shows a significant increase in *il1β* mRNA level compared to *tbk1*$^{+/+}$& *tbk1*$^{+/SH570}$ siblings p=0.0002. b) 12 dpf *tbk1*$^{SH570/SH570}$ shows a significant increase in *tnfα* mRNA level compared to *tbk1*$^{+/+}$& *tbk1*$^{+/SH570}$ siblings p=0.0012. c) 12 dpf *tbk1*$^{SH570/SH570}$ shows a significant increase in *il6* mRNA level compared to *tbk1*$^{+/+}$& *tbk1*$^{+/SH570}$ siblings p=0.0147. d) 12 dpf *tbk1*$^{SH570/SH570}$ shows a significant increase in *il8* mRNA level compared to *tbk1*$^{+/+}$& *tbk1*$^{+/SH570}$ siblings p=0.0011. Each point represents a pool of 10 larvae from 3 independent group.

4.2.2 Increased NFκB:GFP signal in *tbk1* compound heterozygous mutant zebrafish

One of the risks associated with studying a single mutant allele is that we might be seeing increased NFκB signalling due to mutation in a linked gene, or some other unexpected effect of the SH570 allele. As described in chapter (3) we generated a new *tbk1*^{SH643} stable line that carries a frameshift mutation in the kinase domain. Therefore, we tested whether this new allele was able to rescue the increase in NFκB:GFP found in *tbk1*^{SH570} embryos using a complementation assay, where we crossed *tbk1*$^{+/SH570}$ NFκB:GFP hemizygotes with *tbk1*$^{+/SH643}$ zebrafish and examined the GFP signal in their progeny under the fluorescent microscope. We observed two groups of NFκB:GFP zebrafish which we classified as bright and less bright (Figure (4.6b). Genotyping and sequencing of the NFκB:GFP bright embryos revealed that they all carried the mutation in *tbk1* exon4 (c.323_324 ins14; p.Glu109fsX20) and a mutation in *tbk1* Exon 10 (c.1227_1231del5; p.D409Efsx10). Thus, the increased NFκB:GFP signal can be induced by two independent *tbk1* alleles, and the exon 4 mutation fails to complement (rescue) the exon 10 allele. Genotyping and sequencing the NFκB:GFP less bright embryos revealed that some of them carried a mutation in *tbk1* exon 4 but not in *tbk1* exon 10, while some of them carried a mutation in *tbk1* exon 10 but not in *tbk1* exon 4, and some of them were wild type for *tbk1* (see Figure(4.6).

a)

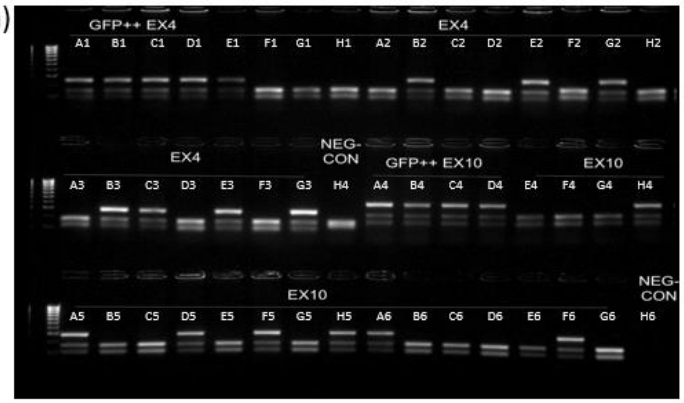

b)

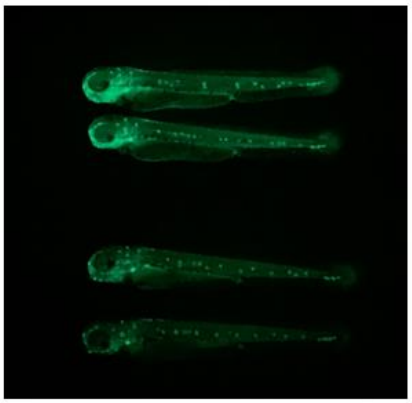

c)

	1	2	3	4	5	6
A	EX4_HET	EX4_WT	EX4_WT	EX10_HET	EX10_HET	EX10_HET
B	EX4_HET	EX4_HET	EX4_HET	EX10_HET	EX10_WT	EX10_WT
C	EX4_HET	EX4_WT	EX4_HET	EX10_HET	EX10_WT	EX10_WT
D	EX4_HET	EX4_WT	EX4_WT	EX10_HET	EX10_HET	EX10_WT
E	EX4_HET	EX4_HET	EX4_HET	EX10_WT	EX10_WT	EX10_WT
F	EX4_WT	EX4_WT	EX4_WT	EX10_WT	EX10_HET	EX10_HET
G	EX4_WT	EX4_HET	EX4_HET	EX10_WT	EX10_WT	EX10_WT
H	EX4_WT	EX4_WT	NEG-CON	EX10_HET	EX10_HET	NEG-CON

- EX4_WT: exon4 wild type
- EX4_HET: exon4 heterozygous c.323_324 ins14; p.Glu109fsX20
- EX10_WT: exon10 wild type
- EX10_HET: exon10 heterozygous c.1227_1231del5; p.D409Efsx10
- NEG_CON: negative control
- GFP++: NFκB:GFP bright
- Green box: NFκB:GFP bright

Figure 4. 6 Compound heterozygous *tbk1* mutations cause increased NFκB:GFP signal. a) Gel image of genotyping tbk1 compound heterozygous, the 1st 23 wells are *tbk1* exon4 and last 23 wells are the same embryos genotyped for *tbk1* exon10. b) is a picture of 2 NFκB:GFP bright zebrafish on the top and 2 less bright NFκB:GFP zebrafish on the bottom. c) is a table of genotyping, the 1st three columns are *tbk1* exon 4 and the last 3 columns are the same embryos genotyped for *tbk1* exon10.

4.2.3 Increased NFκB:GFP signal in *tbk1*$^{SH643/SH643}$ homozygous mutants

To confirm the increased expression of NFκB:GFP in *tbk1*$^{SH570/SH570}$ and in compound heterozygous *tbk1*$^{SH570/SH643}$ we outcrossed *tbk1*$^{+/SH643}$ with *tbk1*$^{+/SH643}$ NFκB:GFP hemizygotes to generate *tbk1* $^{SH643/SH643}$ NFκB:GFP hemizygote progeny. Examining this outcross progeny under the fluorescent microscope at 3 dpf we observed that we have two groups of zebrafish one with a bright GFP signal and the other with a less bright GFP signal. We collected the GFP expressing zebrafish and genotyped them. Comparison of GFP level and genotype showed that all the brightly fluorescing embryos were *tbk1* $^{SH643/SH643}$ while the less bright ones were a mix of *tbk1* $^{+/+}$ and *tbk1* $^{+/SH643}$ (Figure (4.7). Therefore, an independent frameshift mutation in the kinase domain of *tbk1* confirms the effect of *tbk1* mutation on NFκB signalling in zebrafish embryos.

a)

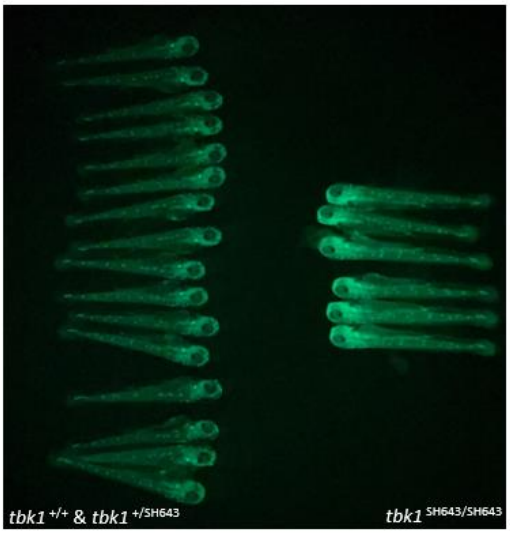

b)

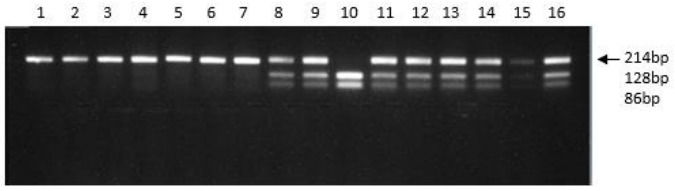

c)

well#	Genotyping	well#	Genotyping
1	*tbk1*$^{SH643/SH643}$	9	*tbk1*$^{+/SH643}$
2	*tbk1*$^{SH643/SH643}$	10	*tbk1*$^{+/+}$
3	*tbk1*$^{SH643/SH643}$	11	*tbk1*$^{+/SH643}$
4	*tbk1*$^{SH643/SH643}$	12	*tbk1*$^{+/SH643}$
5	*tbk1*$^{SH643/SH643}$	13	*tbk1*$^{+/SH643}$
6	*tbk1*$^{SH643/SH643}$	14	*tbk1*$^{+/SH643}$
7	*tbk1*$^{SH643/SH643}$	15	*tbk1*$^{+/SH643}$
8	*tbk1*$^{+/SH643}$	16	*tbk1*$^{+/SH643}$

Figure 4. 7 dpf *tbk1*$^{SH643/SH643}$ have elevated NF*κ*B:GFP signal. a) *tbk1*$^{SH643/SH643}$ zebrafish over expressing NF*κ*B:GFP compared to *tbk1*$^{+/+}$ and *tbk1*$^{+/SH643}$. b) Gel image of *tbk1* exon4 genotyping *tbk1*^{SH643} incross progeny that been selected according to the GFP signals the 1st 7 wells are *tbk1*$^{SH643/SH643}$. c) is a table of *tbk1* exon4 genotyping.

4.2.3.1 Over expression of proinflammatory cytokine genes in *tbk1*$^{SH643/SH643}$

If the *tbk1*^{SH643} mutation in the TBK1 kinase domain affects the same functional pathway as *tbk1*^{SH570} we expect to see similar increased expression of proinflammatory cytokine genes. Thus, we measured the mRNA level of *tnfα*, *il1β*, *il6* and *il8* in 12 dpf *tbk1*^{SH643} zebrafish siblings. We observed significant increases in *il1β*, *tnfα*, *il6* and *il8* mRNA levels in the 12 dpf *tbk1*$^{SH643/SH643}$ compared to *tbk1*$^{+/+}$& *tbk1*$^{+/SH643}$ siblings (see Figure (4.8), suggesting that similar pathways are affected in two independent *tbk1* mutant zebrafish models.

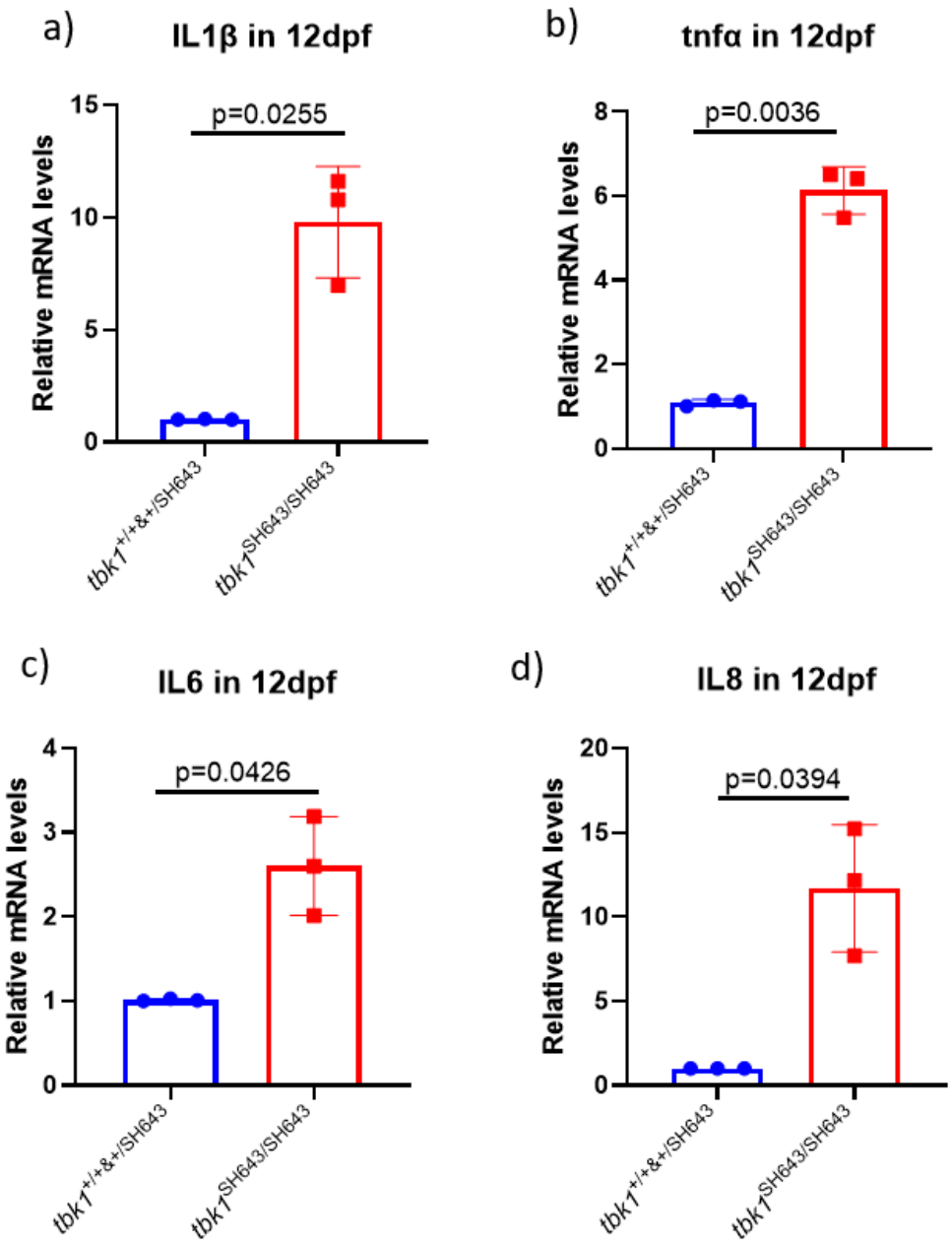

Figure 4. 8 Increased expression of proinflammatory cytokine genes in 12 dpf *tbk1*$^{SH643/SH643}$ zebrafish. a) 12 dpf *tbk1*$^{SH643/SH643}$ shows a significant increase in *il1ϐ* mRNA level compared to *tbk1*$^{+/+}$& *tbk1*$^{+/SH643}$ siblings p=0.0255. b) 12 dpf *tbk1*$^{SH643/SH643}$ shows a significant increase in *tnfα* mRNA level compared to *tbk1*$^{+/+}$& *tbk1*$^{+/SH643}$ siblings p=0.0036. c) 12 dpf *tbk1*$^{SH643/SH643}$ shows a significant increase in *il6* mRNA level compared to *tbk1*$^{+/+}$& *tbk1*$^{+/SH643}$ siblings p=0.0426. d) 12 dpf *tbk1*$^{SH643/SH643}$ shows a significant increase in *il8* mRNA level compared to *tbk1*$^{+/+}$& *tbk1*$^{+/SH643}$ siblings p=0.0394. Each point represents a pool of 10 larvae from 3 independent group.

4.3 A *tbk1*$^{SH570/SH570}$ mxa:mCherry IRF3 reporter line does not provide evidence of altered IRF3 signaling

Since there is crosstalk between IRF3 and NFκB, and TBK1 acts as a downstream kinase in the IRF3 pathway controlling dsDNA mediated IRF3 signaling (Abe and Barber, 2014), we aimed to examine the effect of a TBK1 LOF mutation on IRF3 signaling. To this end we outcrossed *tbk1*$^{+/SH570}$ with an mxa:mCherry irf3 zebrafish reporter line (Levraud et al., 2007) to produce *tbk1*$^{+/SH570}$ mxa:mCherry hemizygotes. Next we out crossed *tbk1*$^{+/SH570}$ with *tbk1*$^{+/SH570}$ mxa:mCherry hemizygotes to generate *tbk1*$^{+/+}$ mxa:mCherry$^{+/-}$, *tbk1*$^{+/SH570}$ mxa:mCherry$^{+/-}$ and *tbk1* $^{SH570/SH570}$ mxa:mCherry$^{+/-}$ progeny.

Under the fluorescent microscope we sorted 3dpf progeny on the basis of red fluorescence that appears in the eye of mxa:mCherry carriers. Under the fluorescent microscope we did not observe any obvious differences between the three genotypes, which was confirmed by measuring the mxa:mCherry fluorescence intensity ($p=0.8151$ (Figure(4.9b). To enhance the antiviral response, we also treated clutches of progeny with compounds that activate interferon pathway signaling including Poly I:C (0.5mg/ml) and brequinar (20mM)(Lucas-Hourani et al., 2013, Moore et al., 2014). We did not detect any difference in the mCherry signal between 5 dpf *tbk1*$^{+/+}$ mxa:mCherry, *tbk1*$^{+/SH570}$ mxa:mCherry and *tbk1* $^{SH570/SH570}$ mxa:mCherry zebrafish even after 48 hours of treatment.

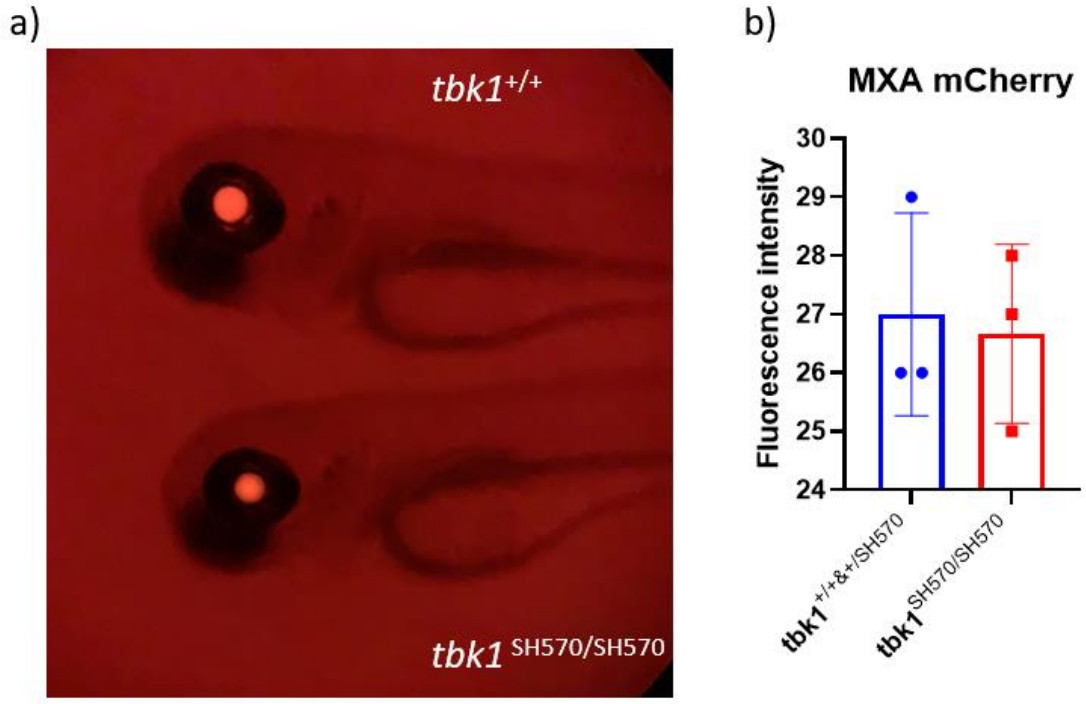

Figure 4. 9 *tbk1*$^{SH570/SH570}$ mxa:mCherry IRF3 reporter line. a) No mxa:mCherry signal was observed in wild type or homozygous mutant TBK1 zebrafish at 5 dpf. b) Measuring mxa:mCherry fluorescence intensity did not reveal any significant difference between *tbk1*$^{+/+,}$ *tbk1*$^{+/SH570}$ and *tbk1*$^{SH570/SH570}$.

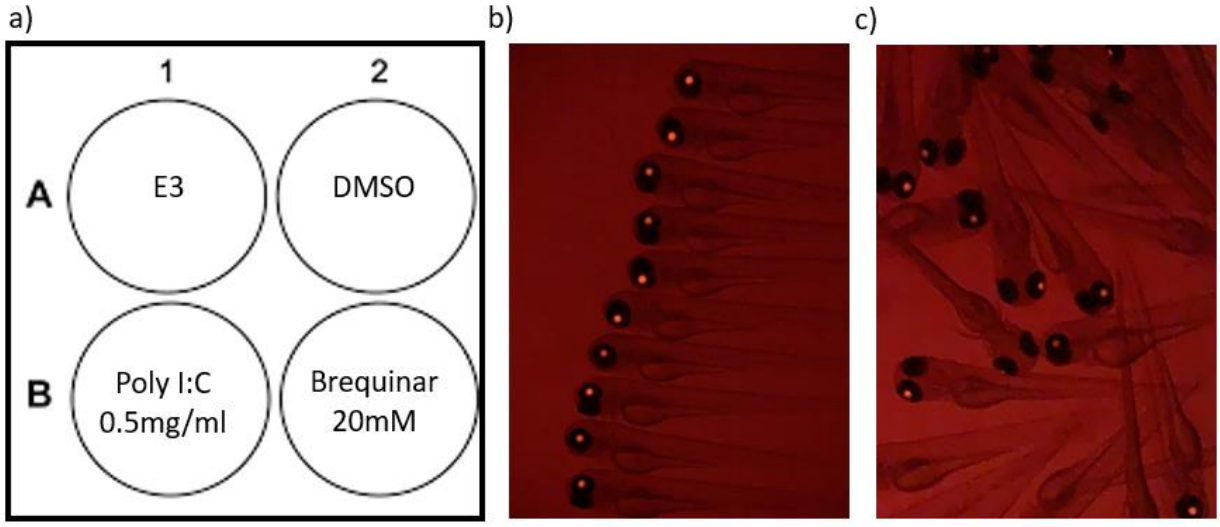

Figure 4.10 *tbk1*$^{SH570/SH570}$ mxa:mCherry zebrafish treated with Poly I:C and brequinar. a) Scheme of the experimental treatment groups.b) tbk1^{SH570} mxa:mCherry treated with Poly I:C did not show any difference between *tbk1*$^{+/+,}$ *tbk1*$^{+/SH570}$ and *tbk1*$^{SH570/SH570}$. c) tbk1^{SH570} mxa:mCherry treated with brequinar did not show any difference in signal between *tbk1*$^{+/+,}$ *tbk1*$^{+/SH570}$ and *tbk1*$^{SH570/SH570}$.

4.3.1 Elevated expression of type I Interferon induced genes in *tbk1*$^{SH570/SH570}$ zebrafish

Since IRF3 regulates type I IFN gene transcription and TBK1 is involved in IRF3 signaling, a LOF mutation in TBK1 could have a downstream impact on type I IFN genes. Although the mxa:mCherry IRF3 reporter line did not reveal altered levels of transcription at the *mxa* promoter in *tbk1*$^{SH570/SH570}$ homozygotes, we decided to use an alternative approach. Therefore, we investigated expression of type I IFN genes which could reveal a downstream impact of TBK1 mutation on the IRF3 signaling pathway. By measuring the mRNA level of type I IFN genes which include *ifnφ1, isg15* and *mxa* in 12 dpf *tbk1*^{SH570} zebrafish siblings we observed increased expression of all the three genes in *tbk1*$^{SH570/SH570}$ (see Figure (4.11). However, this effect was only significant in *isg15* (t-test p value p=0.0438 (see Figure (4.11b). Unfortunately, there was not sufficient time to repeat this experiment with additional batches of 12 dpf embryos to determine whether the other genes would reach statistical significance in a larger study.

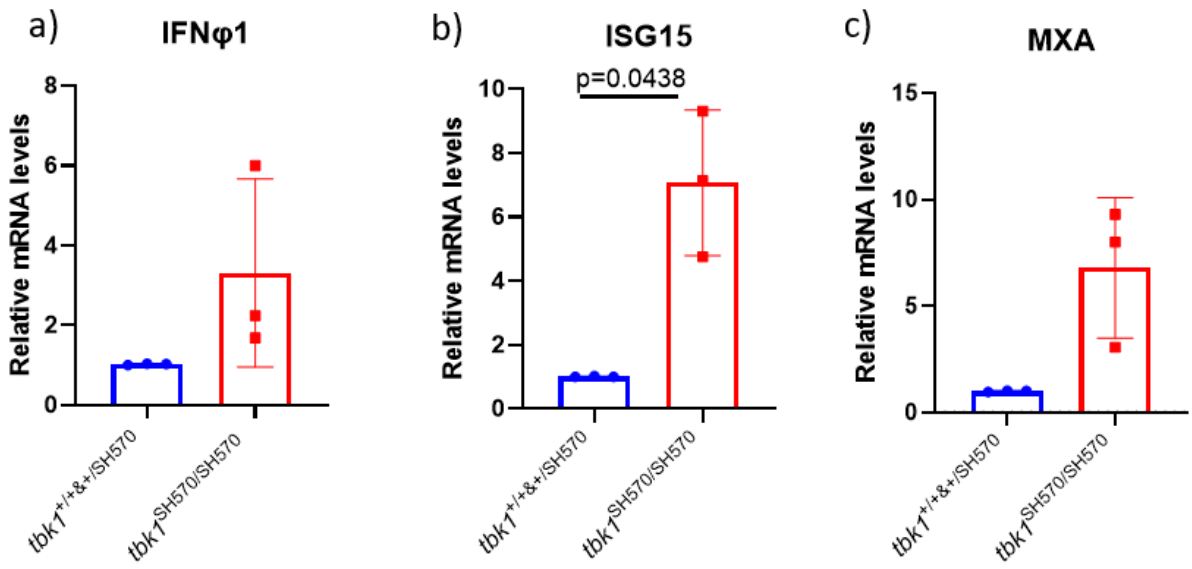

Figure 4. 11 Type I IFN induced gene expression level in 12 dpf *tbk1*$^{SH570/SH570}$. a) 12 dpf *tbk1*$^{SH570/SH570}$ shows no significant increase in *ifnΦ1* mRNA level compared to *tbk1*$^{+/+}$& *tbk1*$^{+/SH570}$ siblings. b) 12 dpf *tbk1*$^{SH570/SH570}$ shows a significant increase in *isg15* mRNA level compared to *tbk1*$^{+/+}$& *tbk1*$^{+/SH570}$ siblings p=0.0438. c) 12 dpf *tbk1*$^{SH570/SH570}$ shows no significant increase in *mxa* mRNA level compared to *tbk1*$^{+/+}$& *tbk1*$^{+/SH570}$ siblings**.** Each point represents a pool of 10 larvae from 3 independent group.

4.3.2 Investigating expression of type I Interferon induced genes in *tbk1*$^{SH643/SH643}$

In order to confirm the elevated expression of type I Interferon genes in *tbk1*^{SH570} mutants we also measured the mRNA level of type I IFN induced genes (*ifnφ1, isg15* and *mxa)* in 12 dpf *tbk1*^{SH643} zebrafish siblings. Similar to what we observed in *tbk1*^{SH570} mutants, *tbk1*$^{SH643/SH643}$ shows higher expression of all the three genes. Likewise, *tbk1*$^{SH643/SH643}$ only shows a significant increase in *isg15* mRNA level (t-test p value P=0.0211 (see Figure (4.12b) replicating the result seen in the *tbk1*^{SH570} mutants.

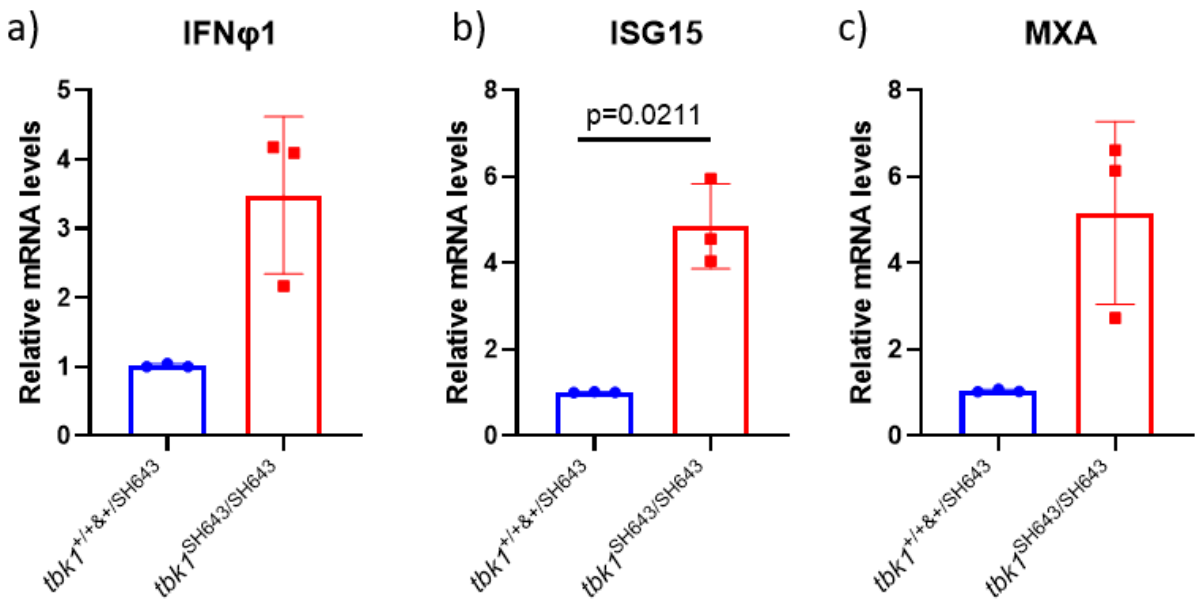

Figure 4. 12 Type I IFN induced gene expression level in 12 dpf *tbk1*$^{SH643/SH643}$. a) 12 dpf *tbk1*$^{SH643/SH643}$ shows no significant increase in cell *ifnΦ1* mRNA level compared to *tbk1*$^{+/+}$& *tbk1*$^{+/SH643}$ siblings. b) 12 dpf *tbk1*$^{SH643/SH643}$ shows a significant increase in *isg15* mRNA level compared to *tbk1*$^{+/+}$& *tbk1*$^{+/SH643}$ siblings p=0.0211. c) 12 dpf *tbk1*$^{SH643/SH643}$ shows no significant increase in *mxa* mRNA level compared to *tbk1*$^{+/+}$& *tbk1*$^{+/SH643}$ siblings. Each point represents a pool of 10 larvae from 3 independent group.

4.4 OPTN as an autophagy receptor for TBK1

An increasing number of studies have highlighted the strong impact of the autophagy pathway in immunity and inflammation(Levine et al., 2011). Recent findings indicate that TBK1 is involved in type I IFN production through OPTN in innate antiviral immunity (Génin et al., 2015). In the previous section we showed that the *tbk1*^{SH650} mutation had some impact on type I IFN induced gene expression. Since there is an overlap between autophagy and the innate immune response, and on account of the involvement of OPTN in IFN production through activation of TBK1 (Weidberg and Elazar, 2011), we wanted to examine if an OPTN LOF mutation (*optn*^{SA0143}) (Paulus and Link, 2014) had a similar impact.

4.4.1 Normal expression of type I Interferon genes in unstimulated *optn*$^{SA0143/SA0143}$

Looking at type I IFN induced genes in 12 dpf *tbk1*$^{SH650/SH650}$ we observed an increase in the mRNA level of *ifnΦ1, isg15* and *mxa* genes, which reached significance for *isg15*. Therefore, we examined expression of the same 3 genes in unstimulated 12 dpf *optn*^{SA0143} zebrafish. In this experiment we were not able to identify homozygous mutants as they have no overt or morphological phenotype, and we knew of no fluorescent reporter gene that would be elevated. Therefore, larvae were genotyped using tail biopsy DNA samples at 12 dpf. By measuring the mRNA level of *ifnΦ1, isg15* and *mxa* genes we found no evidence for an effect of *optn* LOF in 12 dpf zebrafish (Figure (4.13).

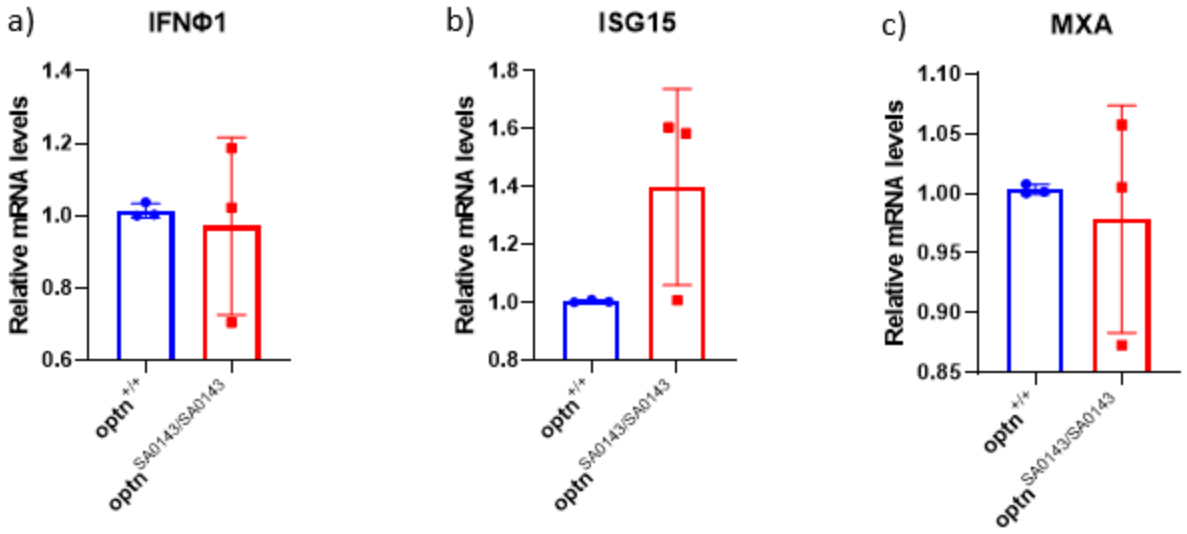

Figure 4. 13 Type I IFN induced gene expression in 12 dpf *optn*$^{SA0143/SA0143.}$ a) 12 dpf *optn*$^{SA0143/SA0143}$ shows no significant increase in cell *ifnΦ1* mRNA level compared to *optn*$^{+/+}$ siblings. b) 12 dpf *optn*$^{SA0143/SA0143}$ shows no significant increase in *isg15* mRNA level compared to *optn*$^{+/+}$ siblings. c) 12 dpf *optn*$^{SA0143/SA0143}$ shows no significant increase in *mxa* mRNA level compared to *optn*$^{+/+}$ siblings. Each point represents a pool of 10 larvae from 3 independent group.

4.4.2 No swimming defect observed in *optn*$^{SA0143/SA0143}$ at 12 dpf

A previous study of 5 dpf *optn*^{SA0143} did not reveal a swimming defect in *optn*$^{SA0143/SA0143}$ (Grierson unpublished observations). Since *tbk1* mutants show defects at 12 dpf we undertook an investigation in *optn*^{SA0143} at this age. We performed three independent experiments on in crosses between *optn*$^{+/SA0143}$ parents to derive experimental cohorts.

Viewpoint was used to calculate four swimming parameters (active duration, slow movement, fast movement and total distance)**.** Figure (4.14) shows that in all cases individual data points were obtained for each embryo to generate the first graph in each panel (i.e. a, d, g, j). This allows us to observe the overall response of the different genotype groups to light/dark switching. No significant differences between *optn*$^{SA0143/SA0143}$ and *optn*$^{+/+}$ were observed in the four parameters see table 4.1 and (Figure (4.14).

Table 4. 1 One-Way ANOVA and Tukey's multiple comparisons test p-value of *optn*^{SA0143}

12 days	One-way ANOVA between group (p-value)		Tukey's multiple comparisons test between Wild type & Homozygous (p-value)	
	Dark	Light	Dark	Light
Active duration	0.0278	0.0097	0.4538	0.3493
Slow movement	0.1229	0.0432	0.8625	0.9408
Fast movement	0.1078	0.0527	0.5553	0.3706
Total distance	0.0640	0.0244	0.5493	0.3783

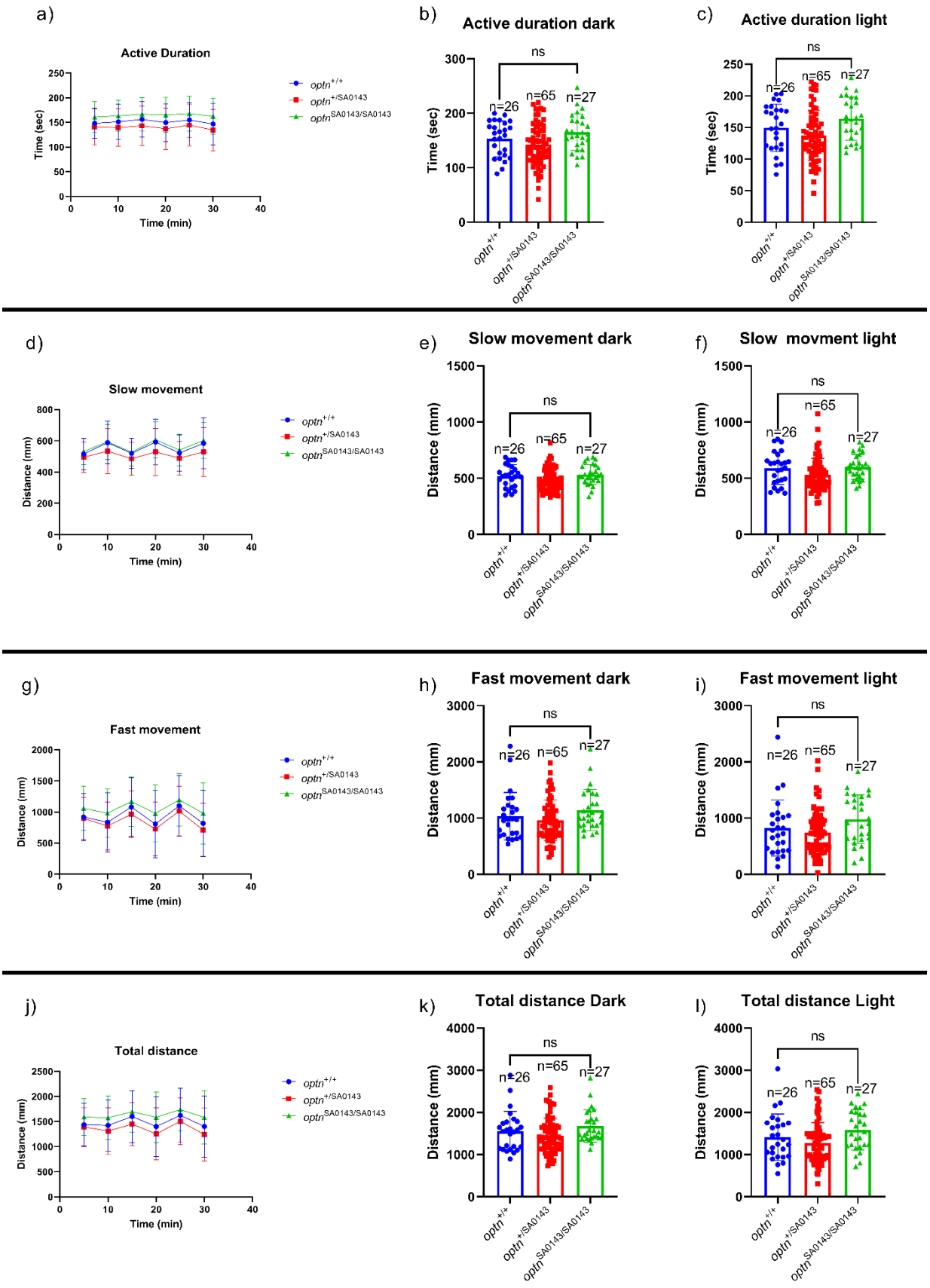
a)
Active Duration
Time (sec)
Time (min)
optn+/+
optn+/SA0143
optnSA0143/SA0143
b)
Active duration dark
Time (sec)
ns
n=26
n=65
n=27
c)
Active duration light
Time (sec)
ns
n=26
n=65
n=27
d)
Slow movement
Distance (mm)
Time (min)
e)
Slow movement dark
Distance (mm)
ns
n=26
n=65
n=27
f)
Slow movment light
Distance (mm)
ns
n=26
n=65
n=27
g)
Fast movement
Distance (mm)
Time (min)
h)
Fast movement dark
Distance (mm)
ns
n=26
n=65
n=27
i)
Fast movement light
Distance (mm)
ns
n=26
n=65
n=27
j)
Total distance
Distance (mm)
Time (min)
k)
Total distance Dark
Distance (mm)
ns
n=26
n=65
n=27
l)
Total distance Light
Distance (mm)
ns
n=26
n=65
n=27

Figure 4. 14 Swimming data for 12 dpf *optn*$^{SA0143/SA0143}$ zebrafish. a) Cumulative plots of 12 day old zebrafish progeny for active duration during dark light switching. b) Histogram of 12 day old zebrafish for active duration in dark cycles shows no significant difference between wild type and homozygous. c) Histogram of 12 day old zebrafish for active duration in light cycles shows no significant difference between wild type and homozygous. d) Cumulative plots of 12 day old zebrafish progeny for slow movement during dark light switching. e) Histogram of 12 day old zebrafish for slow movement in dark cycles shows no significant difference between wild type and homozygous. f) Histogram of 12 day old zebrafish for slow movement in light cycles shows no significant difference between wild type and homozygous ($p=0.0230$). g) Cumulative plots of 12 day old zebrafish progeny for fast movement during dark light switching. h) Histogram of 12 day old zebrafish for fast movement in dark cycles shows no significant difference between wild type and homozygous. i) Histogram of 12 day old zebrafish for fast movement in light cycles shows no significant difference between wild type and homozygous. j) Cumulative plots of 12 day old zebrafish progeny for total distance during dark light switching. k) Histogram of 12 day old zebrafish for total distance in light cycles shows no significant difference between wild type and homozygous. l) Histogram of 5day old zebrafish for total distance in light cycles shows no significant difference between wild type and homozygous. These data are from three independent experiments.

4.4.3 Investigation of possible maternal OPTN effect on swimming in 12 day old null *optn*$^{SA0143/SA0143}$

In the previous section we studied *optn* mutants that were derived from in crosses between *optn*$^{+/SA0143}$ parents. Due to the large volume of the zebrafish maternal zygote, it is known that there may be a strong maternal contribution of mRNA and protein. In order to exclude the possibility that any wild type OPTN from the maternal zygote could rescue a mutant phenotype in *optn*$^{SA0143/SA0143}$ progeny we generated experimental cohorts from three independent biological repeat of either *optn*$^{+/+}$ or *optn*$^{SA0143/SA0143}$ in crosses. The parental fish in this experiment were siblings, thus the 12 dpf zebrafish we studied were cousins (sharing grandparents). This approach controls for potential confounding genetic effects as far as possible. Viewpoint was used to calculate the same four swimming parameters (active duration, slow movement, fast movement and total distance).

Figure (4.15) shows that in all cases individual data points were obtained for each embryo to generate the first graph in each panel (i.e. a, d, g, j). This allows us to observe the overall response of the different genotype groups to light/dark switching. No significant reduction between null *optn*$^{SA0143/SA0143}$ and *optn*$^{+/+}$ was observed in both dark and light cycles of slow movement, fast movement and total distance see table (4.2). Interestingly we observed a significant reduction of active duration in *optn*$^{SA0143/SA0143}$ zebrafish during the dark cycles (t-test $p<0.0001$) but this was not observed in the light cycles (see Figure (4.15). This provides evidence of a maternal effect in the *optn*^{SA0143} mutant line that was potentially masking a small but significant difference in swimming behaviour in *optn* mutants.

Table 4. 2 One-Way ANOVA and Tukey's multiple comparisons test p-value of *optn*^{SA0143}incross

5days	Unpaired t test with Welch's correction (p-value)	
	Dark	Light
Active duration	<0.0001	0.0739
Slow movement	0.1670	0.5998
Fast movement	0.9687	0.2956
Total distance	0.5537	0.3125

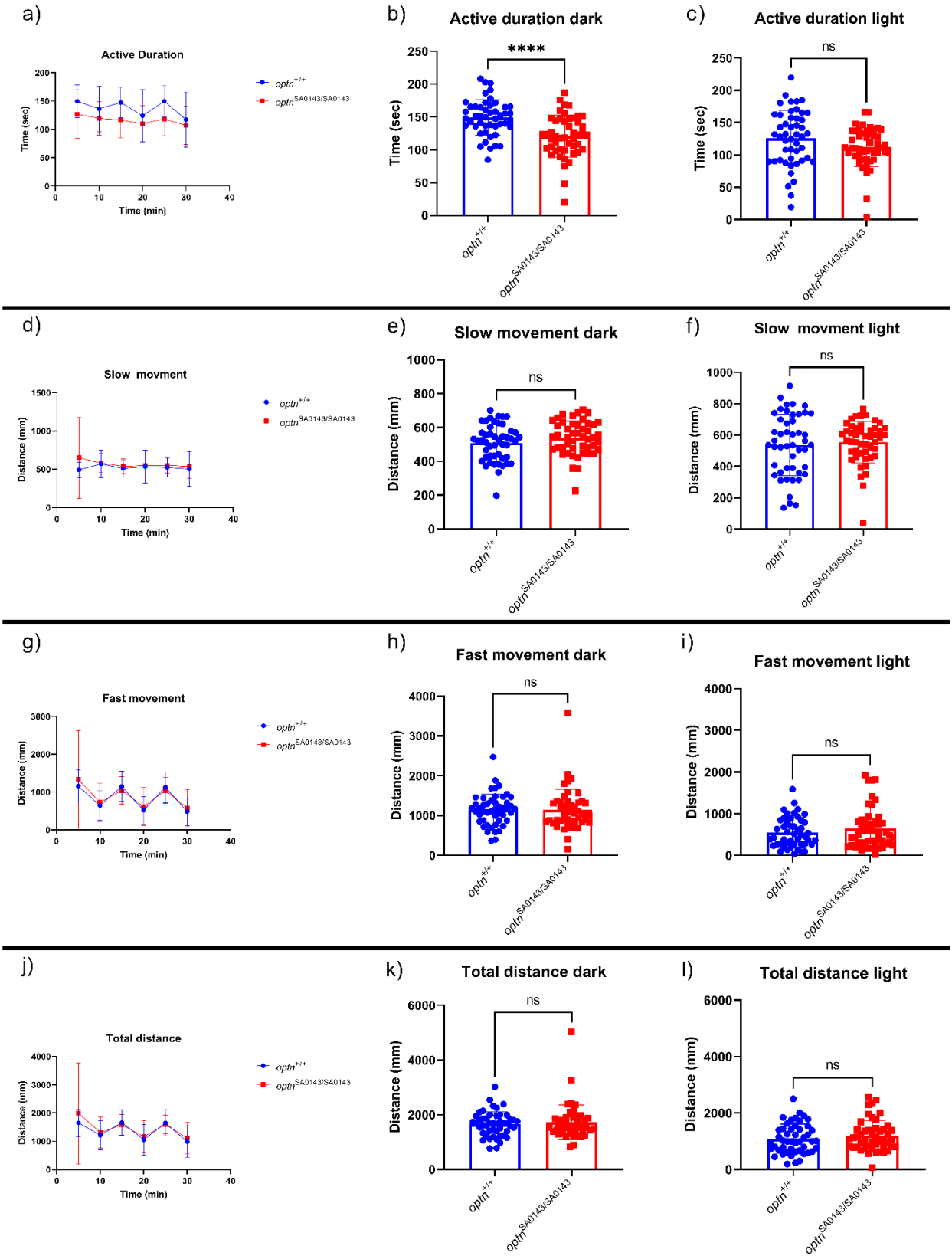
a)
Active Duration
Time (sec)
Time (min)
optn+/+
optnSA0143/SA0143
b)
Active duration dark
****
Time (sec)
c)
Active duration light
ns
Time (sec)
d)
Slow movment
Distance (mm)
Time (min)
e)
Slow movement dark
ns
Distance (mm)
f)
Slow movment light
ns
Distance (mm)
g)
Fast movement
Distance (mm)
Time (min)
h)
Fast movement dark
ns
Distance (mm)
i)
Fast movement light
ns
Distance (mm)
j)
Total distance
Distance (mm)
Time (min)
k)
Total distance dark
ns
Distance (mm)
l)
Total distance light
ns
Distance (mm)

Figure 4. 15 Swimming data for 12 day old *optn*^{SA0143} zebrafish obtained from homozygous parents. a) Cumulative plots of 12 day old zebrafish progeny for active duration during dark light switching. b) Histogram of 12-day old zebrafish for active duration in dark cycles shows a significant difference between wild type and null homozygotes $p<0.0001$. c) Histogram of 12 day old zebrafish for active duration in light cycles shows no significant difference between wild type and null homozgous. d) Cumulative plots of 12 day old zebrafish progeny for slow movement during dark light switching. e) Histogram of 12 day old zebrafish for slow movement in dark cycles shows no significant difference between wild type and null homozgous. f) Histogram of 12 day old zebrafish for slow movement in light cycles shows no significant difference between wild type and null homozygotes ($p=0.0230$). g) Cumulative plots of 12 day old zebrafish progeny for fast movement during dark light switching. h) Histogram of 12 day old zebrafish for fast movement in dark cycles shows no significant difference between wild type and null homozygotes. i) Histogram of 12 day old zebrafish for fast movement in light cycles shows no significant difference between wild type and null homozygotes. j) Cumulative plots of 12 day old zebrafish progeny for total distance during dark light switching. k) Histogram of 12 day old zebrafish for total distance in light cycles shows no significant difference between wild type and null homozygotes. l) Histogram of 12 day old zebrafish for total distance in light cycles shows no significant difference between wild type and null homozygotes. These data are from three independent experiments.

4.4.4 Investigating genetic interaction between *optn* and *tbk1* in zebrafish

In patients there is evidence to support a multiple hit model for ALS pathogenesis involving genetic and environmental factors (A Al-Chalabi 1, 1999). While these factors can be challenging to identify, increasing genetic sequencing of patients has uncovered a significant number of patients bearing >1 mutation (van Blitterswijk et al., 2012a). It is interesting that ALS/FTD patients have been reported in the literature that harbour hemizygous mutations in both *TBK1* and *OPTN* (Lattante et al., 2019, Pottier et al., 2015b), although these occur so rarely that it is impossible to determine the potential for an oligogenic disease mechanism or putative genetic interaction between the two mutant genes.

OPTN is a substrate for TBK1 kinase activity and phosphorylation of OPTN is involved in regulation of autophagy and mitophagy (Richter et al., 2016a). Clearly the effect of homozygous mutation of *optn* on swimming at 12 dpf (Fig 4.15) is much less pronounced than the effect of homozygous mutation of *tbk1* at the same age (Fig 3.24& 3.26). Thus, *optn* can only modestly contribute to the deleterious effects of *tbk1* mutations on swimming in 12 dpf zebrafish. Since we know that OPTN functions downstream of TBK1 in the autophagy pathway, if this pathway is involved in the swimming phenotype, we can predict that in an oligogenic model where both genes are mutated this will not lead to a more severe swimming phenotype.

If on the other hand TBK1 and OPTN function in parallel pathways that affect swimming, we might expect to see a more profound swimming defect when both genes are mutated.

In *tbk1* mutants we observed effects on swimming in response to dark/light stimulus and on thigmotaxis. Therefore, we wished to study the contribution of *tbk1* and *optn* mutations to both phenotypes. In the time available we only performed experiments that tested how introducing hemi- or homozygosity for *tbk1* modifies the $optn^{SA0143/SA0143}$ phenotype (see following section).

4.4.4.1 Generating an oligogenic model with mutations in *tbk1* and *optn*

We outcrossed *tbk1*$^{+/SH570}$ zebrafish with *optn*$^{+/SA0143}$ zebrafish to produce *tbk1*$^{+/SH570}$ *optn*$^{+/SA0143}$ zebrafish then we crossed these fish with *optn*$^{+/SA0143}$ to produce tbk*1*$^{+/SH570}$ *optn*$^{SA0143/SA0143}$. Then we in crossed tbk*1*$^{+/SH570}$ *optn*$^{SA0143/SA0143}$ to produce progeny of tbk*1*$^{+/+}$ *optn*$^{SA0143/SA0143}$, tbk*1*$^{+/SH570}$ *optn*$^{SA0143/SA0143}$ and tbk*1*$^{SH570/SH570}$ *optn*$^{SA0143/SA0143}$ (see Figure (4.16). These fish have no maternal contribution of wild type *optn* mRNA or protein.

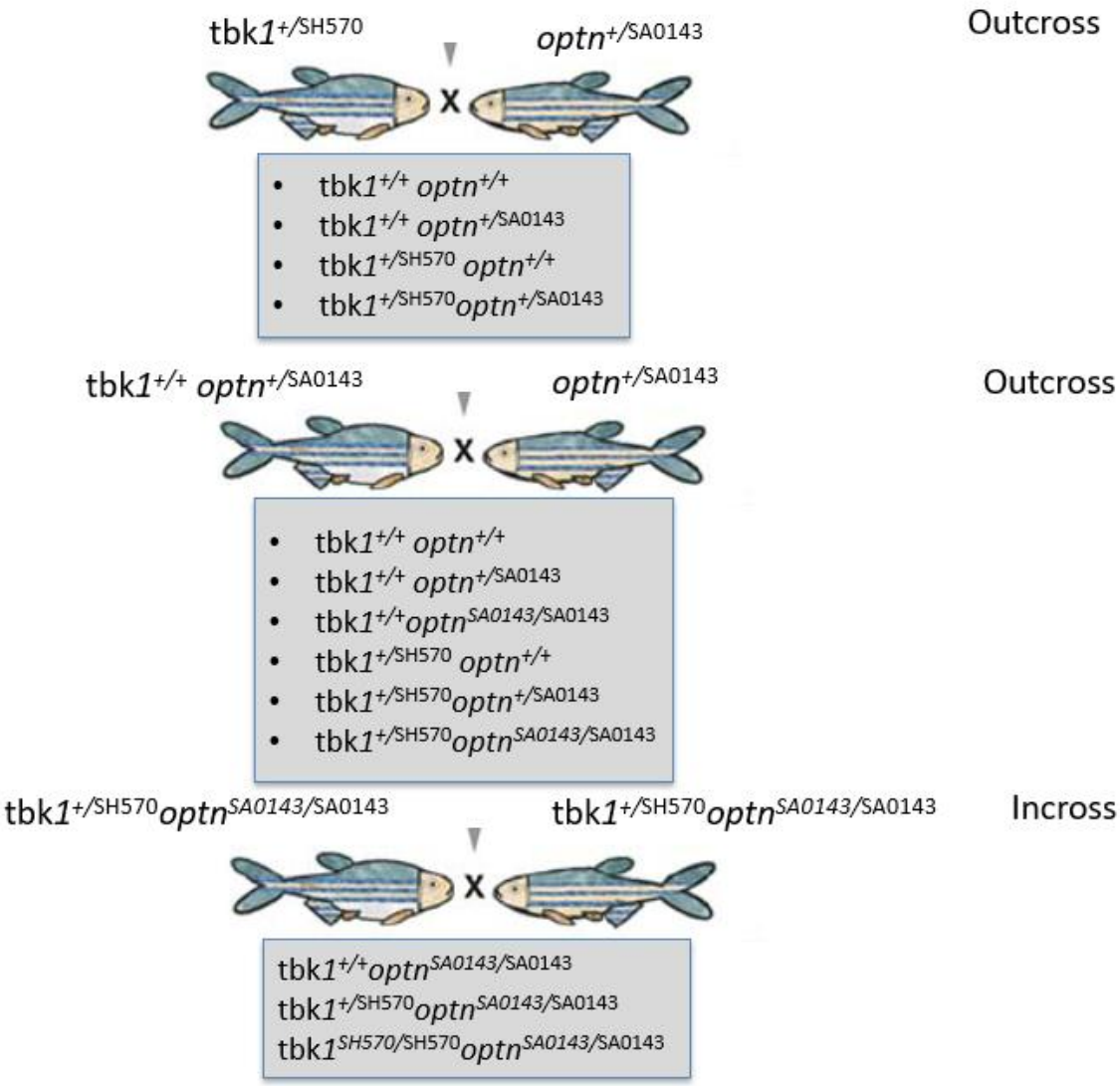

Figure 4. 16 Schematic overview of generating *tbk1*^{SH570} and *optn*^{SA0143} oligogenic models.

4.4.4.1.1 A swimming defect was not detected in *tbk1*$^{+/SH570}$ *optn*$^{SA0143/SA0143}$

A swimming study was conducted using the Viewpoint equipment on 12 dpf progeny from an in cross of *tbk1*$^{+/SH570}$ *optn*$^{SA0143/SA0143}$ parents to examine whether loss of one or both *tbk1* alleles modifies the *optn* phenotype. Viewpoint was used to calculate four swimming parameters (active duration, slow movement, fast movement and total distance)**.** Figure (4.17) shows that in all cases individual data points were obtained for each embryo to generate the first graph in each panel (i.e., a, d, g, j). This allows us to observe the overall response of the different genotype groups to light/dark switching. Similar to what we observed in 12 dpf tbk1$^{SH570/SH570}$ we observe a significant reduction in all four swimming parameters for both dark and lights between *tbk1*$^{SH570/SH570}$ *optn*$^{SA0143/SA0143}$ and *tbk1*$^{+/+}$ *optn*$^{SA0143/SA0143}$ (one-way ANOVA p<0.0001). Tukey's multiple comparison test also shows a significant difference between *tbk1*$^{SH570/SH570}$ *optn*$^{SA0143/SA0143}$ and *tbk1*$^{+/+}$ *optn*$^{SA0143/SA0143}$ (p<0.0001). However, despite a slight reduction in mean fast movement and total distance, when comparing *tbk1*$^{+/SH570}$ *optn*$^{SA0143/SA0143}$ and *tbk1*$^{+/+}$ *optn*$^{SA0143/SA0143}$, we did not observe any significant reduction in any swimming parameter during both the dark and light periods see table (4.3). This suggests that loss of one copy of *tbk1* does not alter the *optn*$^{SA0143/SA0143}$ phenotype, but loss of both causes a similar effect to that observed in *tbk1*$^{SH570/SH570}$ *optn*$^{+/+}$at 12 dpf.

Table 4. 3 One-Way ANOVA and Tukey's multiple comparisons test p-value of *tbk1*$^{+/SH570}$ *optn*$^{SA0143/SA0143}$ incross

12 days	Tukey's multiple comparisons test comparing *tbk1*$^{+/SH570}$ *optn*$^{SA0143/SA0143}$ and *tbk1*$^{+/+}$ *optn*$^{SA0143/SA0143}$ (p-value)	
	Dark	Light
Active duration	0.3158	0.0851
Total distance	0.2927	0.7896
Slow movement	0.3768	0.5744
Fast movement	0.2092	0.4686

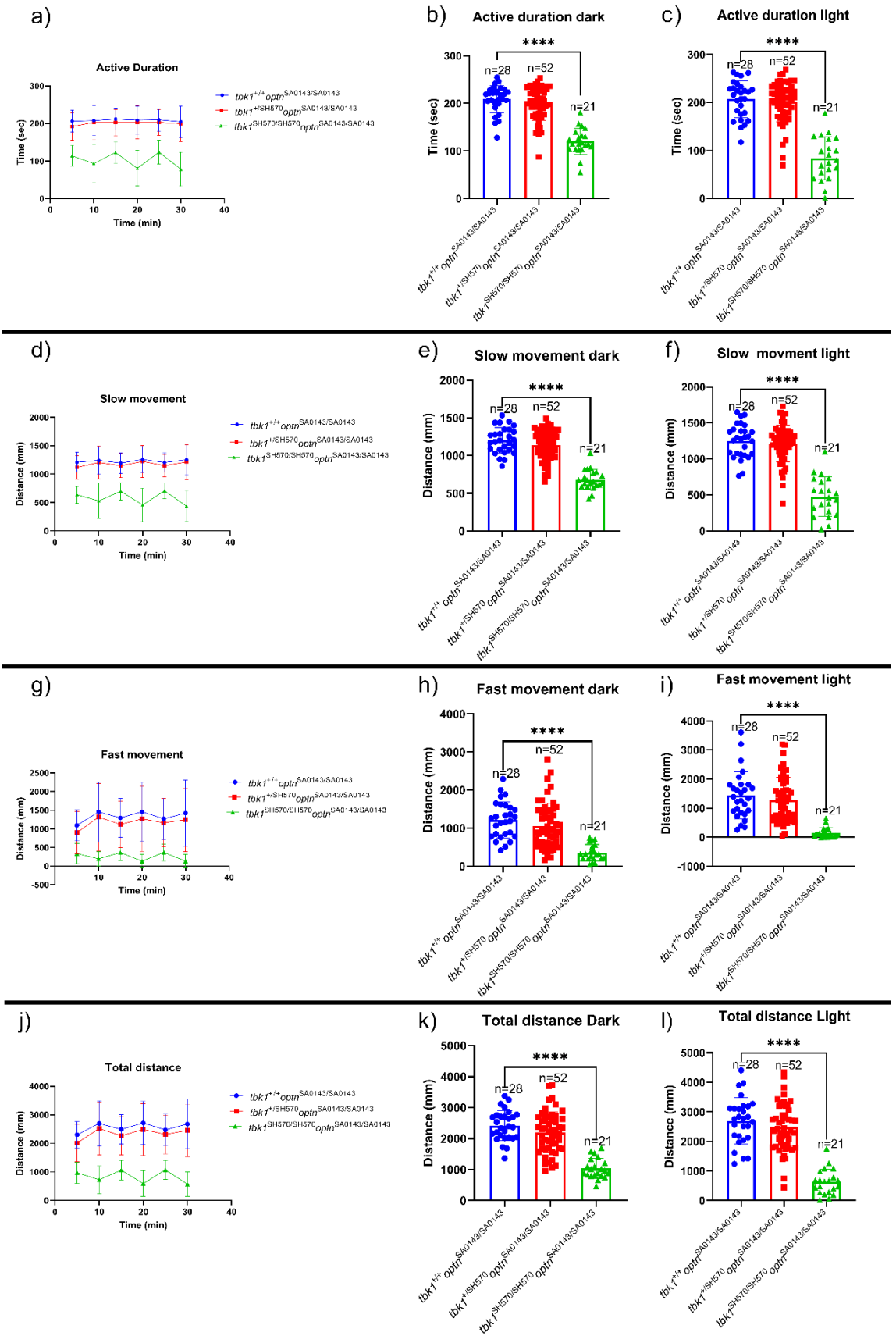
a)
Active Duration
Time (sec)
Time (min)
tbk1+/+optnSA0143/SA0143
tbk1+/SH570optnSA0143/SA0143
tbk1SH570/SH570optnSA0143/SA0143
b)
Active duration dark
****
n=28
n=52
n=21
Time (sec)
c)
Active duration light
****
n=28
n=52
n=21
Time (sec)
d)
Slow movement
Distance (mm)
Time (min)
tbk1+/+optnSA0143/SA0143
tbk1+/SH570optnSA0143/SA0143
tbk1SH570/SH570optnSA0143/SA0143
e)
Slow movement dark
****
n=28
n=52
n=21
Distance (mm)
f)
Slow movment light
****
n=28
n=52
n=21
Distance (mm)
g)
Fast movement
Distance (mm)
Time (min)
tbk1+/+optnSA0143/SA0143
tbk1+/SH570optnSA0143/SA0143
tbk1SH570/SH570optnSA0143/SA0143
h)
Fast movement dark
****
n=28
n=52
n=21
Distance (mm)
i)
Fast movement light
****
n=28
n=52
n=21
Distance (mm)
j)
Total distance
Distance (mm)
Time (min)
tbk1+/+optnSA0143/SA0143
tbk1+/SH570optnSA0143/SA0143
tbk1SH570D/SH570optnSA0143/SA0143
k)
Total distance Dark
****
n=28
n=52
n=21
Distance (mm)
l)
Total distance Light
****
n=28
n=52
n=21
Distance (mm)

Figure 4. 17 Swimming study data for a 12 day old *tbk1*$^{+/SH570}$ *optn*$^{SA0143/SA0143}$ in cross progeny. a) Cumulative plots of 12 day old zebrafish progeny for active duration during dark light switching. b) Histogram of 12-day old zebrafish for active duration in dark cycles shows a significant difference between *tbk1*$^{SH570/SH570}$ *optn*$^{SA0143/SA0143}$ *and tbk1*$^{+/+\&+/SH570}$ *optn*$^{SA0143/SA0143}$ but no significant difference has been observed between *tbk1*$^{+/SH570}$ *optn*$^{SA0143/SA0143}$ *and tbk1*$^{+/+}$ *optn*$^{SA0143/SA0143}$. c) Histogram of 12 day old zebrafish for active duration in light cycles shows a significant difference between *tbk1*$^{SH570/SH570}$ *optn*$^{SA0143/SA0143}$ *and tbk1*$^{+/+\&+/SH570}$ *optn*$^{SA0143/SA0143}$ but no significant difference has been observed between *tbk1*$^{+/SH570}$ *optn*$^{SA0143/SA0143}$ *and tbk1*$^{+/+}$ *optn*$^{SA0143/SA0143}$. e) Histogram of 12 day old zebrafish for slow movement in dark cycles shows a significant difference between *tbk1*$^{SH570/SH570}$ *optn*$^{SA0143/SA0143}$ *and tbk1*$^{+/+\&+/SH570}$ *optn*$^{SA0143/SA0143}$ but no significant difference has been observed between *tbk1*$^{+/SH570}$ *optn*$^{SA0143/SA0143}$ *and tbk1*$^{+/+}$ *optn*$^{SA0143/SA0143}$. g) Cumulative plots of 12 day old zebrafish progeny for fast movement during dark light switching. h) Histogram of 12 day old zebrafish for fast movement in dark cycles shows a significant difference between *tbk1*$^{SH570/SH570}$ *optn*$^{SA0143/SA0143}$ *and tbk1*$^{+/+\&+/SH570}$ *optn*$^{SA0143/SA0143}$ but no significant difference has been observed between *tbk1*$^{+/SH570}$ *optn*$^{SA0143/SA0143}$ *and tbk1*$^{+/+}$ *optn*$^{SA0143/SA0143}$. j) Cumulative plots of 12 day old zebrafish progeny for total distance during dark light switching. k) Histogram of 12 day old zebrafish for total distance in light cycles shows a significant difference between *tbk1*$^{SH570/SH570}$ *optn*$^{SA0143/SA0143}$ *and tbk1*$^{+/+\&+/SH570}$ *optn*$^{SA0143/SA0143}$ but no significant difference has been observed between *tbk1*$^{+/SH570}$ *optn*$^{SA0143/SA0143}$ *and tbk1*$^{+/+}$ *optn*$^{SA0143/SA0143}$. l) Histogram of 12 day old zebrafish for total distance in light cycles shows a significant difference between *tbk1*$^{SH570/SH570}$ *optn*$^{SA0143/SA0143}$ *and tbk1*$^{+/+\&+/SH570}$ *optn*$^{SA0143/SA0143}$ but no significant difference has been observed between *tbk1*$^{+/SH570}$ *optn*$^{SA0143/SA0143}$ *and tbk1*$^{+/+}$ ***optn*$^{SA0143/SA0143}$.** These data are from three independent experiments.

4.4.4.1.2 Altered thigmotaxis was not detected in 12 dpf *tbk1*$^{+/SH570}$ *optn*$^{SA0143/SA0143}$

To investigate any effect on thigmotaxis we conducted similar experiments to those described in (Figure (3.29) (of the previous chapter). Figure (3.29) shows the proportion of time spent swimming in the centre of the field during period of light and dark. When the lights are off we expect fish to enter the centre of the field as they are not able to determine their location relative to the edge (Figure (3.29a). Similar what we observed in 12 dpf *tbk1*$^{SH570/SH570}$**,** the *tbk1*$^{SH570/SH570}$ *optn*$^{SA0143/SA0143}$ larvae spend significantly more time swimming in the centre during light cycles (Figure (3.29b), demonstrating a significant reduction in thigmotactic behaviour between *tbk1*$^{SH570/SH570}$ *optn*$^{SA0143/SA0143}$ and *tbk1*$^{+/+}$ *optn*$^{SA0143/SA0143}$ One-way ANOVA $p<0.0001$ also Tukey's multiple comparisons test show a significant difference $p<0.0001$. However, no significant reduction in thigmotactic behaviour was observed between *tbk1*$^{+/SH570}$ *optn*$^{SA0143/SA0143}$ and *tbk1*$^{+/+}$*optn*$^{SA0143/SA0143}$ Tukey's multiple comparisons test ($p=0.5951$) (see Figure (4.18). This suggests that loss of one copy of *tbk1* does not alter the *optn*$^{SA0143/SA0143}$ phenotype, but loss of both copies causes a similar effect to that observed in *tbk1*$^{SH570/SH570}$ *optn*$^{+/+}$at 12 dpf.

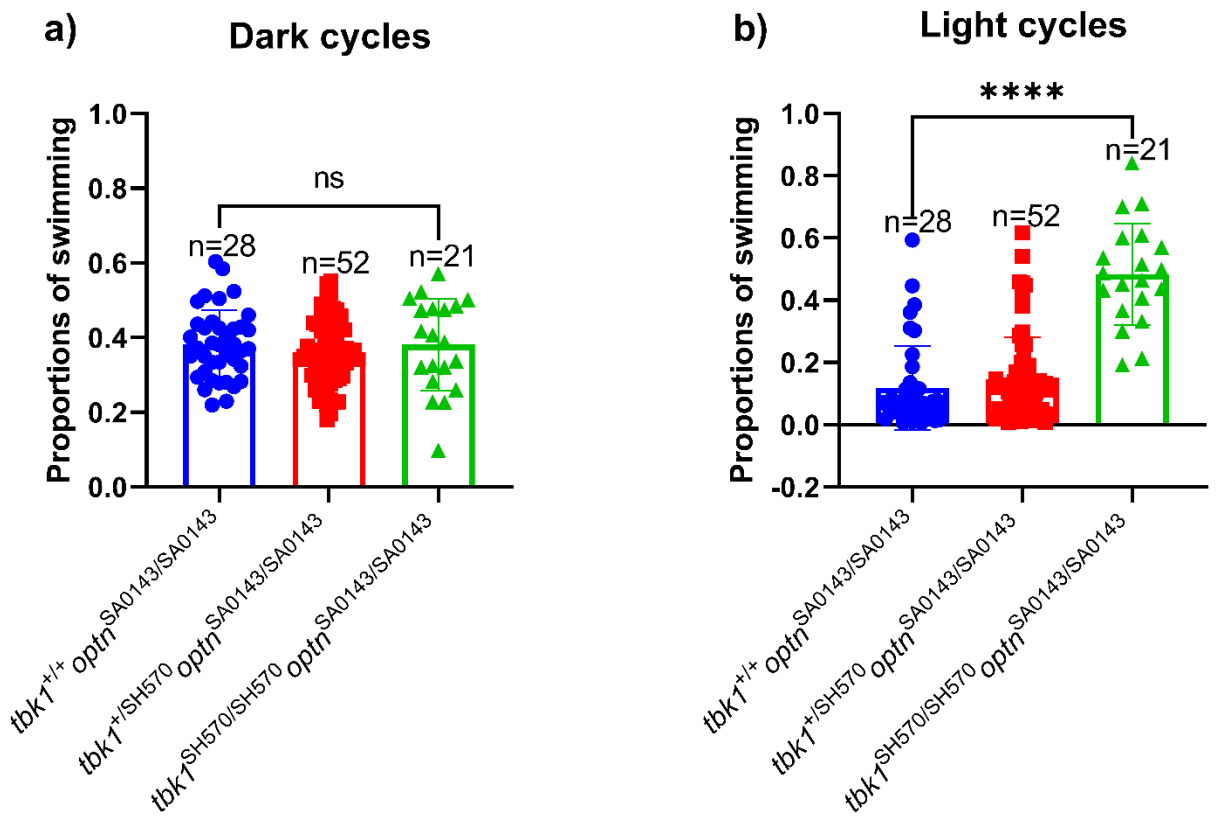

Figure 4. 18 Proportions of swimming for a 12 day old *tbk1*$^{+/SH570}$ *optn*$^{SA0143/SA0143}$ in cross progeny. a) Histogram for total time of proportion of swimming in dark cycles shows no significant difference between the three genotypes b) Histogram for total time for proportion of swimming in light cycles shows a significant difference between *tbk1*$^{SH570/SH570}$ *optn*$^{SA0143/SA0143}$ *and tbk1*$^{+/+\&+/SH570}$ *optn*$^{SA0143/SA0143}$ but no significant difference has been observed between *tbk1*$^{+/SH570}$ *optn*$^{SA0143/SA0143}$ *and tbk1*$^{+/+}$ *optn*$^{SA0143/SA0143}$. These data are from three independent experiments.

4.5 Discussion

TBK1 is a multifunctional kinase expressed in all tissues and implicated in the regulation of multiple pathways. During this project we aimed to identify pathways that are disrupted in *tbk1* mutants that lead to ALS/FTD phenotypes. Due to their overlapping functionality, the crosstalk between them, and prior evidence for their involvement in ALS/FTD, we specifically focussed on three pathways: NFκB, IRF3 and autophagy.

4.5.1 The role of TBK1 in NFκB signaling

As mentioned earlier some studies suggested a role for TBK1 in activating canonical NFκB signaling through phosphorylation and subsequent degradation of IκB. Because *TBK1* knockout mice are early embryonic lethal, most of the evidence for this comes from *in vitro* studies, or *in vivo* knockout in specific cell types. By using a *tbk1* knockout zebrafish which is viable to adulthood we are able to get new insights into *tbk1* function. We crossed our *tbk1* mutants onto a NFκB:GFP reporter line, to test the hypothesis that loss of *tbk1* function will result in reduced NFκB signaling due to reduced IκB phosphorylation and degradation and thus less NFκB translocating to the nucleus to stimulate signaling. Contrary to what we predicted we observed a significant increase in NFκB signaling suggesting the existence of alternative regulation of NFκB signaling in *tbk1* knockout zebrafish.

To confirm these findings, we undertook some additional experiments. If NFκB signaling is upregulated, we would expect to see upregulation of genes which are transcriptionally activated by NFκB. We therefore quantified expression of 4 proinflammatory cytokines using quantitative RT-PCR. By measuring the mRNA levels of *il1β*, *tnfα*, *il6* and *il8* in 5 dpf $tbk1^{SH570/SH570}$ zebrafish we did not observe any significant increase in their expression.

However, by 12 dpf, which is the age that we observed significant defects in swimming and thigmotactic behaviour, we observed a significant increase in expression of all 4 proinflammatory cytokine genes in *tbk1*$^{SH570/SH570}$ zebrafish. It is not clear why we observed the increase in NFκB:GFP as early as 3 dpf, but only see a significant increase in proinflammatory gene expression at 12 dpf. Potentially this could be because RNA is extracted from whole larvae, and NFκB:GFP is only upregulated in a subset of cell types.

On the other hand, there is a possibility that viral infection contributes to upregulation of NFkB and proinflammatory genes in our tbk1 mutant zebrafish model. This is especially likely because picornavirus RNA has been detected in fish housed in our aquaria. Also, it is known that in human cells TBK1 phosphorylates and mediates degradation of a picornavirus coat protein involved in infection (Li et al., 2019). Because picornavirus can be eradicated from zebrafish by bleaching we compared NFκB:GFP in tbk1 mutant embryos, but saw no difference in signal. Even when we raised the *tbk1*$^{+/SH570}$ in cross progeny in contaminated media we did not observe a different impact on *tbk1*$^{+/SH570}$ in cross progeny. Therefore, this is not likely to contribute to the phenotype up to day 5, but might be involved at later stages, for example we see that homozygous mutant larvae are smaller and slower to develop, and it is feasible that this may be due to picornavirus infection.

4.5.2 Confirmation of the *tbk1* mutant phenotype

Our primary findings support the involvement of mutant *tbk1* in NFkB signaling but not in activating canonical NFκB signaling. However, there are alternative explanations for what we observe. For example, a linked mutation in a nearby gene would be coinherited with the *tbk1*^{SH570} allele and thus could account for this phenotype. Alternatively, the *tbk1*^{SH570} mutation may not cause a loss of function of tbk1. This is quite likely since it generates a premature stop codon in the CCD1 domain, and thus a truncated protein could contain the kinase domain and maintain residual kinase activity. Unfortunately, we did not have time to optimise our custom zebrafish anti-tbk1 antibodies, so we do not have experimental proof for loss or truncation of tbk1 protein in this mutant.

To address these two possibilities, we could try to restore tbk1 function either by injecting wild type *tbk1* mRNA into *tbk1*$^{SH570/SH570}$ embryos, but this is not the best approach because we observe NFκB signaling around 3 dpf, by which time any effect of injected mRNA would be expected to be diminished. Therefore, we decided that the best approach would be generating a second *tbk1* mutant zebrafish model that carries a mutation in a more 5' region of the gene, that would abolish kinase activity. For technical reasons we targeted exon 4 and generated the tbk1^{SH643} mutant allele which is located within the serine threonine kinase domain. This mutation truncates within the kinase domain, and we would not expect any truncated protein to have kinase activity.

The new mutant line failed to complement the tbk1$^{+/SH570}$ mutation, and compound hemizygous mutants carrying both alleles showed an increased NFκB:GFP signal similar to tbk1$^{SH570/SH570}$. Therefore, it is extremely unlikely that the effect on NFκB is caused by another gene, but it may still be due to residual activity from the tbk1^{SH570} allele. Next, we conducted crosses of *tbk1*$^{+/SH643}$ and *tbk1*$^{+/SH643}$ NFκB:GFP which demonstrated that this allele also activated NFκB, demonstrating that this is a specific loss of *tbk1* function phenotype. Since *tbk1*^{SH643} mutants also showed upregulation of the same proinflammatory genes we conclude that these effects are also real.

4.5.3 The role of TBK1 in IRF3 signaling

TBK1 kinase activity is critical for IRF3 activation and type I IFNs production (Balka et al., 2020). To investigate the role of zebrafish *tbk1* in IRF3 signaling we outcrossed *tbk1*^{SH570} with an *mxa*:mCherry reporter line that is activated in response to IRF3. We predicted that we will observe a reduction of *mxa*:mCherry signaling because tbk1 kinase activity is needed for IRF3 activation. *mxa*:mCherry signal usually appears in the eyes from 3 dpf, allowing us to identify transgenic embryos. Examining mCherry expressing 5 dpf embryos that were later confirmed by genotyping to include tbk1$^{+/+}$, tbk1$^{+/SH570}$ and tbk1$^{SH570/SH570}$ we did not observe any significant difference in mCherry signal. Viral infection or binding of dsRNA to TLR3 are needed to activate IRF3 (Fitzgerald et al., 2003a).

Considering this fact, we used published approaches (brequinar and Poly I:C) to stimulate IRF3 signaling (Kavaliauskis et al., 2015, Ianevski et al., 2020, White et al., 2011). Treating 3dpf tbk1$^{+/SH570}$ IRF3 *mxa*:mCherry in-cross progeny with brequinar or Poly I:C for 48hr did not result in any significant change in mCherry fluorescence between the three genotypes. Treating a 12 dpf tbk1^{SH570} *mxa*:mCherry larvae with brequinar and PolyI:C would be a sensible next step, since we know other phenotypes manifest at this stage. However due to covid19 restrictions to aquarium access it was not feasible to attempt this protocol in 12 day old fish as it would be a licensed procedure and require regular and close monitoring of the larvae.
Because of these factors we instead looked at genes that are stimulated by Type I IFN signalling. If tbk1 is involved in irf3 activation, we would expect to observe a reduction in production of type I IFNs mRNA levels.
By measuring the mRNA levels of type I IFNs genes *ifnΦ1, isg15* and *mxa* in 12 dpf tbk1^{SH650} zebrafish we observed an increase of the expression of mRNA levels of *ifnΦ1, isg15* and *mxa* in 12 dpf tbk1$^{SH570/SH570}$ zebrafish, however only *isg15* reach statistical significance. It is possible that increasing the number of biological repeats could lead to the other gene expression changes reaching significance.

These findings are not conclusive because *tbk1*^{SH570} *mxa*:mCherry did not show any difference in IRF3 signaling between the three genotypes at 5 dpf. As mentioned we would need to investigate the *mxa*:mCherry phenotype at 12 dpf to confirm the RT-PCR result. Additionally, the increased production of type I IFN stimulated mRNA levels might not necessarily be prompted by mutant *tbk1*. Other than the possibility of viral infection causing the increased production of type I IFNs another explanation could be the dual nature of type I and Type II IFNs (Lee and Ashkar, 2018).

4.5.4 The role of TBK1 in autophagy mediated by OPTN

As mentioned previously ALS/FTD cases have been identified with mutations in both *TBK1* and *OPTN* genes indicating a possible polygenic effect (van Blitterswijk et al., 2012a). In addition TBK1 phosphorylates OPTN and recruitment of TBK1/OPTN drives ubiquitinated mitochondria to autophagosomes (Richter et al., 2016a).

Based on these facts investigating the role of TBK1 in Autophagy mediated by OPTN autophagy receptors is crucial to understand mechanisms of disease. To this end we attempted to leverage zebrafish genetic models to generate an oligogenic zebrafish model *tbk1*$^{+/SH570}$ *optn*$^{SA0143/SA0143}$ that carries a LOF mutation in the *tbk1*1 gene and null mutation in the *optn* gene to examine if this has an impact on the motor function and social behavior of zebrafish.

We showed in the previous chapter, a homozygous *tbk1* LOF mutation resulted in impaired swimming behaviour in zebrafish. If this effect was mediated fully or in part by *optn*, we should expect to see a swimming defect in *optn* homozygous mutants at 12 dpf. We detect a very subtle change in swimming behaviour in 12 dpf *optn* fish, which could represent a very specific effect of an optn-mediated autophagy defect. However, the size of this effect is too small to study, and further work is required to better understand its relevance. We also showed that combining the *optn* and *tbk1* mutations to generate fish that were compound homozygotes, or homozygous for an *optn* mutation and hemizygous for the *tbk1* mutation led to phenotypes that were similar to the tbk1 mutant phenotype. We did not have time to conduct the experiment in this project, but it would be interesting to see if heterozygosity or homozygosity for *optn* affects the *tbk1* mutant phenotype. Combined with the data in this thesis this could allow us to be clear about potential epistatic effects of these mutations relevant to ALS/FTD.

We conducted similar experiments and investigated thigmotaxis. In this case We detect a very subtle change in swimming behaviour in 3 biological repeats using 12 dpf *optn* fish, which could represent a very specific effect of an *optn*-mediated autophagy defect., however we do not know if *optn* mutation alone gives rise to a thigmotaxic phenotype. These experiments are important for a fuller conclusion to be drawn regarding this phenotype.

As previously observed in our model,TBK1 LOF mutation increased the mRNA expression level of type I IFN induced genes and in some mouse models OPTN had a role in the production of IFNs through TBK1 activation (Munitic et al., 2013). Measuring mRNA levels of type I IFN induced genes in progeny of *optn*$^{SA0143/SA0143}$ in cross zebrafish did not demonstrate increase of *ifnφ1, isg15* or *mxα*. This contrasts with what we observed in the 12 dpf *tbk1*$^{SH570/SH570}$ zebrafish. This suggests that the effect of *tbk1* on IFN1 signaling is independent of its interaction with *optn*.

ALS/FTD caused by *TBK1* mutations is inherited in an autosomal dominant manner however the *tbk1*$^{+/SH570}$ zebrafish did not show any significant defect in swimming behaviour. We wondered if we would see a phenotype in *tbk1*$^{+/SH570}$ hemizygotes if we introduced the *optn* mutation. However, we observed no synergistic effect suggesting that the tbk1 swimming defects are operating in the same pathway rather than in parallel. It would be interesting to conduct these studies the other way around, to determine if combining the *optn* mutation on a *tbk1*$^{SH570/SH570}$ background exacerbates the *tbk1* phenotype. If it did then it would suggest that there may be independent pathways involved (Medchalmi et al., 2021, Toth and Atkin, 2018) This would be interesting as our model is based on *tbk1* acting upstream of *optn* (see Figure (4.9).

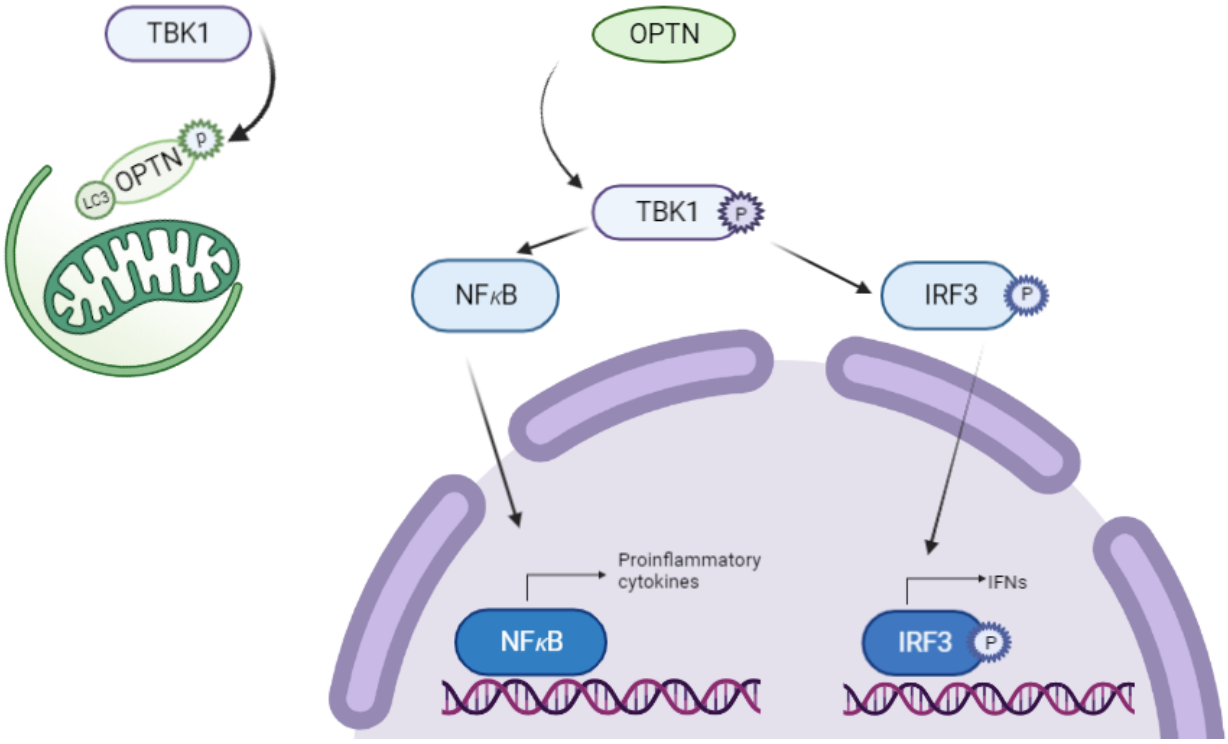

Figure 4. 19 Schematic shows possible ways that tbk1 and optn could function in parallel pathways. On the left is the established role of tbk1 and optn in mitophagy, on the right is an undefined role for optn in modifying tbk1-mediated NFkB signaling.

4.6 Conclusion

Several studies imply a role of *TBK1* in mediating cross talk between the innate immune response and autophagy. Examining the role of TBK1 in three pathways NFκB, IRF3 and autophagy we found that in zebrafish *tbk1* has a potential role in regulating NFκB and IRF3 signaling and show preliminary evidence that could help to determine the basis of any oligogenic effects in ALS/FTD patients with *TBK1* and *OPTN* mutations.

Because *tbk1* homozygotes showed evidence of increased NFκB signaling rather than decreased signaling that the canonical pathway would predict, we decided to investigate the alternative, less well characterised, and somewhat overlapping non-canonical NFκB pathway. In the next chapter we address this pathway and the potential way non-canonical signaling could mediate the upregulation of NFκB in *tbk1* mutants.

Chapter 5

5. Inhibition of map3k14a in noncanonical NF*κ*B signaling in *tbk1*$^{SH570/SH570}$ zebrafish

5.1 Introduction

In the previous chapter we were trying to investigate which pathways downstream of tbk1 are involved in ALS/FTD pathogenesis in zebrafish. Our findings strongly indicate that tbk1 regulates NF*κ*B signaling, as both *tbk1*$^{SH570/SH570}$ NF*κ*B:GFP and *tbk1*$^{SH643/SH643}$ NF*κ*B:GFP reporter lines showed upregulation of NFκB:GFP. Also, both models showed increased mRNA expression levels of NF*κ*B proinflammatory cytokine markers. This seemed contradictory to the role of tbk1 in the canonical pathway, where loss of function is predicted to lead to reduced NF*κ*B signaling. However, studies indicate that TBK1 negatively regulates noncanonical NF*κ*B signaling through phosphorylation-dependent degradation of NIK (Sun et al., 2013). Therefore, we might expect that loss of TBK1 function would lead to increased NIK activity which stimulates NF*κ*B signaling via the noncanonical pathway (Jin et al., 2012). In this chapter we describe experiments that aimed to reduce levels of NIK (map3k14a in zebrafish) in the *tbk1*^{SH570} NFκB:GFP reporter line to prevent the increase in NF*κ*B signaling and consequently rescue any of the pathogenic phenotypes in these fish.

In order to achieve this aim, we used crispant technology (Wu et al., 2018) to reduce map3k14a expression in *tbk1*^{SH570} reporter line embryos. The crispant approach involves injecting Cas9 with a mix of four different gRNAs all targeting the same gene (in this case *map3k14a*) into 1-2 cell embryos. It has been shown that this approach is extremely efficient and can produce phenotypes similar to null alleles of the target gene in F0 zebrafish (Wu et al., 2018). To validate the approach, we looked for evidence of mutations at the gRNA target sites, and for reduction in levels of *map3k14a* mRNA. To test if *map3k14a* crispants affected any of the readouts in *tbk1* mutants we injected the progeny of heterozygous tbk1 mutant in crosses where one parent was a NF*κ*B:GFP hemizygote, and studied the effect on GFP expression, motor function and the expression of proinflammatory cytokine genes downstream of NFκB (summarised in Figure (5.1).

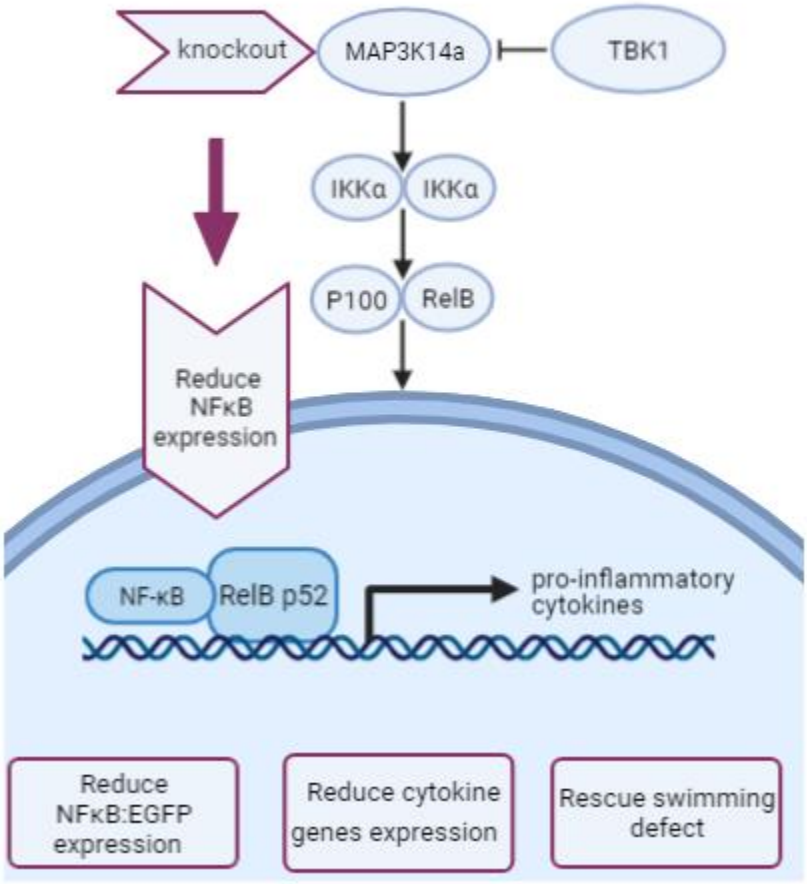

Figure 5. 1 Schematic of plan to rescue the TBK1 phenotype by knocking map3k14a in the *tbk1*$^{SH570/SH570}$ zebrafish. Using crispant to knock map3k14a in the *tbk1*$^{SH570/SH570}$ zebrafish predicting it will reduce NFκB: GFP expression thus proinflammatory cytokines gene expression which will rescue the swimming defect.

5.2 Expression level of *map3k14a* in *tbk1*$^{SH570/SH570}$ zebrafish

Since tbk1 regulates NFκB through phosphorylation of map3k14a leading to its degradation, *tbk1* homozygous mutants should have increased levels of map3k14a protein. However, there are no map3k14a antibodies that have been validated in zebrafish, so this experiment is not currently feasible.

Because we will be investigating *map3k14a* mRNA levels in crispants we first wished to determine if *map3k14a* mRNA levels were normal in *tbk1* mutants. Using qRT-PCR we observed a slight increase in *map3k14a* mRNA levels in *tbk1*$^{SH570/SH570}$ (mean=1.994 in comparison to 0.9381 in pooled *tbk1*$^{+/+}$ and in *tbk1*$^{+/SH570}$). However, this difference failed to reach significance in the 3 biological repeats that were performed (t-test p=0.0724 (see Figure (5.2). Therefore, it is not clear whether *map3k14a* mRNA levels are elevated in the *tbk1*^{SH570} mutant line.

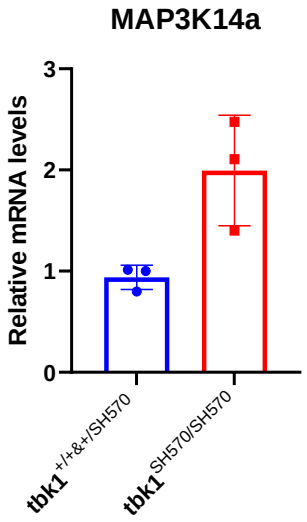

Figure 5. 2 *map3k14a* mRNA level in 12 dpf *tbk1*$^{SH570/SH570}$ zebrafish. *map3k14a* levels were determined using qRT-PCR relative to *eef1a1b*. *map3k14a* mRNA level shows no significant difference between 12 dpf *tbk1*$^{SH570/SH570}$ and pooled *tbk1*$^{+/+}$ and *tbk1*$^{+/SH570}$ larvae (t-test p=0.0724). Each point represents a pool of 10 larvae from 3 independent group.

5.3 Using crispants to study the role of *map3k14a* in *tbk1*^{SH570} zebrafish

To generate *map3k14a* crispants in *tbk1*^{SH570} zebrafish, we crossed *tbk1*$^{+/SH570}$ with *tbk1*$^{+/SH570}$ NFκB:GFP reporter hemizygotes and injected 1-2 cell stage embryos with a mixture containing Cas9 and a pool of 4 different *map3k14a* guide RNAs that were previously reported(Wu et al., 2018). As a control we used Cas9 and a published scrambled guide RNA control. This gRNA represents a random sequence without homology to the zebrafish genome, and does not show any phenotype in a comprehensive screen (Wu et al., 2018) This approach is summarised in (Figure (5.3).

By doing so we obtained 6 groups of experimental larvae: *tbk1*$^{+/+}$, *tbk1*$^{+/SH570}$ and *tbk1*$^{SH570/SH570}$, that were injected with Cas9 and either *map3k14a* or scrambled gRNA. At 3 dpf we used a fluorescence microscope to sort the embryos which are hemizygous carriers of the NFκB:GFP reporter and quantify GFP expression. Strong and weak GFP expressing fish are then raised separately and used for a Viewpoint swimming study on day 12. After this they were sacrificed, a tail biopsy taken for genotyping, and qRT-PCR was used to determine cytokine expression in each experimental group.

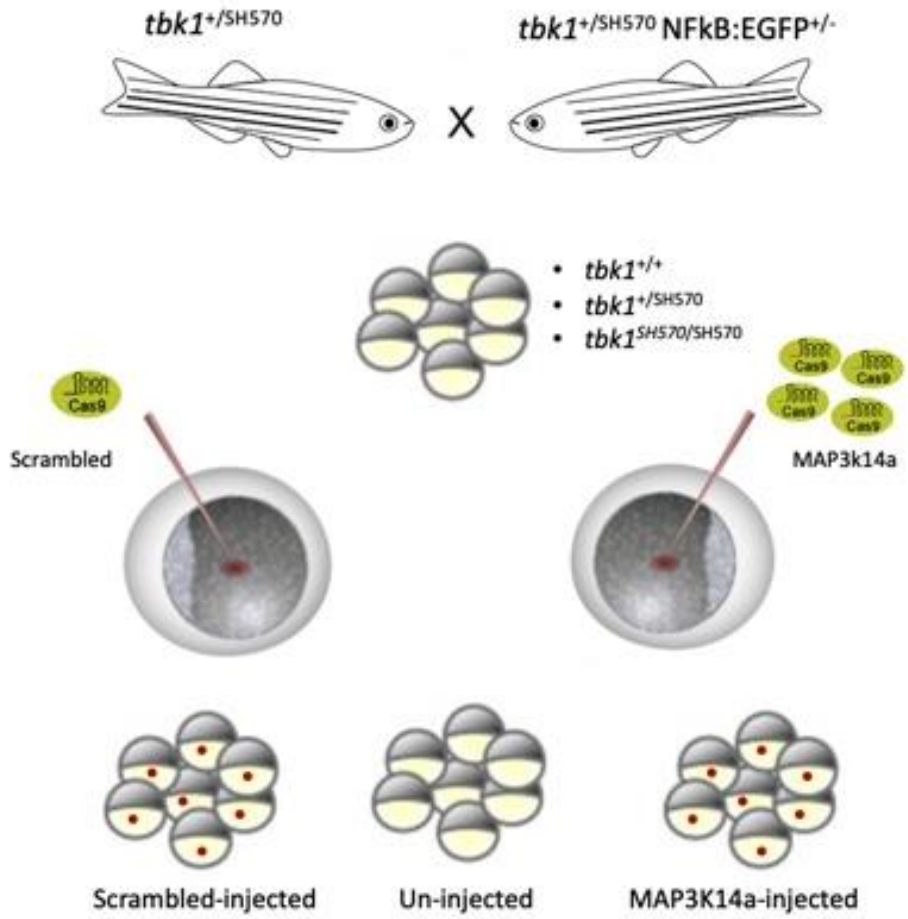

Figure 5. 3 Schematic overview of crispant experimental approach. *tbk1*$^{+/SH570}$ zebrafish were outcrossed with *tbk1*$^{+/SH570}$ NF*κ*B:GFP reporter fish. Out cross progeny were either injected with a mixture of four *map3k14a* gRNA/cas9 or a scrambled control gRNA/cas9. Uninjected embryos were also collected for use as a further control.

5.3.1 Examining *map3k14a* gRNA crispant efficiency

To examine crispant efficiency to introduce mutations in *tbk1*^{SH570} embryos we used high resolution melt analysis (HRMA) of the 4 targets located in exons 4, 5, 11 and 12 to analyse embryos that had previously been genotyped for *tbk1*^{SH570} alleles. For each *map3k14a* target we analysed four scrambled gRNA *tbk1*$^{+/+}$ controls, four *map3k14a* crispant *tbk1*^{SH570} heterozygotes and three *map3k14a* crispant *tbk1*^{SH570} homozygotes.

HMRA detects changes in the meting temperature of DNA duplexes. Heteroduplexes melt differently to homoduplexes, and this can be seen as a shift in the melt curve. If mutagenesis is working efficiently, we would expect to see shifts caused by the presence of mutant and wild type DNA templates. We do not know if all heteroduplexes will shift the melt curve, so we may underestimate the efficiency of the gRNA. The melt curve was shifted in some of the *MAP3K14a* crispant injected embryos compared to uninjected controls, indicating that a mutation has been introduced in the targeted *map3k14a* region. For target 1 (exon 4) and target 2 (exon 5) 5 out of the 7 crispant embryos shows a shift in the melting curve. For target 4 (exon 12) all crispant injected embryos showed a shift in the melting temperature. For target 3 (exon 11) the situation is difficult to interpret. The wild type controls are not tightly clustered, which often means that there can be more than one stable conformation for the DNA duplex. This makes it difficult to see whether the crispant melt curves are different. However, repeating the injection three times and screening the 4 targets of *MAP3K14a*, around 71% of crispant injected embryos show a shift in melting curve (see Figure (5.4).

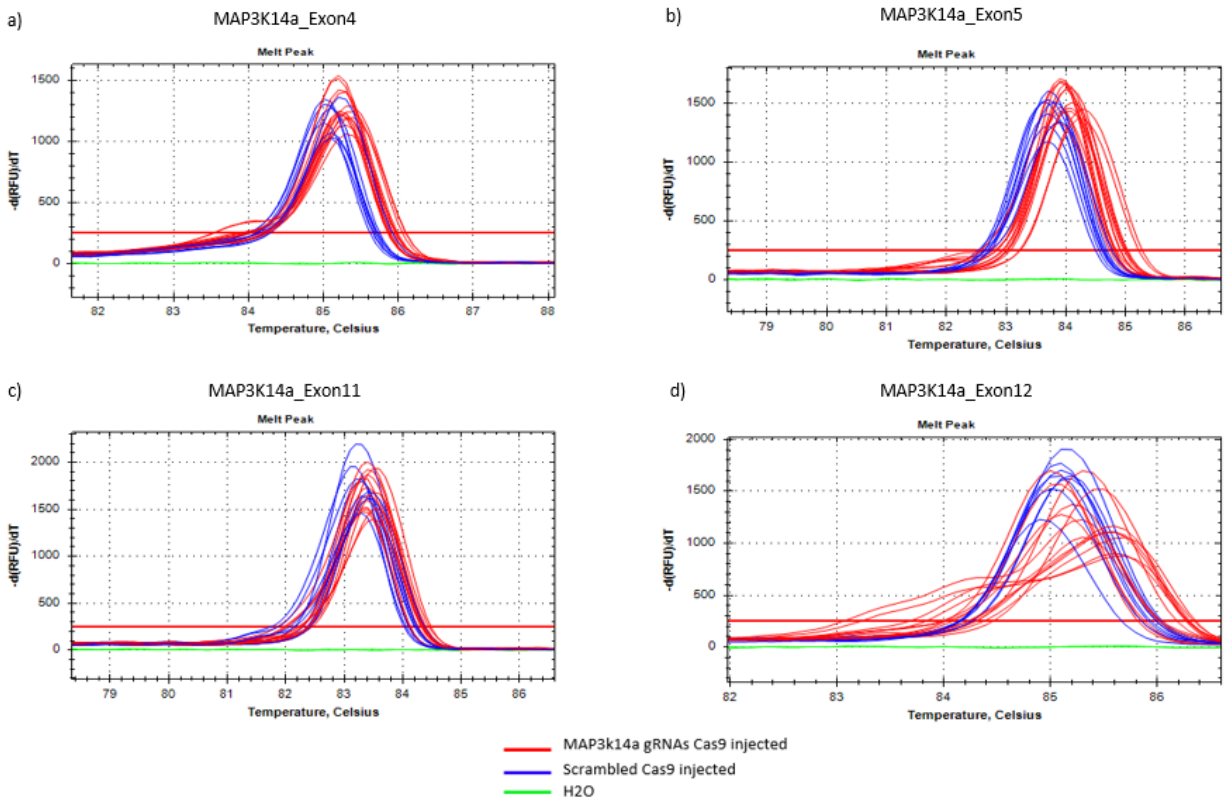

Figure 5. 4 High-resolution melt analysis (HRMA) indicates that mutations have been introduced in crispant embryos. Melt curves are shown for 4 *tbk1*$^{+/+}$ scrambled gRNA crispants (blue lines), 3 *tbk1*$^{SH570/+}$ *map3k14a* crispants (red lines) and 4 *tbk1*$^{SH570/SH570}$ (red lines) crispants from one of the 3 replicate experiments performed. The negative control is shown in green. (a) exon 4, (b) exon 5, (c) exon 11 and (d) exon 12.

To confirm the HMRA data for exon 12, we took advantage of the fact that this gRNA is located close to a BslI site (Figure (5.5b). Thus, BslI will cut the wild type *map3k14a* sequence but if a mutation has been introduced that disrupts that BslI site it will not cut the fragment. We do not know if all mutations will disrupt the BslI site, so we may underestimate the efficiency of the gRNA. BslI will digest the wild type allele giving two fragments of 109 and 142 bp, compared to 251bp if the site is disrupted. Figure (5.4) shows the same samples as (Figure (5.5b) tested using BslI digest. Four of the seven *map3k14a* crispants have a disrupted BslI site in some of the template DNA. Thus, both approaches suggest that the crispant approach has induced mutations at the desired target sites.

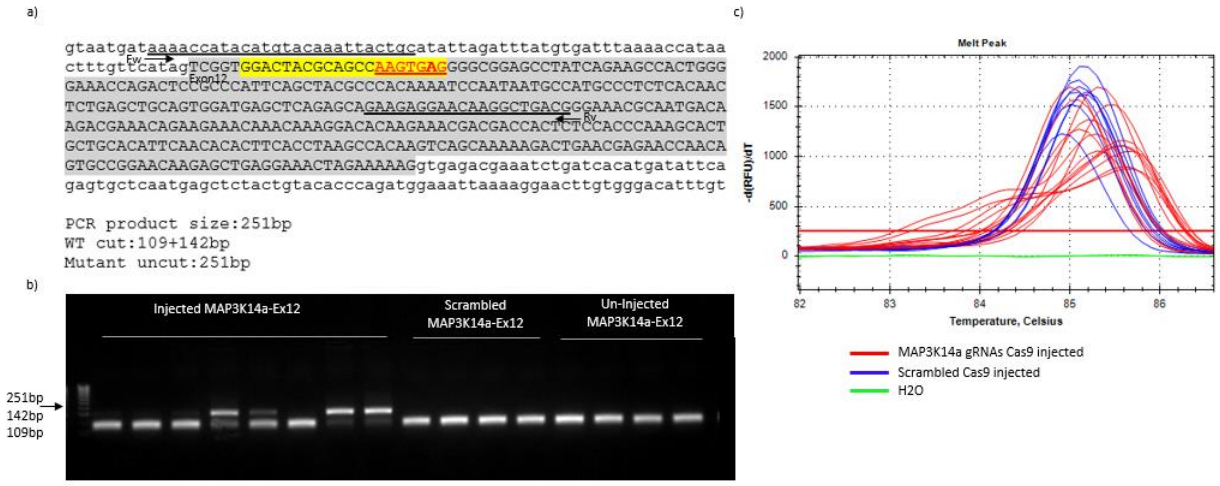

Figure 5. 5 Investigating exon 12 mutation efficiency in crispants using BslI restriction digest. (a) Diagram depicting location of forward (FW) and reverse (RV) primer binding sites. Exon 12 is in uppercase, and the flaking introns in lowercase. The gRNA sequence is highlighted in yellow, underlined red sequence is where BslI will cut). b) Gel image showing disruption of the BslI site is *map3k14a* crispants, but not scrambled crispants or uninjected controls. After BslI digest, wild type gives bands of 109 and142 bp, and undigested PCR product will be 251 bp.c) . Melt curves for map3k14a exon12 shows 4 *tbk1*$^{+/+}$ scrambled gRNA crispants (blue lines), 3 *tbk1*$^{SH570/+}$ *map3k14a* crispants (red lines) and 4 *tbk1*$^{SH570/SH570}$ (red lines) crispants. The negative control is shown in green.

5.3.2 *map3k14a* crispant *tbk1*$^{SH570/SH570}$ zebrafish did not have reduced levels of NF*κ*B:GFP at 3 dpf

If *map3k14a* mediates increased noncanonical NF*κ*B signaling in *tbk1* homozygous mutants we would expect to see a reduced level of NF*κ*B:GFP in *tbk1*$^{SH570/SH570}$ *map3k14a* crispants compared to *tbk1*$^{SH570/SH570}$ scrambled crispants. At 3 dpf we examined the NF*κ*B:GFP fluorescence under a microscope and quantified NF*κ*B:GFP expression by calculating the mean fluorescence signal per larvae in groups of 3 larvae (Figure (5.6). As expected *tbk1*$^{SH570/SH570}$ larvae had significantly higher GFP fluorescence, but we did not see any change in the level of fluorescence in the *map3k14a* crispants.

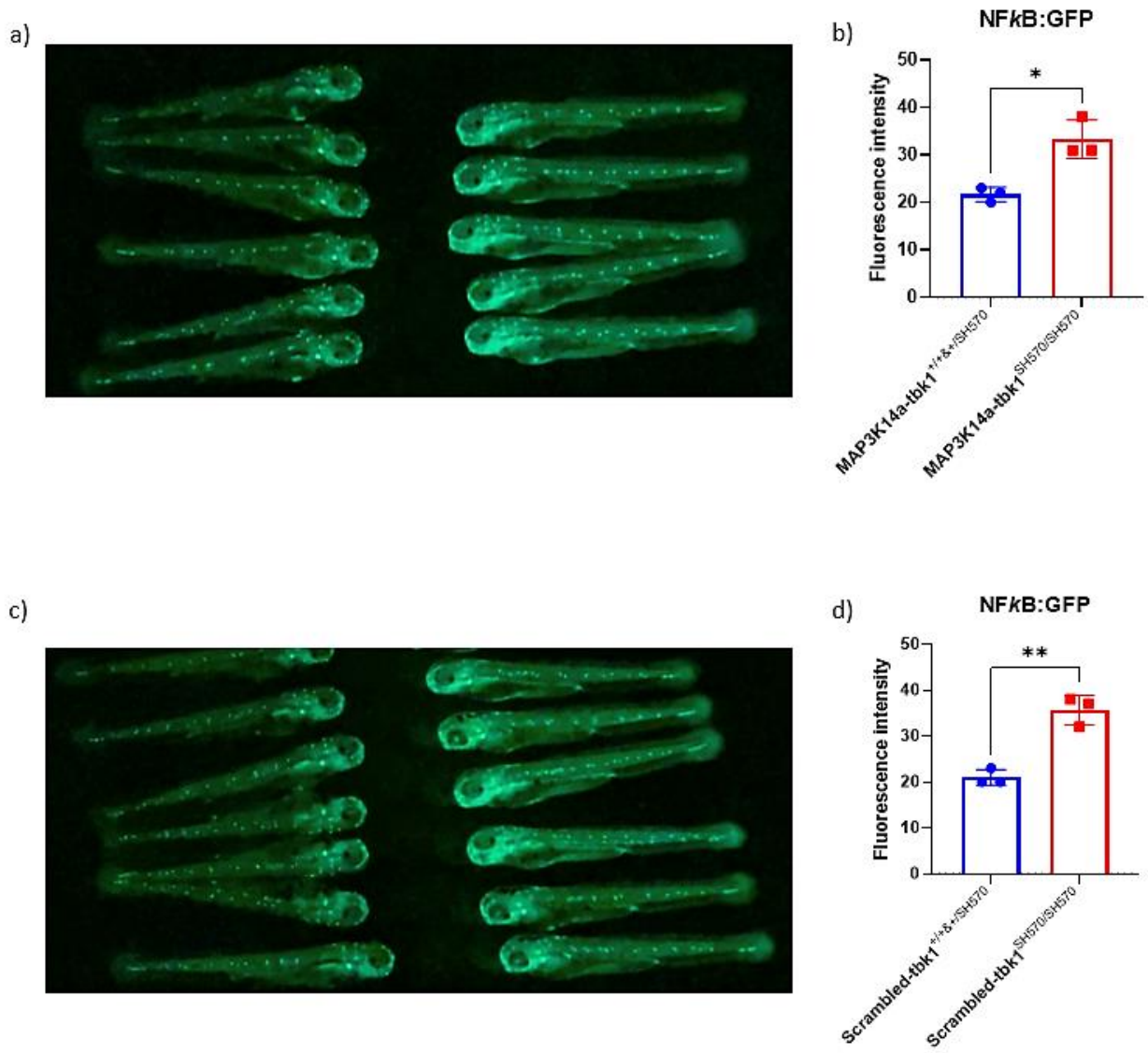

Figure 5. 6 Effect of *ma3k14a* crispant on NFκB:GFP fluorescence in *tbk1*^{SH570}. a) Groups of 3 dpf *map3k14a* crispants selected as low (left) or high (right) GFP fluorescence. All highly fluorescent fish were confirmed by genotyping to be *tbk1*$^{SH570/SH570}$. b) NFκB:GFP mean florescence intensity is significantly higher in *map3k14a* crispant *tbk1*$^{SH570/SH570}$ compared to *map3k14a* injected *tbk1*$^{+/+}$ and *tbk1*$^{+/SH570}$ (p =0.0261). c) Groups of 3 dpf scrambled crispants selected as low (left) or high (right) GFP fluorescence. All highly fluorescent fish were confirmed by genotyping to be *tbk1*$^{SH570/SH570}$. d) NFκB:GFP mean florescence intensity is significantly higher in scrambled crispant *tbk1*$^{SH570/SH570}$ compared to scrambled injected *tbk1*$^{+/+}$ and *tbk1*$^{+/SH570}$ (p =0.0056).

5.3.3 *map3k14a* crispant *tbk1*$^{SH570/SH570}$ zebrafish had defective swimming at 12 dpf

If the increase in NFκB signaling is related to the swimming phenotype in 12 dpf *tbk1*$^{SH570/SH570}$ zebrafish, we predicted that *ma3k14a* crispants may show improvement in their swimming when compared to *tbk1*$^{SH570/SH570}$ scrambled crispants.

As described previously crosses between *tbk1*$^{+/SH570}$ and *tbk1*$^{+/SH570}$ NFκB:GFP reporter hemizygotes were performed and 1-2 cell stage embryos were injected with a mixture containing Cas9 and a pool of 4 different *map3k14a* guide RNAs or a scrambled guide RNA control. Table (5.1) summarises the total number of larvae of each genotype that were used in these experiments.

Table 5. 1 Summary of 12 dpf crispant larvae used in swimming experiments

Crispant	**scrambled**	***map3k14a***	**scrambled**	***map3k14a***	**scrambled**	***map3k14a***
Genotype	**tbk1$^{+/+}$**	**tbk1$^{+/+}$**	**tbk1$^{+/SH570}$**	**tbk1$^{+/SH570}$**	**tbk1$^{SH570/SH570}$**	**tbk1$^{SH570/SH570}$**
Experiment 1	19	13	12	33	9	5
Experiment 2	14	13	28	27	5	7
Experiment 3	17	10	23	30	8	7
Total	50	36	63	80	22	19

We analysed the same swimming parameters as described in the previous chapters (active duration, slow movement, fast movement and total distance). The results are presented in (Figure (5.7), and the statistical analysis is presented in Table 5.2. In all cases individual data points were obtained for each embryo to generate the first graph in each panel (i.e. a, d, g, j). This allows us to observe the overall response of the different genotype groups to light/dark switching.

We first wished to establish whether the crispant *tbk1*$^{+/+}$ and *tbk1*$^{SH570/SH570}$ larvae still showed a significant difference in swimming. Comparing scrambled *tbk1*$^{+/+}$ and scrambled *tbk1*$^{SH570/SH570}$ we observed highly significant difference in all four swimming parameters.

However, when we compared *map3k14a* crispant *tbk1*$^{+/+}$ and *map3k14a* crispant *tbk1*$^{SH570/SH570}$ we see that the results for fast swimming (in the light and the dark) and total distance (in the light) do not reach significance.

It appears that the *map3k14a* crispant has affected some swimming parameters. Figure (5.7) panels (h and i) show that the effect of *map3k14a* appears to be a small reduction in fast swimming in the wild type larvae, rather than a rescue of the *tbk1*$^{SH570/SH570}$ fast swimming phenotype.

Finally, by comparing scrambled and *map3k14a* within each genotype (*tbk1*$^{+/+,}$ *tbk1*$^{+/SH570,}$ and *tbk1*$^{SH570/SH570}$) we can see whether the *map3k14a* crispant rescues any of the swimming defects. There were no significant improvements in swimming in the map3ka14a crispants, therefore according to these results *map3k14a* does not appear to be involved in the motor phenotype in this model.

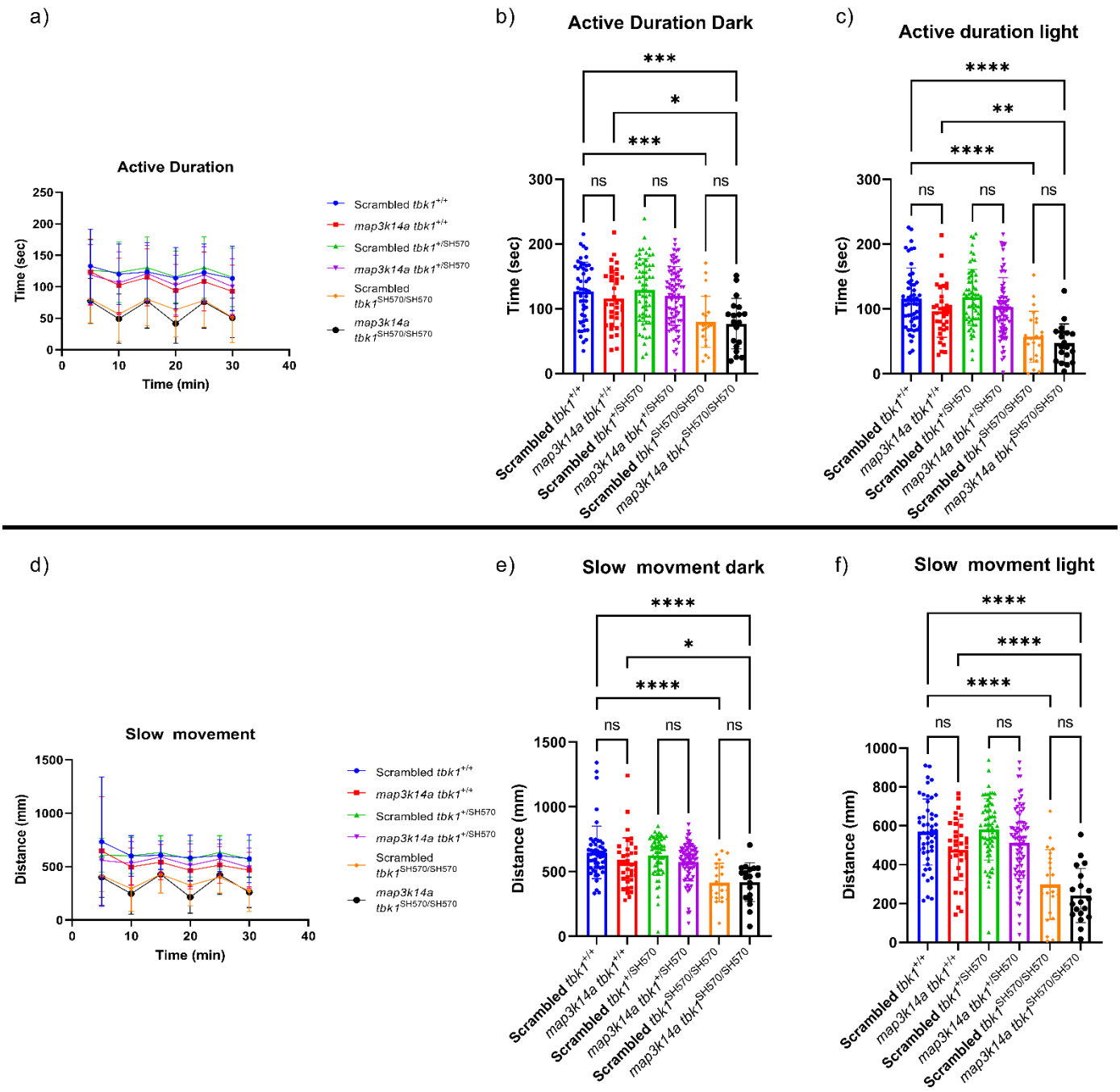
a)
Active Duration
Time (sec)
Time (min)
Scrambled tbk1+/+
map3k14a tbk1+/+
Scrambled tbk1+/SH570
map3k14a tbk1+/SH570
Scrambled tbk1SH570/SH570
map3k14a tbk1SH570/SH570
b)
Active Duration Dark
Time (sec)
ns
c)
Active duration light
Time (sec)
ns
d)
Slow movement
Distance (mm)
Time (min)
e)
Slow movment dark
Distance (mm)
f)
Slow movment light
Distance (mm)

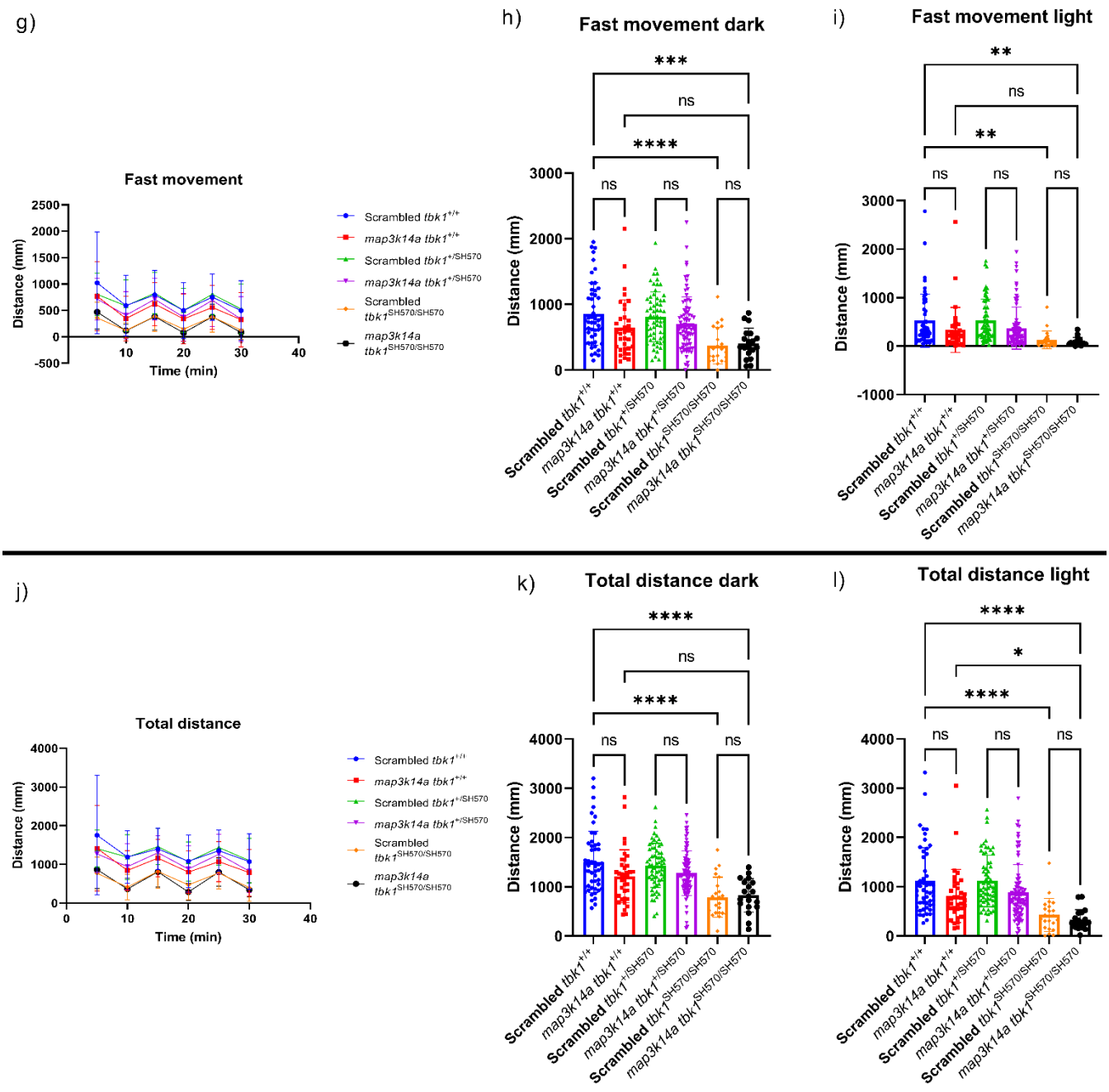

Figure 5. 7 swimming study data for a 12 day old *MAP3K14a* injected *tbk1*$^{SH643/SH643}$ zebrafish. a) Cumulative plots of 12 day old zebrafish *tbk1*^{SH570} for active duration during dark light switching. b) Histogram of 12 day old zebrafish for active duration in dark cycles shows a significant difference between scrambled injected *tbk1*$^{+/+}$ and scrambled injected *tbk1*$^{SH570/SH570}$, *MAP3K14a* injected *tbk1*$^{+/+}$ and *MAP3K14a* injected *tbk1*$^{SH570/SH570}$ and scrambled injected *tbk1*$^{+/+}$ and *MAP3K14a* injected *tbk1*$^{SH570/SH570}$. c) Histogram of 12 day old zebrafish for active duration in light cycles shows significant difference between scrambled injected *tbk1*$^{+/+}$ and scrambled injected *tbk1*$^{SH570/SH570}$, *MAP3K14a* injected *tbk1*$^{+/+}$ and *MAP3K14a* injected *tbk1*$^{SH570/SH570}$ and scrambled injected *tbk1*$^{+/+}$ and *MAP3K14a* injected *tbk1*$^{SH570/SH570}$. d) Cumulative plots of 12 day old zebrafish *tbk1*^{SH570} for slow movement during dark light switching.

e) Histogram of 12 day old zebrafish for slow movement in dark cycles shows significant difference between scrambled injected *tbk1*$^{+/+}$ and scrambled injected *tbk1*$^{SH570/SH570}$, *MAP3K14a* injected *tbk1*$^{+/+}$ and *MAP3K14a* injected *tbk1*$^{SH570/SH570}$ and scrambled injected *tbk1*$^{+/+}$ and *MAP3K14a* injected *tbk1*$^{SH570/SH570}$).
f) Histogram of 12day old zebrafish for slow movement in light cycles shows significant difference between scrambled injected *tbk1*$^{+/+}$ and scrambled injected *tbk1*$^{SH570/SH570}$, *MAP3K14a* injected *tbk1*$^{+/+}$ and *MAP3K14a* injected *tbk1*$^{SH570/SH570}$ and scrambled injected *tbk1*$^{+/+}$ and *MAP3K14a* injected *tbk1*$^{SH570/SH570}$. Cumulative plots of 12 day old zebrafish *tbk1*^{SH570} for fast movement during dark light switching. h) Histogram of 12 day old zebrafish for fast movement in dark cycles shows significant difference between scrambled injected *tbk1*$^{+/+}$ and scrambled injected *tbk1*$^{SH570/SH570}$ and scrambled injected *tbk1*$^{+/+}$ and *MAP3K14a* injected *tbk1*$^{SH570/SH570}$. i) Histogram of 12day old zebrafish for fast movement in light cycles shows significant difference between scrambled injected *tbk1*$^{+/+}$ and scrambled injected *tbk1*$^{SH570/SH570}$ and scrambled injected *tbk1*$^{+/+}$ and *MAP3K14a* injected *tbk1*$^{SH570/SH570}$. j) Cumulative plots of 12 day old zebrafish *tbk1*^{SH570} for total distance during dark light switching. k) Histogram of 12day old zebrafish for total distance in light cycles shows significant difference between scrambled injected *tbk1*$^{+/+}$ and scrambled injected *tbk1*$^{SH570/SH570}$ and scrambled injected *tbk1*$^{+/+}$ and *MAP3K14a* injected *tbk1*$^{SH570/SH570}$.
l) Histogram of 5day old zebrafish for total distance in light cycles shows significant difference between scrambled injected *tbk1*$^{+/+}$ and scrambled injected *tbk1*$^{SH570/SH570}$, *MAP3K14a* injected *tbk1*$^{+/+}$ and *MAP3K14a* injected *tbk1*$^{SH570/SH570}$ and scrambled injected *tbk1*$^{+/+}$ and *MAP3K14a* injected *tbk1*$^{SH570/SH570}$.

Table 5. 2 Summary of statistical analysis of the *map3k14a* crispant effect on swimming

Tukey's multiple comparisons	Active duration Adjusted P Value		Slow movement Adjusted P Value	
	dark	light	dark	light
Scrambled tbk1$^{+/+}$ vs. MAP3K14a tbk1$^{+/+}$	0.8811	0.3217	0.2298	0.1318
Scrambled tbk1$^{+/+}$ vs. Scrambled tbk1$^{+/SH570}$	0.9996	0.9998	0.9689	0.9984
Scrambled tbk1$^{+/+}$ vs. MAP3K14a tbk1$^{+/SH570}$	0.9596	0.5699	0.1257	0.4242
Scrambled tbk1$^{+/+}$ vs. Scrambled tbk1$^{SH570/SH570}$	0.0009	<0.0001	<0.0001	<0.0001
Scrambled tbk1$^{+/+}$ vs. MAP3K14a tbk1$^{SH570/SH570}$	0.0008	<0.0001	<0.0001	<0.0001
MAP3K14a tbk1$^{+/+}$ vs. Scrambled tbk1$^{+/SH570}$	0.71	0.1669	0.592	0.0368
MAP3K14a tbk1$^{+/+}$ vs. MAP3K14a tbk1$^{+/SH570}$	0.9978	0.9758	>0.9999	0.9075
MAP3K14a tbk1$^{+/+}$ vs. Scrambled tbk1$^{SH570/SH570}$	0.0398	0.0113	0.0101	0.0014
MAP3K14a tbk1$^{+/+}$ vs. MAP3K14a tbk1$^{SH570/SH570}$	0.0314	0.001	0.0185	<0.0001
Scrambled tbk1$^{+/SH570}$ vs. MAP3K14a tbk1$^{+/SH570}$	0.8149	0.31	0.4711	0.1375
Scrambled tbk1$^{+/SH570}$ vs. Scrambled tbk1$^{SH570/SH570}$	0.0002	<0.0001	<0.0001	<0.0001
Scrambled tbk1$^{+/SH570}$ vs. MAP3K14a tbk1$^{SH570/SH570}$	0.0002	<0.0001	<0.0001	<0.0001
MAP3K14a tbk1$^{+/SH570}$ vs. Scrambled tbk1$^{SH570/SH570}$	0.0037	0.0002	0.0013	<0.0001
MAP3K14a tbk1$^{+/SH570}$ vs. MAP3K14a tbk1$^{SH570/SH570}$	0.0033	<0.0001	0.0035	<0.0001
Scrambled tbk1$^{SH570/SH570}$ vs. MAP3K14a tbk1$^{SH570/SH570}$	>0.9999	0.9768	>0.9999	0.8938
Tukey's multiple comparisons	Fast movement Adjusted P Value		Total distance Adjusted P Value	
	dark	light	dark	light
Scrambled tbk1$^{+/+}$ vs. MAP3K14a tbk1$^{+/+}$	0.1693	0.3159	0.1122	0.0809
Scrambled tbk1$^{+/+}$ vs. Scrambled tbk1$^{+/SH570}$	0.9927	>0.9999	>0.9999	0.9775
Scrambled tbk1$^{+/+}$ vs. MAP3K14a tbk1$^{+/SH570}$	0.2982	0.3319	0.1695	0.114
Scrambled tbk1$^{+/+}$ vs. Scrambled tbk1$^{SH570/SH570}$	<0.0001	0.005	<0.0001	<0.0001
Scrambled tbk1$^{+/+}$ vs. MAP3K14a tbk1$^{SH570/SH570}$	0.0007	0.0028	<0.0001	<0.0001
MAP3K14a tbk1$^{+/+}$ vs. Scrambled tbk1$^{+/SH570}$	0.3659	0.2233	0.0774	0.2667
MAP3K14a tbk1$^{+/+}$ vs. MAP3K14a tbk1$^{+/SH570}$	0.9804	0.9984	0.9868	0.988
MAP3K14a tbk1$^{+/+}$ vs. Scrambled tbk1$^{SH570/SH570}$	0.1184	0.4993	0.0971	0.0182
MAP3K14a tbk1$^{+/+}$ vs. MAP3K14a tbk1$^{SH570/SH570}$	0.2879	0.3479	0.0244	0.0602
Scrambled tbk1$^{+/SH570}$ vs. MAP3K14a tbk1$^{+/SH570}$	0.6076	0.2059	0.1059	0.4034
Scrambled tbk1$^{+/SH570}$ vs. Scrambled tbk1$^{SH570/SH570}$	0.0002	0.0024	<0.0001	<0.0001
Scrambled tbk1$^{+/SH570}$ vs. MAP3K14a tbk1$^{SH570/SH570}$	0.0021	0.0014	<0.0001	<0.0001
MAP3K14a tbk1$^{+/SH570}$ vs. Scrambled tbk1$^{SH570/SH570}$	0.0087	0.191	0.0076	0.0006
MAP3K14a tbk1$^{+/SH570}$ vs. MAP3K14a tbk1$^{SH570/SH570}$	0.0462	0.115	0.0012	0.0048
Scrambled tbk1$^{SH570/SH570}$ vs. MAP3K14a tbk1$^{SH570/SH570}$	0.9998	0.9997	0.9932	0.9999

5.3.4 *MAP3K14a* crispants do not show significant reduction in *MAP3K14a* mRNA levels

Crispants are a relatively new approach, and we wished to have confidence that *map3k14a* was functionally impaired in the swimming study. In the literature most crispant studies involve phenotypes that can be easily observed such as pigmentation (D'Agati et al., 2017) . However, in the *map3k14a* crispants there were only small, non-significant effects on swimming in *tbk1*$^{+/+}$. We reasoned that crispant larvae with mosaic frameshift mutations should show reduced *map3k14a* expression due to nonsense mediated degradation. Therefore, we extracted RNA from 12 dpf larvae at the end of the swimming study and examined the expression level of *map3k14a* compared to eff1a (Figure (5.8), Table 5.3). Data were normalised to the expression level in scrambled *tbk1*$^{+/+}$ larvae. There was a small but non-significant reduction in map3k14a expression in *tbk1*$^{+/+}$. As seen previously the level of map3k14a was slightly increased in *tbk1*$^{SH570/SH570}$ mutant larvae, and this was not reduced in the crispants. Thus, we do not find evidence for reduced levels of map3k14a that we might expect to see if frameshift mutations in the crispants were causing nonsense mediated degradation.

Table 5. 3 Mean map3k14a mRNA level in 12 dpf crispants

Group	Scrambled tbk1$^{+/+}$	MAP3K14a tbk1$^{+/+}$	Scrambled tbk1$^{SH570/SH570}$	MAP3K14a tbk1$^{SH570/SH570}$
Relative mRNA level	1.011	0.7667	1.189	1.456

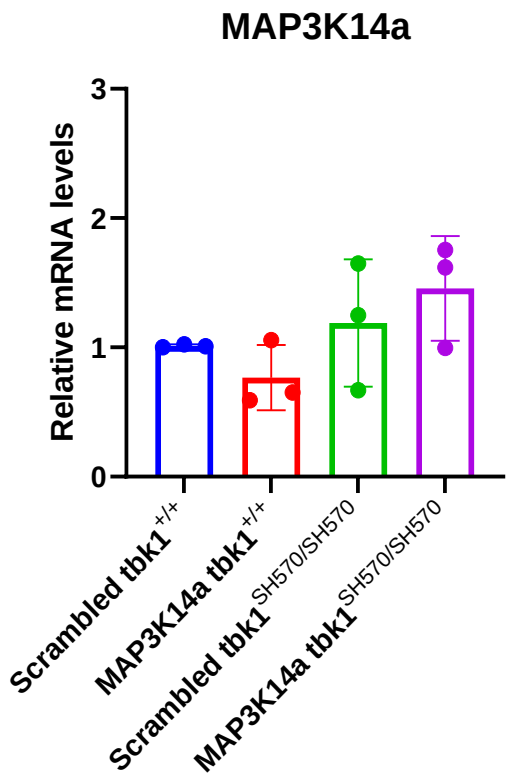

Figure 5. 8 *MAP3K14a* mRNA level in crispant 12 dpf zebrafish. Relative *MAP3K14a* mRNA level shows no significant difference between groups. Each point represents a pool of larvae from 3 independent group.

5.3.5 *MAP3K14a* knockdown/out in *tbk1*$^{SH570/SH570}$ zebrafish present a differential cytokines gene expression

In this chapter, we set out to determine whether map3k14a crispants would show a reduction in the elevated NF*κ*B signaling in *tbk1*$^{SH570/SH570}$ larvae. However, as we showed earlier this was not observed, as there was no effect on NF*κ*B:GFP fluorescence. To look at signaling downstream of NF*κ*B, we also investigated whether the expression of proinflammatory cytokines was reduced in the crispants.

One-way ANOVA demonstrated significant differences in cytokine gene expression (Table 5.4). All four cytokines showed significantly increased expression when comparing *tbk1*$^{SH570/SH570}$ and *tbk1*$^{+/+}$ scrambled crispants. However, Tukey's multiple comparisons test did not show a significant reduction of cytokine expression in map3k14a crispant *tbk1*$^{SH570/SH570}$ larvae.

In contrast there was a small but non-significant increase in cytokine expression in the map3k14a crispant *tbk1*$^{+/+}$ larvae (Figure (5.9), Table 5.4).

Thus, these results are in keeping with the fact that NF*κ*:GFP fluorescence was not reduced in *tbk1*$^{SH570/SH570}$ crispants (Figure (5.9), Table 5.4).

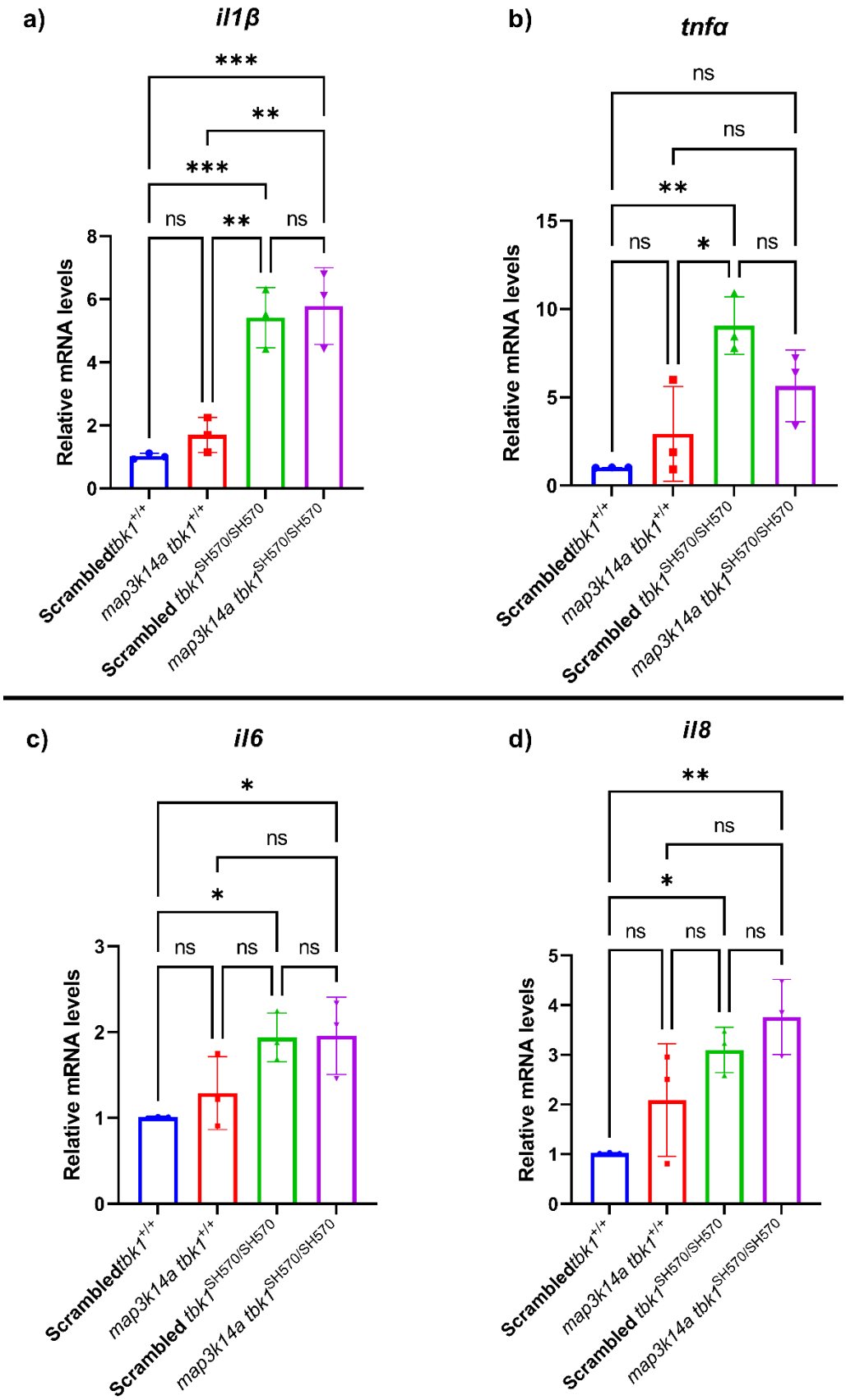
a)
il1β
***
**
***
ns
**
ns
Relative mRNA levels
0
2
4
6
8
Scrambled tbk1+/+
map3k14a tbk1+/+
Scrambled tbk1SH570/SH570
map3k14a tbk1SH570/SH570
b)
tnfα
ns
ns
**
ns
*
ns
Relative mRNA levels
0
5
10
15
Scrambled tbk1+/+
map3k14a tbk1+/+
Scrambled tbk1SH570/SH570
map3k14a tbk1SH570/SH570
c)
il6
*
ns
*
ns
ns
ns
Relative mRNA levels
0
1
2
3
Scrambled tbk1+/+
map3k14a tbk1+/+
Scrambled tbk1SH570/SH570
map3k14a tbk1SH570/SH570
d)
il8
**
ns
*
ns
ns
ns
Relative mRNA levels
0
1
2
3
4
5
Scrambled tbk1+/+
map3k14a tbk1+/+
Scrambled tbk1SH570/SH570
map3k14a tbk1SH570/SH570

Figure 5. 9 Expression of proinflammatory cytokine genes in 12 dpf crispants. a) 12 dpf scrambled injected *tbk1*$^{SH570/SH570}$ showed significantly elevated levels of *tnfα* compared to scrambled injected *tbk1*$^{+/+}$. However, *MAP3K14a* injected *tbk1*$^{SH570/SH570}$ did not show a significant decrease in *tnfα* mRNA levels compared to scrambled injected *tbk1*$^{SH570/SH570}$. b) 12 dpf scrambled injected *tbk1*$^{SH570/SH570}$ showed significantly elevated levels of *il1β* compared to scrambled injected *tbk1*$^{+/+}$. However, *MAP3K14a* injected *tbk1*$^{SH570/SH570}$ did not show a significant decrease in *il1β* mRNA levels compared to scrambled injected *tbk1*$^{SH570/SH570}$. c) 12 dpf scrambled injected *tbk1*$^{SH570/SH570}$ showed significantly elevated levels of *il6* compared to scrambled injected *tbk1*$^{+/+}$. However, *MAP3K14a* injected *tbk1*$^{SH570/SH570}$ did not show a significant decrease in *il6* mRNA levels compared to scrambled injected *tbk1*$^{SH570/SH570}$. d) 12 dpf scrambled injected *tbk1*$^{SH570/SH570}$ showed significantly elevated levels of *il8* compared to scrambled injected *tbk1*$^{+/+}$. However, *MAP3K14a* injected *tbk1*$^{SH570/SH570}$ did not show a significant decrease in *il8* mRNA levels compared to scrambled injected *tbk1*$^{SH570/SH570}$. Each point represents a pool of larvae from 3 independent group.

Table 5. 4 Summary of statistical analysis of the map3k14a crispant effect on gene expression

over all one way ANOVA p-value	IL1β	tnfα	IL6	IL8
	0.0002	0.0038	0.0206	0.0075
Tukey's multiple comparisons test p-value	**IL1β**	**tnfα**	**IL6**	**IL8**
Scrambled tbk1$^{+/+}$ vs. MAP3K14a tbk1$^{+/+}$	0.7456	0.6135	0.7469	0.3301
Scrambled tbk1$^{+/+}$ vs. Scrambled tbk1$^{SH570/SH570}$	0.0008	0.0034	0.0411	0.0308
Scrambled tbk1$^{+/+}$ vs. MAP3K14a tbk1$^{SH570/SH570}$	0.0005	0.0635	0.0373	0.0068
MAP3K14a tbk1$^{+/+}$ vs. Scrambled tbk1$^{SH570/SH570}$	0.0024	0.0164	0.1703	0.3718
MAP3K14a tbk1$^{+/+}$ vs. MAP3K14a tbk1$^{SH570/SH570}$	0.0013	0.3484	0.1549	0.081
Scrambled tbk1$^{SH570/SH570}$ vs. MAP3K14a tbk1$^{SH570/SH570}$	0.9459	0.1942	0.9999	0.6797

5.4 Discussion

In previous chapters we showed that *tbk1* loss of function does not inhibit NF*κ*B signaling as we had hypothesised. In contrast signaling was increased in two different mutant *tbk1* stable lines. We reasoned that the increased NF*κ*B signaling may arise from loss of *tbk1*'s inhibitory role in noncanonical signaling. tbk1 phosphorylates nik (map3k14a*)* leading to degradation of nik by the proteasome (Zhao et al., 2018) and inhibits downstream NF*κ*B signaling (Jin et al., 2012). Thus, loss of tbk1 could lead to constitutively elevated levels of nik, and thus increased noncanonical NF*κ*B signaling.

We hypothesised that inhibiting *map3k14a* in *tbk1*$^{SH570/SH570}$ may reduce the noncanonical NF*κ*B expression and thus reduce cytokine gene expression. We also wanted to see if the noncanonical pathway could be linked to the swimming defect that we observed in the two tbk1 mutant lines. Because time was limited by lockdown and reduced laboratory access, we used a rapid approach (Wu et al., 2018) for direct gene knockout to evaluate the impact in F0 zebrafish. This approach is faster than conventional CRISPR/Cas9 that could take at least a year to generate a stable mutant line (Masselink, 2021).

5.4.1 *map3k14a* crispant efficiency

According to (Wu et al., 2018) the efficiency of crispant gRNA they used is 90%, so we based our approach based on their published data. We used two methods to examine the efficiency of this rapid approach. Firstly, we used HRMA to identify heteroduplex formation. This showed that there were likely to be insertions or deletions in the gRNA target sites, but that the efficiency was low. In addition, the exon 12 target region contained a BslI restriction site which allowed us to look for disruption of this site using restriction enzyme digestion.

Sequencing the targeted gRNA region was not the best approach because F0 *map3k14a* crispant embryos are expected to be highly genetically mosaic, in other words an individual embryo will carry many different mutations.

Although for the swim study and mRNA extraction, we only selected fish that have a disruption in BslI site. At the current time we do not know which *map3k14a* mutations were present in the larvae which were studied in this chapter.

Some F0 crispants have been outcrossed to allow the generation of stable mutant lines. Sequencing the F1 fish will allow us to conduct future studies with defined map3k14a frameshift alleles.

Another way to study the validity of the crispants is to look at *map3k14a* expression. Using qRT-PCR we did not see a significant reduction in map3k14a expression in *tbk1*$^{+/+}$ larvae, although the average expression level was reduced. Potentially, additional repeats of this experiment would demonstrate a significant effect on expression and allow us to conclude that the approach is valid. However, we also saw that *map3k14a* expression was increased in *tbk1*$^{SH570/SH570}$ mutants compared to controls, although this didn't reach significance. Additional repeats of this experiment may allow us to conclude whether the *map3k14a* expression level is higher in *tbk1* loss of function mutants, which could provide evidence for dysfunction of the noncanonical pathway in tbk1 mutants.

5.4.2 NF*κ*B signaling in *map3k14a* crispants

We hypothesised that m*ap3k14a tbk1*$^{SH570/SH570}$ crispants should have reduced NF*κ*B signaling because map3k14a activates the non-canonical NF*κ*B pathway. This should be detected by a reduction of NF*κ*B:GFP fluorescence. However, we did not observe any significant reduction in NF*κ*B:GFP signaling. This finding may not be conclusive, as we only evaluated total larval NF*κ*B:GFP fluorescence using a standard microscope. A more comprehensive approach would be to quantify fluorescence in individual cells or tissues perhaps using confocal microscopy, or biochemical approaches from older fish where we could dissect brain, spinal cord and other tissues and perform ELISA assays for GFP. In addition, the crispants are genetically highly mosaic, therefore even if the efficiency was 100%, and every allele was mutated, the actual mutations in each cell could still be different.

It is important to remember that we are not able to select frameshift mutations in crispants, therefore on average 1 in 3 mutations will be in-frame, and thus not likely to cause loss of map3k14a function. Therefore, a stable frameshift allele of *map3k14a* which we could cross onto *tbk1*$^{SH570/SH570}$ would be the best model to examine the impact of map3k14a on NF*κ*B:GFP signaling.

5.4.3 Proinflammatory cytokine gene expression in *map3k14a* crispants

In addition to looking at the NF*κ*B:GFP reporter gene, we also used qRT-PCR to quantify expression of downstream genes that are activated by NF*κ*B signaling. In the scrambled crispants we saw statistically significant increases in expression of *tnfα*, *il1β*, *il6* and *il8* in *tbk1*$^{SH570/SH570}$ compared to *tbk1*$^{+/+}$, confirming the results we found previously. However, we did not see a significant reduction of expression of these genes in *tbk1*$^{SH570/SH570}$ *map3k14a* crispants.

The mosaic nature of crispants may have contributed to this result, since we are studying total larval mRNA expression, rather than a specific cell population that has loss of function of map3k14a.

5.4.4 Swimming behaviour in *tbk1*$^{SH570/SH570}$ *map3k14a* crispants

We wished to see if a *map3k14a* crispant could rescue the swimming impairments in *tbk1*$^{SH570/SH570}$. As expected, we observed a significant impaired of all 4 swimming parameters studied (active duration, slow movement, fast movement and total distance) in *tbk1*$^{SH570/SH570}$ scrambled crispants compared to *tbk1*$^{+/+}$ scrambled crispants.

When we compared swimming in map3k14a crispants we saw clear but statistically insignificant reduction in mean fast swimming speed and total swimming distance in wild type and *tbk1*$^{+/SH570}$ larvae. The magnitude of this effect was modest, and the variability between individual larvae was high, so a larger number of experimental repeats would be required to determine if this is a reliable and significant result.

However, it is hard to tell if this is specific or an off-target effect of one of the gRNAs. These results would be clearer if we were working with stable *map3k14a* mutant lines.
However, when we compared *tbk1*$^{SH570/SH570}$ scrambled crispants with *tbk1*$^{SH570/SH570}$ *map3k14a* crispants no significant difference was observed in their swimming behavior, and the mean values were similar. This suggests that *map3k14a* does not contribute to the swimming phenotype in *tbk1*$^{SH570/SH570}$.
However, it remains possible that the mosaic nature of the crispants were not sufficient to rescue the phenotype, therefore a further study using a confirmed *map3k14a* frameshift mutant is required. Due to time limitations we only managed to perform 3 replicate experiments using the crispants. In addition, there was reduced survival of the *tbk1*$^{SH570/SH570}$ at 12 dpf because the optimal diet of rotifers was not available at this time.

5.5 Conclusion

We used the rapid crispant approach to try and reduce *map3k14a* function in *tbk1*$^{SH570/SH570}$ zebrafish to restore NF*κ*B signaling, reduce cytokine genes expression and rescue the swimming behaviour in *tbk1*$^{SH570/SH570}$. Contrary to what we predicted, this approach did not show any significant impact on NF*κ*B:GFP fluorescence, cytokine gene expression or swimming behaviour. This suggests that either the crispant approach was not sufficient to block map3k14a function, or the *tbk1* mutation does not impact on the noncanonical NF*κ*B pathway via map3k14a. To overcome this issue and properly exclude the role of *tbk1* in non-canonical NF*κ*B a proper knockout zebrafish that carries compound LOF mutations in both *map3k14a* and *tbk1* is required. Another option would be identifying and using map3k14a inhibitors that could inhibit map3k14a in the *tbk1*$^{SH570/SH570}$ zebrafish. There is also a possibility that tbk1 interacts with or phosphorylates other proteins that are involved in the NF*κ*B signaling pathway thus comparative phosphoproteomic analysis of wild type and *tbk1*$^{SH570/SH570}$ zebrafish would be useful to identify candidate proteins and pathways.

Chapter 6

6. Discussion

6.1 Rationale for this project

ALS/FTD is a complex multifactorial neurodegenerative disorder that presents with a heterogeneous clinical phenotype. It is likely caused by defects in several molecular pathways such as inflammation, autophagy, mitochondrial dysfunction, protein aggregation, RNA metabolism, cellular transport. These pathways affect motor and cortical neurons as well as non-neuronal cells in the CNS. Defects in more than 40 genes have been associated with ALS/FTD.

There are still no truly effective treatments for ALS/FTD, and therefore research into the causes of ALS/FTD is crucial. The improvements in genetic technologies have increased our understanding of the genes and mutations that are involved, but to advance our understanding of disease mechanisms, and to be able to devise therapies, we need more cellular, *in vivo* and clinical research projects.

The recent advancement in genome editing tools such as CRISPR has made it possible to rapidly generate genetic models in cells and organisms. Cell research allows biologists to look in detail at pathways and mechanisms, but ultimately genetic and cell-based discoveries need to be followed up *in vivo*, to understand how they affect function at a whole organism level. In particular in ALS/FTD, because many different cell types are involved in motor function and dementia, it can be hard to fully understand how cellular dysfunction will manifest in this context. Thus, genetic models of ALS/FTD play an important part in research. Many ALS/FTD disease genes have been modelled in vertebrates such as mice, rats, and zebrafish and invertebrates such as yeast and drosophila. In this project, we are interested in the *TBK1* gene, which is one of the genes that has been associated with both ALS and FTD. Genetic and cell-based studies suggest that *TBK1* mutations, although dominantly inherited, cause disease via a loss of function mechanism.

It has been known for many years that a full *TBK1* loss of function model in mice is not possible, because TBK1 is critical for embryonic development in mice, and embryos die at a very early stage of development. For this reason, we chose to study TBK1 loss of function in a different vertebrate model, the zebrafish.

6.2 Hypothesis and aims of this thesis

Whole exome sequencing linked *TBK1* LOF mutation with ALS and FTD (Cirulli et al., 2015b, Freischmidt et al., 2015a). At the start of this project there were no published mouse studies relating to TBK1 in ALS/FTD, although some findings were published during the course of this project (Brenner et al., 2019, Bonnard, 2000, Bruno et al., 2020b, Duan et al., 2019, Gerbino et al., 2020, Sieverding et al., 2021) so we decided to study a much simpler model vertebrate. We hypothesised that a LOF mutation in *tbk1* will cause an ALS/FTD phenotype in zebrafish similar to that which we observe in ALS/FTD patients.

In order to study the effects of *tbk1* LOF mutation in zebrafish and to examine this hypothesis, we used CRISPR/Cas9 to introduce a LOF mutation in the zebrafish *tbk1* gene. Our first aim was to characterise *tbk1* LOF mutation zebrafish to determine whether they show a phenotype similar to that which has been observed in ALS/FTD patients. In addition, we aimed to determine which cellular pathways may be mediating the phenotype we observed. Based on cell-based research, we suspected that the *tbk1* mutation in zebrafish would cause disease via defects in NFκB signaling, IRF3 signaling or autophagy. Lastly, we hoped to restore function in the defective pathway, and determine whether this ameliorated the ALS/FTD phenotype.

6.3 Key findings of this thesis

6.3.1 We generated the first viable vertebrate *tbk1* knockout

TBK1 knockout mice die early in development due to apoptosis and degeneration of the developing liver at embryonic day 14.5 (E14.5) (Bonnard, 2000). When we designed this project, we thought that there was a risk that this would also happen in zebrafish, but we reasoned that it was worth taking this risk for several reasons. Firstly, an E14.5 mouse embryo is equivalent to a 2.5 day old zebrafish.

At this stage zebrafish are able to swim and have a well-developed CNS. Secondly, liver development in zebrafish shows differences with mice, perhaps because zebrafish livers are not hemopoietic organs. Thirdly, zebrafish mutants with abnormal or undeveloped livers do not show lethal effects until >5 days of age. Finally, zebrafish mutants are often viable when the equivalent mouse knockout is lethal. For example, mitofusin 2 knockout is embryonic lethal in mouse but causes adult onset neurodegeneration in fish (Chapman et al., 2013).
As we discovered during this project, we did not see any liver defects in the *tbk1* homozygous mutants that we developed, which may be due to the fact that the liver is not a hemopoietic organ. We were concerned that *tbk1* mutation might lead to reduced viability, and in preliminary studies with in crossed hemizygotes we carefully monitored the survival at different stages. Using standard husbandry conditions, we observed a reduction of survival during the first month of life. The *tbk1*$^{SH570/SH570}$ zebrafish exhibit a significant reduction in size (length, weight) at 14 days old. At 12 days old wild type and heterozygous siblings begin inflation of the second (anterior) swim bladder, but this was not observed in homozygous mutants.
These findings indicate that *tbk1* has a role in zebrafish development. We also observed that the gut of 12 dpf *tbk1* homozygous mutant larvae is empty compared to wild type and heterozygous siblings, which could be linked to the small size of these larvae. An empty gut indicates that the larvae may struggle to eat. This could be attributed to a motor problem with catching food or eating it, or an FTD-like change in behaviour (no interest in feeding).

Because the gut was empty, we decided to change the diet of the larvae. At that time aquarium staff were starting to investigate different diets and had seen that wild type larvae fed live rotifers grew much more quickly than those fed commercial diets. When we tested the effect of this diet in the *tbk1*$^{SH570/SH570}$ larvae we saw improved survival. Shortly after this we noticed that *tbk1*$^{SH570/SH570}$ larvae could be identified because of their increased NF*κ*B:GFP fluorescence when bread into the appropriate reporter background. This made it possible to select the homozygous larvae before 5 dpf, and to raise them in a separate tank in the aquarium. Once we had combined rotifer diet with raising the homozygous mutants separately, we showed that it was feasible to generate equivalent survival rates in *tbk1*$^{SH570/SH570}$ and their wild type and hemizygous siblings.

Thus, we were able to proceed with our characterisation of the zebrafish mutant and determine whether it developed ALS/FTD.

6.3.2 *tbk1* knockout zebrafish show phenotypes consistent with ALS/FTD

Although ALS and FTD are adult-onset diseases with autosomal dominant inheritance, we did not observe any motor dysfunction in our *tbk1* heterozygous zebrafish model at larval or adult stages. It is possible, as has been suggested in mouse *TBK1* heterozygous knockouts(Brenner et al., 2019), that ageing is as key factor in exacerbating the zebrafish *tbk1* LOF mutation. Although we studied heterozygous zebrafish at 12 months, we were not able to look at older fish. Perhaps if we aged sufficient numbers of heterozygous fish to 2 years or older, they may have developed a swimming deficit.

As demonstrated in this thesis, zebrafish *tbk1* homozygous nonsense mutants develop motor defects that can be studied in larval and adult stages. In larvae we saw that the severity of the swimming phenotype was dependent on the presence or absence of maternally contributed wild type *tbk1* mRNA, and thus the progeny of homozygous parents which lacked any maternal wild type *tbk1* mRNA showed significant swimming defects by 5 dpf.

Unfortunately, time became limited due to covid19 and we were unable to confirm that these swimming defects were a result of motor neuron defects, so we currently do not have evidence that these fish are a real model of motor neuron disease. As discussed previously we saw a developmental delay in these fish, so it is possible that this contributes to the swimming defects. However, by 6 and 12 months of age there appeared to be no overall difference in size or morphology of the homozygous mutants, but they still showed a significant impairment in Ucrit. We are not sure if the motor dysfunction in larvae and adults represents the same underlying mechanism. Further investigation is necessary of e.g. neuromuscular junction pathology.

6.3.3 *tbk1* homozygous mutant zebrafish show abnormal emotional and social behaviour

Demonstrating dementia phenotypes in animal models is challenging. In most cases specific tests have been established in order to investigate neurological impairments, such as tests of cognition, social interaction and anxiety. Given the complexity of correlating the FTD clinical phenotype between human and zebrafish we decided to focus on social and emotional behaviours similar to what has been observed in an FTD mouse model (Roberson, 2012). FTD patients can show altered behaviour in the absence of motor symptoms, so it is possible that the basis of the swimming phenotype is not solely related to motor impairment but also reflects a change in emotional behaviour. To investigate this further, we analysed some classical behaviours of zebrafish, such as open field and shoaling behaviour. Examining thigmotactic behaviour at 12 dpf *tbk1*$^{SH570/SH570}$ zebrafish, we observed that *tbk1*$^{SH570/SH570}$ showed significantly reduced thigmotaxis, while *tbk1*$^{+/+}$ and *tbk1*$^{+/SH570}$ siblings avoid swimming in the centre of the dish and prefer to swim near the edge. Another indicator of normal social interaction in zebrafish is shoaling behaviour(Shams et al., 2015). We know that larval *tbk1* mutants are smaller, and it is possible that some swimming changes are either caused by, or correlated with, their reduced size or impaired development.

To mitigate this possibility, we selected the largest homozygous mutants for the shoaling studies, so there was no statistically significant difference in size between homozygous fish and their siblings.

Examining shoaling behaviour at 21 days old we found that tbk*1*$^{SH570/SH570}$ fish showed significant differences in all parameters studied compared to their pooled *tbk1*$^{+/+}$ and *tbk1*$^{+/SH570}$ siblings.

6.3.4 Comparison with mouse models

The finding that zebrafish homozygous mutants bearing a nonsense mutation are viable is particularly interesting in comparison to studies mice. During the course of this project other groups have generated mice that either carry null alleles or pathogenic ALS mutations found in patients(Bruno et al., 2020a, Duan et al., 2019, Brenner et al., 2019, Gerbino et al., 2020, Sieverding et al., 2021). None of the mice that lacked TBK1 kinase activity were viable as homozygotes. To address this, two groups made conditional knockout mice. One model was a conditional knockout in cholinergic neurons including motor neurons (Gerbino et al., 2020), and the other was a conditional knockout in neuronal progenitors, leading to a complete deficiency of *TBK1* in all neurons (Duan et al., 2019). The neuronal knockout showed no conventional motor phenotype, but did show deficits in swimming in a water maze, and impairment in cognition in the water maze (Duan et al., 2019). The cholinergic neuron specific knockout showed no deficits in motor function (Gerbino et al., 2020). Heterozygous mutant mice, that mimic the human ALS patients, also showed no ALS phenotype, but gene expression analysis showed altered neuroinflammatory gene expression in the spinal cord (Gerbino et al., 2020). Two studies crossed *TBK1* mutations onto mutant SOD1 transgenic mice (Gerbino et al., 2020, Brenner et al., 2019). In both cases there was an increase in the progression of motor dysfunction at an early stage, but a reduction in the neuroinflammatory phenotype at a later stage.

Lastly when a *TBK1* heterozygous null allele was introduced on a TDP-43 G298S transgenic mouse model of ALS there was no effect on TDP-43 pathology, motor neuron loss or gliosis, but there was a small decrease in NMJ integrity accompanied by slightly worse motor function (Sieverding et al., 2021).

Thus, it appears that the zebrafish model we have generated is unique because it allows us to study the complete null mutation in all cells in a viable vertebrate model, and it shows a motor and behavioural phenotype.

6.3.5 *tbk1* knockout zebrafish show defects in the expected signaling pathways

The second aim of this project was to determine which of the pathways downstream of *tbk1* is involved in ALS/FTD pathogenesis in zebrafish. The contribution of *TBK1* mutations to ALS/FTD disease pathogenesis is poorly understood as mutations are located throughout the gene. It seems likely that many mutations will reduce OPTN binding or TBK1 kinase activity (Freischmidt et al., 2015a, Freischmidt et al., 2017, Cirulli et al., 2015b). Many studies suggest that TBK1 mediates crosstalk between the innate immune response and autophagy, and there are strong interconnections between these pathways that involve TBK1 (Deretic and Levine, 2018). In the *TBK1* knock in mouse models downstream signaling pathways were impaired in mutant mice that lacked kinase activity, consistent with work in *TBK1* knockout cell lines However no changes in NF-kB signaling were described (Gerbino et al., 2020, Brenner et al., 2019). Therefore, we decided to focus on the role of TBK1 in autophagy, NFκB and IRF3 signalling specifically.

6.4 The role of tbk1 in NFκB signalling

The role of TBK1 in NFκB signalling is well studied, but still not completely understood, as studies suggest that TBK1 activates canonical NFκB signalling through direct phosphorylation of Ikkβ (Fang et al., 2017, Abe and Barber, 2014) but on the other hand TBK1 negatively regulates non-canonical NFκB signaling via phosphorylation of MAP3K14 (Sun, 2017, Jin et al., 2012). These pathways are interconnected and so it may not be possible to separate effects of *TBK1* loss of function on both pathways.

To investigate the role of *tbk1* in NFκB signalling in zebrafish, we used a published NFκB:GFP zebrafish reporter line(Kanther et al., 2011a). Contrary to what we expected, examining *tbk1*$^{SH570/SH570}$ NFκB:GFP hemizygous zebrafish showed an upregulation of the NFκB:GFP reporter gene compared to *tbk1*$^{+/+}$ and $^{+/SH570}$ NFκB:GFP siblings.

We confirmed this was not an off-target effect in the *tbk1*^{SH570} mutant by generating a new mutant with a nonsense mutation in the kinase domain. This also showed the same increase in NFκB:GFP fluorescence, as did compound mutant fish carrying both mutations in the hemizygous state.

To confirm the effect on NFκB signaling we examined mRNA expression of some downstream proinflammatory cytokine genes (Lawrence, 2009b) in *tbk1*$^{SH570/SH570}$ larvae. At 12 dpf, (a timepoint we observe the most significant motor phenotypes), we observed a substantial increase in the relative mRNA level of *il1β, il6, il8* and *tnfα* in *tbk1*$^{SH570/SH570}$. Additionally, examining the cytokine genes in *tbk1*$^{SH643/SH643}$ at 12 dpf we also observed a significant increase in the relative mRNA level of *il1β, il6, il8* and *tnfα*. These findings support the idea that *tbk1* knockout zebrafish upregulate NFκB, increasing the proinflammatory cytokine gene expression. This seems to contradict a role in the canonical pathway and agrees with the role of *tbk1* as a negative regulator of noncanonical NFκB in zebrafish larvae.

Some studies of gene expression were conducted in mouse *TBK1* models of ALS/FTD. No changes in expression were reported for downstream targets of NF*κ*B in total spinal cord extracts from *TBK1* heterozygotes (Brenner et al., 2019), but when microglia were purified, it appeared that *il1β* was downregulated, and when the SOD1 G93A mutant mouse carried a loss of one *TBK1* allele many cytokines showed lower expression in the double mutant compared to the single SOD1 mutation compared to SOD1 G93A mice with two copies of *TBK1* (Brenner et al., 2019). Although NF*κ*B signaling was not directly measured in any of the mouse models of ALS/FTD, reductions in cytokine gene expression in purified microglia from *TBK1* heterozygotes appear to be more consistent with an effect of loss of *TBK1* on canonical NF*κ*B signaling(Brenner et al., 2019).

Of note, in our experiments we are studying global expression changes by measuring whole larvae NF*κ*B:GFP fluorescence or whole larvae mRNA levels, which may be why we see different results.

6.5 IFN stimulated gene expression pathways

TBK1 regulates interferon signaling, and these pathways have been shown to be reduced in mouse heterozygous *TBK1* models (Brenner et al., 2019, Gerbino et al., 2020). In the homozygous mutant zebrafish, we saw significant upregulation of *isg15* expression, and non-significant but elevated levels of other interferon stimulated genes. We did not look at this in more detail, but this may provide further evidence that in zebrafish loss of tbk1 is triggering opposing effects on gene expression to those seen in mice. These findings are not conclusive as the effect could be due to the role of tbk1 regulating irf3 signalling, or due to the overlapping effect of NFκB on interferon signaling pathways (Ivashkiv and Donlin, 2014).

6.6 Relationship of tbk1 and optn in zebrafish models

TBK1 phosphorylates the autophagy receptor OPTN to induce mitophagy, and LOF mutations in either *TBK1*, *OPTN* or both could impair mitophagy leading to the development of ALS/FTD (Moore and Holzbaur, 2016b). In addition, mutations in *OPTN* (Maruyama et al., 2010a) and a gain of function mutation in *TBK1* (Fingert et al., 2011) both cause normal tension glaucoma. We showed that *optn* homozygous zebrafish mutants did not show a conclusive swimming phenotype compared to *tbk1* homozygotes. In the mitophagy pathway tbk1 acts upstream to phosphorylate optn. If the *tbk1* phenotype was due to loss of phosphorylation of optn we would expect to see a severe phenotype in the *optn* mutant, which we do not.

However, because the pathways are interconnected it is difficult to establish the relationship between these genes and their phenotypic effects. To investigate this further we generated *tbk1*$^{+/SH570}$ *optn*$^{sa0143/sa0143}$ zebrafish, and in crossed these to determine the effect of *optn* mutation status on the *tbk1* mutant phenotype. We did not see any effect of the optn mutation on the tbk1 phenotype, however we did not have time to investigate the opposite experiment, where we an *optn* mutation in the *tbk1* homozygous zebrafish.

If this gave a more severe phenotype it would suggest that optn has an effect in tbk1 mutants that is not related to its phosphorylation by tbk1. It is also possible that the larval and adult phenotypes have different causes, and in this project, we did not look at the effect of combining the mutations in older zebrafish, for example studying the effect of combined *optn* and *tbk1* mutations on swimming at 6 and 12 months or examining interferon response or cytokine gene expression in adult fish.

These results are also relevant to oligogenic models of ALS/FTD where patients carry more than one mutation in a known ALS/FTD disease gene. These experimental models may help to determine if one mutation is a bystander or a risk factor in such situations.

6.7 Use of crispants to probe molecular mechanisms in ALS/FTD in zebrafish

Because of the evidence for increased NFkB:GFP signaling in the *tbk1* mutants, we chose to investigate which pathway might be stimulating NFkB in the *tbk1* mutants, and see whether this pathway could be causing the gene expression or swimming phenotypes observed.
Because our data was consistent with increased noncanonical NFkB signaling we chose to inhibit this pathway and determine the effect. We used a crispant approach, as it was reported to be fast and efficient, however negative findings have left us with an inconclusive result. We aimed to block the effect of loss of *tbk1* on map3k14a by mutating *map3k14a*. We obtained some evidence from HRMA and restriction digestion that this may have worked, however we could not see a significant effect on *map3k14a* mRNA expression, which suggests that there could be enough wild type *map3k14a* remaining in the mosaic fish to preserve noncanonical signaling.
In triplicate biological repeat experiments we saw no effect on NFkB:GFP fluorescence, swimming behaviour or cytokine gene expression in *map3k14a* crispants. Whether this relates to the mosaic nature of the crispants, or insufficient mutagenesis is not clear. Once we have generated a stable mutant line which lacks map3k14a kinase activity we can cross this with the *tbk1* mutant lines and look at the same parameters. Therefore, currently we still do not know how loss of *tbk1* is activating NFkB or causing motor phenotypes in this model.

6.8 We have established a platform for future studies

The development of a viable *tbk1* knockout provides a platform for future work. It is critical to use this to determine the basis of the NFkB signaling effects. We have no evidence for cell or tissue specificity of the increase in GFP fluorescence or cytokine expression. Two approaches that would help determine cell/tissue specificity are lightsheet microscopy and single cell RNA sequencing.

The lightsheet microscope allows detailed 3 dimensional analysis of the NFkB:GFP signal, which will allow us to perform comparative imaging of wild type and homozygous tbk1 mutants and identify regions of differential expression. Low magnification imaging suggests that epithelial cells strongly express GFP, particularly in the gut, but we have not formally quantified this. We currently do not know the effect in CNS tissues which is critical to the ALS/FTD focus of this project, and relevant to the opposing effects on NFkB and cytokines that we see in larval zebrafish compared to published findings in mice and cell culture. Confocal microscopy suggests that the GFP signal is present in many cell types, but we have not tried to quantify this. One approach that might help to solve this problem is single cell RNA sequencing of *tbk1*^{SH570} NFkB:GFP larvae. By separating single cell expression profiles on the basis of low/high GFP expression in wild type and mutant larvae we might be able to identify cell types where NF:kB is upregulated on the basis of their gene expression profiles. One limitation of this would be the scale of sequencing that might be necessary to deconvolute the many different cell types in a larval fish. As an alternative we could use a series of cell specific markers for astrocytes, motor neurons and microglia and determine whether the NFκB:GFP signal is altered in these cell types in tbk1 mutants

The zebrafish model is also a potential screening platform to determine drugs and genes that could reverse the swimming phenotype. We observe significant swimming defects at 5 dpf in homozygous *tbk1*^{SH570} mutants derived from homozygous parents, although the magnitude of effect is quite small. We hope that *tbk1*^{SH643} mutants may show a more severe swimming phenotype to allow us to conduct such phenotypic rescue experiment at scale in fish <5.2 dpf that are not restricted by Home Office licensing.

6.9 Future work

It is essential to confirming the impact of the introduced mutation on the protein level using an antibody targeting tbk1 N-terminus. Also performing a whole mount in situ hybridization to determine which tissue are expressing tbk1 could give us an insight of the impact of *tbk1* mutation. Further next-generation hybridization chain reaction implements simultaneous mapping of multiple mRNA targets. This approach could be applied to identify the expression of tbk1 and other downstream substrates such as optn, irf3 and map3k14a(Harry M. T. Choi, 2014).

GFP reporter zebrafish expressing GFP in single cell types such as motor neurons (Flanagan-Steet et al., 2005) or macrophages and microglia (Ellett et al., 2011) could be used in combination with cell sorting of GFP expressing cells to analyse phosphoproteins individual cell types, but the amount of protein required for mass spectrometry may be difficult to achieve.

The most important studies that need to be conducted are investigations into the basis of swimming defects in *tbk1* mutants. This could involve staining and analysis of the NMJ in adult fish at 6 and 12 months, as well as larval fish at 12 days. Similar studies in *mfn2* mutant zebrafish previously conducted in the laboratory showed defects in the NMJ in adult fish with swimming defects (Chapman et al., 2013). Any significant alterations at the NMJ in homozygous *tbk1* mutants would support to the idea that the swimming phenotype is primarily a result of motor dysfunction. Besides, we should examine motor axon length and branching also motor neuron count and morphology as these are indicators of motor neuron degeneration as axonopathy indicate motor cell death (Morrice et al., 2018). Imaging studies to investigate the activation and morphology of microglia are also crucial as these cells are relevant to immune surveillance and neuronal defects, and it is activation is a common feature of ALS/FTD pathogenesis (Lall and Baloh, 2017).

TDP-43 DNA/RNA binding protein aggregation is associated with ALS pathogenesis, defects in autophagy mediated by loss of tbk1 could cause aggregation, so performing optogenetics methods on the spinal motor neuron could enable the functional analysis of aggregation of protein in our model (Asakawa et al., 2021).

It is also important to look at the effect of *map3k14a* on NFκB signaling and swimming phenotypes. As mentioned above stable *map3k14a* F1 fish have been obtained, which will allow these studies.

Screening for chemical NFκB inhibitors and anti-inflammatory drugs which could reduce inflammation and improve the ALS/FTD like phenotype in our model and would give us an indication of the relevance of neuroimmune defects in our model.

Lastly more information is needed about dysfunctional pathways downstream of *tbk1* in the mutant zebrafish which may cause the phenotypes we observe. Because tbk1 is a protein kinase we could use phosphoproteomics to determine which tbk1 substrates are not phosphorylated in the mutants. This could provide clues about the dysfunctional pathways which may be causing the swimming phenotypes. tbk1 substrates have been identified using mass spectrometry of phosphoproteins(Kim et al., 2013b), but doing this in whole larvae containing thousands of cell types with different proteomes may lead to confusing results.

Chapter 7

7. References

A AL-CHALABI 1, P. M. A., P NILSSON, B CHIOZA, J L ANDERSSON, C RUSS, C E SHAW, J F POWELL, P N LEIGH 1999. <Deletions of the heavy neurofilament subunit tail in amyotrophic lateral sclerosis>. *Human molecular Genetics,* 8**,** 157-164.

A.M. ISAACS1, P. JOHANNSEN2, I. HOLM4,5, J.E. NIELSEN2,3 AND THE FREJA CONSORTIUM6 2011. Frontotemporal Dementia Caused by CHMP2B Mutations. *Bentham Science,* 8**,** 246-251.

ABE, T. & BARBER, G. N. 2014. Cytosolic-DNA-Mediated, STING-Dependent Proinflammatory Gene Induction Necessitates Canonical NF- B Activation through TBK1. *Journal of Virology,* 88**,** 5328-5341.

ADITI, GLASS, L., DAWSON, T. R. & WENTE, S. R. 2016. An amyotrophic lateral sclerosis-linked mutation in GLE1 alters the cellular pool of human Gle1 functional isoforms. *Adv Biol Regul,* 62**,** 25-36.

AHMAD, L., ZHANG, S. Y., CASANOVA, J. L. & SANCHO-SHIMIZU, V. 2016. Human TBK1: A Gatekeeper of Neuroinflammation. *Trends Mol Med,* 22**,** 511-527.

AHMED, R. M., IRISH, M., PIGUET, O., HALLIDAY, G. M., ITTNER, L. M., FAROOQI, S., HODGES, J. R. & KIERNAN, M. C. 2016. Amyotrophic lateral sclerosis and frontotemporal dementia: distinct and overlapping changes in eating behaviour and metabolism. *The Lancet Neurology,* 15**,** 332-342.

AHMETI, K. B., AJROUD-DRISS, S., AL-CHALABI, A., ANDERSEN, P. M., ARMSTRONG, J., BIRVE, A., BLAUW, H. M., BROWN, R. H., BRUIJN, L., CHEN, W., CHIO, A., COMEAU, M. C., CRONIN, S., DIEKSTRA, F. P., SORAYA GKAZI, A., GLASS, J. D., GRAB, J. D., GROEN, E. J., HAINES, J. L., HARDIMAN, O., HELLER, S., HUANG, J., HUNG, W. Y., CONSORTIUM, I., JAWORSKI, J. M., JONES, A., KHAN, H., LANDERS, J. E., LANGEFELD, C. D., LEIGH, P. N., MARION, M. C., MCLAUGHLIN, R. L., MEININGER, V., MELKI, J., MILLER, J. W., MORA, G., PERICAK-VANCE, M. A., RAMPERSAUD, E., ROBBERECHT, W., RUSSELL, L. P., SALACHAS, F., SARIS, C. G., SHATUNOV, A., SHAW, C. E., SIDDIQUE, N., SIDDIQUE, T., SMITH, B. N., SUFIT, R., TOPP, S., TRAYNOR, B. J., VANCE, C., VAN DAMME, P., VAN DEN BERG, L. H., VAN ES, M. A., VAN VUGHT, P. W., VELDINK, J. H., YANG, Y., ZHENG, J. G. & CONSORTIUM, A. 2013. Age of onset of amyotrophic lateral sclerosis is modulated by a locus on 1p34.1. *Neurobiol Aging,* 34**,** 357 e7-19.

AL-CHALABI, A., FANG, F., HANBY, M. F., LEIGH, P. N., SHAW, C. E., YE, W. & RIJSDIJK, F. 2010. An estimate of amyotrophic lateral sclerosis heritability using twin data. *Journal of Neurology, Neurosurgery & Psychiatry,* 81**,** 1324-1326.

ALLAN FORCE, M. L., * F. BRYAN PICKETT,† ANGEL AMORES,* YI-LIN YAN* AND JOHN POSTLETHWAIT* 1998. Preservation of Duplicate Genes by Complementary, Degenerative Mutations.

ALTAN, E., KUBISKI, S. V., BOROS, A., REUTER, G., SADEGHI, M., DENG, X., CREIGHTON, E. K., CRIM, M. J. & DELWART, E. 2019. A Highly Divergent Picornavirus Infecting the Gut

Epithelia of Zebrafish (Danio rerio) in Research Institutions Worldwide. *Zebrafish,* 16**,** 291-299.

ASAKAWA, K., HANDA, H. & KAWAKAMI, K. 2021. Illuminating ALS Motor Neurons With Optogenetics in Zebrafish. *Front Cell Dev Biol,* 9**,** 640414.

BAI, J., GONG, W., WANG, C., GAO, Y., HONG, W. & CHEN, S. X. 2016. Dynamic methylation pattern of cyp19a1a core promoter during zebrafish ovarian folliculogenesis. *Fish Physiology and Biochemistry,* 42**,** 947-954.

BALKA, K. R., LOUIS, C., SAUNDERS, T. L., SMITH, A. M., CALLEJA, D. J., D'SILVA, D. B., MOGHADDAS, F., TAILLER, M., LAWLOR, K. E., ZHAN, Y., BURNS, C. J., WICKS, I. P., MINER, J. J., KILE, B. T., MASTERS, S. L. & DE NARDO, D. 2020. TBK1 and IKKepsilon Act Redundantly to Mediate STING-Induced NF-kappaB Responses in Myeloid Cells. *Cell Rep,* 31**,** 107492.

BALLA, K. M., RICE, M. C., GAGNON, J. A. & ELDE, N. C. 2020. Linking Virus Discovery to Immune Responses Visualized during Zebrafish Infections. *Current Biology,* 30**,** 2092-2103.e5.

BANDMANN, O. & BURTON, E. A. 2010. Genetic zebrafish models of neurodegenerative diseases. *Neurobiol Dis,* 40**,** 58-65.

BANG, J., SPINA, S. & MILLER, B. L. 2015. Frontotemporal dementia. *The Lancet,* 386**,** 1672-1682.

BANNWARTH, S., AIT-EL-MKADEM, S., CHAUSSENOT, A., GENIN, E. C., LACAS-GERVAIS, S., FRAGAKI, K., BERG-ALONSO, L., KAGEYAMA, Y., SERRE, V., MOORE, D. G., VERSCHUEREN, A., ROUZIER, C., LE BER, I., AUGE, G., COCHAUD, C., LESPINASSE, F., N'GUYEN, K., DE SEPTENVILLE, A., BRICE, A., YU-WAI-MAN, P., SESAKI, H., POUGET, J. & PAQUIS-FLUCKLINGER, V. 2014. A mitochondrial origin for frontotemporal dementia and amyotrophic lateral sclerosis through CHCHD10 involvement. *Brain,* 137**,** 2329-45.

BEARD, J. D. & KAMEL, F. 2015. Military service, deployments, and exposures in relation to amyotrophic lateral sclerosis etiology and survival. *Epidemiol Rev,* 37**,** 55-70.

BEGHI, E., LOGROSCINO, G., CHIO, A., HARDIMAN, O., MITCHELL, D., SWINGLER, R., TRAYNOR, B. J. & CONSORTIUM, E. 2006. The epidemiology of ALS and the role of population-based registries. *Biochim Biophys Acta,* 1762**,** 1150-7.

BEN-NERIAH, M. K. A. Y. 2000. PHOSPHORYLATION MEETS UBIQUITINATION:The Control of NF-jB Activity. *Immunology,* 18**,** 621–663.

BLACK, H. A., LEIGHTON, D. J., CLEARY, E. M., ROSE, E., STEPHENSON, L., COLVILLE, S., ROSS, D., WARNER, J., PORTEOUS, M., GORRIE, G. H., SWINGLER, R., GOLDSTEIN, D., HARMS, M. B., CONNICK, P., PAL, S., AITMAN, T. J. & CHANDRAN, S. 2017. Corrigendum to "Genetic epidemiology of motor neuron disease-associated variants in the Scottish population." [Neurobiol. Aging 51 (2017) 178.e11-178.e20]. *Neurobiol Aging,* 56**,** 214.

BONNARD, M. 2000. Deficiency of T2K leads to apoptotic liver degeneration and impaired NF-kappaB-dependent gene transcription. *The EMBO Journal,* 19**,** 4976-4985.

BORGHERO, G., PUGLIATTI, M., MARROSU, F., MARROSU, M. G., MURRU, M. R., FLORIS, G., CANNAS, A., OCCHINERI, P., CAU, T. B., LOI, D., TICCA, A., TRACCIS, S., MANERA, U., CANOSA, A., MOGLIA, C., CALVO, A., BARBERIS, M., BRUNETTI, M., GIBBS, J. R., RENTON, A. E., ERRICHIELLO, E., ZOLEDZIEWSKA, M., MULAS, A., QIAN, Y., DIN, J., PLINER, H. A., TRAYNOR, B. J., CHIO, A., ITALSGEN & CONSORTIA, S. 2016. TBK1 is associated with ALS and ALS-FTD in Sardinian patients. *Neurobiol Aging,* 43**,** 180 e1-5.

BORRONI, B., BONVICINI, C., ALBERICI, A., BURATTI, E., AGOSTI, C., ARCHETTI, S., PAPETTI, A., STUANI, C., DI LUCA, M., GENNARELLI, M. & PADOVANI, A. 2009. Mutation within TARDBP leads to frontotemporal dementia without motor neuron disease. *Hum Mutat,* 30**,** E974-83.

BORRONI, B., FERRARI, F., GALIMBERTI, D., NACMIAS, B., BARONE, C., BAGNOLI, S., FENOGLIO, C., PIACERI, I., ARCHETTI, S., BONVICINI, C., GENNARELLI, M., TURLA, M., SCARPINI, E., SORBI, S. & PADOVANI, A. 2014. Heterozygous TREM2 mutations in frontotemporal dementia. *Neurobiol Aging,* 35**,** 934 e7-10.

BRAM, R. J. 2012. TBK1 suppression of IgA in the NIK of time. *Nature Immunology,* 13**,** 1027-1029.

BRENNER, D., SIEVERDING, K., BRUNO, C., LÜNINGSCHRÖR, P., BUCK, E., MUNGWA, S., FISCHER, L., BROCKMANN, S. J., ULMER, J., BLIEDERHÄUSER, C., PHILIBERT, C. E., SATOH, T., AKIRA, S., BOILLÉE, S., MAYER, B., SENDTNER, M., LUDOLPH, A. C., DANZER, K. M., LOBSIGER, C. S., FREISCHMIDT, A. & WEISHAUPT, J. H. 2019. Heterozygous Tbk1 loss has opposing effects in early and late stages of ALS in mice. *Journal of Experimental Medicine,* 216**,** 267-278.

BRUNEEL, B. & WITTEN, P. E. 2015. Power and challenges of using zebrafish as a model for skeletal tissue imaging. *Connective Tissue Research,* 56**,** 161-173.

BRUNO, C., SIEVERDING, K., FREISCHMIDT, A., SATOH, T., WALTHER, P., MAYER, B., LUDOLPH, A. C., AKIRA, S., YILMAZER-HANKE, D., DANZER, K. M., LOBSIGER, C. S., BRENNER, D. & WEISHAUPT, J. H. 2020a. Haploinsufficiency of TANK-binding kinase 1 prepones age-associated neuroinflammatory changes without causing motor neuron degeneration in aged mice. *Brain Communications,* 2.

BRUNO, C., SIEVERDING, K., FREISCHMIDT, A., SATOH, T., WALTHER, P., MAYER, B., LUDOLPH, A. C., AKIRA, S., YILMAZER-HANKE, D., DANZER, K. M., LOBSIGER, C. S., BRENNER, D. & WEISHAUPT, J. H. 2020b. Haploinsufficiency of TANK-binding kinase 1 prepones age-associated neuroinflammatory changes without causing motor neuron degeneration in aged mice. *Brain Commun,* 2**,** fcaa133.

BURATTI, E. 2001. Nuclear factor TDP-43 and SR proteins promote in vitro and in vivo CFTR exon 9 skipping. *The EMBO Journal,* 20**,** 1774-1784.

BUSKE, C. & GERLAI, R. 2011. Shoaling develops with age in Zebrafish (Danio rerio). *Progress in Neuro-Psychopharmacology and Biological Psychiatry,* 35**,** 1409-1415.

BUTTERFIELD, R. J., RAMACHANDRAN, D., HASSTEDT, S. J., OTTERUD, B. E., LEPPERT, M. F., SWOBODA, K. J. & FLANIGAN, K. M. 2009. A novel form of juvenile recessive ALS maps to loci on 6p25 and 21q22. *Neuromuscul Disord,* 19**,** 279-87.

C. MÜNCH, M. R. S., PHD; T. MEYER, MD; V. HOMBERG, MD; A.D. SPERFELD, MD; A. KURT, MD; & J. PRUDLO, M. G. P., PHD; C.O. HANEMANN, MD; G. STUMM, MD; AND A.C. LUDOLPH, MD 2004. <Point mutations of the p150 subunit of dynactin (DCTN1) gene in ALS>. *NEUROLOGY,* 63**,** 724–726.

CHAPMAN, A. L., BENNETT, E. J., RAMESH, T. M., DE VOS, K. J. & GRIERSON, A. J. 2013. Axonal Transport Defects in a Mitofusin 2 Loss of Function Model of Charcot-Marie-Tooth Disease in Zebrafish. *PLoS One,* 8**,** e67276.

CHAU, T. L., GIOIA, R., GATOT, J. S., PATRASCU, F., CARPENTIER, I., CHAPELLE, J. P., O'NEILL, L., BEYAERT, R., PIETTE, J. & CHARIOT, A. 2008. Are the IKKs and IKK-related kinases TBK1 and IKK-epsilon similarly activated? *Trends Biochem Sci,* 33**,** 171-80.

CHEN, B., LI, C., YAO, J., SHI, L., LIU, W., WANG, F., HUO, S., ZHANG, Y., LU, Y., ASHRAF, U., YE, J. & LIU, X. 2020. Zebrafish NIK Mediates IFN Induction by Regulating Activation of IRF3 and NF-kappaB. *J Immunol,* 204**,** 1881-1891.

CHENG, T. F., BRZOSTEK, S., ANDO, O., VAN SCOY, S., KUMAR, K. P. & REICH, N. C. 2006. Differential Activation of IFN Regulatory Factor (IRF)-3 and IRF-5 Transcription Factors during Viral Infection. *The Journal of Immunology,* 176**,** 7462-7470.

CHERAN, G., SILVERMAN, H., MANOOCHEHRI, M., GOLDMAN, J., LEE, S., WU, L., CINES, S., FALLON, E., KELLY, B. D., OLSZEWSKA, D. A., HEIDEBRINK, J., SHAIR, S., CAMPBELL, S., PAULSON, H., LYNCH, T., COSENTINO, S. & HUEY, E. D. 2018. Psychiatric symptoms in preclinical behavioural-variant frontotemporal dementia in MAPT mutation carriers. *J Neurol Neurosurg Psychiatry,* 89**,** 449-455.

CHEW, T. S., O'SHEA, N. R., SEWELL, G. W., OEHLERS, S. H., MULVEY, C. M., CROSIER, P. S., GODOVAC-ZIMMERMANN, J., BLOOM, S. L., SMITH, A. M. & SEGAL, A. W. 2015. Optineurin deficiency contributes to impaired cytokine secretion and neutrophil recruitment in bacteria driven colitis. *Disease Models & Mechanisms,* 8**,** 817-829.

CHI, H., ZHANG, Z., BOGWALD, J., ZHAN, W. & DALMO, R. A. 2011. Cloning, expression analysis and promoter structure of TBK1 (TANK-binding kinase 1) in Atlantic cod (Gadus morhua L.). *Fish Shellfish Immunol,* 30**,** 1055-63.

CHI, Z. L., AKAHORI, M., OBAZAWA, M., MINAMI, M., NODA, T., NAKAYA, N., TOMAREV, S., KAWASE, K., YAMAMOTO, T., NODA, S., SASAOKA, M., SHIMAZAKI, A., TAKADA, Y. & IWATA, T. 2010. Overexpression of optineurin E50K disrupts Rab8 interaction and leads to a progressive retinal degeneration in mice. *Hum Mol Genet,* 19**,** 2606-15.

CHIO, A., BORGHERO, G., PUGLIATTI, M., TICCA, A., CALVO, A., MOGLIA, C., MUTANI, R., BRUNETTI, M., OSSOLA, I., MARROSU, M. G., MURRU, M. R., FLORIS, G., CANNAS, A., PARISH, L. D., COSSU, P., ABRAMZON, Y., JOHNSON, J. O., NALLS, M. A., AREPALLI, S., CHONG, S., HERNANDEZ, D. G., TRAYNOR, B. J., RESTAGNO, G. & ITALIAN AMYOTROPHIC LATERAL SCLEROSIS GENETIC, C. 2011. Large proportion of amyotrophic lateral sclerosis cases in Sardinia due to a single founder mutation of the TARDBP gene. *Arch Neurol,* 68**,** 594-8.

CHOW, C. Y., LANDERS, J. E., BERGREN, S. K., SAPP, P. C., GRANT, A. E., JONES, J. M., EVERETT, L., LENK, G. M., MCKENNA-YASEK, D. M., WEISMAN, L. S., FIGLEWICZ, D., BROWN, R. H. & MEISLER, M. H. 2009. Deleterious variants of FIG4, a phosphoinositide phosphatase, in patients with ALS. *Am J Hum Genet,* 84**,** 85-8.

CHRISTIAN, F., SMITH, E. L. & CARMODY, R. J. 2016. The Regulation of NF-kappaB Subunits by Phosphorylation. *Cells,* 5.

CHUN HAO WONG, C. S. A. B. S. 2018. *Characterisation of ARPP21 as a novel causative gene for amyotrophic lateral sclerosis.* Doctor of Philosophy, King's College London.

CIRULLI, E. T., LASSEIGNE, B. N., PETROVSKI, S., SAPP, P. C., DION, P. A., LEBLOND, C. S., COUTHOUIS, J., LU, Y. F., WANG, Q., KRUEGER, B. J., REN, Z., KEEBLER, J., HAN, Y., LEVY, S. E., BOONE, B. E., WIMBISH, J. R., WAITE, L. L., JONES, A. L., CARULLI, J. P., DAY-WILLIAMS, A. G., STAROPOLI, J. F., XIN, W. W., CHESI, A., RAPHAEL, A. R., MCKENNA-

YASEK, D., CADY, J., VIANNEY DE JONG, J. M., KENNA, K. P., SMITH, B. N., TOPP, S., MILLER, J., GKAZI, A., CONSORTIUM, F. S., AL-CHALABI, A., VAN DEN BERG, L. H., VELDINK, J., SILANI, V., TICOZZI, N., SHAW, C. E., BALOH, R. H., APPEL, S., SIMPSON, E., LAGIER-TOURENNE, C., PULST, S. M., GIBSON, S., TROJANOWSKI, J. Q., ELMAN, L., MCCLUSKEY, L., GROSSMAN, M., SHNEIDER, N. A., CHUNG, W. K., RAVITS, J. M., GLASS, J. D., SIMS, K. B., VAN DEERLIN, V. M., MANIATIS, T., HAYES, S. D., ORDUREAU, A., SWARUP, S., LANDERS, J., BAAS, F., ALLEN, A. S., BEDLACK, R. S., HARPER, J. W., GITLER, A. D., ROULEAU, G. A., BROWN, R., HARMS, M. B., COOPER, G. M., HARRIS, T., MYERS, R. M. & GOLDSTEIN, D. B. 2015a. Exome sequencing in amyotrophic lateral sclerosis identifies risk genes and pathways. *Science,* 347**,** 1436-41.

CIRULLI, E. T., LASSEIGNE, B. N., PETROVSKI, S., SAPP, P. C., DION, P. A., LEBLOND, C. S., COUTHOUIS, J., LU, Y. F., WANG, Q., KRUEGER, B. J., REN, Z., KEEBLER, J., HAN, Y., LEVY, S. E., BOONE, B. E., WIMBISH, J. R., WAITE, L. L., JONES, A. L., CARULLI, J. P., DAY-WILLIAMS, A. G., STAROPOLI, J. F., XIN, W. W., CHESI, A., RAPHAEL, A. R., MCKENNA-YASEK, D., CADY, J., VIANNEY DE JONG, J. M. B., KENNA, K. P., SMITH, B. N., TOPP, S., MILLER, J., GKAZI, A., AL-CHALABI, A., VAN DEN BERG, L. H., VELDINK, J., SILANI, V., TICOZZI, N., SHAW, C. E., BALOH, R. H., APPEL, S., SIMPSON, E., LAGIER-TOURENNE, C., PULST, S. M., GIBSON, S., TROJANOWSKI, J. Q., ELMAN, L., MCCLUSKEY, L., GROSSMAN, M., SHNEIDER, N. A., CHUNG, W. K., RAVITS, J. M., GLASS, J. D., SIMS, K. B., VAN DEERLIN, V. M., MANIATIS, T., HAYES, S. D., ORDUREAU, A., SWARUP, S., LANDERS, J., BAAS, F., ALLEN, A. S., BEDLACK, R. S., HARPER, J. W., GITLER, A. D., ROULEAU, G. A., BROWN, R., HARMS, M. B., COOPER, G. M., HARRIS, T., MYERS, R. M. & GOLDSTEIN, D. B. 2015b. Exome sequencing in amyotrophic lateral sclerosis identifies risk genes and pathways. *Science,* 347**,** 1436-1441.

CLARK, K., PEGGIE, M., PLATER, L., SORCEK, R. J., YOUNG, E. R., MADWED, J. B., HOUGH, J., MCIVER, E. G. & COHEN, P. 2011. Novel cross-talk within the IKK family controls innate immunity. *Biochem J,* 434**,** 93-104.

CLEMENT, J. F., MELOCHE, S. & SERVANT, M. J. 2008. The IKK-related kinases: from innate immunity to oncogenesis. *Cell Res,* 18**,** 889-99.

COLLETTE K. HAND, J. K., 2,3 FRANC¸OIS SALACHAS,4 FRANC¸OIS GROS-LOUIS,1, ANA AME´LIA SIMO˜ES LOPES, V. M.-P., 2 ROBERT H. BROWN, JR.,5 & VINCENT MEININGER, W. C., 2,3 AND GUY A. ROULEAU1 2002. <A Novel Locus for Familial Amyotrophic Lateral Sclerosis, on Chromosome 18q>. *Hum. Genet,* 70**,** 251–256.

COOPER-KNOCK, J., MOLL, T., RAMESH, T., CASTELLI, L., BEER, A., ROBINS, H., FOX, I., NIEDERMOSER, I., VAN DAMME, P., MOISSE, M., ROBBERECHT, W., HARDIMAN, O., PANADES, M. P., ASSIALIOUI, A., MORA, J. S., BASAK, A. N., MORRISON, K. E., SHAW, C. E., AL-CHALABI, A., LANDERS, J. E., WYLES, M., HEATH, P. R., HIGGINBOTTOM, A., WALSH, T., KAZOKA, M., MCDERMOTT, C. J., HAUTBERGUE, G. M., KIRBY, J. & SHAW, P. J. 2019. Mutations in the Glycosyltransferase Domain of GLT8D1 Are Associated with Familial Amyotrophic Lateral Sclerosis. *Cell Reports,* 26**,** 2298-2306.e5.

COUTHOUIS, J., HART, M. P., ERION, R., KING, O. D., DIAZ, Z., NAKAYA, T., IBRAHIM, F., KIM, H. J., MOJSILOVIC-PETROVIC, J., PANOSSIAN, S., KIM, C. E., FRACKELTON, E. C., SOLSKI, J. A., WILLIAMS, K. L., CLAY-FALCONE, D., ELMAN, L., MCCLUSKEY, L., GREENE, R., HAKONARSON, H., KALB, R. G., LEE, V. M., TROJANOWSKI, J. Q., NICHOLSON, G. A.,

BLAIR, I. P., BONINI, N. M., VAN DEERLIN, V. M., MOURELATOS, Z., SHORTER, J. & GITLER, A. D. 2012. Evaluating the role of the FUS/TLS-related gene EWSR1 in amyotrophic lateral sclerosis. *Hum Mol Genet,* 21**,** 2899-911.

D'AGATI, G., BELTRE, R., SESSA, A., BURGER, A., ZHOU, Y., MOSIMANN, C. & WHITE, R. M. 2017. A defect in the mitochondrial protein Mpv17 underlies the transparent casper zebrafish. *Dev Biol,* 430**,** 11-17.

DANIEL R. ROSEN*, T. S., DAVID PATTERSONT,DENISE A. FIGLEWICZ§, PETER SAPP*II, AFIF HENTATIT,DEIRDRE DONALDSONT, JUN GOTO§,JEREMIAH P. O'REGAN*II, HAN-XIANG DENGT,ZOHRA RAHMANIT, ALDIS KRIZUS§,, DIANE MCKENNA-YASEK*, A. C., SANDRA M. GASTON*~, RALPH BERGERT, RUDOLPH E. TANZI~, JOHN J. HALPERIN#, BRIAN HERZFELDTT, RAYMOND VAN DEN BERGH**, WU-YEN HUNGT, & THOMAS BIRDTT, G. D., DONALD W. MULDERH, CELESTINE SMYTHT, NIGEL G. LAING§§, EDWIN SORIANOT, MARGARET A. PERICAK-VANCELL 11, JONATHAN HAINES. GUY A. ROULEAU§, JAMES S. GUSELLA.H. ROBERT HORVITZLL & ROBERT H. BROWN JR* 1993. <Mutations in Cu/Zn superoxide dismutase gene are associated with familial amyotrophic lateral sclerosis >. *Nature,* 362**,** 59-62.

DE MAJO, M., TOPP, S. D., SMITH, B. N., NISHIMURA, A. L., CHEN, H.-J., GKAZI, A. S., MILLER, J., WONG, C. H., VANCE, C., BAAS, F., TEN ASBROEK, A. L. M. A., KENNA, K. P., TICOZZI, N., REDONDO, A. G., ESTEBAN-PÉREZ, J., TILOCA, C., VERDE, F., DUGA, S., MORRISON, K. E., SHAW, P. J., KIRBY, J., TURNER, M. R., TALBOT, K., HARDIMAN, O., GLASS, J. D., DE BELLEROCHE, J., GELLERA, C., RATTI, A., AL-CHALABI, A., BROWN, R. H., SILANI, V., LANDERS, J. E. & SHAW, C. E. 2018. ALS-associated missense and nonsense TBK1 mutations can both cause loss of kinase function. *Neurobiology of Aging,* 71**,** 266.e1-266.e10.

DEJESUS-HERNANDEZ, M., MACKENZIE, I. R., BOEVE, B. F., BOXER, A. L., BAKER, M., RUTHERFORD, N. J., NICHOLSON, A. M., FINCH, N. A., FLYNN, H., ADAMSON, J., KOURI, N., WOJTAS, A., SENGDY, P., HSIUNG, G. Y., KARYDAS, A., SEELEY, W. W., JOSEPHS, K. A., COPPOLA, G., GESCHWIND, D. H., WSZOLEK, Z. K., FELDMAN, H., KNOPMAN, D. S., PETERSEN, R. C., MILLER, B. L., DICKSON, D. W., BOYLAN, K. B., GRAFF-RADFORD, N. R. & RADEMAKERS, R. 2011. Expanded GGGGCC hexanucleotide repeat in noncoding region of C9ORF72 causes chromosome 9p-linked FTD and ALS. *Neuron,* 72**,** 245-56.

DENG, H.-X. 2011. Differential Involvement of Optineurin in Amyotrophic Lateral Sclerosis With or Without <emph type="ital">SOD1</emph> Mutations. *Archives of Neurology,* 68**,** 1057.

DENG, H. X., CHEN, W., HONG, S. T., BOYCOTT, K. M., GORRIE, G. H., SIDDIQUE, N., YANG, Y., FECTO, F., SHI, Y., ZHAI, H., JIANG, H., HIRANO, M., RAMPERSAUD, E., JANSEN, G. H., DONKERVOORT, S., BIGIO, E. H., BROOKS, B. R., AJROUD, K., SUFIT, R. L., HAINES, J. L., MUGNAINI, E., PERICAK-VANCE, M. A. & SIDDIQUE, T. 2011. Mutations in UBQLN2 cause dominant X-linked juvenile and adult-onset ALS and ALS/dementia. *Nature,* 477**,** 211-5.

DERETIC, V. & LEVINE, B. 2018. Autophagy balances inflammation in innate immunity. *Autophagy,* 14**,** 243-251.

DESCHAUER, M., GAUL, C., BEHRMANN, C., PROKISCH, H., ZIERZ, S. & HAACK, T. B. 2012. C19orf12 mutations in neurodegeneration with brain iron accumulation mimicking juvenile amyotrophic lateral sclerosis. *J Neurol,* 259**,** 2434-9.

DIEHL, J., MONSCH, A. U., AEBI, C., WAGENPFEIL, S., KRAPP, S., GRIMMER, T., SEELEY, W., FORSTL, H. & KURZ, A. 2005. Frontotemporal dementia, semantic dementia, and Alzheimer's disease: the contribution of standard neuropsychological tests to differential diagnosis. *J Geriatr Psychiatry Neurol,* 18**,** 39-44.

DOBSON-STONE, C., HALLUPP, M., SHAHHEYDARI, H., RAGAGNIN, A. M. G., CHATTERTON, Z., CAREW-JONES, F., SHEPHERD, C. E., STEFEN, H., PARIC, E., FATH, T., THOMPSON, E. M., BLUMBERGS, P., SHORT, C. L., FIELD, C. D., PANEGYRES, P. K., HECKER, J., NICHOLSON, G., SHAW, A. D., FULLERTON, J. M., LUTY, A. A., SCHOFIELD, P. R., BROOKS, W. S., RAJAN, N., BENNETT, M. F., BAHLO, M., SHANKARACHARYA, LANDERS, J. E., PIGUET, O., HODGES, J. R., HALLIDAY, G. M., TOPP, S. D., SMITH, B. N., SHAW, C. E., MCCANN, E., FIFITA, J. A., WILLIAMS, K. L., ATKIN, J. D., BLAIR, I. P. & KWOK, J. B. 2020. CYLD is a causative gene for frontotemporal dementia – amyotrophic lateral sclerosis. *Brain,* 143**,** 783-799.

DUAN, W., GUO, M., YI, L., ZHANG, J., BI, Y., LIU, Y., LI, Y., LI, Z., MA, Y., ZHANG, G., LIU, Y., SONG, X. & LI, C. 2019. Deletion of Tbk1 disrupts autophagy and reproduces behavioral and locomotor symptoms of FTD-ALS in mice. *Aging,* 11**,** 2457-2476.

EACHUS, H., BRIGHT, C., CUNLIFFE, V. T., PLACZEK, M., WOOD, J. D. & WATT, P. J. 2017. Disrupted-in-Schizophrenia-1 is essential for normal hypothalamic-pituitary-interrenal (HPI) axis function. *Human Molecular Genetics,* 26**,** 1992-2005.

ELDEN, A. C., KIM, H. J., HART, M. P., CHEN-PLOTKIN, A. S., JOHNSON, B. S., FANG, X., ARMAKOLA, M., GESER, F., GREENE, R., LU, M. M., PADMANABHAN, A., CLAY-FALCONE, D., MCCLUSKEY, L., ELMAN, L., JUHR, D., GRUBER, P. J., RUB, U., AUBURGER, G., TROJANOWSKI, J. Q., LEE, V. M., VAN DEERLIN, V. M., BONINI, N. M. & GITLER, A. D. 2010. Ataxin-2 intermediate-length polyglutamine expansions are associated with increased risk for ALS. *Nature,* 466**,** 1069-75.

ELLETT, F., PASE, L., HAYMAN, J. W., ANDRIANOPOULOS, A. & LIESCHKE, G. J. 2011. mpeg1 promoter transgenes direct macrophage-lineage expression in zebrafish. *Blood,* 117**,** e49-e56.

FAISAL FECTO, M. J. Y., MD, PHD; S. PAVAN VEMULA; ERDONG LIU, MD; YI YANG, MS; WENJIE CHEN, MD;, JIAN GUO ZHENG, M. Y. S., MD, PHD; NAILAH SIDDIQUE, RN, MSN; HASAN ARRAT, MD; SANDRA DONKERVOORT, MS; & SENDA AJROUD-DRISS, M. R. L. S., MD; SCOTT L. HELLER, MD; HAN-XIANG DENG, MD, PHD; TEEPU SIDDIQUE, MD 2011. SQSTM1 Mutations in Familial and Sporadic Amyotrophic Lateral Sclerosis. *ARCH NEUROL,* 68.

FANG, R., WANG, C., JIANG, Q., LV, M., GAO, P., YU, X., MU, P., ZHANG, R., BI, S., FENG, J.-M. & JIANG, Z. 2017. NEMO–IKKβ Are Essential for IRF3 and NF-κB Activation in the cGAS–STING Pathway. *The Journal of Immunology,* 199**,** 3222-3233.

FENG, S. M., CHE, C. H., FENG, S. Y., LIU, C. Y., LI, L. Y., LI, Y. X., HUANG, H. P. & ZOU, Z. Y. 2019. Novel mutation in optineurin causing aggressive ALS+/−frontotemporal dementia. *Annals of Clinical and Translational Neurology,* 6**,** 2377-2383.

FERRARI, R., HERNANDEZ, D. G., NALLS, M. A., ROHRER, J. D., RAMASAMY, A., KWOK, J. B. J., DOBSON-STONE, C., BROOKS, W. S., SCHOFIELD, P. R., HALLIDAY, G. M., HODGES, J. R., PIGUET, O., BARTLEY, L., THOMPSON, E., HAAN, E., HERNÁNDEZ, I., RUIZ, A., BOADA, M., BORRONI, B., PADOVANI, A., CRUCHAGA, C., CAIRNS, N. J., BENUSSI, L., BINETTI, G.,

GHIDONI, R., FORLONI, G., GALIMBERTI, D., FENOGLIO, C., SERPENTE, M., SCARPINI, E., CLARIMÓN, J., LLEÓ, A., BLESA, R., WALDÖ, M. L., NILSSON, K., NILSSON, C., MACKENZIE, I. R. A., HSIUNG, G.-Y. R., MANN, D. M. A., GRAFMAN, J., MORRIS, C. M., ATTEMS, J., GRIFFITHS, T. D., MCKEITH, I. G., THOMAS, A. J., PIETRINI, P., HUEY, E. D., WASSERMANN, E. M., BABORIE, A., JAROS, E., TIERNEY, M. C., PASTOR, P., RAZQUIN, C., ORTEGA-CUBERO, S., ALONSO, E., PERNECZKY, R., DIEHL-SCHMID, J., ALEXOPOULOS, P., KURZ, A., RAINERO, I., RUBINO, E., PINESSI, L., ROGAEVA, E., ST GEORGE-HYSLOP, P., ROSSI, G., TAGLIAVINI, F., GIACCONE, G., ROWE, J. B., SCHLACHETZKI, J. C. M., UPHILL, J., COLLINGE, J., MEAD, S., DANEK, A., VAN DEERLIN, V. M., GROSSMAN, M., TROJANOWSKI, J. Q., VAN DER ZEE, J., DESCHAMPS, W., VAN LANGENHOVE, T., CRUTS, M., VAN BROECKHOVEN, C., CAPPA, S. F., LE BER, I., HANNEQUIN, D., GOLFIER, V., VERCELLETTO, M., BRICE, A., NACMIAS, B., SORBI, S., BAGNOLI, S., PIACERI, I., NIELSEN, J. E., HJERMIND, L. E., RIEMENSCHNEIDER, M., MAYHAUS, M., IBACH, B., GASPARONI, G., PICHLER, S., GU, W., ROSSOR, M. N., et al. 2014. Frontotemporal dementia and its subtypes: a genome-wide association study. *The Lancet Neurology,* 13**,** 686-699.

FINCH, N., BAKER, M., CROOK, R., SWANSON, K., KUNTZ, K., SURTEES, R., BISCEGLIO, G., ROVELET-LECRUX, A., BOEVE, B., PETERSEN, R. C., DICKSON, D. W., YOUNKIN, S. G., DERAMECOURT, V., CROOK, J., GRAFF-RADFORD, N. R. & RADEMAKERS, R. 2009. Plasma progranulin levels predict progranulin mutation status in frontotemporal dementia patients and asymptomatic family members. *Brain,* 132**,** 583-91.

FINGERT, J. H., ROBIN, A. L., STONE, J. L., ROOS, B. R., DAVIS, L. K., SCHEETZ, T. E., BENNETT, S. R., WASSINK, T. H., KWON, Y. H., ALWARD, W. L., MULLINS, R. F., SHEFFIELD, V. C. & STONE, E. M. 2011. Copy number variations on chromosome 12q14 in patients with normal tension glaucoma. *Hum Mol Genet,* 20**,** 2482-94.

FISHMAN, M. C. 2001. Zebrafish—the Canonical
Vertebrate.

FITZGERALD, K. A., MCWHIRTER, S. M., FAIA, K. L., ROWE, D. C., LATZ, E., GOLENBOCK, D. T., COYLE, A. J., LIAO, S.-M. & MANIATIS, T. 2003a. IKKε and TBK1 are essential components of the IRF3 signaling pathway. *Nature Immunology,* 4**,** 491-496.

FITZGERALD, K. A., MCWHIRTER, S. M., FAIA, K. L., ROWE, D. C., LATZ, E., GOLENBOCK, D. T., COYLE, A. J., LIAO, S. M. & MANIATIS, T. 2003b. IKKepsilon and TBK1 are essential components of the IRF3 signaling pathway. *Nat Immunol,* 4**,** 491-6.

FLANAGAN-STEET, H., FOX, M. A., MEYER, D. & SANES, J. R. 2005. Neuromuscular synapses can form in vivo by incorporation of initially aneural postsynaptic specializations. *Development,* 132**,** 4471-4481.

FREISCHMIDT, A., MÜLLER, K., LUDOLPH, A. C., WEISHAUPT, J. H. & ANDERSEN, P. M. 2017. Association of Mutations in TBK1 With Sporadic and Familial Amyotrophic Lateral Sclerosis and Frontotemporal Dementia. *JAMA Neurology,* 74**,** 110.

FREISCHMIDT, A., WIELAND, T., RICHTER, B., RUF, W., SCHAEFFER, V., MÜLLER, K., MARROQUIN, N., NORDIN, F., HÜBERS, A., WEYDT, P., PINTO, S., PRESS, R., MILLECAMPS, S., MOLKO, N., BERNARD, E., DESNUELLE, C., SORIANI, M.-H., DORST, J., GRAF, E., NORDSTRÖM, U., FEILER, M. S., PUTZ, S., BOECKERS, T. M., MEYER, T., WINKLER, A. S., WINKELMAN, J., DE CARVALHO, M., THAL, D. R., OTTO, M., BRÄNNSTRÖM, T., VOLK, A. E., KURSULA, P., DANZER, K. M., LICHTNER, P., DIKIC, I.,

MEITINGER, T., LUDOLPH, A. C., STROM, T. M., ANDERSEN, P. M. & WEISHAUPT, J. H. 2015a. Haploinsufficiency of TBK1 causes familial ALS and fronto-temporal dementia. *Nature Neuroscience,* 18**,** 631-636.

FREISCHMIDT, A., WIELAND, T., RICHTER, B., RUF, W., SCHAEFFER, V., MULLER, K., MARROQUIN, N., NORDIN, F., HUBERS, A., WEYDT, P., PINTO, S., PRESS, R., MILLECAMPS, S., MOLKO, N., BERNARD, E., DESNUELLE, C., SORIANI, M. H., DORST, J., GRAF, E., NORDSTROM, U., FEILER, M. S., PUTZ, S., BOECKERS, T. M., MEYER, T., WINKLER, A. S., WINKELMAN, J., DE CARVALHO, M., THAL, D. R., OTTO, M., BRANNSTROM, T., VOLK, A. E., KURSULA, P., DANZER, K. M., LICHTNER, P., DIKIC, I., MEITINGER, T., LUDOLPH, A. C., STROM, T. M., ANDERSEN, P. M. & WEISHAUPT, J. H. 2015b. Haploinsufficiency of TBK1 causes familial ALS and fronto-temporal dementia. *Nat Neurosci,* 18**,** 631-6.

FUJITA, F., TANIGUCHI, Y., KATO, T., NARITA, Y., FURUYA, A., OGAWA, T., SAKURAI, H., JOH, T., ITOH, M., DELHASE, M., KARIN, M. & NAKANISHI, M. 2003. Identification of NAP1, a Regulatory Subunit of I B Kinase-Related Kinases That Potentiates NF- B Signaling. *Molecular and Cellular Biology,* 23**,** 7780-7793.

GARDNER, R. C. & YAFFE, K. 2015. Epidemiology of mild traumatic brain injury and neurodegenerative disease. *Mol Cell Neurosci,* 66**,** 75-80.

GÉNIN, P., CUVELIER, F., LAMBIN, S., CÔRTE-REAL FILIPE, J., AUTRUSSEAU, E., LAURENT, C., LAPLANTINE, E. & WEIL, R. 2015. Optineurin Regulates the Interferon Response in a Cell Cycle-Dependent Manner. *PLOS Pathogens,* 11**,** e1004877.

GERBINO, V., KAUNGA, E., YE, J., CANZIO, D., O'KEEFFE, S., RUDNICK, N. D., GUARNIERI, P., LUTZ, C. M. & MANIATIS, T. 2020. The Loss of TBK1 Kinase Activity in Motor Neurons or in All Cell Types Differentially Impacts ALS Disease Progression in SOD1 Mice. *Neuron,* 106**,** 789-805.e5.

GERLAI, R. 2010. Zebrafish antipredatory responses: A future for translational research? *Behavioural Brain Research,* 207**,** 223-231.

GILMORE, T. D. 2006. Introduction to NF-kappaB: players, pathways, perspectives. *Oncogene,* 25**,** 6680-4.

GIULIA GUARGUAGLINI, P. I. D., *‡ YORK D. STIERHOF,§ TIM HOLMSTRO¨M,* 2005. The Forkhead-associated Domain Protein Cep170 Interacts with Polo-like Kinase 1 and Serves as a Marker for Mature Centrioles. *Molecular Biology of the Cell,* 16**,** 1095–1107.

GIULIA GUARGUAGLINI, P. I. D., *‡ YORK D. STIERHOF,§ TIM HOLMSTRO¨M,* STEFAN DUENSING,¶ AND ERICH A. NIGG* 2004.

The Forkhead-associated Domain Protein Cep170 Interacts with Polo-like Kinase 1 and Serves as a Marker for Mature Centrioles.

GLEASON, C. E., ORDUREAU, A., GOURLAY, R., ARTHUR, J. S. C. & COHEN, P. 2011. Polyubiquitin Binding to Optineurin Is Required for Optimal Activation of TANK-binding Kinase 1 and Production of Interferon β. *Journal of Biological Chemistry,* 286**,** 35663-35674.

GOMEZ-TORTOSA, E., VAN DER ZEE, J., RUGGIERO, M., GIJSELINCK, I., ESTEBAN-PEREZ, J., GARCIA-REDONDO, A., BORREGO-HERNANDEZ, D., NAVARRO, E., SAINZ, M. J., PEREZ-PEREZ, J., CRUTS, M., VAN BROECKHOVEN, C., GUERRERO-LOPEZ, R. & CONSORTIUM, E. E. 2017. Familial primary lateral sclerosis or dementia associated with Arg573Gly TBK1 mutation. *J Neurol Neurosurg Psychiatry,* 88**,** 996-997.

GONCALVES, A., BURCKSTUMMER, T., DIXIT, E., SCHEICHER, R., GORNA, M. W., KARAYEL, E., SUGAR, C., STUKALOV, A., BERG, T., KRALOVICS, R., PLANYAVSKY, M., BENNETT, K. L., COLINGE, J. & SUPERTI-FURGA, G. 2011. Functional dissection of the TBK1 molecular network. *PLoS One,* 6**,** e23971.

GOTKINE, M., DE MAJO, M., WONG, C. H., TOPP, S. D., MICHAELSON-COHEN, R., EPSZTEJN-LITMAN, S., EIGES, R., Y, Y. L., KANAAN, M., SHAKED, H. M., ALAHMADY, N., VANCE, C., NEWHOUSE, S. J., BREEN, G., NISHIMURA, A. L., SHAW, C. E. & SMITH, B. N. 2021. A recessive S174X mutation in Optineurin causes amyotrophic lateral sclerosis through a loss of function via allele-specific nonsense-mediated decay. *Neurobiology of Aging*.

GRAY, C. M., REMOUCHAMPS, C., MCCORKELL, K. A., SOLT, L. A., DEJARDIN, E., ORANGE, J. S. & MAY, M. J. 2014. Noncanonical NF- B Signaling Is Limited by Classical NF- B Activity. *Science Signaling,* 7**,** ra13-ra13.

GREENWAY, M. J., ANDERSEN, P. M., RUSS, C., ENNIS, S., CASHMAN, S., DONAGHY, C., PATTERSON, V., SWINGLER, R., KIERAN, D., PREHN, J., MORRISON, K. E., GREEN, A., ACHARYA, K. R., BROWN, R. H., JR. & HARDIMAN, O. 2006. ANG mutations segregate with familial and 'sporadic' amyotrophic lateral sclerosis. *Nat Genet,* 38**,** 411-3.

GROS-LOUIS, F., LARIVIERE, R., GOWING, G., LAURENT, S., CAMU, W., BOUCHARD, J. P., MEININGER, V., ROULEAU, G. A. & JULIEN, J. P. 2004. A frameshift deletion in peripherin gene associated with amyotrophic lateral sclerosis. *J Biol Chem,* 279**,** 45951-6.

HAMDAN, T. A., BHAT, H., CHAM, L. B., ADOMATI, T., LANG, J., LI, F., MURTAZA, A., HARDT, C., LANG, P. A., DUHAN, V. & LANG, K. S. 2020. Map3k14 as a Regulator of Innate and Adaptive Immune Response during Acute Viral Infection. *Pathogens,* 9**,** 96.

HAMILTON, N., RUTHERFORD, H. A., PETTS, J. J., ISLES, H. M., WEBER, T., HENNEKE, M., GÄRTNER, J., DUNNING, M. J. & RENSHAW, S. A. 2020. The failure of microglia to digest developmental apoptotic cells contributes to the pathology of RNASET2-deficient leukoencephalopathy. *Glia,* 68**,** 1531-1545.

HARDIMAN, O., AL-CHALABI, A., CHIO, A., CORR, E. M., LOGROSCINO, G., ROBBERECHT, W., SHAW, P. J., SIMMONS, Z. & VAN DEN BERG, L. H. 2017. Amyotrophic lateral sclerosis. *Nat Rev Dis Primers,* 3**,** 17071.

HARRY M. T. CHOI, V. A. B., AND NILES A. PIERCE 2014. Next-Generation in Situ Hybridization Chain Reaction: Higher Gain, Lower Cost, Greater Durability. *American Chemical Society,* 8**,** 4284–4294.

HE, L., CHEN, L. & LI, L. 2017. The TBK1-OPTN Axis Mediates Crosstalk Between Mitophagy and the Innate Immune Response: A Potential Therapeutic Target for Neurodegenerative Diseases. *Neuroscience Bulletin,* 33**,** 354-356.

HELGASON, E., PHUNG, Q. T. & DUEBER, E. C. 2013. Recent insights into the complexity of Tank-binding kinase 1 signaling networks: the emerging role of cellular localization in the activation and substrate specificity of TBK1. *FEBS Lett,* 587**,** 1230-7.

HEMMI, H., TAKEUCHI, O., SATO, S., YAMAMOTO, M., KAISHO, T., SANJO, H., KAWAI, T., HOSHINO, K., TAKEDA, K. & AKIRA, S. 2004. The roles of two IkappaB kinase-related kinases in lipopolysaccharide and double stranded RNA signaling and viral infection. *J Exp Med,* 199**,** 1641-50.

HEO, J. M., ORDUREAU, A., PAULO, J. A., RINEHART, J. & HARPER, J. W. 2015. The PINK1-PARKIN Mitochondrial Ubiquitylation Pathway Drives a Program of OPTN/NDP52 Recruitment and TBK1 Activation to Promote Mitophagy. *Mol Cell,* 60**,** 7-20.

HERMAN, M., CIANCANELLI, M., OU, Y. H., LORENZO, L., KLAUDEL-DRESZLER, M., PAUWELS, E., SANCHO-SHIMIZU, V., PEREZ DE DIEGO, R., ABHYANKAR, A., ISRAELSSON, E., GUO, Y., CARDON, A., ROZENBERG, F., LEBON, P., TARDIEU, M., HEROPOLITANSKA-PLISZKA, E., CHAUSSABEL, D., WHITE, M. A., ABEL, L., ZHANG, S. Y. & CASANOVA, J. L. 2012. Heterozygous TBK1 mutations impair TLR3 immunity and underlie herpes simplex encephalitis of childhood. *J Exp Med,* 209**,** 1567-82.

HEWAMADDUMA, C. A., GRIERSON, A. J., MA, T. P., PAN, L., MOENS, C. B., INGHAM, P. W., RAMESH, T. & SHAW, P. J. 2013. Tardbpl splicing rescues motor neuron and axonal development in a mutant tardbp zebrafish. *Hum Mol Genet,* 22**,** 2376-86.

HOBSON, E. V. & MCDERMOTT, C. J. 2016. Supportive and symptomatic management of amyotrophic lateral sclerosis. *Nat Rev Neurol,* 12**,** 526-38.

HODGES, J. R. & MILLER, B. 2001. The classification, genetics and neuropathology of frontotemporal dementia. Introduction to the special topic papers: Part I. *Neurocase,* 7**,** 31-5.

HOGAN, A. L., DON, E. K., RAYNER, S. L., LEE, A., LAIRD, A. S., WATCHON, M., WINNICK, C., TARR, I. S., MORSCH, M., FIFITA, J. A., GWEE, S. S. L., FORMELLA, I., HORTLE, E., YUAN, K. C., MOLLOY, M. P., WILLIAMS, K. L., NICHOLSON, G. A., CHUNG, R. S., BLAIR, I. P. & COLE, N. J. 2017. Expression of ALS/FTD-linked mutant CCNF in zebrafish leads to increased cell death in the spinal cord and an aberrant motor phenotype. *Hum Mol Genet,* 26**,** 2616-2626.

HOU, F., SUN, L., ZHENG, H., SKAUG, B., JIANG, Q. X. & CHEN, Z. J. 2011. MAVS forms functional prion-like aggregates to activate and propagate antiviral innate immune response. *Cell,* 146**,** 448-61.

IANEVSKI, A., YAO, R., BIZA, S., ZUSINAITE, E., MANNIK, A., KIVI, G., PLANKEN, A., KURG, K., TOMBAK, E. M., USTAV, M., JR., SHTAIDA, N., KULESSKIY, E., JO, E., YANG, J., LYSVAND, H., LOSETH, K., OKSENYCH, V., AAS, P. A., TENSON, T., VITKAUSKIENE, A., WINDISCH, M. P., FENSTAD, M. H., NORDBO, S. A., USTAV, M., BJORAS, M. & KAINOV, D. E. 2020. Identification and Tracking of Antiviral Drug Combinations. *Viruses,* 12.

ILSE GIJSELINCK, P. S. V. M., MD, JULIE VAN DER ZEE, P. A. S., MD STÉPHANIE PHILTJENS, MSC BAVO HEEMAN, PHD SEBASTIAAN ENGELBORGHS,, PHD, MATHIEU VANDENBULCKE, PHD, GREET DE BAETS, P. V. B. U., BSC, IVY CUIJT, M., MARLEEN VAN DEN BROECK, BSC, KARIN PEETERS, B., MARIA MATTHEIJSSENS, B. F. R., PHD RIK VANDENBERGHE, PHD PETER DE JONGHE, PHD PATRICK CRAS, PHD, PETER P. DE DEYN, P. J.-J. M., PHD MARC CRUTS, PHD CHRISTINE VAN, BROECKHOVEN, D. O. B. O. T. & CONSORTIUM, B. 2015. Loss of TBK1 is a frequent cause of frontotemporal dementia in a Belgian cohort. *Neurology,* 85**,** 2116-2125.

ITAN, Y., SHANG, L., BOISSON, B., PATIN, E., BOLZE, A., MONCADA-VELEZ, M., SCOTT, E., CIANCANELLI, M. J., LAFAILLE, F. G., MARKLE, J. G., MARTINEZ-BARRICARTE, R., DE JONG, S. J., KONG, X. F., NITSCHKE, P., BELKADI, A., BUSTAMANTE, J., PUEL, A., BOISSON-DUPUIS, S., STENSON, P. D., GLEESON, J. G., COOPER, D. N., QUINTANA-MURCI, L., CLAVERIE, J. M., ZHANG, S. Y., ABEL, L. & CASANOVA, J. L. 2015. The human gene

damage index as a gene-level approach to prioritizing exome variants. *Proc Natl Acad Sci U S A,* 112**,** 13615-20.

IVASHKIV, L. B. & DONLIN, L. T. 2014. Regulation of type I interferon responses. *Nature Reviews Immunology,* 14**,** 36-49.

J. WITTBRODT, A. M., 2 AND M. SCHARTL 1998. <More genes in fish_Wittbrodt_et_al-1998-BioEss.pdf>.

J.D. ROHRER, M. R. G., MS, J. VANDROVCOVA, P. J. U., BSC, REIMAN, D., J. BECK, B., A.M. ISAACS, D., A. AUTHIER, M., R. FERRARI, B., N.C. FOX, M., FRCP I.R.A. MACKENZIE, PHD J.D. WARREN, PHD,, FRACP, R. DE SILVA, D., J. HOLTON, P., T. REVESZ, M., J. HARDY, P., S. MEAD, P., MRCP M.N. ROSSOR, MD, & FRCP 2009. The heritability and genetics of frontotemporal lobar degeneration.

JIN, J., XIAO, Y., CHANG, J.-H., YU, J., HU, H., STARR, R., BRITTAIN, G. C., CHANG, M., CHENG, X. & SUN, S.-C. 2012. The kinase TBK1 controls IgA class switching by negatively regulating noncanonical NF-κB signaling. *Nature Immunology,* 13**,** 1101-1109.

JOHNSON, J. O., MANDRIOLI, J., BENATAR, M., ABRAMZON, Y., VAN DEERLIN, V. M., TROJANOWSKI, J. Q., GIBBS, J. R., BRUNETTI, M., GRONKA, S., WUU, J., DING, J., MCCLUSKEY, L., MARTINEZ-LAGE, M., FALCONE, D., HERNANDEZ, D. G., AREPALLI, S., CHONG, S., SCHYMICK, J. C., ROTHSTEIN, J., LANDI, F., WANG, Y. D., CALVO, A., MORA, G., SABATELLI, M., MONSURRO, M. R., BATTISTINI, S., SALVI, F., SPATARO, R., SOLA, P., BORGHERO, G., CONSORTIUM, I., GALASSI, G., SCHOLZ, S. W., TAYLOR, J. P., RESTAGNO, G., CHIO, A. & TRAYNOR, B. J. 2010. Exome sequencing reveals VCP mutations as a cause of familial ALS. *Neuron,* 68**,** 857-64.

JOHNSON, J. O., PIORO, E. P., BOEHRINGER, A., CHIA, R., FEIT, H., RENTON, A. E., PLINER, H. A., ABRAMZON, Y., MARANGI, G., WINBORN, B. J., GIBBS, J. R., NALLS, M. A., MORGAN, S., SHOAI, M., HARDY, J., PITTMAN, A., ORRELL, R. W., MALASPINA, A., SIDLE, K. C., FRATTA, P., HARMS, M. B., BALOH, R. H., PESTRONK, A., WEIHL, C. C., ROGAEVA, E., ZINMAN, L., DRORY, V. E., BORGHERO, G., MORA, G., CALVO, A., ROTHSTEIN, J. D., ITALSGEN, DREPPER, C., SENDTNER, M., SINGLETON, A. B., TAYLOR, J. P., COOKSON, M. R., RESTAGNO, G., SABATELLI, M., BOWSER, R., CHIO, A. & TRAYNOR, B. J. 2014. Mutations in the Matrin 3 gene cause familial amyotrophic lateral sclerosis. *Nat Neurosci,* 17**,** 664-666.

JULIAN, T. H., GLASCOW, N., BARRY, A. D. F., MOLL, T., HARVEY, C., KLIMENTIDIS, Y. C., NEWELL, M., ZHANG, S., SNYDER, M. P., COOPER-KNOCK, J. & SHAW, P. J. 2021. Physical exercise is a risk factor for amyotrophic lateral sclerosis: Convergent evidence from Mendelian randomisation, transcriptomics and risk genotypes. *EBioMedicine,* 68**,** 103397.

KALUEFF, A. V., STEWART, A. M. & GERLAI, R. 2014. Zebrafish as an emerging model for studying complex brain disorders. *Trends Pharmacol Sci,* 35**,** 63-75.

KANTHER, M., SUN, X., MUHLBAUER, M., MACKEY, L. C., FLYNN, E. J., 3RD, BAGNAT, M., JOBIN, C. & RAWLS, J. F. 2011a. Microbial colonization induces dynamic temporal and spatial patterns of NF-kappaB activation in the zebrafish digestive tract. *Gastroenterology,* 141**,** 197-207.

KANTHER, M., SUN, X., MÜHLBAUER, M., MACKEY, L. C., FLYNN, E. J., BAGNAT, M., JOBIN, C. & RAWLS, J. F. 2011b. Microbial Colonization Induces Dynamic Temporal and Spatial

Patterns of NF-κB Activation in the Zebrafish Digestive Tract. *Gastroenterology,* 141**,** 197-207.

KARIN, M. 1999. The Beginning of the End: I B Kinase (IKK) and NF- B Activation.

KASICA-JAROSZ, N., PODLASZ, P. & KALECZYC, J. 2018. Pituitary adenylate cyclase-activating polypeptide (PACAP-38) plays an inhibitory role against inflammation induced by chemical damage to zebrafish hair cells. *PLoS One,* 13**,** e0198180.

KAVALIAUSKIS, A., ARNEMO, M., KIM, S. H., ULANOVA, L., SPETH, M., NOVOA, B., DIOS, S., EVENSEN, O., GRIFFITHS, G. W. & GJOEN, T. 2015. Use of Poly(I:C) Stabilized with Chitosan As a Vaccine-Adjuvant Against Viral Hemorrhagic Septicemia Virus Infection in Zebrafish. *Zebrafish,* 12**,** 421-31.

KAWASE, K., ALLINGHAM, R. R., MEGURO, A., MIZUKI, N., ROOS, B., SOLIVAN-TIMPE, F. M., ROBIN, A. L., RITCH, R. & FINGERT, J. H. 2012. Confirmation of TBK1 duplication in normal tension glaucoma. *Experimental Eye Research,* 96**,** 178-180.

KELLER, M. F., FERRUCCI, L., SINGLETON, A. B., TIENARI, P. J., LAAKSOVIRTA, H., RESTAGNO, G., CHIÒ, A., TRAYNOR, B. J. & NALLS, M. A. 2014. Genome-Wide Analysis of the Heritability of Amyotrophic Lateral Sclerosis. *JAMA Neurology,* 71**,** 1123.

KENNA, K. P., VAN DOORMAAL, P. T., DEKKER, A. M., TICOZZI, N., KENNA, B. J., DIEKSTRA, F. P., VAN RHEENEN, W., VAN EIJK, K. R., JONES, A. R., KEAGLE, P., SHATUNOV, A., SPROVIERO, W., SMITH, B. N., VAN ES, M. A., TOPP, S. D., KENNA, A., MILLER, J. W., FALLINI, C., TILOCA, C., MCLAUGHLIN, R. L., VANCE, C., TROAKES, C., COLOMBRITA, C., MORA, G., CALVO, A., VERDE, F., AL-SARRAJ, S., KING, A., CALINI, D., DE BELLEROCHE, J., BAAS, F., VAN DER KOOI, A. J., DE VISSER, M., TEN ASBROEK, A. L., SAPP, P. C., MCKENNA-YASEK, D., POLAK, M., ASRESS, S., MUNOZ-BLANCO, J. L., STROM, T. M., MEITINGER, T., MORRISON, K. E., CONSORTIUM, S., LAURIA, G., WILLIAMS, K. L., LEIGH, P. N., NICHOLSON, G. A., BLAIR, I. P., LEBLOND, C. S., DION, P. A., ROULEAU, G. A., PALL, H., SHAW, P. J., TURNER, M. R., TALBOT, K., TARONI, F., BOYLAN, K. B., VAN BLITTERSWIJK, M., RADEMAKERS, R., ESTEBAN-PEREZ, J., GARCIA-REDONDO, A., VAN DAMME, P., ROBBERECHT, W., CHIO, A., GELLERA, C., DREPPER, C., SENDTNER, M., RATTI, A., GLASS, J. D., MORA, J. S., BASAK, N. A., HARDIMAN, O., LUDOLPH, A. C., ANDERSEN, P. M., WEISHAUPT, J. H., BROWN, R. H., JR., AL-CHALABI, A., SILANI, V., SHAW, C. E., VAN DEN BERG, L. H., VELDINK, J. H. & LANDERS, J. E. 2016. NEK1 variants confer susceptibility to amyotrophic lateral sclerosis. *Nat Genet,* 48**,** 1037-42.

KEOGH, M. J., WEI, W., ARYAMAN, J., WILSON, I., TALBOT, K., TURNER, M. R., MCKENZIE, C. A., TROAKES, C., ATTEMS, J., SMITH, C., AL SARRAJ, S., MORRIS, C. M., ANSORGE, O., PICKERING-BROWN, S., JONES, N., IRONSIDE, J. W. & CHINNERY, P. F. 2018. Oligogenic genetic variation of neurodegenerative disease genes in 980 postmortem human brains. *J Neurol Neurosurg Psychiatry*.

KETTLEBOROUGH, R. N., BUSCH-NENTWICH, E. M., HARVEY, S. A., DOOLEY, C. M., DE BRUIJN, E., VAN EEDEN, F., SEALY, I., WHITE, R. J., HERD, C., NIJMAN, I. J., FENYES, F., MEHROKE, S., SCAHILL, C., GIBBONS, R., WALI, N., CARRUTHERS, S., HALL, A., YEN, J., CUPPEN, E. & STEMPLE, D. L. 2013. A systematic genome-wide analysis of zebrafish protein-coding gene function. *Nature,* 496**,** 494-7.

KIM, H. J., KIM, N. C., WANG, Y. D., SCARBOROUGH, E. A., MOORE, J., DIAZ, Z., MACLEA, K. S., FREIBAUM, B., LI, S., MOLLIEX, A., KANAGARAJ, A. P., CARTER, R., BOYLAN, K. B.,

WOJTAS, A. M., RADEMAKERS, R., PINKUS, J. L., GREENBERG, S. A., TROJANOWSKI, J. Q., TRAYNOR, B. J., SMITH, B. N., TOPP, S., GKAZI, A. S., MILLER, J., SHAW, C. E., KOTTLORS, M., KIRSCHNER, J., PESTRONK, A., LI, Y. R., FORD, A. F., GITLER, A. D., BENATAR, M., KING, O. D., KIMONIS, V. E., ROSS, E. D., WEIHL, C. C., SHORTER, J. & TAYLOR, J. P. 2013a. Mutations in prion-like domains in hnRNPA2B1 and hnRNPA1 cause multisystem proteinopathy and ALS. *Nature,* 495**,** 467-73.

KIM, J. Y., WELSH, E. A., OGUZ, U., FANG, B., BAI, Y., KINOSE, F., BRONK, C., REMSING RIX, L. L., BEG, A. A., RIX, U., ESCHRICH, S. A., KOOMEN, J. M. & HAURA, E. B. 2013b. Dissection of TBK1 signaling via phosphoproteomics in lung cancer cells. *Proc Natl Acad Sci U S A,* 110**,** 12414-9.

KIM, Y. E., OH, K. W., NOH, M. Y., NAHM, M., PARK, J., LIM, S. M., JANG, J. H., CHO, E. H., KI, C. S., LEE, S. & KIM, S. H. 2017. Genetic and functional analysis of TBK1 variants in Korean patients with sporadic amyotrophic lateral sclerosis. *Neurobiol Aging,* 50**,** 170 e1-170 e6.

KLIONSKY, D. J. 2007. Autophagy: from phenomenology to molecular understanding in less than a decade. *Nature reviews molecular cell biology,* 8**,** 931-937.

KORAC, J., SCHAEFFER, V., KOVACEVIC, I., CLEMENT, A. M., JUNGBLUT, B., BEHL, C., TERZIC, J. & DIKIC, I. 2013. Ubiquitin-independent function of optineurin in autophagic clearance of protein aggregates. *J Cell Sci,* 126**,** 580-92.

KUMAR, H., KAWAI, T. & AKIRA, S. 2011. Pathogen recognition by the innate immune system. *Int Rev Immunol,* 30**,** 16-34.

LAAKSOVIRTA, H., PEURALINNA, T., SCHYMICK, J. C., SCHOLZ, S. W., LAI, S.-L., MYLLYKANGAS, L., SULKAVA, R., JANSSON, L., HERNANDEZ, D. G., GIBBS, J. R., NALLS, M. A., HECKERMAN, D., TIENARI, P. J. & TRAYNOR, B. J. 2010. Chromosome 9p21 in amyotrophic lateral sclerosis in Finland: a genome-wide association study. *The Lancet Neurology,* 9**,** 978-985.

LALL, D. & BALOH, R. H. 2017. Microglia and C9orf72 in neuroinflammation and ALS and frontotemporal dementia. *Journal of Clinical Investigation,* 127**,** 3250-3258.

LAMB, R., ROHRER, J. D., REAL, R., LUBBE, S. J., WAITE, A. J., BLAKE, D. J., WALTERS, R. J., LASHLEY, T., REVESZ, T., HOLTON, J. L. & MORRIS, H. R. 2019. A novel TBK1 mutation in a family with diverse frontotemporal dementia spectrum disorders. *Cold Spring Harb Mol Case Stud,* 5.

LARABI, A., DEVOS, J. M., NG, S. L., NANAO, M. H., ROUND, A., MANIATIS, T. & PANNE, D. 2013. Crystal structure and mechanism of activation of TANK-binding kinase 1. *Cell Rep,* 3**,** 734-46.

LARDELLI, D. M. 2017. Using zebrafish in human disease research:
some advantages, disadvantages and
ethical considerations. *Transgenics and modelling* 23-28.

LATTANTE, S., DORONZIO, P. N., MARANGI, G., CONTE, A., BISOGNI, G., BERNARDO, D., RUSSO, T., LAMBERTI, D., PATRIZI, S., APOLLO, F. P., LUNETTA, C., SCARLINO, S., POZZI, L., ZOLLINO, M., RIVA, N. & SABATELLI, M. 2019. Coexistence of variants in TBK1 and in other ALS-related genes elucidates an oligogenic model of pathogenesis in sporadic ALS. *Neurobiol Aging,* 84**,** 239 e9-239 e14.

LAWRENCE, T. 2009a. The Nuclear Factor NF- B Pathway in Inflammation. *Cold Spring Harbor Perspectives in Biology,* 1**,** a001651-a001651.

LAWRENCE, T. 2009b. The nuclear factor NF-kappaB pathway in inflammation. *Cold Spring Harb Perspect Biol,* 1**,** a001651.

LE BER, I., CAMUZAT, A., GUERREIRO, R., BOUYA-AHMED, K., BRAS, J., NICOLAS, G., GABELLE, A., DIDIC, M., DE SEPTENVILLE, A., MILLECAMPS, S., LENGLET, T., LATOUCHE, M., KABASHI, E., CAMPION, D., HANNEQUIN, D., HARDY, J., BRICE, A., FRENCH, C. & GENETIC RESEARCH NETWORK ON, F. F.-A. 2013. SQSTM1 mutations in French patients with frontotemporal dementia or frontotemporal dementia with amyotrophic lateral sclerosis. *JAMA Neurol,* 70**,** 1403-10.

LE BER, I., DE SEPTENVILLE, A., MILLECAMPS, S., CAMUZAT, A., CAROPPO, P., COURATIER, P., BLANC, F., LACOMBLEZ, L., SELLAL, F., FLEURY, M. C., MEININGER, V., CAZENEUVE, C., CLOT, F., FLABEAU, O., LEGUERN, E., BRICE, A., FRENCH, C. & GENETIC RESEARCH NETWORK ON, F. F.-A. 2015. TBK1 mutation frequencies in French frontotemporal dementia and amyotrophic lateral sclerosis cohorts. *Neurobiol Aging,* 36**,** 3116 e5-3116 e8.

LEE, A. J. & ASHKAR, A. A. 2018. The Dual Nature of Type I and Type II Interferons. *Front Immunol,* 9**,** 2061.

LEVINE, B., MIZUSHIMA, N. & VIRGIN, H. W. 2011. Autophagy in immunity and inflammation. *Nature,* 469**,** 323-335.

LEVRAUD, J. P., BOUDINOT, P., COLIN, I., BENMANSOUR, A., PEYRIERAS, N., HERBOMEL, P. & LUTFALLA, G. 2007. Identification of the zebrafish IFN receptor: implications for the origin of the vertebrate IFN system. *J Immunol,* 178**,** 4385-94.

LI, F., XIE, X., WANG, Y., LIU, J., CHENG, X., GUO, Y., GONG, Y., HU, S. & PAN, L. 2016. Structural insights into the interaction and disease mechanism of neurodegenerative disease-associated optineurin and TBK1 proteins. *Nat Commun,* 7**,** 12708.

LI, F., XU, D., WANG, Y., ZHOU, Z., LIU, J., HU, S., GONG, Y., YUAN, J. & PAN, L. 2018. Structural insights into the ubiquitin recognition by OPTN (optineurin) and its regulation by TBK1-mediated phosphorylation. *Autophagy,* 14**,** 66-79.

LI, S., LU, L. F., LI, Z. C., ZHANG, C., ZHOU, X. Y., ZHOU, Y. & ZHANG, Y. A. 2019. Zebrafish MVP Recruits and Degrades TBK1 To Suppress IFN Production. *J Immunol,* 202**,** 559-566.

LI, S., WANG, L., BERMAN, M., KONG, Y. Y. & DORF, M. E. 2011. Mapping a dynamic innate immunity protein interaction network regulating type I interferon production. *Immunity,* 35**,** 426-40.

LIN, R. H., C ; PITHA, P ; HISCOTT, J 1998. Virus-dependent phosphorylation of the IRF-3 transcription factor regulates nuclear translocation, transactivation potential, and proteasome-mediated degradation. *Molecular and Cellular Biology,* 18**,** 2986-2996.

LISTER, J. A., ROBERTSON, C. P., LEPAGE, T., JOHNSON, S. L. & RAIBLE, D. W. 1999. nacre encodes a zebrafish microphthalmia-related protein that regulates neural-crest-derived pigment cell fate. *Development,* 126**,** 3757-3767.

LIU, T., ZHANG, L., JOO, D. & SUN, S. C. 2017. NF-kappaB signaling in inflammation. *Signal Transduct Target Ther,* 2.

LOCKSHIN, J. B. A. R. 1977. Ultrastructural Study of the Normal Degeneration of the Intersegmental Muscles of Antheraea polyphemus and Manduca sexta (Insecta, Lepidoptera) with Particular Reference to Cellular Autophagy. *Journal of Morphology,* 154**,** 39-58.

LOGROSCINO, G., TRAYNOR, B. J., HARDIMAN, O., CHIO, A., COURATIER, P., MITCHELL, J. D., SWINGLER, R. J., BEGHI, E. & EURALS 2008. Descriptive epidemiology of amyotrophic lateral sclerosis: new evidence and unsolved issues. *J Neurol Neurosurg Psychiatry,* 79**,** 6-11.

LUCAS-HOURANI, M., DAUZONNE, D., JORDA, P., COUSIN, G., LUPAN, A., HELYNCK, O., CAIGNARD, G., JANVIER, G., ANDRÉ-LEROUX, G., KHIAR, S., ESCRIOU, N., DESPRÈS, P., JACOB, Y., MUNIER-LEHMANN, H., TANGY, F. & VIDALAIN, P.-O. 2013. Inhibition of Pyrimidine Biosynthesis Pathway Suppresses Viral Growth through Innate Immunity. *PLoS Pathogens,* 9**,** e1003678.

LUTY, A. A., KWOK, J. B., DOBSON-STONE, C., LOY, C. T., COUPLAND, K. G., KARLSTROM, H., SOBOW, T., TCHORZEWSKA, J., MARUSZAK, A., BARCIKOWSKA, M., PANEGYRES, P. K., ZEKANOWSKI, C., BROOKS, W. S., WILLIAMS, K. L., BLAIR, I. P., MATHER, K. A., SACHDEV, P. S., HALLIDAY, G. M. & SCHOFIELD, P. R. 2010. Sigma nonopioid intracellular receptor 1 mutations cause frontotemporal lobar degeneration-motor neuron disease. *Ann Neurol,* 68**,** 639-49.

M.L. GORNO-TEMPINI, M., PHD, A.E. HILLIS, M., S. WEINTRAUB, P., A. KERTESZ, M., M. MENDEZ, M., S.F. CAPPA, M., J.M. OGAR, M., J.D. ROHRER, M., S. BLACK, M., B.F. BOEVE, M., F. MANES, M., N.F. DRONKERS, P. R. V., MD,, PHD, K. RASCOVSKY, P., K. PATTERSON, P. B. L. M., MD, KNOPMAN, D. S. & J.R. HODGES, M. M. M. M., MD* M. GROSSMAN, MD* 2011. Classification of primary progressive aphasia and its variants. *Neurology,* 76**,** 1006–1014.

MANKOURI, J., FRAGKOUDIS, R., RICHARDS, K. H., WETHERILL, L. F., HARRIS, M., KOHL, A., ELLIOTT, R. M. & MACDONALD, A. 2010. Optineurin Negatively Regulates the Induction of IFNβ in Response to RNA Virus Infection. *PLoS Pathogens,* 6**,** e1000778.

MANUELA NEUMANN, 11* DEEPAK M. SAMPATHU,1* LINDA K. KWONG,1* ADAM C. TRUAX,1, MATTHEW C. MICSENYI, T. T. C., 2 JENNIFER BRUCE,1 THERESA SCHUCK,1 MURRAY GROSSMAN,3,4 CHRISTOPHER M. CLARK,3,4 LEO F. MCCLUSKEY,3 BRUCE L. MILLER,6 ELIEZER MASLIAH,7, IAN R. MACKENZIE, H. F., 9 WOLFGANG FEIDEN,10 HANS A. KRETZSCHMAR,11 & JOHN Q. TROJANOWSKI, 4,5 VIRGINIA M.-Y. LEE1,4,5† 2006. Ubiquitinated TDP-43 in
Frontotemporal Lobar Degeneration
and Amyotrophic Lateral Sclerosis. *SCIENCE,* 314**,** 130-133.

MARUYAMA, H., MORINO, H., ITO, H., IZUMI, Y., KATO, H., WATANABE, Y., KINOSHITA, Y., KAMADA, M., NODERA, H., SUZUKI, H., KOMURE, O., MATSUURA, S., KOBATAKE, K., MORIMOTO, N., ABE, K., SUZUKI, N., AOKI, M., KAWATA, A., HIRAI, T., KATO, T., OGASAWARA, K., HIRANO, A., TAKUMI, T., KUSAKA, H., HAGIWARA, K., KAJI, R. & KAWAKAMI, H. 2010a. Mutations of optineurin in amyotrophic lateral sclerosis. *Nature,* 465**,** 223-226.

MARUYAMA, H., MORINO, H., ITO, H., IZUMI, Y., KATO, H., WATANABE, Y., KINOSHITA, Y., KAMADA, M., NODERA, H., SUZUKI, H., KOMURE, O., MATSUURA, S., KOBATAKE, K., MORIMOTO, N., ABE, K., SUZUKI, N., AOKI, M., KAWATA, A., HIRAI, T., KATO, T., OGASAWARA, K., HIRANO, A., TAKUMI, T., KUSAKA, H., HAGIWARA, K., KAJI, R. & KAWAKAMI, H. 2010b. Mutations of optineurin in amyotrophic lateral sclerosis. *Nature,* 465**,** 223-6.

MASSELINK, W. 2021. Crispants take the spotlight. *Lab Animal,* 50**,** 95-96.
MCCALL, A. L., DHINDSA, J. S., PUCCI, L. A., KAHN, A. F., FUSCO, A. F., BISWAS, D. D., STRICKLAND, L. M., TSENG, H. C. & ELMALLAH, M. K. 2020. Respiratory pathology in the Optn(-/-) mouse model of Amyotrophic Lateral Sclerosis. *Respir Physiol Neurobiol,* 282**,** 103525.
MEDCHALMI, S., TARE, P., SAYYAD, Z. & SWARUP, G. 2021. A glaucoma- and ALS-associated mutant of OPTN induces neuronal cell death dependent on Tbk1 activity, autophagy and ER stress. *FEBS J,* 288**,** 4576-4595.
MENKE, R. A. L., KÖRNER, S., FILIPPINI, N., DOUAUD, G., KNIGHT, S., TALBOT, K. & TURNER, M. R. 2014. Widespread grey matter pathology dominates the longitudinal cerebral MRI and clinical landscape of amyotrophic lateral sclerosis. *Brain,* 137**,** 2546-2555.
MIKKO HALLMAN, M. R., AND R. ALAN EZEKOWITZ 2001. Toll-like Receptors as Sensors of Pathogens. *Pediatric Research,* 50**,** 315-321.
MILLER1, J. R. H. A. B. 2001. <The Classification Genetics and Neuropathology of Frontotemporal Dementia Introduction to the Special Topic Papers Part I.pdf>. *Neurocase,* Vol. 7**,** pp. 31–35.
MILLER, N. & GERLAI, R. 2007. Quantification of shoaling behaviour in zebrafish (Danio rerio). *Behavioural Brain Research,* 184**,** 157-166.
MILLER, N. & GERLAI, R. 2012. From Schooling to Shoaling: Patterns of Collective Motion in Zebrafish (Danio rerio). *PLoS ONE,* 7**,** e48865.
MITCHELL, J., PAUL, P., CHEN, H. J., MORRIS, A., PAYLING, M., FALCHI, M., HABGOOD, J., PANOUTSOU, S., WINKLER, S., TISATO, V., HAJITOU, A., SMITH, B., VANCE, C., SHAW, C., MAZARAKIS, N. D. & DE BELLEROCHE, J. 2010. Familial amyotrophic lateral sclerosis is associated with a mutation in D-amino acid oxidase. *Proc Natl Acad Sci U S A,* 107**,** 7556-61.
MITSUHARU SATO, H. S., † NAOKI HATA,* MASATAKA ASAGIRI,* KOUETSU OGASAWARA,*, KAZUKI NAKAO, T. N., * MOTOYA KATSUKI,‡ SHIGERU NOGUCHI,† NOBUYUKI TANAKA,* & TANIGUCHI*§, A. T. 2000. Distinct and Essential Roles of Transcription Factors IRF-3 and IRF-7 in Response
to Viruses for IFN- / Gene Induction.
MOORE, A. S. & HOLZBAUR, E. L. 2016a. Dynamic recruitment and activation of ALS-associated TBK1 with its target optineurin are required for efficient mitophagy. *Proc Natl Acad Sci U S A,* 113**,** E3349-58.
MOORE, A. S. & HOLZBAUR, E. L. F. 2016b. Dynamic recruitment and activation of ALS-associated TBK1 with its target optineurin are required for efficient mitophagy. *Proceedings of the National Academy of Sciences,* 113**,** E3349-E3358.
MOORE, T. C., KUMM, P. M., BROWN, D. M. & PETRO, T. M. 2014. Interferon response factor 3 is crucial to poly-I:C induced NK cell activity and control of B16 melanoma growth. *Cancer Letters,* 346**,** 122-128.
MORRICE, J. R., GREGORY-EVANS, C. Y. & SHAW, C. A. 2018. Modeling Environmentally-Induced Motor Neuron Degeneration in Zebrafish. *Scientific Reports,* 8.
MORTON, S., HESSON, L., PEGGIE, M. & COHEN, P. 2008. Enhanced binding of TBK1 by an optineurin mutant that causes a familial form of primary open angle glaucoma. *FEBS Lett,* 582**,** 997-1002.

MOSER, C. V., STEPHAN, H., ALTENRATH, K., KYNAST, K. L., RUSSE, O. Q., OLBRICH, K., GEISSLINGER, G. & NIEDERBERGER, E. 2015. TANK-binding kinase 1 (TBK1) modulates inflammatory hyperalgesia by regulating MAP kinases and NF-kappaB dependent genes. *J Neuroinflammation,* 12**,** 100.

MUNITIC, I., GIARDINO TORCHIA, M. L., MEENA, N. P., ZHU, G., LI, C. C. & ASHWELL, J. D. 2013. Optineurin Insufficiency Impairs IRF3 but Not NF-κB Activation in Immune Cells. *The Journal of Immunology,* 191**,** 6231-6240.

N. PARKINSON, P. P. G. I., MD*; M.O. SMITH, BSC; R. HIGHLEY, PHD; G. SKIBINSKI, PHD;, P.M. ANDERSEN, M. K. E. M., PHD; H.S. PALL, MD; O. HARDIMAN, PHD; J. COLLINGE, MD; & P.J. SHAW, M. A. E. M. C. F., PHD*; 2006. <ALS phenotypes with mutations in CHMP2B (charged multivesicular body

protein 2B)>. *Neurology,* 67**,** 1074-1077.

NAGABHUSHANA, A., BANSAL, M. & SWARUP, G. 2011. Optineurin Is Required for CYLD-Dependent Inhibition of TNFα-Induced NF-κB Activation. *PLoS ONE,* 6**,** e17477.

NEWTON, K. & DIXIT, V. M. 2012. Signaling in innate immunity and inflammation. *Cold Spring Harb Perspect Biol,* 4.

NICOLAS, A., KENNA, K. P., RENTON, A. E., TICOZZI, N., FAGHRI, F., CHIA, R., DOMINOV, J. A., KENNA, B. J., NALLS, M. A., KEAGLE, P., RIVERA, A. M., VAN RHEENEN, W., MURPHY, N. A., VAN VUGT, J. J. F. A., GEIGER, J. T., VAN DER SPEK, R. A., PLINER, H. A., SHANKARACHARYA, SMITH, B. N., MARANGI, G., TOPP, S. D., ABRAMZON, Y., GKAZI, A. S., EICHER, J. D., KENNA, A., MORA, G., CALVO, A., MAZZINI, L., RIVA, N., MANDRIOLI, J., CAPONNETTO, C., BATTISTINI, S., VOLANTI, P., LA BELLA, V., CONFORTI, F. L., BORGHERO, G., MESSINA, S., SIMONE, I. L., TROJSI, F., SALVI, F., LOGULLO, F. O., D'ALFONSO, S., CORRADO, L., CAPASSO, M., FERRUCCI, L., MORENO, C. D. A. M., KAMALAKARAN, S., GOLDSTEIN, D. B., GITLER, A. D., HARRIS, T., MYERS, R. M., PHATNANI, H., MUSUNURI, R. L., EVANI, U. S., ABHYANKAR, A., ZODY, M. C., KAYE, J., FINKBEINER, S., WYMAN, S. K., LENAIL, A., LIMA, L., FRAENKEL, E., SVENDSEN, C. N., THOMPSON, L. M., VAN EYK, J. E., BERRY, J. D., MILLER, T. M., KOLB, S. J., CUDKOWICZ, M., BAXI, E., BENATAR, M., TAYLOR, J. P., RAMPERSAUD, E., WU, G., WUU, J., LAURIA, G., VERDE, F., FOGH, I., TILOCA, C., COMI, G. P., SORARÙ, G., CEREDA, C., CORCIA, P., LAAKSOVIRTA, H., MYLLYKANGAS, L., JANSSON, L., VALORI, M., EALING, J., HAMDALLA, H., ROLLINSON, S., PICKERING-BROWN, S., ORRELL, R. W., SIDLE, K. C., MALASPINA, A., HARDY, J., SINGLETON, A. B., JOHNSON, J. O., AREPALLI, S., SAPP, P. C., MCKENNA-YASEK, D., et al. 2018. Genome-wide Analyses Identify KIF5A as a Novel ALS Gene. *Neuron,* 97**,** 1268-1283.e6.

NISHIMURA, A. L., MITNE-NETO, M., SILVA, H. C., RICHIERI-COSTA, A., MIDDLETON, S., CASCIO, D., KOK, F., OLIVEIRA, J. R., GILLINGWATER, T., WEBB, J., SKEHEL, P. & ZATZ, M. 2004. A mutation in the vesicle-trafficking protein VAPB causes late-onset spinal muscular atrophy and amyotrophic lateral sclerosis. *Am J Hum Genet,* 75**,** 822-31.

NOAD, J., VON DER MALSBURG, A., PATHE, C., MICHEL, M. A., KOMANDER, D. & RANDOW, F. 2017. LUBAC-synthesized linear ubiquitin chains restrict cytosol-invading bacteria by activating autophagy and NF-κB. *Nature Microbiology,* 2**,** 17063.

NORTON, W. H. J. 2012. Measuring Larval Zebrafish Behavior: Locomotion, Thigmotaxis, and Startle. Humana Press.

OAKES, J. A., DAVIES, M. C. & COLLINS, M. O. 2017. TBK1: a new player in ALS linking autophagy and neuroinflammation. *Molecular Brain,* 10.

OECKINGHAUS, A. & GHOSH, S. 2009. The NF-kappaB family of transcription factors and its regulation. *Cold Spring Harb Perspect Biol,* 1**,** a000034.

OMAR M E ALBAGHA1, S. E. W., MICAELA R VISCONTI1, NEREA ALONSO1, KIRSTEEN GOODMAN2, MARIA LUISA BRANDI3, TIM CUNDY4, PUI YAN JENNY CHUNG5, ROSEMARY DARGIE6, JEAN-PIERRE DEVOGELAER7, ALBERTO FALCHETTI3, WILLIAM D FRASER8, LUIGI GENNARI9, FERNANDO GIANFRANCESCO10, MICHAEL J HOOPER11, WIM VAN HUL5, GIANLUCA ISAIA12, GEOFF C NICHOLSON13, RANUCCIO NUTI9, SOCRATES PAPAPOULOS14, JAVIER DEL PINO MONTES15, THOMAS RATAJCZAK16,17, SARAH L REA16,17, DOMENICO RENDINA18, ROGELIO GONZALEZ-SARMIENTO19, MARCO DI STEFANO12, LYNLEY C WARD16, JOHN P WALSH16,20 & STUART H RALSTON1 2011. Genome-wide association identifies three new susceptibility loci for Paget's disease of bone. *Nature Genetics,* 43**,** 685-689.

ORLACCHIO, A., BABALINI, C., BORRECA, A., PATRONO, C., MASSA, R., BASARAN, S., MUNHOZ, R. P., ROGAEVA, E. A., ST GEORGE-HYSLOP, P. H., BERNARDI, G. & KAWARAI, T. 2010. SPATACSIN mutations cause autosomal recessive juvenile amyotrophic lateral sclerosis. *Brain,* 133**,** 591-8.

PANNE, D., MCWHIRTER, S. M., MANIATIS, T. & HARRISON, S. C. 2007. Interferon Regulatory Factor 3 Is Regulated by a Dual Phosphorylation-dependent Switch. *Journal of Biological Chemistry,* 282**,** 22816-22822.

PASINELLI, P. & BROWN, R. H. 2006. Molecular biology of amyotrophic lateral sclerosis: insights from genetics. *Nat Rev Neurosci,* 7**,** 710-23.

PAULUS, J. D. & LINK, B. A. 2014. Loss of optineurin in vivo results in elevated cell death and alters axonal trafficking dynamics. *PLoS One,* 9**,** e109922.

PEARSON, W. R. 2013. An introduction to sequence similarity ("homology") searching. *Curr Protoc Bioinformatics,* Chapter 3**,** Unit3 1.

PFLUG, K. M. & SITCHERAN, R. 2020. Targeting NF-κB-Inducing Kinase (NIK) in Immunity, Inflammation, and Cancer. *International Journal of Molecular Sciences,* 21**,** 8470.

PICKRELL, A. M. & YOULE, R. J. 2015. The roles of PINK1, parkin, and mitochondrial fidelity in Parkinson's disease. *Neuron,* 85**,** 257-73.

PILLAI, S., NGUYEN, J., JOHNSON, J., HAURA, E., COPPOLA, D. & CHELLAPPAN, S. 2015. Tank binding kinase 1 is a centrosome-associated kinase necessary for microtubule dynamics and mitosis. *Nat Commun,* 6**,** 10072.

PILLI, M., ARKO-MENSAH, J., PONPUAK, M., ROBERTS, E., MASTER, S., MANDELL, M. A., DUPONT, N., ORNATOWSKI, W., JIANG, S., BRADFUTE, S. B., BRUUN, J. A., HANSEN, T. E., JOHANSEN, T. & DERETIC, V. 2012. TBK-1 promotes autophagy-mediated antimicrobial defense by controlling autophagosome maturation. *Immunity,* 37**,** 223-34.

PLAUT, I. 2000. EFFECTS OF FIN SIZE ON SWIMMING PERFORMANCE, SWIMMING BEHAVIOUR AND ROUTINE ACTIVITY OF ZEBRAFISH DANIO RERIO. *Journal of experimental biology,* 203**,** 813-820.

PODLASZ, P., SALLINEN, V., CHEN, Y. C., KUDO, H., FEDOROWSKA, N. & PANULA, P. 2012. Galanin gene expression and effects of its knock-down on the development of the nervous system in larval zebrafish. *Journal of Comparative Neurology,* 520**,** 3846-3862.

POTTIER, C., BIENIEK, K. F., FINCH, N., VAN DE VORST, M., BAKER, M., PERKERSEN, R., BROWN, P., RAVENSCROFT, T., VAN BLITTERSWIJK, M., NICHOLSON, A. M., DETURE, M., KNOPMAN, D. S., JOSEPHS, K. A., PARISI, J. E., PETERSEN, R. C., BOYLAN, K. B., BOEVE, B. F., GRAFF-RADFORD, N. R., VELTMAN, J. A., GILISSEN, C., MURRAY, M. E., DICKSON, D. W. & RADEMAKERS, R. 2015a. Whole-genome sequencing reveals important role for TBK1 and OPTN mutations in frontotemporal lobar degeneration without motor neuron disease. *Acta Neuropathol,* 130**,** 77-92.

POTTIER, C., BIENIEK, K. F., FINCH, N., VAN DE VORST, M., BAKER, M., PERKERSEN, R., BROWN, P., RAVENSCROFT, T., VAN BLITTERSWIJK, M., NICHOLSON, A. M., DETURE, M., KNOPMAN, D. S., JOSEPHS, K. A., PARISI, J. E., PETERSEN, R. C., BOYLAN, K. B., BOEVE, B. F., GRAFF-RADFORD, N. R., VELTMAN, J. A., GILISSEN, C., MURRAY, M. E., DICKSON, D. W. & RADEMAKERS, R. 2015b. Whole-genome sequencing reveals important role for TBK1 and OPTN mutations in frontotemporal lobar degeneration without motor neuron disease. *Acta Neuropathologica,* 130**,** 77-92.

POZZI, L., VALENZA, F., MOSCA, L., DAL MAS, A., DOMI, T., ROMANO, A., TARLARINI, C., FALZONE, Y. M., TREMOLIZZO, L., SORARU, G., CERRI, F., FERRARO, P. M., BASAIA, S., AGOSTA, F., FAZIO, R., COMOLA, M., COMI, G., FERRARI, M., QUATTRINI, A., LUNETTA, C., PENCO, S., BONANOMI, D., CARRERA, P. & RIVA, N. 2017. TBK1 mutations in Italian patients with amyotrophic lateral sclerosis: genetic and functional characterisation. *J Neurol Neurosurg Psychiatry,* 88**,** 869-875.

PRESSMAN, P. S. & MILLER, B. L. 2014. Diagnosis and management of behavioral variant frontotemporal dementia. *Biol Psychiatry,* 75**,** 574-81.

RABINOVICI, G. D. & MILLER, B. L. 2010. Frontotemporal lobar degeneration: epidemiology, pathophysiology, diagnosis and management. *CNS Drugs,* 24**,** 375-98.

RADEMAKERS, R., CRUTS, M. & VAN BROECKHOVEN, C. 2004. The role of tau (MAPT) in frontotemporal dementia and related tauopathies. *Hum Mutat,* 24**,** 277-95.

RADULESCU, A. E. & CLEVELAND, D. W. 2010. NuMA after 30 years: the matrix revisited. *Trends Cell Biol,* 20**,** 214-22.

RAINERO, I. R., E; MICHELERIO, A; D'AGATA, F; GENTILE, SALVATORE; PINESSI, LORENZO 2017. Recent advances in the molecular genetics of frontotemporal lobar degeneration.

RAINIER, S., BUI, M., MARK, E., THOMAS, D., TOKARZ, D., MING, L., DELANEY, C., RICHARDSON, R. J., ALBERS, J. W., MATSUNAMI, N., STEVENS, J., COON, H., LEPPERT, M. & FINK, J. K. 2008. Neuropathy target esterase gene mutations cause motor neuron disease. *Am J Hum Genet,* 82**,** 780-5.

RAMESH, T., LYON, A. N., PINEDA, R. H., WANG, C., JANSSEN, P. M., CANAN, B. D., BURGHES, A. H. & BEATTIE, C. E. 2010. A genetic model of amyotrophic lateral sclerosis in zebrafish displays phenotypic hallmarks of motoneuron disease. *Dis Model Mech,* 3**,** 652-62.

RAN, F. A., HSU, P. D., WRIGHT, J., AGARWALA, V., SCOTT, D. A. & ZHANG, F. 2013. Genome engineering using the CRISPR-Cas9 system. *Nat Protoc,* 8**,** 2281-2308.

REIKO SHINKURA1*, K. K., FUMIHIKO MATSUDA1, KEI TASHIRO3, KOICHI IKUTA1, MISAO SUZUKI4, & KATSUMI KOGISHI2, T. S. T. H. 1999. <NAlymphoplasia is caused by a point mutation in the

mouse gene encoding Nf-κb−inducing kinase>. *nature genetics,* 22**,** 74-77.

RENTON, A. E., CHIO, A. & TRAYNOR, B. J. 2014. State of play in amyotrophic lateral sclerosis genetics. *Nat Neurosci,* 17**,** 17-23.

RENTON, A. E., MAJOUNIE, E., WAITE, A., SIMON-SANCHEZ, J., ROLLINSON, S., GIBBS, J. R., SCHYMICK, J. C., LAAKSOVIRTA, H., VAN SWIETEN, J. C., MYLLYKANGAS, L., KALIMO, H., PAETAU, A., ABRAMZON, Y., REMES, A. M., KAGANOVICH, A., SCHOLZ, S. W., DUCKWORTH, J., DING, J., HARMER, D. W., HERNANDEZ, D. G., JOHNSON, J. O., MOK, K., RYTEN, M., TRABZUNI, D., GUERREIRO, R. J., ORRELL, R. W., NEAL, J., MURRAY, A., PEARSON, J., JANSEN, I. E., SONDERVAN, D., SEELAAR, H., BLAKE, D., YOUNG, K., HALLIWELL, N., CALLISTER, J. B., TOULSON, G., RICHARDSON, A., GERHARD, A., SNOWDEN, J., MANN, D., NEARY, D., NALLS, M. A., PEURALINNA, T., JANSSON, L., ISOVIITA, V. M., KAIVORINNE, A. L., HOLTTA-VUORI, M., IKONEN, E., SULKAVA, R., BENATAR, M., WUU, J., CHIO, A., RESTAGNO, G., BORGHERO, G., SABATELLI, M., CONSORTIUM, I., HECKERMAN, D., ROGAEVA, E., ZINMAN, L., ROTHSTEIN, J. D., SENDTNER, M., DREPPER, C., EICHLER, E. E., ALKAN, C., ABDULLAEV, Z., PACK, S. D., DUTRA, A., PAK, E., HARDY, J., SINGLETON, A., WILLIAMS, N. M., HEUTINK, P., PICKERING-BROWN, S., MORRIS, H. R., TIENARI, P. J. & TRAYNOR, B. J. 2011. A hexanucleotide repeat expansion in C9ORF72 is the cause of chromosome 9p21-linked ALS-FTD. *Neuron,* 72**,** 257-68.

REZAIE, T. 2002. Adult-Onset Primary Open-Angle Glaucoma Caused by Mutations in Optineurin. *Science,* 295**,** 1077-1079.

RICHARD, E. B. A. M. 2015. Rewriting The Book Of Life:
A New Era in Precision Gene Editing.

RICHTER, B., SLITER, D. A., HERHAUS, L., STOLZ, A., WANG, C., BELI, P., ZAFFAGNINI, G., WILD, P., MARTENS, S., WAGNER, S. A., YOULE, R. J. & DIKIC, I. 2016a. Phosphorylation of OPTN by TBK1 enhances its binding to Ub chains and promotes selective autophagy of damaged mitochondria. *Proceedings of the National Academy of Sciences,* 113**,** 4039-4044.

RICHTER, B., SLITER, D. A., HERHAUS, L., STOLZ, A., WANG, C., BELI, P., ZAFFAGNINI, G., WILD, P., MARTENS, S., WAGNER, S. A., YOULE, R. J. & DIKIC, I. 2016b. Phosphorylation of OPTN by TBK1 enhances its binding to Ub chains and promotes selective autophagy of damaged mitochondria. *Proc Natl Acad Sci U S A,* 113**,** 4039-44.

RIORDAN, S. M., HERUTH, D. P., ZHANG, L. Q. & YE, S. Q. 2015. Application of CRISPR/Cas9 for biomedical discoveries. *Cell Biosci,* 5**,** 33.

ROBERSON, E. D. 2012. Mouse models of frontotemporal dementia. *Ann Neurol,* 72**,** 837-49.

ROHRER, J. D. & WARREN, J. D. 2011. Phenotypic signatures of genetic frontotemporal dementia. *Curr Opin Neurol,* 24**,** 542-9.

RUBINSTEIN, A. L. 2003. Zebrafish: From disease modeling to drug discovery
Current Opinion in Drug Discovery & Development 218-223.

RUTHERFORD, N. J., ZHANG, Y. J., BAKER, M., GASS, J. M., FINCH, N. A., XU, Y. F., STEWART, H., KELLEY, B. J., KUNTZ, K., CROOK, R. J., SREEDHARAN, J., VANCE, C., SORENSON, E., LIPPA, C., BIGIO, E. H., GESCHWIND, D. H., KNOPMAN, D. S., MITSUMOTO, H., PETERSEN, R. C., CASHMAN, N. R., HUTTON, M., SHAW, C. E., BOYLAN, K. B., BOEVE, B., GRAFF-RADFORD, N. R., WSZOLEK, Z. K., CASELLI, R. J., DICKSON, D. W., MACKENZIE, I. R., PETRUCELLI, L. & RADEMAKERS, R. 2008. Novel mutations in TARDBP (TDP-43) in patients with familial amyotrophic lateral sclerosis. *PLoS Genet,* 4**,** e1000193.

S.H. APPEL, W. Z., D.R. BEERS, J.S. HENKEL 2011. the Microglial-Motoneuron dialogue in als
SABATELLI, M., EUSEBI, F., AL-CHALABI, A., CONTE, A., MADIA, F., LUIGETTI, M., MANCUSO, I., LIMATOLA, C., TRETTEL, F., SOBRERO, F., DI ANGELANTONIO, S., GRASSI, F., DI CASTRO, A., MORICONI, C., FUCILE, S., LATTANTE, S., MARANGI, G., MURDOLO, M., ORTESCHI, D., DEL GRANDE, A., TONALI, P., NERI, G. & ZOLLINO, M. 2009. Rare missense variants of neuronal nicotinic acetylcholine receptor altering receptor function are associated with sporadic amyotrophic lateral sclerosis. *Hum Mol Genet,* 18**,** 3997-4006.
SABERI, S., STAUFFER, J. E., SCHULTE, D. J. & RAVITS, J. 2015. Neuropathology of Amyotrophic Lateral Sclerosis and Its Variants. *Neurologic Clinics,* 33**,** 855-876.
SAKAI, C., IJAZ, S. & HOFFMAN, E. J. 2018. Zebrafish Models of Neurodevelopmental Disorders: Past, Present, and Future. *Front Mol Neurosci,* 11**,** 294.
SCHLECHTER, N., GLANZMANN, B., HOAL, E. G., SCHOEMAN, M., PETERSEN, B. S., FRANKE, A., LAU, Y. L., URBAN, M., VAN HELDEN, P. D., ESSER, M. M., MOLLER, M. & KINNEAR, C. 2017. Exome Sequencing Identifies a Novel MAP3K14 Mutation in Recessive Atypical Combined Immunodeficiency. *Front Immunol,* 8**,** 1624.
SCHMITTGEN, T. D. & LIVAK, K. J. 2008. Analyzing real-time PCR data by the comparative C(T) method. *Nat Protoc,* 3**,** 1101-8.
SCHNÖRR, S. J., STEENBERGEN, P. J., RICHARDSON, M. K. & CHAMPAGNE, D. L. 2012a. Assessment of Thigmotaxis in Larval Zebrafish. Humana Press.
SCHNÖRR, S. J., STEENBERGEN, P. J., RICHARDSON, M. K. & CHAMPAGNE, D. L. 2012b. Measuring thigmotaxis in larval zebrafish. *Behavioural Brain Research,* 228**,** 367-374.
SEKIGUCHI, T., KANOUCHI, T., SHIBUYA, K., NOTO, Y. I., YAGI, Y., INABA, A., ABE, K., MISAWA, S., ORIMO, S., KOBAYASHI, T., KAMATA, T., NAKAGAWA, M., KUWABARA, S., MIZUSAWA, H. & YOKOTA, T. 2014. Spreading of amyotrophic lateral sclerosis lesions--multifocal hits and local propagation? *Journal of Neurology, Neurosurgery & Psychiatry,* 85**,** 85-91.
SHAMS, S., CHATTERJEE, D. & GERLAI, R. 2015. Chronic social isolation affects thigmotaxis and whole-brain serotonin levels in adult zebrafish. *Behavioural Brain Research,* 292**,** 283-287.
SHARMA, S., TENOEVER, B. R., GRANDVAUX, N., ZHOU, G. P., LIN, R. & HISCOTT, J. 2003. Triggering the interferon antiviral response through an IKK-related pathway. *Science,* 300**,** 1148-51.
SHARON J. SHA, M., MS* LEONEL T. TAKADA, MD* KATHERINE P. RANKIN,, PHD, JENNIFER S. YOKOYAMA, PHD, NICOLA J. RUTHERFORD, BSC, JAMIE C. FONG, M., CGC BABER KHAN, BA, ANNA KARYDAS, B. M. C. B., BSC MARIELY DEJESUS-, HERNANDEZ, B. M. P., PHD GIOVANNI COPPOLA, MD DANIEL H. GESCHWIND,, MD, P., ROSA RADEMAKERS, P. S. E. L., MD WILLIAM SEELEY, MD BRUCE L. MILLER, MD‡ ADAM L. BOXER, MD, & PHD‡ 2012. Frontotemporal dementia due to
C9ORF72 mutations. *Neurology,* 79**,** 1002-1011.
SHEN, R. R. & HAHN, W. C. 2011. Emerging roles for the non-canonical IKKs in cancer. *Oncogene,* 30**,** 631-41.
SHEN, W.-C., LI, H.-Y., CHEN, G.-C., CHERN, Y. & TU, P.-H. 2015. Mutations in the ubiquitin-binding domain of OPTN/optineurin interfere with autophagy-mediated degradation of misfolded proteins by a dominant-negative mechanism. *Autophagy,* 11**,** 685-700.

SHENG CHEN1, P. S., XIAOJIE ZHANG AND WEIDONG LE 2013. <genetics of ALS _1750-1326-8-28.pdf>.

SHIH, V. F.-S., TSUI, R., CALDWELL, A. & HOFFMANN, A. 2011. A single NFκB system for both canonical and non-canonical signaling. *Cell Research,* 21**,** 86-102.

SHINJI HADANO1, COLLETTE K. HAND3, HITOSHI OSUGA1,2, YOSHIKO YANAGISAWA1, ASAKO OTOMO1, REBECCA S., DEVON4, N. M., JUNKO SHOWGUCHI-MIYATA2, YOSHINORI OKADA2, ROSHNI SINGARAJA4, DENISE A., FIGLEWICZ5, T. K., BETSY A. HOSLER6, TALLY SAGIE7, JENNIFER SKAUG8, JAMAL NASIR4,9, ROBERT H. & BROWN, J., STEPHEN W. SCHERER8, GUY A. ROULEAU3, MICHAEL R. HAYDEN4 & JOH-E IKEDA1,2,10 2001. <A gene encoding a putative GTPase
regulator is mutated in familial
amyotrophic lateral sclerosis 2>. *Nature,* 29**,** 166-173.

SHINKURA, R., KITADA, K., MATSUDA, F., TASHIRO, K., IKUTA, K., SUZUKI, M., KOGISHI, K., SERIKAWA, T. & HONJO, T. 1999. Alymphoplasia is caused by a point mutation in the mouse gene encoding Nf-κb-inducing kinase. *Nature Genetics,* 22**,** 74-77.

SIEVERDING, K., ULMER, J., BRUNO, C., SATOH, T., TSAO, W., FREISCHMIDT, A., AKIRA, S., WONG, P. C., LUDOLPH, A. C., DANZER, K. M., LOBSIGER, C. S., BRENNER, D. & WEISHAUPT, J. H. 2021. Hemizygous deletion of Tbk1 worsens neuromuscular junction pathology in TDP-43 transgenic mice. *Experimental Neurology,* 335**,** 113496.

SIMPSON, C. L., LEMMENS, R., MISKIEWICZ, K., BROOM, W. J., HANSEN, V. K., VAN VUGHT, P. W., LANDERS, J. E., SAPP, P., VAN DEN BOSCH, L., KNIGHT, J., NEALE, B. M., TURNER, M. R., VELDINK, J. H., OPHOFF, R. A., TRIPATHI, V. B., BELEZA, A., SHAH, M. N., PROITSI, P., VAN HOECKE, A., CARMELIET, P., HORVITZ, H. R., LEIGH, P. N., SHAW, C. E., VAN DEN BERG, L. H., SHAM, P. C., POWELL, J. F., VERSTREKEN, P., BROWN, R. H., JR., ROBBERECHT, W. & AL-CHALABI, A. 2009. Variants of the elongator protein 3 (ELP3) gene are associated with motor neuron degeneration. *Hum Mol Genet,* 18**,** 472-81.

SMITH, B. N., TICOZZI, N., FALLINI, C., GKAZI, A. S., TOPP, S., KENNA, K. P., SCOTTER, E. L., KOST, J., KEAGLE, P., MILLER, J. W., CALINI, D., VANCE, C., DANIELSON, E. W., TROAKES, C., TILOCA, C., AL-SARRAJ, S., LEWIS, E. A., KING, A., COLOMBRITA, C., PENSATO, V., CASTELLOTTI, B., DE BELLEROCHE, J., BAAS, F., TEN ASBROEK, A. L., SAPP, P. C., MCKENNA-YASEK, D., MCLAUGHLIN, R. L., POLAK, M., ASRESS, S., ESTEBAN-PEREZ, J., MUNOZ-BLANCO, J. L., SIMPSON, M., CONSORTIUM, S., VAN RHEENEN, W., DIEKSTRA, F. P., LAURIA, G., DUGA, S., CORTI, S., CEREDA, C., CORRADO, L., SORARU, G., MORRISON, K. E., WILLIAMS, K. L., NICHOLSON, G. A., BLAIR, I. P., DION, P. A., LEBLOND, C. S., ROULEAU, G. A., HARDIMAN, O., VELDINK, J. H., VAN DEN BERG, L. H., AL-CHALABI, A., PALL, H., SHAW, P. J., TURNER, M. R., TALBOT, K., TARONI, F., GARCIA-REDONDO, A., WU, Z., GLASS, J. D., GELLERA, C., RATTI, A., BROWN, R. H., JR., SILANI, V., SHAW, C. E. & LANDERS, J. E. 2014. Exome-wide rare variant analysis identifies TUBA4A mutations associated with familial ALS. *Neuron,* 84**,** 324-31.

SMITH, B. N., TOPP, S. D., FALLINI, C., SHIBATA, H., CHEN, H.-J., TROAKES, C., KING, A., TICOZZI, N., KENNA, K. P., SORAGIA-GKAZI, A., MILLER, J. W., SATO, A., DIAS, D. M., JEON, M., VANCE, C., WONG, C. H., DE MAJO, M., KATTUAH, W., MITCHELL, J. C., SCOTTER, E. L., PARKIN, N. W., SAPP, P. C., NOLAN, M., NESTOR, P. J., SIMPSON, M., WEALE, M., LEK, M., BAAS, F., VIANNEY DE JONG, J. M., TEN ASBROEK, A. L. M. A., REDONDO, A. G., ESTEBAN-

PÉREZ, J., TILOCA, C., VERDE, F., DUGA, S., LEIGH, N., PALL, H., MORRISON, K. E., AL-CHALABI, A., SHAW, P. J., KIRBY, J., TURNER, M. R., TALBOT, K., HARDIMAN, O., GLASS, J. D., DE BELLEROCHE, J., MAKI, M., MOSS, S. E., MILLER, C., GELLERA, C., RATTI, A., AL-SARRAJ, S., BROWN, R. H., SILANI, V., LANDERS, J. E. & SHAW, C. E. 2017. Mutations in the vesicular trafficking protein annexin A11 are associated with amyotrophic lateral sclerosis. *Science Translational Medicine,* 9**,** eaad9157.

STEWART, A. M., BRAUBACH, O., SPITSBERGEN, J., GERLAI, R. & KALUEFF, A. V. 2014. Zebrafish models for translational neuroscience research: from tank to bedside. *Trends Neurosci,* 37**,** 264-78.

STOLZ, A., ERNST, A. & DIKIC, I. 2014. Cargo recognition and trafficking in selective autophagy. *Nat Cell Biol,* 16**,** 495-501.

SUN, S.-C. 2012. The noncanonical NF-κB pathway. *Immunological Reviews,* 246**,** 125-140.

SUN, S.-C. 2017. The non-canonical NF-κB pathway in immunity and inflammation. *Nature Reviews Immunology,* 17**,** 545-558.

SUN, S.-C., CHANG, J.-H. & JIN, J. 2013. Regulation of nuclear factor-κB in autoimmunity. *Trends in Immunology,* 34**,** 282-289.

SYNOFZIK, M., MAETZLER, W., GREHL, T., PRUDLO, J., VOM HAGEN, J. M., HAACK, T., REBASSOO, P., MUNZ, M., SCHOLS, L. & BISKUP, S. 2012. Screening in ALS and FTD patients reveals 3 novel UBQLN2 mutations outside the PXX domain and a pure FTD phenotype. *Neurobiol Aging,* 33**,** 2949 e13-7.

T. J. KWIATKOWSKI JR., D. A. B., 1,2 A. L. LECLERC,1,2 E. TAMRAZIAN,1 C. R. VANDERBURG,3 C. RUSS,1,4 A. DAVIS,1 J. GILCHRIST,5 E. J. KASARSKIS,6 T. MUNSAT,7, † P. VALDMANIS, G. A. R., 8, B. A. HOSLER, P. C., 9 P. J. DE JONG,10 Y. YOSHINAGA,10 J. L. HAINES,11 M. A. PERICAK-VANCE,12 J. YAN,13 N. TICOZZI,1,2,14 T. SIDDIQUE,13 D. MCKENNA-YASEK,1 P. C. SAPP,1,15 H. R. HORVITZ,15 & J. E. LANDERS, 2 R. H. BROWN JR.1,2* 2009. <Mutations in the FUS/TLS Gene on Chromosome 16 Cause Familial Amyotrophic Lateral Sclerosis>. *SCIENCE,* 323**,** 1205-1208.

T. MEYER, M. A. S., MD; J.S. DULLINGER, MD; J. BROCKE, MD; K.-T. HOFFMANN; C.H. NOLTE, MD; & A. HOPT, M. U. K., PHD; P. ANDERSEN, MD; J.T. EPPLEN, MD; AND P. LINKE, MD 2005. Early-onset ALS with long-term survival associated with spastin gene mutation. *NEUROLOGY,* 65**,** 141–143.

TAKAHASHI, Y., FUKUDA, Y., YOSHIMURA, J., TOYODA, A., KURPPA, K., MORITOYO, H., BELZIL, V. V., DION, P. A., HIGASA, K., DOI, K., ISHIURA, H., MITSUI, J., DATE, H., AHSAN, B., MATSUKAWA, T., ICHIKAWA, Y., MORITOYO, T., IKOMA, M., HASHIMOTO, T., KIMURA, F., MURAYAMA, S., ONODERA, O., NISHIZAWA, M., YOSHIDA, M., ATSUTA, N., SOBUE, G., JACALS, FIFITA, J. A., WILLIAMS, K. L., BLAIR, I. P., NICHOLSON, G. A., GONZALEZ-PEREZ, P., BROWN, R. H., JR., NOMOTO, M., ELENIUS, K., ROULEAU, G. A., FUJIYAMA, A., MORISHITA, S., GOTO, J. & TSUJI, S. 2013. ERBB4 mutations that disrupt the neuregulin-ErbB4 pathway cause amyotrophic lateral sclerosis type 19. *Am J Hum Genet,* 93**,** 900-5.

TEYSSOU, E., VANDENBERGHE, N., MOIGNEU, C., BOILLEE, S., COURATIER, P., MEININGER, V., PRADAT, P. F., SALACHAS, F., LEGUERN, E. & MILLECAMPS, S. 2014. Genetic analysis of SS18L1 in French amyotrophic lateral sclerosis. *Neurobiol Aging,* 35**,** 1213 e9-1213 e12.

THU, Y. M. & RICHMOND, A. 2010. NF-kappaB inducing kinase: a key regulator in the immune system and in cancer. *Cytokine Growth Factor Rev,* 21**,** 213-26.

TICOZZI, N., VANCE, C., LECLERC, A. L., KEAGLE, P., GLASS, J. D., MCKENNA-YASEK, D., SAPP, P. C., SILANI, V., BOSCO, D. A., SHAW, C. E., BROWN, R. H., JR. & LANDERS, J. E. 2011. Mutational analysis reveals the FUS homolog TAF15 as a candidate gene for familial amyotrophic lateral sclerosis. *Am J Med Genet B Neuropsychiatr Genet,* 156B**,** 285-90.

TODA, Y., KASHIWAGI, K., MABUCHI, F., IIJIMA, H., TSUKAHARA, S., YAMAGATA, Z. & TANG, S. 2003. The association between Japanese primary open-angle glaucoma and normal tension glaucoma patients and the optineurin gene. *Human Genetics,* 113**,** 276-279.

TOSHCHAKOV, V., JONES, B. W., PERERA, P. Y., THOMAS, K., CODY, M. J., ZHANG, S., WILLIAMS, B. R., MAJOR, J., HAMILTON, T. A., FENTON, M. J. & VOGEL, S. N. 2002. TLR4, but not TLR2, mediates IFN-beta-induced STAT1alpha/beta-dependent gene expression in macrophages. *Nat Immunol,* 3**,** 392-8.

TOTH, R. P. & ATKIN, J. D. 2018. Dysfunction of Optineurin in Amyotrophic Lateral Sclerosis and Glaucoma. *Front Immunol,* 9**,** 1017.

UNTERHOLZNER, L., SUMNER, R. P., BARAN, M., REN, H., MANSUR, D. S., BOURKE, N. M., RANDOW, F., SMITH, G. L. & BOWIE, A. G. 2011. Vaccinia virus protein C6 is a virulence factor that binds TBK-1 adaptor proteins and inhibits activation of IRF3 and IRF7. *PLoS Pathog,* 7**,** e1002247.

VAN BLITTERSWIJK, M., VAN ES, M. A., HENNEKAM, E. A., DOOIJES, D., VAN RHEENEN, W., MEDIC, J., BOURQUE, P. R., SCHELHAAS, H. J., VAN DER KOOI, A. J., DE VISSER, M., DE BAKKER, P. I., VELDINK, J. H. & VAN DEN BERG, L. H. 2012a. Evidence for an oligogenic basis of amyotrophic lateral sclerosis. *Hum Mol Genet,* 21**,** 3776-84.

VAN BLITTERSWIJK, M., VAN ES, M. A., HENNEKAM, E. A. M., DOOIJES, D., VAN RHEENEN, W., MEDIC, J., BOURQUE, P. R., SCHELHAAS, H. J., VAN DER KOOI, A. J., DE VISSER, M., DE BAKKER, P. I. W., VELDINK, J. H. & VAN DEN BERG, L. H. 2012b. Evidence for an oligogenic basis of amyotrophic lateral sclerosis. *Human Molecular Genetics,* 21**,** 3776-3784.

VAN DER ZEE, J., GIJSELINCK, I., VAN MOSSEVELDE, S., PERRONE, F., DILLEN, L., HEEMAN, B., BAUMER, V., ENGELBORGHS, S., DE BLEECKER, J., BAETS, J., GELPI, E., ROJAS-GARCIA, R., CLARIMON, J., LLEO, A., DIEHL-SCHMID, J., ALEXOPOULOS, P., PERNECZKY, R., SYNOFZIK, M., JUST, J., SCHOLS, L., GRAFF, C., THONBERG, H., BORRONI, B., PADOVANI, A., JORDANOVA, A., SARAFOV, S., TOURNEV, I., DE MENDONCA, A., MILTENBERGER-MILTENYI, G., SIMOES DO COUTO, F., RAMIREZ, A., JESSEN, F., HENEKA, M. T., GOMEZ-TORTOSA, E., DANEK, A., CRAS, P., VANDENBERGHE, R., DE JONGHE, P., DE DEYN, P. P., SLEEGERS, K., CRUTS, M., VAN BROECKHOVEN, C., GOEMAN, J., NUYTTEN, D., SMETS, K., ROBBERECHT, W., DAMME, P. V., BLEECKER, J., SANTENS, P., DERMAUT, B., VERSIJPT, J., MICHOTTE, A., IVANOIU, A., DERYCK, O., BERGMANS, B., DELBECK, J., BRUYLAND, M., WILLEMS, C., SALMON, E., PASTOR, P., ORTEGA-CUBERO, S., BENUSSI, L., GHIDONI, R., BINETTI, G., HERNANDEZ, I., BOADA, M., RUIZ, A., SORBI, S., NACMIAS, B., BAGNOLI, S., SORBI, S., SANCHEZ-VALLE, R., LLADO, A., SANTANA, I., ROSARIO ALMEIDA, M., FRISONI, G. B., MAETZLER, W., MATEJ, R., FRAIDAKIS, M. J., KOVACS, G. G., FABRIZI, G. M. & TESTI, S. 2017. TBK1 Mutation Spectrum in an Extended European Patient Cohort with Frontotemporal Dementia and Amyotrophic Lateral Sclerosis. *Hum Mutat,* 38**,** 297-309.

VANCE, C., ROGELJ, B., HORTOBAGYI, T., DE VOS, K. J., NISHIMURA, A. L., SREEDHARAN, J., HU, X., SMITH, B., RUDDY, D., WRIGHT, P., GANESALINGAM, J., WILLIAMS, K. L., TRIPATHI, V.,

AL-SARAJ, S., AL-CHALABI, A., LEIGH, P. N., BLAIR, I. P., NICHOLSON, G., DE BELLEROCHE, J., GALLO, J. M., MILLER, C. C. & SHAW, C. E. 2009. Mutations in FUS, an RNA processing protein, cause familial amyotrophic lateral sclerosis type 6. *Science,* 323**,** 1208-1211.

VERHEIJEN, J., VAN DER ZEE, J., GIJSELINCK, I., VAN DEN BOSSCHE, T., DILLEN, L., HEEMAN, B., GOMEZ-TORTOSA, E., LLADO, A., SANCHEZ-VALLE, R., GRAFF, C., PASTOR, P., PASTOR, M. A., BENUSSI, L., GHIDONI, R., BINETTI, G., CLARIMON, J., DE MENDONCA, A., GELPI, E., TSOLAKI, M., DIEHL-SCHMID, J., NACMIAS, B., ALMEIDA, M. R., BORRONI, B., MATEJ, R., RUIZ, A., ENGELBORGHS, S., VANDENBERGHE, R., DE DEYN, P. P., CRUTS, M., VAN BROECKHOVEN, C., SLEEGERS, K., CONSORTIUM, B. & CONSORTIUM, E. E. 2018. Common and rare TBK1 variants in early-onset Alzheimer disease in a European cohort. *Neurobiol Aging,* 62**,** 245 e1-245 e7.

WATTS, G. D., THOMASOVA, D., RAMDEEN, S. K., FULCHIERO, E. C., MEHTA, S. G., DRACHMAN, D. A., WEIHL, C. C., JAMROZIK, Z., KWIECINSKI, H., KAMINSKA, A. & KIMONIS, V. E. 2007. Novel VCP mutations in inclusion body myopathy associated with Paget disease of bone and frontotemporal dementia. *Clin Genet,* 72**,** 420-6.

WEIDBERG, H. & ELAZAR, Z. 2011. TBK1 Mediates Crosstalk Between the Innate Immune Response and Autophagy. *Science Signaling,* 4**,** pe39-pe39.

WEIL, R., LAPLANTINE, E., CURIC, S. & GENIN, P. 2018. Role of Optineurin in the Mitochondrial Dysfunction: Potential Implications in Neurodegenerative Diseases and Cancer. *Front Immunol,* 9**,** 1243.

WHITE, R. M., CECH, J., RATANASIRINTRAWOOT, S., LIN, C. Y., RAHL, P. B., BURKE, C. J., LANGDON, E., TOMLINSON, M. L., MOSHER, J., KAUFMAN, C., CHEN, F., LONG, H. K., KRAMER, M., DATTA, S., NEUBERG, D., GRANTER, S., YOUNG, R. A., MORRISON, S., WHEELER, G. N. & ZON, L. I. 2011. DHODH modulates transcriptional elongation in the neural crest and melanoma. *Nature,* 471**,** 518-22.

WILD, P., FARHAN, H., MCEWAN, D. G., WAGNER, S., ROGOV, V. V., BRADY, N. R., RICHTER, B., KORAC, J., WAIDMANN, O., CHOUDHARY, C., DOTSCH, V., BUMANN, D. & DIKIC, I. 2011. Phosphorylation of the Autophagy Receptor Optineurin Restricts Salmonella Growth. *Science,* 333**,** 228-233.

WILLMANN, K. L., KLAVER, S., DOĞU, F., SANTOS-VALENTE, E., GARNCARZ, W., BILIC, I., MACE, E., SALZER, E., DOMÍNGUEZ CONDE, C., SIC, H., MÁJEK, P., BANERJEE, P. P., VLADIMER, G. I., HASKOLOĞLU, Ş., GÖKALP BOLKENT, M., KÜPESIZ, A., CONDINO-NETO, A., COLINGE, J., SUPERTI-FURGA, G., PICKL, W. F., VAN ZELM, M. C., EIBEL, H., ORANGE, J. S., IKINCIOĞULLARı, A. & BOZTUĞ, K. 2014. Biallelic loss-of-function mutation in NIK causes a primary immunodeficiency with multifaceted aberrant lymphoid immunity. *Nature Communications,* 5**,** 5360.

WOO, J. A., LIU, T., TROTTER, C., FANG, C. C., DE NARVAEZ, E., LEPOCHAT, P., MASLAR, D., BUKHARI, A., ZHAO, X., DEONARINE, A., WESTERHEIDE, S. D. & KANG, D. E. 2017. Loss of function CHCHD10 mutations in cytoplasmic TDP-43 accumulation and synaptic integrity. *Nat Commun,* 8**,** 15558.

WRIGHT, D. & KRAUSE, J. 2006. Repeated measures of shoaling tendency in zebrafish (Danio rerio) and other small teleost fishes. *Nat Protoc,* 1**,** 1828-31.

WU, C. H., FALLINI, C., TICOZZI, N., KEAGLE, P. J., SAPP, P. C., PIOTROWSKA, K., LOWE, P., KOPPERS, M., MCKENNA-YASEK, D., BARON, D. M., KOST, J. E., GONZALEZ-PEREZ, P.,

FOX, A. D., ADAMS, J., TARONI, F., TILOCA, C., LECLERC, A. L., CHAFE, S. C., MANGROO, D., MOORE, M. J., ZITZEWITZ, J. A., XU, Z. S., VAN DEN BERG, L. H., GLASS, J. D., SICILIANO, G., CIRULLI, E. T., GOLDSTEIN, D. B., SALACHAS, F., MEININGER, V., ROSSOLL, W., RATTI, A., GELLERA, C., BOSCO, D. A., BASSELL, G. J., SILANI, V., DRORY, V. E., BROWN, R. H., JR. & LANDERS, J. E. 2012. Mutations in the profilin 1 gene cause familial amyotrophic lateral sclerosis. *Nature,* 488**,** 499-503.

WU, R. S., LAM, I. I., CLAY, H., DUONG, D. N., DEO, R. C. & COUGHLIN, S. R. 2018. A Rapid Method for Directed Gene Knockout for Screening in G0 Zebrafish. *Developmental Cell,* 46**,** 112-125.e4.

XI, Y., NOBLE, S. & EKKER, M. 2011. Modeling neurodegeneration in zebrafish. *Curr Neurol Neurosci Rep,* 11**,** 274-82.

XIAO, G. & SUN, S.-C. 2000. Negative Regulation of the Nuclear Factor κB-inducing Kinase by a cis-Acting Domain. *Journal of Biological Chemistry,* 275**,** 21081-21085.

XIAO, T. S. 2017. Innate immunity and inflammation. *Cell Mol Immunol,* 14**,** 1-3.

XIE, X. H., ZANG, N., LI, S. M., WANG, L. J., DENG, Y., HE, Y., YANG, X. Q. & LIU, E. M. 2012. Resveratrol Inhibits respiratory syncytial virus-induced IL-6 production, decreases viral replication, and downregulates TRIF expression in airway epithelial cells. *Inflammation,* 35**,** 1392-401.

YIN, L. 2001. Defective Lymphotoxin-beta Receptor-Induced NF-kappa B Transcriptional Activity in NIK-Deficient Mice. *Science,* 291**,** 2162-2165.

YING, H., SHEN, X., PARK, B. & YUE, B. Y. J. T. 2010. Posttranslational Modifications, Localization, and Protein Interactions of Optineurin, the Product of a Glaucoma Gene. *PLoS ONE,* 5**,** e9168.

YING, H. & YUE, B. Y. J. T. 2012. Cellular and Molecular Biology of Optineurin. Elsevier.

YU, T., YI, Y. S., YANG, Y., OH, J., JEONG, D. & CHO, J. Y. 2012. The pivotal role of TBK1 in inflammatory responses mediated by macrophages. *Mediators Inflamm,* 2012**,** 979105.

YUICHIRO TOJIMA , A. F., MIREILLE DELHASE , YI CHEN ,, SHIGETSUGU HATAKEYAMAK, K.-I. N. K., YOKO KANEKO ,, YUJI NIMURA , N. M., KYOJI IKEDA , MICHAEL KARIN & NAKANISHI, M. 2000a. NAK is an IkB kinase-activating kinase. *NATURE,* 404**,** 778-782.

YUICHIRO TOJIMA , A. F., MIREILLE DELHASE , YI CHEN ,, SHIGETSUGU HATAKEYAMAK, K.-I. N. K., YOKO KANEKO ,, YUJI NIMURA , N. M., KYOJI IKEDA , MICHAEL KARIN & NAKANISHI, M. 2000b. NAK is an IkB kinase-activating kinase. *NATURE,* VOL 404**,** 778-782.

YUK, J. M. & JO, E. K. 2013. Crosstalk between autophagy and inflammasomes. *Mol Cells,* 36**,** 393-9.

ZHANG, K. Y., YANG, S., WARRAICH, S. T. & BLAIR, I. P. 2014. Ubiquilin 2: a component of the ubiquitin-proteasome system with an emerging role in neurodegeneration. *Int J Biochem Cell Biol,* 50**,** 123-6.

ZHAO, P., WONG, K. I., SUN, X., REILLY, S. M., UHM, M., LIAO, Z., SKOROBOGATKO, Y. & SALTIEL, A. R. 2018. TBK1 at the Crossroads of Inflammation and Energy Homeostasis in Adipose Tissue. *Cell,* 172**,** 731-743.e12.

ZHU, G., WU, C.-J., ZHAO, Y. & ASHWELL, J. D. 2007. Optineurin Negatively Regulates TNFα-Induced NF-κB Activation by Competing with NEMO for Ubiquitinated RIP. *Current Biology,* 17**,** 1438-1443.

ZIV, L., MUTO, A., SCHOONHEIM, P. J., MEIJSING, S. H., STRASSER, D., INGRAHAM, H. A., SCHAAF, M. J. M., YAMAMOTO, K. R. & BAIER, H. 2013. An affective disorder in zebrafish with mutation of the glucocorticoid receptor. *Molecular Psychiatry,* 18**,** 681-691.